IRE Transactions

on Microwave Theory and Techniques

Volume MTT-5 APRIL, 1957 Number 2

In This Issue

For complete Table of Contents, see page 79.

PUBLISHED BY THE
essional Group on Microwave Theory and Techniques

IRE PROFESSIONAL GROUP ON MICROWAVE THEORY AND TECHNIQUES

The Professional Group on Microwave Theory and Techniques is an association of IRE members with professional interest in the field of Microwave Theory and Techniques. All IRE members are eligible for membership and will receive all Group publications upon payment of the prescribed annual assessment of $3.00.

IRE TRANSACTIONS®

on Microwave Theory and Techniques

Published by the Institute of Radio Engineers, Inc., for the Professional Group on Microwave Theory and Techniques, at 1 East 79th Street, New York 21, New York. Responsibility for the contents rests upon the authors, and not upon the IRE, the Group, or its members. Price per copy: IRE PGMTT members, $1.90; IRE members, $2.85, nonmembers, $5.70. Annual subscription price: IRE members, $8.50; colleges and public libraries, $12.75; nonmembers, $17.00.

Address all manuscripts to Kiyo Tomiyasu, General Electric Company, Palo Alto, Calif.

IRE Transactions on Microwave Theory and Techniques

Published by the Professional Group on Microwave Theory and Techniques

Volume MTT-5 APRIL, 1957 Number 2

TABLE OF CONTENTS

A Message from the Editor

Beginning with the next issue of these TRANSACTIONS, Kiyo Tomiyasu will be the Editor.

The last two years have seen these TRANSACTIONS grow both in size and quality of contents. The growth has been a healthy one, and there appears to be every reason to believe that it will continue.

In closing my term of office, I would like to thank the various people who have helped to make these TRANSACTIONS possible. These people include the members of the editorial board whose names are listed below, the Administrative Committee of the Professional Group, the editorial staff at IRE Headquarters, and the many fine authors without whom these TRANSACTIONS would not exist.

Editorial Board Members
Past and Present

Eugene Feldman
Irving Goldstein
Henry Jasik
Donald D. King
Richard C. LaRosa
Roderic V. Lowman
Marshall C. Pease
Wilbur L. Pritchard
John Reed
William E. Waller
Ernest Wantuch
Gershon Wheeler

—THEODORE S. SAAD

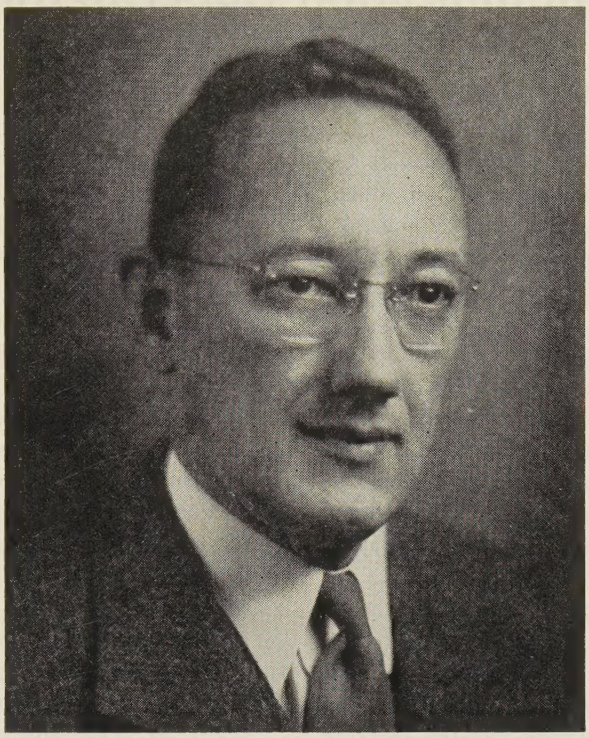

Alfred C. Beck

Alfred C. Beck was born in Granville, N. Y., on July 26, 1905. He received the E.E. degree from Rensselaer Polytechnic Institute in 1927. During the summers of 1926 and 1927 he worked in the Test Department of the New York Edison Company on various electric power projects, and through the academic year, 1927–1928, he was an instructor in mathematics at Rensselaer Polytechnic Institute. Graduate courses in communications during that year, and experience as a radio amateur (W2AGG), convinced him that his interests were along the lines of radio communication.

In July, 1928, he became a member of the technical staff of Bell Telephone Laboratories, Inc., assigned to the Radio Research Department at Cliffwood, N. J. He worked on antennas for the transatlantic and ship-to-shore radiotelephone systems, including inverted vees, rhombics, comb antennas, and MUSA arrangements. In 1930, this group moved and formed the Holmdel Radio Research Laboratory, where he is still located.

In the latter 1930's, attention turned to research on microwave radio repeaters for Bell System use. However, the national defense requirements for radar soon took full time, and communications work had to be postponed. There followed about five years of work on antennas, waveguide components, and microwave equipment for naval fire control and other military radar applications.

After World War II, work was resumed on broad-band Bell System transmission methods. A few years were spent with the development, assembly, and testing of microwave radio repeater systems.

For the past several years, Mr. Beck has been working on special waveguides, components, experimental installations, and testing methods for long-distance communication using circular electric waveguides.

Mr. Beck has a number of publications and patents in the radio field. He is a New York State licensed professional engineer and a member of Sigma Xi. He has served in a number of IRE capacities, including chairman of the New York Section and chairman of the PGMTT Administrative Committee.

Communication Superhighways

ALFRED C. BECK
Bell Telephone Laboratories, Inc., Holmdel, N. J.

Because of advances in communication, it has been said that more progress has been made in science and general living conditions in the last fifty years than in all the thousands of years preceding. Part of this is due to transportation improvements in all divisions—land, water, and air. Today, auto trips from New York to Chicago in about fifteen hours demonstrate strikingly what a big advance turnpikes make in surface travel. Such thoroughfares are important for the trucking industry, too, and government is pushing superhighway construction all over the country. On these highways traffic has exceeded all estimates, thus proving their value.

The telephone is one of the important parts of the communication art which has contributed so much to our way of living. In its early days, amplification became a necessity for extending the talking distances, and fifty years ago the birth of the electron tube made this practical, as well as ushering in the electronic art which gave us our profession. And this tube, by the process of modulation, led to carrier systems, stacking up many individual channels on single transmission lines that became highways of communication. This was a big advance, greatly reducing the cost and increasing the amount of long distance traffic.

As this process continued to higher frequencies, the increase in losses prompted the use of better transmission lines, one example being the coaxial. Then, as high frequency techniques improved, microwave art produced broader bandwidth systems, wider communication highways which, like the auto highways, are handling more and more traffic.

Other communication requirements have also contributed to this traffic increase. The telephone made possible talking and hearing at a distance. Many years ago, a Bell System research executive said that he was sure people were just as anxious to see at a distance as they were to hear at a distance. The big strides of television in the field have proved the truth of this observation. This has placed large bandwidth requirements on our communication systems, which may well be tremendous, if business and personal television service, even in a small part akin to the telephone service, become a reality. The demand for data transmission is now growing fast too, and other new communication needs are constantly arising.

All of this will require communications superhighways, if it is to be transmitted at a low enough cost for public acceptance. Such superhighways, because of their large bandwidth, must come in the microwave frequency range or higher. So this becomes one of the big challenges and opportunities in microwave theory and techniques.

Radio highways through the air, using the higher frequencies of the spectrum, form an important part of our art and have occupied many pages of the TRANSACTIONS. But radio has definite limitations in available bands, interference, fading, and congestion at large traffic centers. Then too, rain, water vapor, and oxygen place an upper limit on transmission through the air of still higher frequencies which we are learning to generate and use, and which will be necessary for superhighways.

Many of these limitations can be avoided by putting the high frequency waves inside pipes—that is, using waveguides for long distance transmission. This provides a shielded system, avoiding interference and sharing with other services, and permits the use of a nonabsorbing atmosphere. It has been found that one form, using the circular electric mode, has the unique theoretical property of decreasing attenuation with increasing frequency. Experiments have shown its validity, and the conditions for achieving this property. This appears to open vast new frequency areas, perhaps many times larger than the whole radio spectrum now in use, for communication applications. These waveguides have losses that are low enough for economical long distance service in the future. Like most new things, this medium does have difficulties and problems to be overcome, and here is a challenge. Advances in the waveguide art, and in all of the associated microwave technology, are coming rapidly to help us, and more are needed.

Considering the increasing importance of communication in our civilization, it is comforting to know that microwave theory and techniques hold the possibility of supplying communication superhighways when we need them. There is much work to be done, and the opportunities in research, development, installation, and maintenance give great promise for the future of our profession and all those connected with it.

Report of Advances in Microwave Theory and Techniques—1956*

DONALD D. KING†

MICROWAVE THEORY and techniques include the transmission, control, and measurement of waves of centimeter or millimeter length. The methods applicable in this region differ sufficiently from those at lower frequency to constitute a rather well-defined discipline. This area is the subject of our review. Several subjects contiguous to the microwave domain are excluded. Thus, antenna and propagation problems do not exhibit so clearcut a change with wavelength, and are mentioned only indirectly. The electronic aspects of microwave generators are also omitted, although much work on the circuits for these generators is necessarily included.

The year 1956 in microwaves has been dominated by the continuing advance in the use of gyromagnetic media for circuit elements. What might be called the ferrite revolution is extending rapidly to embrace more and more useful devices for the control of microwaves. The host of new practical applications for ferrites has been accompanied by a corresponding advance in the basic physics of the solid state. The close community of interest of both physicists and engineers in the microwave properties of ferrites offers the best explanation for the intense and fruitful effort in this area during the year.

Less spectacular but important advances are being made on certain types of waveguides and linear circuit elements for microwaves. Measurement techniques also show steady progress during the year. Traveling wave devices of various kinds remain the most active area of research in microwave active elements. However, interest in gas discharges appears to be increasing, and this field holds some promise of new microwave active elements. The smaller scale efforts in detectors and noise sources continue unabated.

The general subjects mentioned above provide four broad headings under which the individual work is listed. These are: I. Ferrites, II. Waveguides, III. Measurements, and IV. Sources and Detectors. These are now considered in turn.

I. Ferrites

Research in ferrites follows two complementary channels: the study of ferrite materials, and the investigation of circuit elements using ferrites. In the early developments, these two aspects often could not be distinguished, since special circuit elements were needed to study the new materials. At least the more obvious circuit elements have now been realized, and in some instances have already become standard items. Progress in ferrite circuit elements continues at a rapid pace, and enjoys the advantage of many standardized ferrite materials. The need for improvement in these ferrites is basic to much of the future development of the field, and occupies the first place in this review. Following the review of materials and their properties in waveguides, the various special circuit elements utilizing ferrites are taken up.

The work being considered is confined to published papers which may be generally accessible to others active in the field. However, two important conferences must be mentioned in connection with ferrites. The first of these was held in Cambridge, Mass. on April 2–4, 1956. The papers presented at this meeting provided the most complete and unified coverage of the ferrite field to date; they included both tutorial discussions of basic theory, and detailed papers on various special applications. These papers have since been published and are included in the bibliography wherever applicable.

Another conference on ferrites took place in London on October 29–November 2, 1956. Many important contributions were made at this conference which have not yet appeared in print. A few of these papers are incorporated into the bibliography to record their significant contribution. Many of these papers will be published in the *Proceedings of the Institution of Electrical Engineers*, part B during 1957.

The success of these two conferences, both in terms of important scientific contributions, and in numbers of interested technical people attending, is a measure of the vitality of ferrite research throughout the world.

Properties of Ferrite Materials

No single figure of merit describes the quality of a given ferrite for all circuit applications. Important properties which must be considered are:

1) Tensor susceptibility.
2) Dielectric constant.
3) Ferromagnetic resonance linewidth.
4) Curie temperature.
5) Saturation magnetization.

For the circuit designer, the tensor susceptibility and dielectric constant, both complex, specify the electrical performance. The frequency dependence of the former limits the bandwidth of many ferrite devices. In particular, the magnetic loss at low frequency constitutes a basic limitation of present materials. Except for certain resonance devices, a narrow resonance line-

* Manuscript received by the PGMTT, January 25, 1957.
† Electronic Communications, Inc., Baltimore 18, Md.

width is also desirable. At present, the dielectric constant and loss are not a major limitation on ferrite performance. However, changes in ferrite composition or extension to higher frequencies may alter the situation.

At the Curie temperature, the saturation magnetization vanishes, and the ferrite properties disappear. This places an absolute limit on the operating temperature, and hence generally on the power handling capacity.

The basic theory of ferrites has been described in considerable detail by theoretical physicists in papers intended to provide the foundation for engineering applications.

[1] J. H. Van Vleck, "Fundamental theory of ferro- and ferrimagnetism," PROC. IRE, vol. 44, pp. 1248–1258; October, 1956.
[2] N. Bloembergen, "Magnetic resonance in ferrites," PROC. IRE, vol. 44, pp. 1259–1269; October, 1956
[3] J. O. Artman, "Microwave resonance relations in anisotropic single crystal ferrites," PROC. IRE, vol. 44, pp. 1284–1293; October, 1956.
[4] G. T. Rado, "On the electromagnetic characterization of ferromagnetic media: permeability tensors and spin wave equations," IRE TRANS., vol. AP-4, pp. 512–525; July, 1956.

A good start has been made at extending the analysis of ferrite behavior to high-signal levels. Important saturation effects exist on which considerable experimental data has been accumulated.

[5] H. Suhl, "The nonlinear behavior of ferrites at high microwave signal levels," PROC. IRE, vol. 44, pp. 1270–1283; October, 1956.
[6] N. G. Sakiotis, H. N. Chait, and M. L. Kales, "Nonlinearity of microwave ferrite media," IRE TRANS., vol. AP-4, pp. 111–115; April, 1956.

In the study of new ferrite materials, particular interest has been attracted to rare earth ferrites and to hexagonal crystal structures.

[7] F. Bertaut, "Structure of the ferrimagnetic ferrites of the rare earths," *Compt. Rend. Acad. Sci. Paris*, vol. 242, p. 282; April, 1956.
[8] F. Bertaut and R. Pauthenet, "Crystalline structure and magnetic properties of ferrites having the general formula 5 Fe_2O_3—$3M_2O_3$," presented at the Convention on Ferrites, October 29–November 2, 1956.
[9] E. W. Gorter, "Saturation magnetization of new ferrimagnetic oxides with hexagonal crystal structures," presented at the Convention on Ferrites, October 29–November 2, 1956.
[10] P. B. Braun, G. H. Jonker, and H. P. J. Wijn, "A new class of oxidic ferromagnetic materials with hexagonal crystal structures," presented at the Convention on Ferrites, October 29–November 2, 1956.

A few additional materials which have been examined in some detail are the following:

[11] L. G. Van Uitert, "Nickel copper ferrites for microwave applications," *J. Appl. Phys.*, vol. 27, pp. 723–727; July, 1956.
[12] P. E. Tannenwald and M. H. Seavey, "Anisotropy of cobalt-substituted Mn ferrite single crystals," PROC. IRE, vol. 44, pp. 1343–1344; October, 1956.
[13] F. Mayer, "Study of magnetic rotatory polarization in copper ferrite at 10 kmc/s," *Compt. Rend. Acad. Sci. Paris*, vol. 242, pp. 81–83; January, 1956.

Permeability and dielectric properties of ferrites have been determined by a variety of methods and in considerable detail.

[14] E. B. Mullen and E. R. Carlson, "Permeability tensor values from waveguide measurements," PROC. IRE, vol. 44, pp. 1318–1322; October, 1956.
[15] E. G. Spencer, L. S. Ault, and R. C. LeCraw, "Intrinsic tensor permeabilities on ferrite rods, spheres, and disks," PROC. IRE, vol. 44, pp. 1311–1317; October, 1956.
[16] R. C. LeCraw and E. G. Spencer, "Tensor permeabilities of ferrites below magnetic saturation," 1956 IRE CONVENTION RECORD, Part 5, pp. 66–74.
[17] E. G. Spencer, R. C. LeCraw, and F. Reggia, "Measurement of microwave dielectric constants and tensor permeabilities of ferrite spheres," PROC. IRE, vol. 44, pp. 790–800; June, 1956.
[18] L. G. Van Uitert, "Dielectric properties of and conductivity in ferrites," PROC. IRE, vol. 44, pp. 1294–1302; October, 1956.
[19] S. Sensiper, "Resonance loss properties of ferrites in 9 kmc region," PROC. IRE, vol. 44, pp. 1323–1342; October, 1956.

The preparation and chemical aspects of ferrites have been discussed in a paper which in many respects is basic to all ferrite applications.

[20] D. L. Fresh, "Methods of preparation and crystal chemistry of ferrites," PROC. IRE, vol. 44, pp. 1303–1310; October, 1956.

Wave Propagation in Ferrites

Microwave applications inevitably involve the propagation of EM waves in ferrite materials. Here, the boundary conditions assumed are of paramount importance. Circular waveguide is perhaps the most common and useful configuration. For more complicated geometries, the mathematical complications become formidable. In spite of this, some progress has been made, both by approximation and by numerical solution.

Several reviews of the general problem have appeared which serve well to put the various problems in perspective.

[21] P. S. Epstein, "Theory of wave propagation in a gyromagnetic medium," *Rev. Mod. Phys.*, vol. 28, pp. 3–17; January, 1956.
[22] M. L. Kales, "Topics in guided-wave propagation in magnetized ferrites," PROC. IRE, vol. 44, pp. 1403–1409; October, 1956.
[23] G. H. B. Thompson, "Ferrites in waveguides," *J. Brit. IRE*, vol. 16, pp. 311–328; June, 1956.

Papers dealing with more specific waveguide cross sections containing ferrites include the following.

[24] L. R. Walker and H. Suhl, "Propagation in circular waveguides filled with gyromagnetic material," IRE TRANS., vol. AP-4, pp. 492–494; July, 1956.
[25] J. L. Melchor, W. P. Ayers, and P. H. Vartanian, "Energy concentration effects in ferrite loaded wave guides," *J. Appl. Phys.*, vol. 27, pp. 72–77; January, 1956.
[26] A. A. van Trier, "Some topics in the microwave application of gyrotropic media," IRE TRANS., vol. AP-4, pp. 502–507; July, 1956.
[27] N. Karayianis and J. C. Cacheris, "Birefringence of ferrites in circular waveguides," PROC. IRE, vol. 44, pp. 1414–1420; October, 1956.
[28] K. J. Button and Benjamin Lax, "Theory of ferrites in rectangular waveguide," IRE TRANS., vol. AP-4, pp. 531–537; July, 1956.
[29] H. Seidel, "Anomalous propagation in ferrite-loaded waveguide," PROC. IRE, vol. 44, pp. 1410–1413; October, 1956.
[30] P. H. Vartanian and E. T. Jaynes, "Propagation in ferrite-filled transversely magnetized waveguide," IRE TRANS., vol. MTT-4, pp. 140–143; July, 1956.
[31] B. J. Duncan and L. Swern, "Temperature behavior of ferrimagnetic resonance in ferrites located in waveguide," *J. Appl. Phys.*, vol. 27, pp. 209–215; March, 1956.

More general boundary conditions have also been treated, including an experimental study of radiation from ferrite-filled apertures.

[32] J. Sontif-Guichard, "Calculation of the Faraday effect in a gyroparamagnetic medium," *Compt. Rend. Acad. Sci. Paris*, vol. 242, pp. 1868–1871; April 9, 1956.
[33] J. Sontif-Guichard, "Equation of circularly polarized waves in a gyroparamagnetic medium," *Compt. Rend. Acad. Sci. Paris*, vol. 242, pp. 1418–1421; March, 1956.
[34] D. J. Angelakos and M. M. Korman, "Radiation from ferrite-filled apertures," PROC. IRE, vol. 44, pp. 1463–1467; October, 1956.

Isolators

The component which makes the most obvious use of nonreciprocal ferrite properties is the isolator. It is probably the most outstanding ferrite component, since it offers properties which cannot be attained at all with linear elements, and does so with elegance and dispatch.

The general configuration of isolators and other ferrite circuit elements involves a section of waveguide partially filled with ferrite material of a particular shape. For most circuit elements, the distribution of ferrite is uniform along the direction of propagation. The properties of these ferrite devices have been reviewed in several papers covering both the basic theory and the generally attainable performance at the present time.

[35] C. L. Hogan, "The elements of nonreciprocal microwave devices," PROC. IRE, vol. 44, pp. 1345–1367; October, 1956.
[36] B. Lax, "Frequency and loss characteristics of microwave ferrite devices," PROC. IRE, vol. 44, pp. 1368–1385; October, 1956.
[37] G. S. Heller, "Ferrites as microwave circuit elements," PROC. IRE, vol. 44, pp. 1386–1393; October, 1956.
[38] C. L. Hogan, "The low-frequency problem in the design of microwave gyrators and associated elements," IRE TRANS., vol. AP-4, pp. 495–501; July, 1956.

An important contribution to the analysis of such elements has been the introduction of matrix methods for the solution of transverse propagation characteristics. This type of analysis holds promise for a number of waveguide types.

[39] J. H. Rowen, "A novel approach to the analysis of ferrite-loaded waveguide structures," presented at the London Convention on Ferrites, October 29–November 2, 1956.

An example of the possibilities for ferrite isolators in strip line was also given earlier in the year.

[40] L. Lewin, "A resonant absorption isolator in microstrip for 4 kmc/s," presented at the London Convention on Ferrites, October 29–November 2, 1956.
[41] O. A. Fix, "A balanced stripline isolator," 1956 IRE CONVENTION RECORD, Part 5, pp. 99–105.

A large number of papers has appeared on various isolator designs. In many of these considerable material of importance to the basic understanding of isolator operations is included, as well as specific information on a practical engineering design.

[42] S. Weisbaum and H. Seidel, "The field displacement isolator," *Bell Sys. Tech. J.*, vol. 35, pp. 877–898; July, 1956.
[43] S. Weisbaum and H. Boyet, "A double-slab ferrite field displacement isolator at 11 kmc," PROC. IRE, vol. 44, pp. 554–555; April, 1956.
[44] M. T. Weiss, "Improved rectangular waveguide resonance isolators," IRE TRANS., vol. MTT-4, pp. 240–243; October, 1956.
[45] P. H. Vartanian, J. L. Melchor, and W. P. Ayres, "Broadband ferrite microwave isolator," IRE TRANS., vol. MTT-4, pp. 8–13; January, 1956.
[46] P. H. Vartanian, J. L. Melchor, and W. P. Ayres, "Broadbanding ferrite microwave isolators," 1956 IRE CONVENTION RECORD, Part 5, pp. 79–83.
[47] A. Langley Morris, "The 45° rotation ferrite isolator," presented at the London Convention on Ferrites, October 29–November 2, 1956.
[48] R. F. Sullivan, "A miniaturized high temperature isolator," 1956 IRE CONVENTION RECORD, Part 5, pp. 75–78.
[49] W. Eichin, "A unidirectional attenuator with delay line and ferrite element for the 4-kmc/s frequency band," *Nachrichtentech Z.*, vol. 9, pp. 168–172; April, 1956.
[50] B. N. Enander, "A new ferrite isolator," PROC. IRE, vol. 44, pp. 1421–1430; October, 1956.

Modulators

Control of attenuation by means of the external magnetic field is easily achieved in ferrite devices. The resulting possibilities for modulation and gain control are very attractive. A number of papers have reported successful devices of this type.

[51] P. Fire and P. H. Vartanian, "An amplitude regulator for microwave signal sources," 1956 IRE CONVENTION RECORD, Part 5, pp. 166–171.
[52] W. W. H. Clarke, W. M. Searle, and F. T. Vail, "A ferrite microwave modulator employing feedback," *Proc. IEE*, vol. 103, Part B, pp. 485–490; July, 1956.
[53] J. C. Cacheris and H. A. Dropkin, "Compact microwave single-sideband modulator using ferrites," IRE TRANS., vol. MTT-4, pp. 152–155; July, 1956.
[54] H. G. Beljers, "Amplitude modulation of centimetre waves by means of ferroxcube," *Philips Tech. Rev.*, vol. 18, pp. 82–86; September, 1956.
[55] J. P. Vinding, "Automatic gain control system for microwaves," IRE TRANS., vol. MTT-4, pp. 244–245; October, 1956.

Frequency modulation is also possible by means of cavity tuning. An example of this has been given.

[56] G. R. Jones, J. C. Cacheris, and C. A. Morrison, "Magnetic tuning of resonant cavities and wideband frequency modulation of klystrons," PROC. IRE, vol. 44, pp. 1431–1438; October, 1956.

A rather different action, namely frequency doubling, has also been obtained in ferrites. Although not modulation in the usual sense, this important effect is listed here for want of a better heading.

[57] W. P. Ayres, P. H. Vartanian, and J. L. Melchor, "Frequency doubling in ferrites," *J. Appl. Phys.*, vol. 27, pp. 188–189; February, 1956.

Circulators and Directional Couplers

A circulator may be defined as a device in which energy is transferred from port to port without amplitude change. Phase shifts may be tolerated, and energy need not return from a port by the same path as it came to that port. Such a device in nonreciprocal form is only practicable with ferrite elements. The network properties of circulators have been analyzed very effectively in terms of group theory and topology. In terms of the former, a circulator is defined as a device whose scattering matrix operates on the incident voltages so as to produce the same result as the operation of a cyclic substitution. In the language of topology, a circulator is any structure which may be represented by an "oriented 1-circuit."

With the aid of these concepts, possible symmetries for circulators can be specified, and rules for determining the results of complicated interconnections of circulators can be set up.

[58] Milton A. Treuhaft, "Network properties of circulators based on the scattering concept." PROC. IRE, vol. 44, pp. 1394–1402; October, 1956.

Several circulator schemes have been developed with widely differing physical arrangements.

[59] E. A. Ohm, "A broad-band microwave circulator," IRE TRANS., vol. MTT-4, pp. 210–217; October, 1956.
[60] P. J. Allen, "The turnstile circulator," IRE TRANS., vol. MTT-4, pp. 223–227; October, 1956.

A directional coupler based on the nonreciprocal scattering from a ferrite post has also been developed. This device is closely related to circulators.

[61] A. D. Berk and E. Strumwasser, "Ferrite directional couplers," PROC. IRE, vol. 44, pp. 1439–1445; October, 1956.

Phase Shifters

The differential phase shifts which underlie the operation of the ferrite devices mentioned so far may be used explicitly in phase shifters. Both reciprocal and nonreciprocal types are possible, and offer new possibilities in electrical control of transmission characteristics over broad bands.

[62] S. Weisbaum and H. Boyet, "Broad-band nonreciprocal phase shifts—analysis of two ferrite slabs in rectangular waveguide," *J. Appl. Phys.*, vol. 27, pp. 519–524; May, 1956.
[63] H. Scharfman, "Three new ferrite phase shifters," PROC. IRE, vol. 44, pp. 1456–1459; October, 1956.
[64] H. N. Chait and N. C. Sakiotis, "The design of nonreciprocal phase shift sections," 1956 IRE CONVENTION RECORD, Part 5, pp. 58–65.
[65] R. F. Sookov, "Ferrite microwave phase shifters," 1956 IRE CONVENTION RECORD, Part 5, pp. 84–98.

Filters

The insertion of a ferrite post into a resonant cavity permits electrical tuning over a considerable bandwidth. The basic theory of a ferrite post in a section of waveguide has been analyzed in general terms and applied to this problem.

[66] P. S. Epstein and A. D. Berk, "Ferrite post in a rectangular waveguide," *J. Appl. Phys.*, vol. 27, pp. 1328–1334; November, 1956.

Several specific filter designs and their capabilities have been described during the year. These are evidently the forerunners of a family of devices for electrical frequency control over the entire microwave spectrum.

[67] C. E. Fay, "Ferrite-tuned resonant cavities," PROC. IRE, vol. 44, pp. 1446–1448; October, 1956.
[68] C. E. Nelson, "Ferrite-tunable microwave cavities and the introduction of a new reflectionless, tunable microwave filter," PROC. IRE, vol. 44, pp. 1449–1455; October, 1956.
[69] James H. Burgess, "Ferrite-tunable filter for use in S-band," PROC. IRE, vol. 44, pp. 1460–1462; October, 1956.

After reviewing the ferrite contributions in the various areas of development, it appears that not only new elements are being created: operations which have been successfully performed by linear elements are being accomplished with ferrites to considerable advantage. It may not be too extravagant a prediction to state that within a few years most microwave circuit elements will rely on ferrites in one way or another.

II. WAVEGUIDES

The bandwidth and attenuation requirements for waveguides are becoming increasingly severe. As a result, strong effects are underway to improve the performance of TEM lines, whose bandwidth is inherently greater than that of hollow guides. Where allowable transmission loss does not permit the use of such lines, extremely high frequencies and precise mode control must be relied on to produce adequate bandwidth and attenuation characteristics. The trend to broad-band systems increases the importance of filters, transformers, and other elements suitable for separating and controlling various portions of the spectrum being transmitted. Most of the published work on waveguides is concerned with these aspects of the field.

TEM Lines

As in previous years, various types of strip or planar lines are being developed as compact broad-band transmission systems. Refinements in characteristic impedance determination are the principal contribution being made.

[70] R. H. Bates, "The characteristic impedance of the shielded slab line," IRE TRANS., vol. MTT-4, pp. 28–33; January, 1956.
[71] R. M. Chisholm, "The characteristic impedance of trough and slab lines," IRE TRANS., vol. MTT-4, pp. 166–172; July, 1956.
[72] J. M. C. Dukes, "An investigation into some fundamental properties of strip transmission lines with the aid of an electrolytic tank," *Proc. IEE*, vol. 103, Part B, pp. 319–333; May, 1956.

An important application of TEM lines is coupling to various types of radiators. Here, a better understanding of both strip and coaxial line coupling has been achieved.

[73] A. D. Frost, C. R. McGeoch, and C. R. Mingins, "The excitation of surface waveguides and radiating slots by strip-circuit transmission lines," IRE TRANS., vol. MTT-4, pp. 218–223; October, 1956.
[74] R. E. Collin, "The characteristic impedance of a slotted coaxial line," IRE TRANS., vol. MTT-4, pp. 4–8; January, 1956.

Tapered TEM lines have long served as transformers. This subject, which received considerable attention in 1955, has been examined further. As a result, the various Fourier and Tchebycheff formulations have been brought more clearly into focus, and several useful, practical formulas and charts have been published.

[75] R. W. Klopfenstein, "A transmission line taper of improved design," PROC. IRE, vol. 44, pp. 31–35; January, 1956.
[76] R. E. Collin, "The optimum tapered transmission line matching section," PROC. IRE, vol. 44, pp. 539–548; April, 1956. (Also p. 1055; August, 1956.)
[77] J. Willis and N. K. Sinha, "Non-uniform transmission lines as impedance transformers," *Proc. IEE*, vol. 103, Part B, pp. 166–172; March, 1956.
[78] J. Willis and N. K. Sinha, "Impedance transformers," *Wireless Eng.*, vol. 33, pp. 204–208; September, 1956.
[79] E. F. Bolinder, "Fourier transforms and tapered transmission lines," PROC. IRE, vol. 44, p. 557; April, 1956.

Hollow Waveguides

The TE_{01} circular mode provides minimum theoretical attenuation in hollow pipes. To achieve this, an ingenious helical guide has been developed: by replacing the cylindrical conductor of a circular waveguide with a helical coil of fine wire, only circular components of current can be supported. Consequently, only the TE_{0n} type modes are sustained by the guide. Other modes penetrate the guide wall and are absorbed by a lossy outer coating.

[80] S. P. Morgan and J. A. Young, "Helix waveguide," *Bell Sys. Tech. J.*, vol. 35, pp. 1347–1385; November, 1956.

The problem of unwanted mode control in large guides is being attacked very effectively. By making the guide lossy for undesired modes, their amplitudes

are kept low; the interaction with the transmission mode is thereby reduced. Conversion to other modes occurs primarily in bends and discontinuities, hence particular attention must be concentrated here.

[81] A. P. King and E. A. Marcutili, "Transmission loss due to resonance of converted modes," *Bell Sys. Tech. J.*, vol. 35, pp. 899–906; July, 1956.

Techniques for evaluating the performance of low-loss guide are now highly refined. The use of very short pulses for transmission is particularly effective.

[82] A. P. King, "Observed 5–6 mm. attenuation for the circular electric wave in small and medium-sized pipes," *Bell Sys. Tech. J.*, vol. 35, pp. 1115–1128; September, 1956.
[83] A. Sander, "The excitation and propagation of E_{0n} modes in a circular waveguide with coaxial lines at input and output," *Arch. Elekt. Übertragung*, vol. 10, pp. 77–85; March, 1956.
[84] W. Schaffeld and H. Bayer, "Propagation of electromagnetic waves in circular waveguides with finite wall conductivity at frequencies near cut-off," *Arch. Elekt. Übertragung*, vol. 10, pp. 89–97; March, 1956.
[85] A. S. Beck, "Waveguide investigations with millimicrosecond pulses," *Bell Sys. Tech. J.*, vol. 35, pp. 35–66; January, 1956.
[86] O. E. DeLange, "Experiments on the regeneration of binary microwave pulses," *Bell Sys. Tech. J.*, vol. 35, pp. 67–90; January, 1956.

Several extensions of existing theory on circular guides complete the contributions noted on hollow waveguides.

[87] A. D. Berk, "Variational principles for electromagnetic resonators and waveguides," IRE Trans., vol. AP-4, pp. 104–111; April, 1956.
[88] M. Handelsman, "The susceptance of a circular iris to the dominant TE_{11} mode in circular waveguide," 1956 IRE Convention Record, Part 5, pp. 133–140.

Surface Waves and Periodic Structures

Various structures have been used as surface waveguides. Perhaps the simplest of these is the dielectric-coated wire. Coupling phenomenon for lines of this type have been studied.

[89] D. Marcuse, "Investigation of the energy exchange and the field distribution for parallel surface-wave transmission lines," *Arch. Elekt. Übertragung*, vol. 10, pp. 117–124; March, 1956.

A method for confining a wave between two strips with the aid of a small dielectric spacer has been described. The resulting structure has a cross section resembling the letter H, and offers very low attenuation for loosely-bound waves.

[90] F. J. Tischer, "H-guide—a waveguide for microwaves," 1956 IRE Convention Record, Part 5, pp. 44–47.

The use of periodic structures as waveguides continues to grow. The most generally useful of these is the helix. Several papers extend the theoretical treatment of this structure so common in traveling-wave tubes.

[91] N. N. Smirnov, "Propagation of waves along an infinitely long helix," *Compt. Rend. Acad. Sci. U.R.S.S.*, vol. 108, pp. 243–246; May 11, 1956.
[92] S. Kh. Kogan, "Theory of helical lines," *Compt. Rend. Acad. Sci. U.R.S.S.*, vol. 107, pp. 541–544; April, 1956.
[93] C. P. Allen and G. M. Clarke, "Interpretation of wavelength measurements on tape helices," *Proc. IEE*, vol. 103, Part C, pp. 171–176; March, 1956.

When used to support the inner conductor of coaxial cables, the helix appears in a different role. The physical conditions needed to provide good support with a dielectric helix result in well defined stop bands at higher frequencies.

[94] J. W. E. Griemsmann, "An approximate analysis of coaxial line with helical dielectric support," IRE Trans., vol. MTT-4, pp. 13–23; January, 1956.

Diaphragms or irises in tubes provide another common method of obtaining relatively slow guided waves. Theoretical work continues here, with emphasis on formulating a more exact analysis for lossy structures and on representation for measurements.

[95] E. G. Solov'ev, "Propagation of electromagnetic waves between two circular cylindrical surfaces in the presence of longitudinal, periodically spaced diaphragms," *Radiotekhnika Moscow*, vol. 11, pp. 57–60; January, 1956.
[96] P. N. Butcher, "A new treatment of lossy periodic waveguides," *Proc. IEE*, vol. 103, Part B, pp. 301–306; May, 1956.
[97] R. L. Kyhl, "The use of non-Euclidean geometry in measurements of periodically loaded transmission lines," IRE Trans., vol. MTT-4, pp. 111–115; April, 1956.

The use of current sheets to provide slow guided waves has also been proposed.

[98] F. Bertein and W. Chahid, "Production of slow electromagnetic waves by means of cylindrical current sheets," *Compt. Rend. Acad. Sci. Paris*, vol. 242, pp. 2918–2920; June 18, 1956.

The launching of surface waves over corrugated or dielectric coated surfaces is being accomplished with surprising efficiency with dipole radiators. Calculations based on Sommerfeld's integrals and comparative measurements on smooth and reactive surfaces confirm efficiencies up to 80 per cent for the radially symmetric surface wave.

[99] W. M. G. Fernando and H. E. M. Barlow, "An investigation of the properties of radial cylindrical surface waves launched over flat reactive surfaces," *Proc. IEE*, vol. 103, Part B, pp. 307–318; May, 1956.

The theoretical treatment of propagation in periodic structures is facilitated by considering an infinite medium. A number of interesting periodic structures can then be studied with a view to obtaining a quantitative understanding of their propagation characteristics.

[100] R. I. Primich, "A semi-infinite array of parallel metallic plates of finite thickness for microwave systems," IRE Trans., vol. MTT-4, pp. 156–166; July, 1956.
[101] Z. A. Kaprielian, "Electromagnetic transmission characteristics of a lattice of infinitely long conducting cylinders," *J. Appl. Phys.*, vol. 27, pp. 1491–1502; December, 1956.
[102] H. T. Ward, W. D. Puro, and D. M. Bowie, "Artificial dielectrics utilizing cylindrical and spherical voids," Proc. IRE, vol. 44, pp. 171–175; February, 1956.
[103] I. Kay and H. E. Moses, "Reflectionless transmission dielectrics and scattering potentials," *J. Appl. Phys.*, vol. 27, pp. 1503–1508; December, 1956.
[104] Ya. N. Fel'd, "Paired systems of infinite linear algebraic equations, linked with infinite periodic structures," *Compt. Rend. Acad. Sci. U.R.S.S.*, vol. 106, pp. 215–218; January, 1956.

Filters

The impact of Striplines on microwave filter design has been very significant. The possibilities of filters using multiple combinations of Stripline elements are surprisingly great. In addition to providing flexible filter elements, the Stripline components are easily designed and built. Several papers have dealt rather extensively with this subject; practical designs as well as the theory are tabulated and discussed.

[105] S. B. Cohn and F. S. Coale, "Directional channel-separation filters," Proc. IRE, vol. 44, pp. 1018–1024; August, 1956.
[106] E. H. Bradley, "Design and development of stripline filters," IRE Trans., vol. MTT-4, pp. 86–93; April, 1956.

Waveguide filters are the subject of a number of papers. Several new ideas have been advanced, including the use of circular polarization and symmetry to increase power capability and efficiency at constant input resistance.

[107] R. W. Klopfenstein and J. Epstein, "The polarguide—a constant resistance waveguide filter," PROC. IRE, vol. 44, pp. 210–218; February, 1956.
[108] E. M. T. Jones, "Synthesis of wide-band microwave filters to have prescribed insertion loss," 1956 IRE CONVENTION RECORD, Part 5, pp. 119–128.
[109] P. A. Rizzi, "Microwave filters utilizing the cut-off effect," IRE TRANS., vol. MTT-4, pp. 36–40; January, 1956.
[110] M. H. N. Potok, "Waveguide filters," *Wireless Eng.*, vol. 33, pp. 79–82; April, 1956.
[111] G. Craven and L. Lewin, "Design of microwave filters with quarter-wave couplings," *Proc. IEE*, vol. 103, Part B, pp. 173–177; March, 1956.

Two new tunable filters have been described. One of these uses two crossed modes in a square-cylinder resonator. A double tuned response is thereby obtained with only a single resonator. The second device is electrically tunable over a 10:1 frequency range starting at 600 mc. The paramagnetic resonance of hydrazyl provides the tuning element.

[112] N. A. Spencer, "Crossed-mode tunable selector for microwaves," 1956 IRE CONVENTION RECORD, Part 5, pp. 129–132.
[113] P. H. Vartanian and J. L. Melchor, "Broad-band microwave frequency meter," PROC. IRE, vol. 44, pp. 175–178; February, 1956.

A microwave filter has been developed which relies on a traveling-wave resonance rather than the conventional standing wave. A closed transmission line loop supports the traveling wave. Two directional couplers provide coupling to four output terminal pairs. The device is a constant resistance circuit with very low input standing-wave ratio. The traveling-wave filter seems particularly well-suited to multiplexing applications because of its terminal arrangement and low reflection.

[114] F. S. Coale, "A traveling-wave directional filter," IRE TRANS., vol. MTT-4, pp. 256–260; October, 1956.

Directional Couplers and Junctions

Directional couplers are easily realized in Striplines. Because of the simple structures involved, tuned elements can be combined easily with directional coupling to yield a variety of useful response patterns.

[115] E. M. T. Jones and J. T. Bolljahn, "Coupled-strip-transmission-line filters and directional couplers," IRE TRANS., vol. MTT-4, pp. 75–81; April, 1956.

Lumped-element couplers for lower frequencies have been reviewed and new data provided.

[116] P. Lombardini, R. F. Schwartz, and P. J. Kelly, "Criteria for the design of loop-type directional couplers for the L band," IRE TRANS. vol. MTT-4, pp. 234–239; October, 1956.

The recently developed finline circuits offer interesting possibilities in a variety of functions. Directional couplers, twists, bends, and hybrid junctions have been described for use with hollow waveguide carrying one or several modes.

[117] S. D. Robertson, "Recent advances in finline circuits," IRE TRANS., vol. MTT-4, pp. 263–267; October, 1956.

Several papers have appeared on waveguide junctions and the systematic representation of their properties.

[118] R. S. Potter, "A trimode turnstile waveguide junction," 1956 IRE CONVENTION RECORD, Part 5, pp. 36–43.
[119] J. A. Ortusi, "The amplitude concept of an electromagnetic wave and its application to junction problems in waveguides," IRE TRANS. vol. AP-4, pp. 156–162; April, 1956.
[120] P. A. Loth, "Recent advances in waveguide hybrid junctions," IRE TRANS., vol. MTT-4, pp. 268–271; October, 1956.
[121] J. Reed and G. J. Wheeler, "A method of analysis of symmetrical four-port networks," IRE TRANS., vol. MTT-4, pp. 246–252; October, 1956.

From the point of view of fabrication, waveguide junctions are often clumsy and space-consuming. An interesting scheme of construction has been proposed in which guides are arranged in a single plane with adjacent walls common. Considerable simplification in construction results from this arrangement.

[122] L. Lewin, "Miniaturization of microwave assemblies," IRE TRANS., vol. MTT-4, pp. 261–262; October, 1956.

A variety of articles on transitions and joints have appeared during the year. One of the most interesting of these is an annular rotary joint with coupling through an array of slots forming an extended directional coupler between two waveguide rings.

[123] K. Tomiyasu, "A new annular waveguide rotary joint," PROC. IRE, vol. 44, pp. 548–553; April, 1956.

A somewhat related device is the serrated choke proposed by the same author for broad-band applications.

[124] K. Tomiyasu and J. J. Bolus, "Characteristics of a new serrated choke," IRE TRANS., vol. MTT-4, pp. 33–36; January, 1956.

Another ingenious device is a high-speed phase shifter utilizing circular polarization and rotating helical coupling units.

[125] W. Sichak and D. J. Levine, "Microwave high-speed continuous phase shifter," *Elec. Communication*, vol. 33, pp. 224–227; September, 1956.

Several transitions and a switching tee complete the circuit elements noted in this review.

[126] R. D. Tompkins, "A broad-band dual-mode circular waveguide transducer," IRE TRANS., vol. MTT-4, pp. 181–183; July, 1956.
[127] F. Mayer, "Transitions from the TE_{01} mode in a rectangular waveguide to the TE_{11} mode in a circular waveguide," *J. Phys. Radium*, vol. 17, Suppl. 3 Phys. Appl., pp. 52A-53A; March, 1956.
[128] R. L. Fogel, "An orthogonal mode transducer," 1956 IRE CONVENTION RECORD, Part 5, pp. 53–57.
[129] J. W. E. Griemsmann and S. S. Kasai, "Broad-band waveguide series T for switching," IRE TRANS., vol. MTT-4, pp. 252–255; October, 1956.

As can be seen from the papers listed, the designers of waveguides and linear circuit elements have been both active and ingenious during 1956.

III. MEASUREMENTS

Progress in measurements for the most part reflects a continuing refinement and extension of proven techniques. However, some basically new approaches have appeared during the year, both in technique and representation. The impact of advances in solid-state physics are now beginning to be felt in the measurements field; in future years, this influence will undoubtedly grow.

Impedance Measurements

The techniques of impedance measurements rest on long-established foundations. As can be seen from their titles, the papers in this field belong largely in the category of reports on refinements and extensions of the art.

[130] A. C. MacPherson and D. M. Kerns, "A new technique for the measurement of microwave standing wave ratios," PROC. IRE, vol. 44, pp. 1024–1030; August, 1956.
[131] E. E. Conrad, C. S. Porter, N. J. Doctor, and P. J. Franklin, "Extension of the 'thin-sample method' for measurement of initial complex permeability and permittivity," *J. Appl. Phys.*, vol. 27, pp. 346–350; April, 1956.
[132] H. L. Bachman, "Automatic plotter for waveguide impedance," *Electronics*, vol. 29, pp. 184–187; March, 1956.
[133] J. P. Vinding, "The Z-Scope, an automatic impedance plotter," 1956 IRE CONVENTION RECORD, Part 5, pp. 178–183.
[134] W. R. Thurston, "A transadmittance meter for vhf-uhf measurements," 1956 IRE CONVENTION RECORD, Part 5, pp. 3–7.
[135] M. M. Zimet and S. Friedman, "Measurement of electron tube admittance matrix parameters at ultra high frequencies," 1956 IRE CONVENTION RECORD, Part 5, pp. 8–14.
[136] C. Polk, "Standing-wave ratio of inaccessible load," *Comm. and Elect.*, No. 23, pp. 9–11; March, 1956.
[137] D. M. Bowie and K. S. Kelleher, "Rapid measurement of dielectric constant and loss tangent," IRE TRANS., vol. MTT-4, pp. 137–140; July, 1956.

Power Measurement

In the domain of power measurement, the Hall effect has been put to use for microwave power measurement. By mounting *n*-type germanium in a slot-excited cavity, sufficient magnetic field at 4000 mc was obtained to give about 5 μv/watt Hall output. The resulting directional wattmeter offers great promise as a sensitive power indicator.

[138] H. E. M. Barlow and L. M. Stephenson, "The Hall effect and its application to power measurement at microwave frequencies," *Proc. IEE*, vol. 103, Part B, pp. 110–112; January, 1956. (Also Monograph No. 191R, August, 1956.)

Two other wattmeters of novel design have also been described.

[139] R. A. Bailey "A resonant cavity torque-operated wattmeter for microwave power," *Proc. IEE*, vol. 103, Part C, pp. 59–63; March, 1956.
[140] J. A. Lane, "A film radiometer for centimetre wavelengths," *Nature*, Lond., vol. 177, p. 392; February 25, 1956.

Four-Pole Methods

Determination of the properties of a four-pole can be achieved by several elegant methods. The mathematical representation of four poles is particularly important to the measuring procedure, and hence is included at this point in the review. One of the most interesting advances in this area has been a proposed representation for nonreciprocal two-ports. A modified Wheeler form is used in which the nonreciprocal properties appear in two bilaterally matched elements: a one-way phase-shifter and a one-way attenuator.

[141] H. M. Altschuler and W. K. Kahn, "Nonreciprocal two-ports represented by modified Wheeler networks," IRE TRANS., vol. MTT-4, pp. 228–233; October, 1956.

Graphical representations of four-poles by various formalisms have been extended by a number of investigators.

[142] F. L. Wentworth and D. R. Barthel, "A simplified calibration of two-port transmission line devices," IRE TRANS., vol. MTT-4, pp. 173–175; July, 1956.
[143] H. F. Mathis, "Some properties of image circles," IRE TRANS., vol. MTT-4, pp. 48–50; January, 1956.
[144] E. F. Bolinder, "Impedance and polarization ratio transformations by a graphical method using isometric circles," IRE TRANS., vol. MTT-4, pp. 176–180; July, 1956.
[145] H. Schering, "The mean geometrical distances of a circle," *Elektrotech. Z.*, Edn. A, vol. 77, pp. 12–13, January, 1956.

Resonators and Related Measurements

Cavity resonators are an important tool for many microwave measurements. Perhaps the most direct application of cavity techniques is in the measurement of dielectric and magnetic properties of materials. Several papers have appeared describing improvements and extensions of these techniques to new materials and geometries.

[146] S. Saito and K. Kurokawa, "A precision resonance method for measuring dielectric properties of low-loss solid materials in the microwave region," PROC. IRE, vol. 44, pp. 35–42; January, 1956.
[147] R. A. Waldron, "Ferrites in resonant cavities," *Brit. J. Appl. Phys.*, vol. 7, p. 114; March, 1956.
[148] V. L. Patrushev, "Calculation of the natural frequency for a single reentrant cavity partly filled with an absorbing dielectric," *Compt. Rend. Acad. Sci. U.R.S.S.*, vol. 107, pp. 409–412; March 21, 1956.
[149] J. G. Linhart, I. M. Templeton, and R. Dunsmuir, "A microwave resonant cavity method for measuring the resistivity of semi-conducting materials," *Brit. J. Appl. Phys.*, vol. 7, pp. 36–38; January, 1956.
[150] F. Gross, "Temperature dependence of loss angle and dielectric constant of solid insulating materials in the 4 kmc/s range," *Nachrichtentech. Z.*, vol. 9, pp. 124–128; March, 1956.
[151] R. Servant and J. Gougeon, "Birefringence and rectilinear dichroism of paper at 9350 mc/s," *Compt. Rend. Acad. Sci. Paris*, vol. 242, pp. 2318–2320; May 7, 1956.
[152] I. Bady, "Measurement of the complex dielectric constant of materials from 100 to 1200 mc over a wide range of temperature," 1956 IRE CONVENTION RECORD, Part 5, pp. 172–177.

The cavity itself remains an object of interest for several investigators.

[153] G. Boudouris, "Spherical-frustrum cavities," *Ondé Elect.*, vol 36, pp. 104–121; February, 1956.
[154] H. Urbarz, "Measurement of the Q-factor of cavity resonators using a straight test line," *Nachrichtentech. Z.*, vol. 9, pp. 112–118; March, 1956.
[155] U. Adelsberger, "The rod wavemeter for the frequency range 180–80,000 mc/s—construction and measurement results," *Arch. Elect. Übertragung*, vol. 10, pp. 51–57; February, 1956.
[156] J. R. G. Twisleton, "An X-band magnetron Q-measuring apparatus," *Proc. IEE*, vol. 103, Part B, pp. 339–342; May, 1956.
[157] E. O. Bowers and C. W. Curtis, "A resonant cavity frequency duplexer," 1956 IRE CONVENTION RECORD, Part 5, pp. 113–118.
[158] C. Colani, "A simple microwave discriminator," *Frequenz*, vol. 10, pp. 25–26; January, 1956.
[159] D. W. Fraser and E. G. Holmes, "Frequency control in the 300–1200 mc region," PROC. IRE, vol. 44, pp. 1531–1541; November, 1956.

Optical techniques occupy a definite place at the upper end of the microwave spectrum. Two papers of particular interest on spectroscopic methods complete the measurements portion of this review.

[160] C. A. Burrus and W. Gordy, "Millimeter and submillimeter wave spectroscopy," *Phys. Rev.*, vol. 101, pp. 599–602; January 15, 1956.
[161] P. H. Sollom and J. Brown, "A centimetre-wave parallel-plate spectrometer," *Proc. IEE*, vol. 103, Part B, pp. 419–428; May, 1956.

IV. Sources and Detectors

The available sources and detectors determine the usable microwave spectrum. Of these, the former constitute the principal limitation today. Both traveling-wave devices, and more conventional klystrons, and magnetrons are being actively improved. In recent years, the primary effort has been concentrated on traveling-wave tubes of various types. This trend is continuing, both in improving existing types, and in the development of new principles of operation.

Much original work is also underway in gas discharges and related problems in physical electronics with microwave applications. These include both oscillators and noise sources. The crystal diode remains preeminent in the detector field, but some potential competition may be in sight.

Traveling-Wave Devices

The characteristics of transverse current traveling-wave tubes have been studied both theoretically and experimentally. The most unusual feature of this type of tube is its large signal behavior: output independent of input level over a 20–30 db range has been attained. This is attributed to the presence of many individual beam elements along the axis of the helix. Saturation for different power levels occurs at different positions along the helix. However, the particular beam element which saturates is immaterial to the output of the entire tube. Hence, a uniform limiting action over a wide range is achieved.

[162] D. A. Dunn, W. A. Harman, L. M. Field, and G. S. Kino, "Theory of the transverse-current traveling-wave tube," Proc. IRE, vol. 44, pp. 879–887; July, 1956.
[163] D. A. Dunn and W. A. Harman, " An experimental transverse-current traveling-wave tube," Proc. IRE, vol. 44, pp. 888–896; July, 1956.

A different transverse type tube has been developed with novel focusing elements. Two flat helices confine an electron sheet between them. The helix elements are bifilar, and provide a steady periodic focusing field. The resulting tube appears well suited to low-noise amplification in the uhf region.

[164] R. Adler, O. M. Kromhout, and P. A. Clavier, "Transverse-field traveling-wave tubes with periodic electrostatic focusing," Proc. IRE, vol. 44, pp. 82–89; January, 1956.

The Carcinotron continues in the forefront of microwave oscillators, as evidenced by the continuing studies on this configuration.

[165] P. Palluel and A. K. Goldberger, "The O-type carcinotron tube," Proc. IRE, vol. 44, pp. 333–345; March, 1956.
[166] P. Palluel, "Recent developments of O-type carcinotrons," *Ondé Elect.*, vol. 36, pp. 318–335; April, 1956.
[167] A. Bobenrieth and O. Cahen, "Travelling-wave valves for 4-cm waves: Research and development at the Centre National d'Etudes des Telecommunications," *Ondé Elect.*, vol. 36, pp. 307–317; April, 1956.

High power developments are also recorded.

[168] W. W. Siekanowicz and F. Sterzer, "A developmental wide-band, 100-watt, 20 db S-band traveling-wave amplifier utilizing periodic permanent magnets," Proc. IRE, vol. 44, pp. 55–61; January, 1956.
[169] M. Chodorow and E. J. Nalor, "The design of high-power traveling-wave tubes," Proc. IRE, vol. 44, pp. 649–659; May, 1956.
[170] J. P. Laico, H. L. McDowell, and C. R. Moster, "A medium power traveling-wave tube for 6000 mc radio relay," *Bell Sys. Tech. J.*, vol. 35, pp. 1285–1346; November, 1956.

A few circuit applications of traveling-wave tubes should also be mentioned.

[171] P. D. Lacy, "Microwave spectrum synthesis with the traveling-wave tube," 1956 IRE Convention Record, Part 5, pp. 48–52.
[172] N. Sawazaki and T. Honma, "New microwave repeater system using traveling-wave tubes," Proc. IRE, vol. 44, pp. 19–24; January, 1956.

Klystrons and Magnetrons

The klystron has been the object of several investigations.

[173] I. L. Bershtein, "Fluctuation of oscillations of a klystron generator," *Compt. Rend. Acad. Sci. U.R.S.S.*, vol. 106, pp. 453–456; January, 1956.
[174] R. L. Bell and M. Hillier, "An 8-mm klystron power oscillator," Proc. IRE, vol. 44, pp. 1155–1159; September, 1956.
[175] J. R. M. Vaughan, "Klystron modulators and Schlömilch series," *J. Electronics*, vol. 1, pp. 430–438; January, 1956.
[176] J. I. Davis, "Technique of pulsing low power reflex klystrons," IRE Trans., vol. MTT-4, pp. 40–47; January, 1956.
[177] Y. Matsuo, "Multi-beam velocity-type frequency multiplier," Proc. IRE, vol. 44, pp. 101–106; January, 1956.

Two papers of particular interest have appeared on circuit applications of klystrons and magnetrons. One deals with the use of precision quench frequencies to produce a series of standard frequencies from a klystron. The other presents a simplified theory of the long-lines effect in magnetrons.

[178] N. Sawazaki and T. Honma, "A new microwave frequency standard by quenching oscillator control," IRE Trans., vol. MTT-4, pp. 116–121; April, 1956.
[179] W. L. Pritchard, "Long-line effect and pulsed magnetrons," IRE Trans., vol. MTT-4, pp. 97–110; April, 1956.

Other Electronic Sources

Plasma oscillations are an interesting potential source of microwaves. The immediate prospects for practical generators are dim. However, investigation continues actively, and all avenues have not yet been fully explored.

[180] M. A. Lampert, "Plasma oscillations at extremely high frequencies," *J. Appl. Phys.*, vol. 27, pp. 5–11; January, 1956.
[181] F. Diamand, A. Gozzini, and T. Kahon, "Interaction of centimeter waves with a plasma in the presence of magnetic field," *Compt. Rend. Acad. Sci. Paris.*, vol. 242, pp. 90–93; January, 1956.
[182] D. Gabor, "Plasma oscillations," IRE Trans. vol. AP-4, pp. 526–530; July, 1956.
[183] J. Corte and J. L. Delcroix, "Plasma oscillations and resonance frequencies in a magnetron in the Brillouin state," *Compt. Rend. Acad. Sci. Paris*, vol. 242, pp. 57–90; January 4, 1956.

Cerenkov radiation is another potential source of millimeter waves which is under study.

[184] H. Lashinsky, "Cerenkov radiation from extended electron beams near a medium of complex index of refraction," *J. Appl. Phys.*, vol. 27, pp. 631–635; June, 1956.
[185] M. A. Lampert, "Incidence of an electromagnetic wave on a 'Cerenkov electron gas,' " *Phys. Rev.*, vol. 102, pp. 299–304; April 15, 1956.

Gas discharges have long been used as noise sources and switches and considerable effort is noted in this area.

[186] R. I. Skinner, "Wide-band noise sources using cylindrical gas-discharge tubes in two-conductor lines," *Proc. IEE*, vol. 103, Part B, pp. 491–495; July, 1956.
[187] G. K. Hart, F. R. Stevenson, and M. S. Tanenbaum, "High-power breakdown of microwave structures," 1956 IRE Convention Record, Part 5, pp. 199–205.
[188] R. H. Geiger and P. E. Dorney, "Coaxial components employing gaseous discharges at microwave frequencies," 1956 IRE Convention Record, Part 5, pp. 193–198.
[189] G. M. Pateyuk, "Investigation of the high-frequency discharge," *Th. Eksp. Teor. Fiz.*, vol. 30, pp. 12–17; January, 1956.

Even the spark serves as an often unwelcome microwave source. Its potential as a useful generator has been studied systematically.

[190] M. H. N. Potok, "Researches into spark generation of microwaves," *Proc. IEE*, vol. 103, Part B, pp. 781–786; November, 1956.

Detection

Noise measurements are basic to receiver development, and continue to be refined.

[191] W. Klein and W. Friz, "The gas-discharge tube as a device for noise measurement in the centimetre wave-band," *J. Electronics*, vol. 1, pp. 589–600; May, 1956.
[192] C. H. Mayer, "Improved microwave noise measurements using ferrites," IRE Trans., vol. MTT-4, pp. 24–28; January, 1956.
[193] E. Maxwell and B. J. Leon, "Absolute measurement of receiver noise figures at uhf," IRE Trans., vol. MTT-4, pp. 81–85; April, 1956.
[194] Peter D. Strum, "A note on noise temperature," IRE Trans., vol. MTT-4, pp. 145–151; July, 1956.
[195] V. A. Hughes, "Absolute calibration of a standard temperature noise source for use with S-band radiometers," *Proc. IEE*, vol. 103, Part B, pp. 669–672; September, 1956.
[196] H. Sutcliffe, "Noise measurements in the 3-cm band using a hot source," *Proc. IEE*, vol. 103, Part B, pp. 673–676; September, 1956.

Several important advances in microwave detectors and receivers have been recorded. First among these is an electron beam device with sensitivity comparable to a crystal and extremely wide bandwidths. This device utilizes the stop-band phenomenon of periodic magnetic focusing to sort the electrons in the beam according to their rf velocity modulation.

[197] J. T. Mendel, "Microwave detector," Proc. IRE, vol. 44, pp. 503–508; April, 1956.

Two superheterodyne systems of unusual capability have been realized. The first utilizes multiple coherent local oscillator signals to cover wide band continuously. Injection of both a microwave and a vhf signal into the mixer produces the desired spectrum.

The second scheme actually synchronizes two swept oscillators to produce a broad-band response with full superheterodyne sensitivity.

[198] M. Cohn and W. C. King, "A sideband-mixing superheterodyne receiver," Proc. IRE, vol. 44, pp. 1595–1599; November, 1956.
[199] D. L. Favin, "A swept, broad band microwave double detection system with automatic synchronization," 1956 IRE Convention Record, Part 5, pp. 184–192.

In the field of crystals, the technique of fabricating and mounting millimeter detector elements has been perfected to the point where performance comparable to that at lower frequencies is achieved.

[200] W. M. Sharpless, "Wafer-type millimeter wave rectifiers," *Bell Sys. Tech. J.*, vol. 35, pp. 1385–1402; November, 1956.

The last reference under detectors, and in the entire review, concerns the effects of microwaves on the human body. Fortunately, the prognosis is generally favorable: at frequencies above 3000 mc, only superficial heating is to be expected, with adequate sensory perception to provide warning. Only at lower frequencies is there danger of damage to tissues from exposure to radiation.

[201] H. P. Schwan and K. Li, "Hazards due to total body irradiation by radar," Proc. IRE, vol. 44, pp. 1572–1581; November, 1956.

Conclusion

The number of papers and their titles give only a poor estimate of the progress made in microwave theory and techniques. More important, the quality of work has been almost uniformly high, insofar as it is possible to determine at this time. The results of future years, built on the achievements of the present, will prove the importance of the advances made during the year 1956.

Acknowledgment

The assistance of Dr. H. Scharfman and Dr. D. Angelakos in providing valuable information, particularly on the London Conference on Ferrites, is gratefully acknowledged.

Coupled Strip Transmission Lines with Rectangular Inner Conductors*

JAMES D. HORGAN†

Summary—A method is presented for determining the capacitance of electrostatic fields which have hitherto proved intractable because their solutions required the evaluation of hyperelliptic integrals. The method is illustrated by applying it to the determination of the characteristic impedance of a strip transmission line. The results compare favorably with the results of existing solutions. The method is then used to determine the characteristic impedance of coupled strip transmission lines with inner conductors of rectangular shape. Curves are included which permit the determination of this impedance over a wide range of line proportions.

Introduction

THE OBJECTIVES of this paper are: 1) to present a method for determining the capacitance of electric fields which have hitherto proved intractable because their solutions, using conformal mapping techniques, required evaluation of hyperelliptic integrals, and 2) through use of this method, to determine the characteristic impedance of the coupled strip lines of Fig. 1. In the method to be described, the field is divided into two or more simpler configurations, and ordinary conformal mapping techniques are used to find potential distributions in each region. These distributions serve to furnish a first approximation to the correct capacitance and also provide the curvilinear coordinate systems necessary for obtaining a second approximation. Second approximations to the correct potential functions are obtained by using the first terms in Fourier series involving the curvilinear coordinates. Parameters associated with these terms are adjusted so that the capacitance obtained is a maximum. As a result, the capacitance and impedance values are correct to within one or two per cent over the range of proportions investigated. The method described can also be applied to determine the permeance of magnetic fields, the conductance of electric current fields, and the conductance of thermal fields with similarly complicated boundary shapes.

In order to present the method clearly, treatment of the coupled strip lines is preceded by application of the method to the simpler case of the strip transmission line of Fig. 2. The capacitance and characteristic impedance of such a line has been accurately determined,[1] and therefore a check on the accuracy of the method is afforded. After this problem has been treated, the method is applied to determine the characteristic impedance of the coupled strip transmission lines.

* Manuscript received by the PGMTT, June 1, 1956.

† Elec. Eng. Dept., Marquette University, Milwaukee, Wis.

[1] N. A. Begovich, "Capacity and characteristic impedance of strip transmission lines with rectangular inner conductors," IRE TRANS., vol. MTT-3, pp. 127–133; March, 1955.

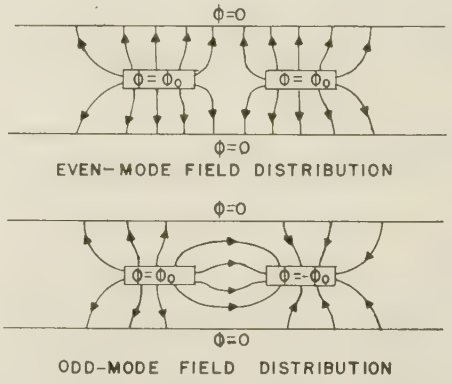

Fig. 1—Field distributions of the even and odd modes in coupled strip line.

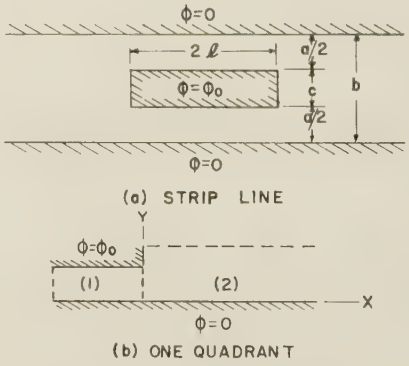

Fig. 2—Strip line configuration.

To determine the capacitance per unit length of the strip transmission line of Fig. 2, an insulating partition is visualized as dividing the quadrant of Fig. 2(b) into the regions 1 and 2. Potential functions are obtained for each region, using conformal transformations as necessary. These functions are the first approximations to the true potential distributions. To obtain the true distributions, an infinite Fourier series could be added in each region, with coefficients evaluated so that all boundary conditions, including those at the surface common to both regions, would be satisfied. However, there are difficulties involved in evaluating these coefficients. Such difficulties may be avoided by seeking a second approximation in which only the first term of the series in each region is retained. The approximation is made to yield an accurate value for the capacitance by: 1) choosing a coordinate system (Fig. 3) in such a way that individual terms in the series exactly satisfy all boundary conditions except those at the matching surface, and 2) determining the coefficients in the series terms in a manner which yields maximum capacitance.

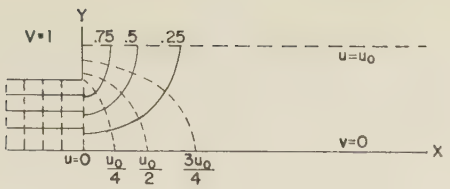

Fig. 3—Strip line coordinate system.

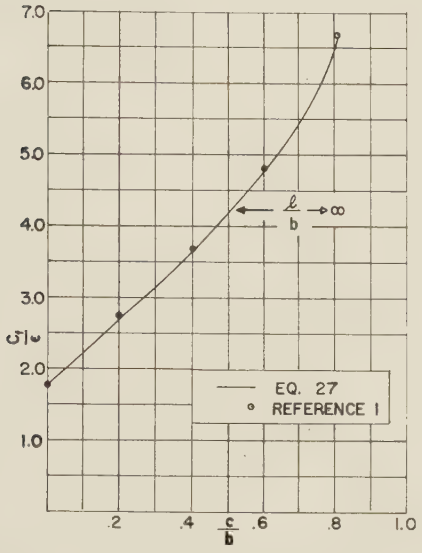

Fig. 4—Fringing capacitance for strip line.

The results of such analysis, shown in Fig. 4 in comparison with the results of Begovich,[1] are accurate to within two per cent of the fringe capacitance. The error, expressed as a percentage of total capacitance, is less than two per cent.

Strip Transmission Line

The problem to be discussed in this section is that of determining the characteristic impedance of the strip transmission line shown in Fig. 2(a). Such a line can propagate a transverse electromagnetic wave (TEM) for which the characteristic impedance, Z_0, is[2]

$$Z_0 = \frac{\sqrt{\mu\epsilon}}{C} = \frac{120\pi}{\sqrt{\epsilon_r}} \cdot \frac{\epsilon}{C}, \tag{1}$$

where ϵ_r is the relative dielectric constant of the material in the space between the electrodes, ϵ is the permittivity, and C is the capacitance per unit length. Thus, the crux of the problem is the determination of the capacitance. The general plan of attack is to determine the potential distribution, the field intensity, the stored energy, and from this, to find the relative capacitance.

In order to determine the potential distribution, an insulating partition is visualized as dividing the field quadrant into the regions 1 and 2 as shown in Fig. 2(b). In region 1 the potential function which satisfies Laplace's equation and the boundary conditions is

$$\phi_1(x, y) = 2y/a, \tag{2}$$

where ϕ_0 in Fig. 2 is taken as unity without loss of generality. In region 2 it is convenient to express the potential in terms of a new system of curvilinear coordinates (u, v), selected so that

$$\phi_2(u, v) = v. \tag{3}$$

Since equipotential surfaces coincide with surfaces of constant value of the coordinate v, the coordinate system (u, v) must be conformally related to the (x, y) system and must satisfy the boundary conditions indicated in Fig. 3 and stated below:

$$\begin{aligned} v &= 0; \quad y = 0; \quad 0 < x \\ v &= 1; \quad x = 0; \quad a/2 < y < b/2 \\ u &= 0; \quad x = 0; \quad 0 < y < a/2 \\ u &= u_0; \quad y = b/2; \quad 0 < x. \end{aligned} \tag{4}$$

The important relations between (x, y) and (u, v) are developed in the appendix, using the Schwarz-Christoffel transformation. It is shown there that

$$u_0 = K(k)/K(k') \tag{5}$$

$$k = \cos(\pi a/2b) \tag{6}$$

$$k' = \sin(\pi a/2b), \tag{7}$$

where $K(k)$ and $K(k')$ are complete elliptic integrals of the first kind. Consideration of the above leads to a first approximation for the capacitance of Fig. 2(a):

$$C/\epsilon = 81/a + 4K(k)/K(k'). \tag{8}$$

To obtain a more accurate solution, the insulating partition is removed and the approximate potential solutions are augmented as follows:

$$\phi_1(x, y) = 2y/a + \sum_{m=1}^{\infty} a_m e^{m2\pi x/a} \sin m2\pi y/a \tag{9}$$

$$\phi_2(u, v) = v + \sum_{n=1}^{\infty} b_n e^{-n\pi u} \sin n\pi v. \tag{10}$$

For simplicity, (9) is written for the case of $1/a$ approaching infinity, although it is easily generalized by including a negative exponential term.

Each individual term in the two series satisfies all boundary conditions except those at the matching surface, $u = 0$. One method of obtaining the exact potential solutions involves evaluating the coefficients a_m and b_n so that both the potential and the normal component of displacement are continuous across the matching surface. The difficulties associated with this method are great, because the series involve trigonometric functions of two different arguments.

Another method, the one to be pursued here, involves determining the coefficients a_m and b_n in such a way that the potential is continuous across the matching surface,

[2] S. Ramo and J. R. Whinnery, "Fields and Waves in Modern Radio," John Wiley and Sons, Inc., New York, N.Y.; 1944.

and the capacitance attains its maximum value.[3] To pursue this method, the capacitance is expressed as

$$C = 2W/\phi_0^2, \tag{11}$$

where W is the total energy stored in the field and ϕ_0 is the total potential difference across the conductors. In turn, W is expressed as

$$W = (\epsilon/2)\int\int\int E^2 dV, \tag{12}$$

where E is the magnitude of the field intensity and V is the volume of the field. Thus, assuming the potential difference as unity, capacitance as a function of potential distributions becomes

$$C/\epsilon = 4\int_0^{a/2}\int_{-1}^{0}[(\partial\phi_1/\partial x)^2 + (\partial\phi_1/\partial y)^2]dxdy + 4\int_0^1\int_0^{u_0}[(\partial\phi_2/\partial u)^2 + (\partial\phi_2/\partial v)^2]dudv. \tag{13}$$

Now if the potentials in (9) and (10) are substituted in (13) the result is, for the case of $1/a$ approaching infinity, the expression relating capacitance to the undetermined coefficients, a_m and b_n.

$$C/\epsilon = 81/a + 4u_0 + 2\pi\sum_m m{a_m}^2 + 2\pi\sum_n (1 - e^{-2n\pi u_0})n{b_n}^2. \tag{14}$$

The maximum value of this capacitance is desired, subject to the condition of continuity of the potential $\phi(0, v)$ at the matching surface as expressed by

$$\phi(0, v) = 2y/a + \sum_m a_m \sin m2\pi y/a = v + \sum_n b_n \sin n\pi v. \tag{15}$$

To introduce the potential $\phi(0, v)$ into the capacitance (14), a_m and b_n are expressed in terms of this potential by multiplying (15) by the appropriate sin function, and integrating. When these results are substituted in (14), capacitance is expressed in terms of the potential at the matching surface:

$$C/\epsilon = 81/a + 4u_0 + 2\pi\sum_m m\left\{(4/a)\int_0^{a/2}[\phi(0, v) - 2y/a]\sin m2\pi y/a\,dy\right\}^2 + 2\pi\sum_n n(1 - e^{-n2\pi u_0})\left\{2\int_0^1[\phi(0, v) - v]\sin n\pi v dv\right\}^2. \tag{16}$$

The specific problem at hand now is this: find the function $\phi(0, v)$ which will result in the maximum value of the capacitance. This can be solved approximately by assuming that the potential at the matching surface can be represented by the first term in either of the series in (15). That is, assume

$$\phi(0, v) \approx 2y/a + a_1 \sin 2\pi y/a \approx v + b_1 \sin v. \tag{17}$$

Then, using (17) and the relation between a_m and $\phi(0, v)$ as obtained from (15), a_1 can be expressed in terms of b_1.

$$a_1 = B_0 + B_1 b_1 \tag{18}$$

$$B_0 = (4/a)\int_0^{a/2}(v - 2y/a)\sin 2\pi y/a\,dy \tag{19}$$

$$B_1 = (4/a)\int_0^{a/2}(\sin \pi v)\sin 2\pi y/a\,dy. \tag{20}$$

As shown in the appendix, along the matching surface, y and v are related as follows:

$$v = 1 - F(\theta', k')/K(k') \tag{21}$$

$$\cos\theta' = (k/k')\tan \pi y/b. \tag{22}$$

In (21), $F(\theta', k')$ is the incomplete elliptic integral of the first kind.

Eqs. (18)–(22) serve to uniquely determine a_1 in terms of b_1. Eqs. (19) and (20) are integrated, using numerical or graphical methods.

It is now possible to express the capacitance in terms of the single parameter, b_1:

$$C/\epsilon = 81/a + 4u_0 + 2\pi[(B_0 + B_1 b_1)^2 + (1 - e^{-2\pi u_0}){b_1}^2]. \tag{23}$$

When this is maximized with respect to b_1, the result is

$$b_1 = \frac{-B_0 B_1}{1 - e^{-2\pi u_0} + {B_1}^2}. \tag{24}$$

If $u_0 \gg 1/2\pi$, this reduces to

$$b_1 = \frac{-B_0}{B_1 + \dfrac{1}{B_1}}. \tag{25}$$

When (24) or (25) is substituted in (23), the capacitance is determined. In order to compare the results of this method with results obtained previously,[1] the capacitance is written in the form

$$C/\epsilon = 81/a + C_f/\epsilon, \tag{26}$$

where C_f is the fringe capacitance, given by

$$C_f/\epsilon = 4u_0 + 2\pi[(B_0 + B_1 b_1)^2 + {b_1}^2]. \tag{27}$$

In Fig. 4, this fringe capacitance is plotted as a function of the ratio c/b for the case of $1/b$ approaching infinity. The results of Begovich[1] are also shown for comparison. A maximum deviation of about two per cent of the fringe capacitance is indicated. It should be noted that this deviation approaches zero as $1/b$ ap-

[3] J. W. S. Rayleigh, "The Theory of Sound," Macmillan and Co., Ltd., London, Eng., vol. 2, p. 175; 1896.

proaches zero. Also, when this deviation is expressed as a percentage of total capacitance, the figure is less than two per cent.

Coupled Strip Line: Odd Mode

In this section, the following problem is taken up: for the coupled strip line operating in the odd mode, determine the characteristic impedance. As indicated in Fig. 1, the odd mode is excited by maintaining the inner conductors at equal and opposite potentials with respect to the parallel ground planes. For transverse electromagnetic (TEM) wave propagation on such a line, the characteristic impedance, measured from one strip to ground, can be determined from (1), if the capacitance is taken as that of one strip to ground. As in the previous example, the crux of the problem is the determination of this capacitance. Because of symmetry, attention can be focused on the problem of determining the capacitance of the quadrant shown in Fig. 5.

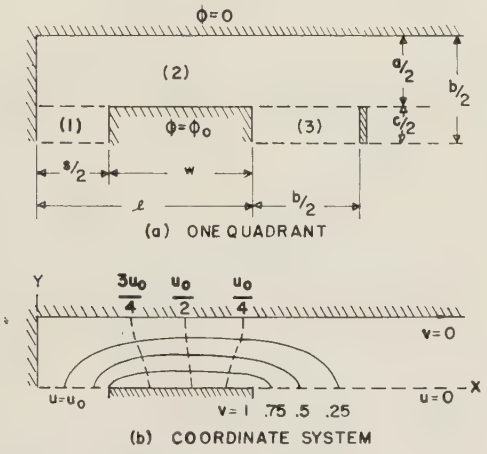

Fig. 5—Quadrant of coupled line in odd mode.

Following the general scheme of the previous section, insulating partitions are assumed to divide the field into the regions marked 1, 2, and 3. In region 1, the potential which satisfies Laplace's equation and the boundary conditions indicated in Fig. 5 is

$$\phi_1(x, y) = 2x/s, \tag{28}$$

where ϕ_0 is taken as unity without loss of generality. In region 2 the solution is

$$\phi_2(u, v) = v, \tag{29}$$

where the coordinate system (u, v) is that sketched in Fig. 5. It is conformally related to the coordinate system (x, y) and satisfies the boundary conditions indicated in Fig. 5. The important relations between (x, y) and (u, v) are developed in the appendix, using the Schwarz-Christoffel transformation. It is shown there that

$$u_0 = 2K(k_0)/K(k_0') \tag{30}$$

$$k_0 = (\tanh \pi w/2a)(\coth \pi(w + s)/2a) \tag{31}$$

$$k_0' = \sqrt{1 - k_0^2}. \tag{32}$$

In region 3 it is impossible to write down a potential solution with the partition in place because the field extends infinitely to the right. Practically, this situation can be remedied by imagining a conducting plate at zero potential to exist at some distance to the right of the conductor as indicated in Fig. 5. In effect, the assumption is made that the energy stored in that portion of region 3 to the right of this conducting plate is negligibly small compared with the energy stored in the entire field. The placement of this plate is somewhat arbitrary. The choice here is a location $b/2$ units to the right of the conductor. Then, in region 3 a suitable potential is

$$\phi_3(x, y) = 1 - 2(x - 1)/b. \tag{33}$$

Corresponding to the above potentials, the first approximation for the capacitance of one strip to ground, operating in the odd mode, is

$$C_0/\epsilon = 4K(k_0)/K(k_0') + 2c/s + 2c/b. \tag{34}$$

To obtain a more accurate solution, the insulating partitions are removed and the approximate solutions for potential are augmented as follows:

$$\phi_1(x, y) = 2x/s + \sum_{m=1}^{\infty} a_m(e^{m2\pi y/s} + e^{-m2\pi c/s}e^{-m2\pi y/s}) \sin m2\pi x/s \tag{35}$$

$$\phi_2(u, v) = v + \sum_{n=1}^{\infty} (b_n e^{-n\pi(u_0-u)} + d_n e^{-n\pi u}) \sin n\pi v \tag{36}$$

$$\phi_3(x, y) = 1 - 2(x - 1)/b + \sum_{p=1}^{\infty} c_p(e^{p2\pi y/b} + e^{-p2\pi c/b}\, e^{-p2\pi y/b}) \sin p2\pi(x - 1)/b. \tag{37}$$

Eq. (37) is valid only for $(x-1)$ less than $b/2$.

By considering energy storage, it is possible to write the equation for capacitance in a form analogous to (13). By substituting the potential equations (35)–(37) in this form, the relation between capacitance and the coefficients a_m, b_n, d_n, and c_p is obtained.

$$C_0/\epsilon = 4K(k_0)/K(k_0') + 2c/s + 2c/b + \pi \sum_{m=1}^{\infty} (1 - e^{-m4\pi c/s}) m a_m^2 + \pi \sum_{p=1}^{\infty} (1 - e^{-p4\pi c/b}) p c_p^2 + \pi \sum_{n=1}^{\infty} (1 - e^{-n2\pi u_0})(n)(b_n^2 + d_n^2). \tag{38}$$

In order to introduce the condition of continuity of potential at the matching surface, these potentials are written in terms of the coefficients:

$$\phi(u_0, v) = 2x/s + \sum_{m=1}^{\infty} (1 + e^{-m2\pi c/s}) a_m \sin m2\pi x/s \approx v + \sum_{n=1}^{\infty} b_n \sin n\pi v \tag{39}$$

$$\phi(0, v) = 1 - 2(x-1)/b + \sum_{p=1}^{\infty} (1 + e^{-p2\pi c/b}) c_p \sin p2\pi(x-1)/b \approx v + \sum_{n=1}^{\infty} d_n \sin nv. \quad (40)$$

In writing (39)–(40) the following assumptions were made:

$$d_n e^{-\pi u_0} \ll b_n \qquad b_n e^{-\pi u_0} \ll d_n. \quad (41)$$

It is now possible to relate capacitance to the potentials at the matching surfaces by determining the Fourier coefficients as functions of these potentials from (39)–(40) and substituting these expressions in (38). As in the previous example, these functions $\phi(u_0, v)$ and $\phi(0, v)$ must then be chosen to result in the maximum value of capacitance. The problem is solved approximately by assuming the form of these potential functions as

$$\phi(u_0, v) = v + b_1 \sin \pi v \approx 2x/s + a_1(1 + e^{-2\pi c/s}) \sin 2\pi x/s$$
$$\phi(0, v) = v + d_1 \sin \pi v \approx 1 - 2(x-1)/b + c_1(1 + e^{-2\pi c/b}) \sin 2\pi(x-1)/b. \quad (42)$$

Using these approximations, a_1 and c_1 can be related to b_1 and d_1:

$$a_1 = B_0 + B_1 b_1 \quad (43)$$

$$c_1 = D_0 + D_1 d_1 \quad (44)$$

$$B_0 = \frac{4}{s(1 + e^{-2\pi c/s})} \int_0^{s/2} (v - 2x/s) \sin 2\pi x/s \, dx \quad (45)$$

$$B_1 = \frac{4}{s(1 + e^{-2\pi c/s})} \int_0^{s/2} (\sin \pi v) \sin 2\pi x/s \, dx \quad (46)$$

$$D_0 = \frac{4}{b(1 + e^{-2\pi c/b})} \cdot \int_0^{b/2} [v - 2(x-1)/b] \sin 2\pi(x-1)/b \, dx \quad (47)$$

$$D_1 = \frac{4}{b(1 + e^{-2\pi c/b})} \int_0^{b/2} (\sin \pi v) \sin 2\pi(x-1)/b \, dx. \quad (48)$$

As shown in the appendix, along the matching surfaces, x and v are implicitly related by the following:

$$v = 1 - F(\theta', k_0')/K(k_0') \quad (49)$$

$$\sin \theta' = (1/k_0')\sqrt{1 - 1/t^2} \quad (50)$$

$$t = (1/k_0) \frac{t' - 1}{t' + 1} \quad (51)$$

$$t' = \frac{1 - k_0}{1 + k_0} \frac{\sinh^2 \pi x/a}{\sinh^2 \pi s/2a}. \quad (52)$$

Eqs. (43)–(52) serve to determine a_1 in terms of b_1 and to determine c_1 in terms of d_1. The integrations in (45)–(48) are carried out using numerical or graphical methods. It is now possible to express the capacitance in terms of the two parameters b_1 and d_1:

$$C_0/\epsilon = 4K(k_0)/K(k_0') + 2c/s + 2c/b + \pi(1 - e^{-4\pi c/s})(B_0 + B_1 b_1)^2 + \pi(1 - e^{-2\pi u_0})(b_1^2 + d_1^2) + \pi(1 - e^{-4\pi c/b})(D_0 + D_1 d_1)^2. \quad (53)$$

When this is maximized with respect to b_1 and then with respect to d_1, the results are

$$b_1 = \frac{-B_0}{B_1 + \dfrac{1 - e^{-2\pi u_0}}{1 - e^{-4\pi c/s}} \dfrac{1}{B_1}} \quad (54)$$

$$d_1 = \frac{-D_0}{D_1 + \dfrac{1 - e^{-2\pi u_0}}{1 - e^{-4\pi c/b}} \dfrac{1}{D_1}}. \quad (55)$$

When the last two equations are substituted in (53), the capacitance is determined. In order to present curves from which capacitance is easily obtained, it is convenient to rewrite (53) as

$$C_0/\epsilon = 4K(k_0)/K(k_0') + 2\Delta C_f'/\epsilon + 2\Delta C_f'_0/\epsilon. \quad (56)$$

In this, k_0 and k_0' are given by (31)–(32) and $\Delta C_f'/\epsilon$ and $\Delta C_{f0}'/\epsilon$, plotted in Figs. 6 and 7, are defined as

$$\Delta C_f'/\epsilon = c/b + (\pi/2)[(1 - e^{-2\pi u_0}) d_1^2 + (1 - e^{-4\pi c/b})(D_0 + D_1 d_1)^2]$$
$$\Delta C_{f0}'/\epsilon = c/s + (\pi/2)[(1 - e^{-2\pi u_0}) b_1^2 + (1 - e^{-4\pi c/s})(B_0 + B_1 b_1)^2]. \quad (57)$$

The notation used above is consistent with that used in Cohn.[4]

The first term in (56) is the capacitance of one strip to ground, operating in the odd mode, when the thickness c is zero. $\Delta C_f'/\epsilon$ is the correction for the additional fringing from the outer end of one conductor to one ground plane. $\Delta C_{f0}'/\epsilon$ is the correction for additional fringing from one half of the inner end of one conductor to the zero potential surface. Fig. 6 is a plot of the fringing capacitance correction for the outer end of the conductor. The correction is practically independent of w as long as w/b is greater than 0.2 and is independent of s as long as s/b is greater than unity. Fig. 7 shows a similar plot for the fringing capacitance correction at the inner end.

Coupled Strip Line: Even Mode

To determine the characteristic impedance for the line operating in the even mode, in which the inner conductors are maintained at equal potentials with

[4] S. B. Cohn, "Shielded coupled-strip transmission line," IRE Trans., vol. MTT-3, pp. 29–38; October, 1955.

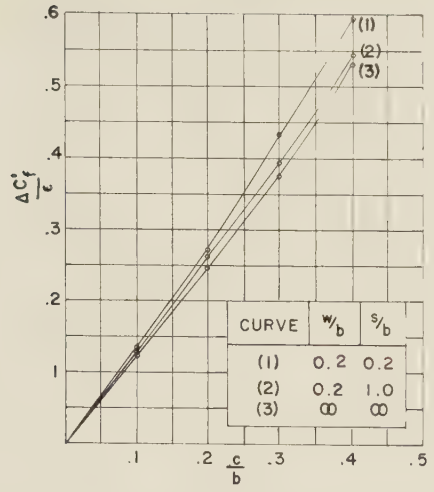

Fig. 6—Correction to outer fringing capacitance.

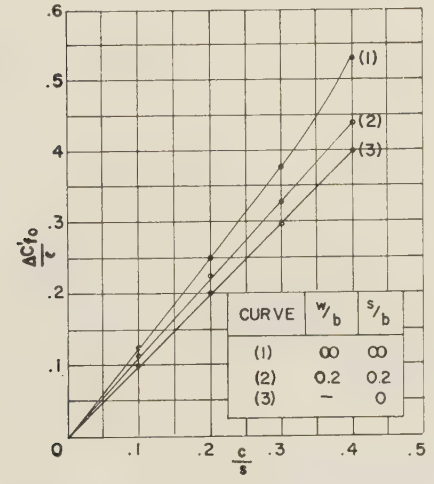

Fig. 7—Correction to inner fringing capacitance.

respect to the ground planes, attention is focused on one quadrant of the field as shown in Fig. 8. Insulating partitions are visualized as dividing the field into three regions as indicated. Following a scheme which parallels that for the odd mode, a first approximation for the capacitance can be written as

$$C_\theta/\epsilon = 4K(k_e)/K(k_e') + 2c/b, \tag{58}$$

where C_e/ϵ is the capacitance of one strip to ground and k_e and k_e' are given by

$$k_e = (\tanh \pi w/2a)(\tanh \pi(w + s)/2a) \tag{59}$$

$$k_e' = \sqrt{1 - k_\theta^2}. \tag{60}$$

With the partitions as shown, no field can exist in region 1 and therefore the corresponding capacitance term is zero.

A second approximation for the potentials can be written as

$$\phi_1(x, y) = v(0, 0) + [1 - v(0, 0)]2x/s \tag{61}$$

$$\phi_2(u, v) = v + \sum_{n=1}^{\infty} d_n(e^{-n\pi u} + e^{-2n\pi u_0}e^{n\pi u}) \sin n\pi v \tag{62}$$

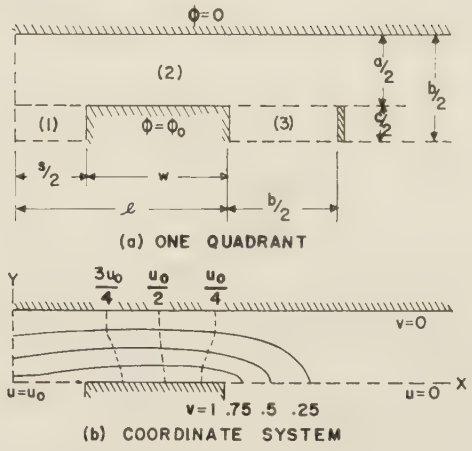

Fig. 8—Quadrant of coupled line in even mode.

$$\phi_3(x, y) = 1 - 2(x - 1)/b + \sum_{p=1}^{\infty} c_p(e^{p2\pi y/b} - e^{-p2\pi y/b}e^{-p2\pi c/b}) \sin p^2\pi(x - 1)/b \tag{63}$$

where $v(0, 0)$ is the value of v for $x = 0$ and $y = 0$. In this case the added series solution is not introduced in $\phi_1(x, y)$ since the relatively weak field in region 1 contributes little to the total capacitance. Following the procedure set out in the preceding section, an expression similar to (56) is obtained:

$$C_e/\epsilon = 4K(k_e)/K(k_e') + 2\Delta C_f'/\epsilon + 2\Delta C_{fe}'/\epsilon. \tag{64}$$

Here, k_e and k_e' are given by (59)–(60), $\Delta C_f'/\epsilon$ is given by Fig. 6 for most practical cases, and $\Delta C_{fe}'/\epsilon$ is defined as

$$\Delta C_{fe}'/\epsilon = [1 - v(0, 0)]^2(c/s). \tag{65}$$

For most proportions, this term is negligible compared with the other terms in the expression for capacitance.

Appendix

Coordinate System: Strip Line

Fig. 9 shows the transformations used in establishing the coordinate system suitable for the strip transmission line of Fig. 2. According to the Schwarz-Christoffel theorem, the variables z and t are related by

$$dz/dt = A_1(t)^{-1/2}(t - 1)^{-1/2}. \tag{66}$$

This can be integrated to give

$$z = (jb/2)[1/2 - (1/\pi) \sin^{-1}(2t - 1)] \tag{67}$$

where the constant of integration has been adjusted to satisfy the boundary condition at $z = 0$. Again, relating w and t by means of the Schwarz-Christoffel method,

$$dw/dt = B_1(t)^{-1/2}(t - 1)^{-1/2}(t - k^2)^{-1/2} \tag{68}$$

which, when integrated, yields

$$w = u_0[1 - F(\theta, k)/K(k)] + j1 \tag{69}$$

$$\sin \theta = \sqrt{t}/k. \tag{70}$$

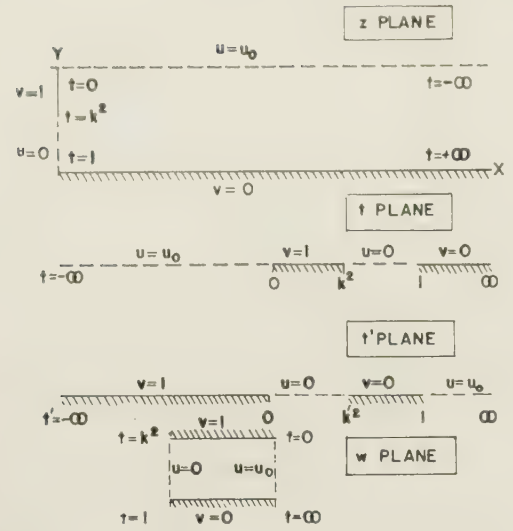

Fig. 9—Transformations for strip line coordinate system.

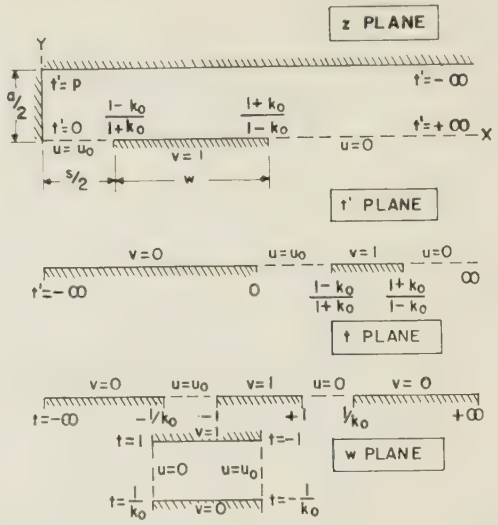

Fig. 10—Transformations for odd mode coordinate system.

Here, $F(\theta, k)$ is the incomplete elliptic integral of the first kind; $K(k)$ is the complete elliptic integral of the first kind. B_1 has been made equal to $-u_0/2K(k)$ in order to satisfy the boundary conditions at $t=0$ and $t=k^2$. Unforuntately, (69) is useful only in the range $0<t<k^2$. To obtain an expression which is useful along the matching surface, $u=0$, the transformation

$$t' = 1 - k^2/t \tag{71}$$

is utilized. Then

$$dw/dt' = (-ju_0/2K(k))(t' - 1)^{-1/2}(t' - k'^2)^{-1/2}(t')^{-1/2} \tag{72}$$

$$k' = \sqrt{1 - k^2}. \tag{73}$$

Eq. (72) can be integrated to give

$$w = j[1 - (u_0)F(\theta', k')/K(k)] \tag{74}$$

$$\sin\theta' = \sqrt{t'}/k'. \tag{75}$$

In order to satisfy the boundary condition at $t'=k^2$,

$$u_0 = K(k)/K(k'), \tag{76}$$

and therefore, along $u=0$,

$$v = 1 - F(\theta', k')/K(k'). \tag{77}$$

In order to relate θ' and k' directly to the z plane, (67), (71), (73), and (75) can be manipulated to give

$$\cos\theta' = (k/k')\tan\pi y/b. \tag{78}$$

Coordinate Systems: Coupled Lines

Fig. 10 shows the transformations used in establishing the coordinate system suitable for the odd mode operation of the coupled strip line shown in Fig. 5. According to the Schwarz-Christoffel transformation, z and t' are related by

$$dz/dt' = A_1(t')^{-1/2}(t' - p)^{-1/2}, \tag{79}$$

which may be integrated to give

$$z = (a/\pi)\ln[\sqrt{t'/-p} + \sqrt{(t'/-p) + 1}]. \tag{80}$$

Along $y=0$, (80) can be manipulated to give the relation between t' and x:

$$t' = \frac{1 - k_0}{1 + k_0}\frac{\sinh^2 \pi x/a}{\sinh^2 \pi s/2a}. \tag{81}$$

Further, by considering the value of t' at $x=s/2$ and at $x=(w+s/2)$, the expression for k_0 can be obtained.

$$k_0 = (\tanh \pi w/2a)(\coth \pi(w + s)/2a). \tag{82}$$

Inspection of Fig. 11 shows that t and t' are related by

$$t = \frac{1}{k_0}\frac{t' - 1}{t' + 1}. \tag{83}$$

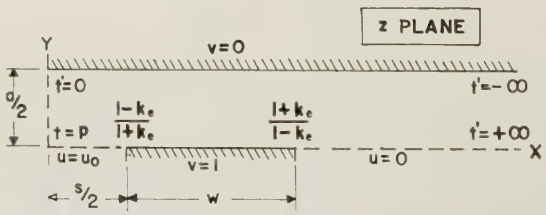

Fig. 11—Transformations for even mode coordinate system.

Now w and t can be related by means of the Schwarz-Christoffel transformation:

$$dw/dt = B_1(t^2 - 1)^{-1/2}(t^2 - 1/k^2)^{-1/2}, \tag{84}$$

which may be ingerated to give

$$w = [K(k_0)/K(k_0')][1 - F(\theta, k_0)/K(k_0)] + j1 \tag{85}$$

$$\sin\theta = t. \tag{86}$$

Eq. (85) is practically useful only in the range $-1<t<1$, that is, along $v=1$. To obtain an expression which is useful along the matching surfaces $u=0$ and $u=u_0$, (85) can be transformed to[5]

[5] P. F. Byrd and M. D. Friedmann, "Handbook of Elliptic Integrals for Engineers and Physicists," Springer Verlag, Berlin, Germany, Art. 115.02; 1954.

$$w = u + j[1 - F(\theta', k_0')/K(k_0')] \quad (87)$$

$$k_0' = \sqrt{1 - k_0^2} \quad (88)$$

$$\sin \theta' = (1/k_0')\sqrt{1 - 1/t^2}. \quad (89)$$

Eqs. (87), (89), (83), and (81) give the implicit relation between x and v along the matching surfaces.

Fig. 11 shows the z plane for the even mode operation of the coupled strip line. From it, it can be seen that the t plane, the t' plane, and the w plane sketches are identical with the odd mode sketches, except for replacing k_0 by k_e. Eqs. (89) and (86) apply, and by analogy with (85),

$$w = [K(k_e)/K(k_e')][1 - F(\theta, k_e)/K(k_e)] + j1. \quad (90)$$

Along $y=0$, by analogy with (87),

$$w = u + j[1 - F(\theta', k_e')/K(k_e')]. \quad (91)$$

Eq. (79) applies to Fig. 11 as well as to Fig. 10. When it is integrated, and boundary conditions are applied, the result is

$$z = (a/\pi) \ln [\sqrt{t'/p} + \sqrt{(t'/p) - 1}]. \quad (92)$$

Along $y=0$ this can be written as

$$t' = \frac{1 - k_e \cosh^2 \pi x/a}{1 + k_e \cosh^2 \pi s/2a}. \quad (93)$$

By considering the value of t' at $x=s/2$ and at $x=(w+s/2)$ the expression for k_e can be obtained:

$$k_e = (\tanh \pi w/2a)(\tanh \pi(w + s)/2a). \quad (94)$$

Eqs. (91), (89), (83), and (93) serve to give the implicit relation between x and v along $y=0$.

ACKNOWLEDGMENT

The author wishes to express his sincere thanks to Prof. T. J. Higgins of the University of Wisconsin for his advice and encouragement during the course of this investigation.

The Impedance of a Wire Grid Parallel to a Dielectric Interface*

JAMES R. WAIT†

Summary—**Analysis is given for the problem of reflection of a plane wave at oblique incidence on a wire grid which is parallel to a plane interface between two homogeneous dielectrics. It is assumed that the wire grid is a periodic structure and consists of thin cylindrical wires of homogeneous material. The equivalent circuit is derived where it is shown that the space on either side of the interface can be represented by a transmission line, and the grid itself is represented by a pure shunt element across one of the lines.**

INTRODUCTION

THERE HAVE been many investigations of the electromagnetic properties of thin parallel wires composed of conductive material. The first quantitative study was made by Lamb[1] in 1898 who considered the plane wave incident normally on the grid. He showed that if the diameter, $2a$, of the parallel wires was small, the reflection and transmission could be varied by changing the spacing. In 1914, von Ignatowsky[2] made a very exhaustive analysis of the scattering of incident plane waves by single metallic grids including the case where the wire spacing is comparable to the wavelength. His formulas have been reduced, extended, and applied by other authors since that time.[3–11] A very illuminating treatment has been given by MacFarlane[5] who indicated that a single grid can be represented by an impedance shunted across an infinite transmission line whose characteristic impedance is proportional to the intrinsic impedance of the

* Manuscript received by the PGMTT, June 1, 1956.

† National Bureau of Standards, Boulder, Colo.

[1] H. Lamb, "Passage of E. M. waves through wire grids," *Proc. London Math. Soc.*, vol. 29, pp. 523–543; 1898.

[2] W. von Ignatowsky, "Theory of the grating," *Ann. der Phys.*, vol. 44, pp. 369–436; May, 1914.

[3] R. Gans, "Hertzian gratings," *Ann. Physik*, vol. 61, pp. 447–464; March, 1920.

[4] W. Wessel, "On the Passage of E.M. waves through a wire grid," *Hochfrequenztechnik*, vol. 54, pp. 62–69; January, 1939.

[5] G. G. MacFarlane, "Surface impedance of an infinite wire grid, at oblique angles of incidence" (parallel polarization), *J. IEE*, vol. 93 (III A), pp. 1523–1527; December, 1946.

[6] R. Honerjager, "E.M. properties of wire grids," *Ann. der Physik*, vol. 4, pp. 25–35; January, p. 1948.

[7] E. A. Lewis and J. Casey, "E.M. reflection and transmission by a grating of resistive wires," *J. Appl. Phys.*, vol. 23, pp. 605–606; June, 1952.

[8] W. E. Groves, "Transmission of E.M. waves through a pair of parallel wire grids," *J. Appl. Phys.*, vol. 24, pp. 845–854; July, 1953.

[9] G. von Trentini, "Gratings as circuit elements of electric waves in space," *Zeit. angew. Phys.*, vol. 5, pp. 221–231; June, 1953.

[10] J. R. Wait, "Reflection from a wire grid parallel to a conducting Plane," *Can. J. Phys.*, vol. 32, pp. 571–579; September, 1954.

[11] J. R. Wait, "Reflection at arbitrary incidence from a parallel wire grid." *App. Sci. Res.*, vol. B IV, pp. 393–400; March, 1954.

Note: In this reference $\cos \theta \cos \phi_0 Z_i d/\eta_0$ should be replaced by $\cos^{-1} \theta \cos \phi_0 Z_i d/\eta_0$ in (25).

surrounding infinite medium. He showed that this shunt impedance was proportional to log $(d/2\pi a)+F(\theta, d)$ where F is a correction factor which is a function of angle of incidence θ and the spacing d.

Recently it has been suggested by Jones and Cohn[12] that a wire grid, if suitably located near an air-interface of a dielectric lens, can effectively simulate a quarter-wave matching network. Considering the case where the wire grid is embedded within the lens medium of intrinsic impedance Z, it can be readily shown[12] that the conditions for the matching the lens to the exterior (air) medium of intrinsic impedance Z' are

$$X_g/Z = \tan 2\phi$$

and

$$Z'/Z = \tan^2 \phi$$

where ϕ is the "electrical" distance in radians from the lens surface to the embedded grid whose impedance is $Z_g \cong iX_g$.

The use of MacFarlane's expression for Z_g in the above application is not strictly correct as the $F(\theta, d)$ function that he rigorously computed is only valid in the case where the grid is in an infinite medium. For dielectric lens matching, the value of ϕ is usually of the order of $\pi/4$ radians corresponding to an air-lens interface to grid separation of the order of $\frac{1}{8}$ wavelength. It will be shown that some error can be introduced if account is not taken of the interface. The following analysis treats fully the problem of a parallel wire grid embedded in a homogeneous dielectric at a fixed distance from a plane interface. While the analysis employs the terminology appropriate to lossless dielectrics, the extension to dissipative media on either or both sides of the interface is effected by regarding the respective dielectric constants to be complex.

Outline of Solution

With respect to a Cartesian coordinate system, the wire grid is contained in the plane $x=h$ and is parallel to a plane interface, at $x=0$, of two dielectrics. The grid is composed of an array of wires parallel to the z axis and spaced a distance d between centers. The wires are taken to be of circular cross section and the diameter is assumed to be small compared to d. The medium $(x>0)$ surrounding the wire grid is homogeneous with a dielectric constant ϵ. The homogeneous medium beyond the interface $(x<0)$ has a dielectric constant ϵ'.

A plane wave with the electric field of magnitude E_0 parallel to the z axis, impinges on the grid with angle of incidence θ as indicated in Fig. 1. The primary or incident field is given by

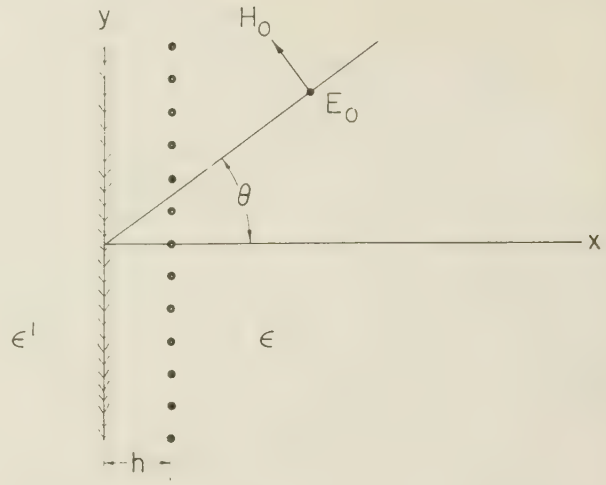

Fig. 1—The wire grid parallel to a plane interface between two dielectrics.

$$E_i = E_0 \exp\left[i2\pi\lambda^{-1}(x\cos\theta + y\sin\theta)\right] \quad (1)$$

where the time factor $\exp(i\omega t)$ has been omitted and

$$2\pi\lambda^{-1} = (\epsilon\mu)^{1/2}\omega \quad (2)$$

where λ is the wavelength in the incident medium and μ is the permeability which is assumed to be the same for both dielectrics. The currents induced on the wires will all be of equal magnitude I but will have a progressive change of phase between adjacent wires of $2\pi\lambda^{-1}d\sin\theta$ radians.

In the absence of a grid a reflected wave

$$E_r = E_0 R \exp\cdot\left[i(2\pi/\lambda)(-x\cos\theta + y\sin\theta)\right] \quad (3)$$

for $x>0$, and a transmitted wave

$$E_t = E_0 T \exp\cdot\left[i(2\pi/\lambda')(x\cos\theta' + y\sin\theta')\right] \quad (4)$$

for $x<0$, will be set up. R and T are Fresnel reflection coefficients given by

$$R = T - 1 = (K' - K)/(K' + K) \quad (5)$$

where

$$K = \eta/\cos\theta, \quad K' = \eta'/\cos\theta', \quad \eta = (\mu/\epsilon)^{1/2}$$

and

$$\sin\theta' = (\lambda'/\lambda)\sin\theta = (\epsilon/\epsilon')^{1/2}\sin\theta = (\eta'/\eta)\sin\theta.$$

It is now necessary to consider the field E_w of the wire grid carrying a current of magnitude I. From a previous analysis,[10] it is known that:

$$E_w = \frac{i\mu\omega I}{4\pi}\exp\cdot\left[i(2\pi/\lambda)y\sin\theta\right]\cdot\sum_{m=-\infty}^{+\infty}\frac{\exp\left[i2\pi my/d\right]\exp\left[-(2\pi/d)\,|\,x-h\,|\,\sqrt{(m+D\sin\theta)^2-D^2}\right]}{\sqrt{(m+D\sin\theta)^2-D^2}} \quad (6)$$

where $D=d/\lambda$. To satisfy the boundary conditions at the interface, a further secondary field E_w^s in the incident medium must be introduced, and further transmitted field E_w^t, given by

[12] E. M. T. Jones and S. B. Cohn, "Surface matching of dielectric lenses," *J. Appl. Phys.*, vol. 26, pp. 452–457; April, 1955.

$$E_w^s = \frac{i\mu\omega I}{4\pi} \exp\left[i(2\pi/\lambda) y \sin\theta\right] \cdot \sum_{m=-\infty}^{+\infty} \frac{R_m \exp\left[i2\pi m y/d\right] \exp\left[-(2\pi/d)(x+h)\sqrt{(m+D\sin\theta)^2 - D^2}\right]}{\sqrt{(m+D\sin\theta)^2 - D^2}} \tag{7}$$

and

$$E_w^t = \frac{i\mu\omega I}{4\pi} \exp\left[i(2\pi/\lambda) y \sin\theta\right] \cdot \sum_{m=-\infty}^{+\infty} \frac{T_m \exp\left[i2\pi m y/d\right] \exp\left[(2\pi/d) x\sqrt{(m+D\sin\theta)^2 - (D')^2}\right]}{\sqrt{(m+D\sin\theta)^2 - D^2} \exp\left[(2\pi/d) h\sqrt{(m+D\sin\theta)^2 - D^2}\right]} \tag{8}$$

where $D' = d/\lambda'$. R_m and T_m are analogous to Fresnel reflection coefficients and are given by

$$R_m = T_m - 1 = \frac{\sqrt{(m+D\sin\theta)^2 - D^2} - \sqrt{(m+D\sin\theta)^2 - (D')^2}}{\sqrt{(m+D\sin\theta)^2 - D^2} + \sqrt{(m+D\sin\theta)^2 - (D')^2}} \cdot \tag{9}$$

where

$$Z_g = \frac{i\mu\omega d}{2\pi}\left(\log\frac{d}{2\pi a} + \Delta\right) + (1+i)\frac{d}{2\pi a}\left(\frac{\bar{\mu}\omega}{2\bar{\sigma}}\right)^{1/2} \tag{12}$$

with

$$\Delta = \frac{1}{2}\sum_{m=1}^{\infty}\left[\frac{1 + R_m \exp\left[-4\pi H D^{-1}\sqrt{(m+D\sin\theta)^2 - D^2}\right]}{\sqrt{(m+D\sin\theta)^2 - D^2}} + \frac{1 + R_{-m}\exp\left[-4\pi H D^{-1}\sqrt{(m-D\sin\theta)^2 - D^2}\right]}{\sqrt{(m-D\sin\theta)^2 - D^2}} - \frac{2}{m}\right] \tag{13}$$

The total field is then

$$\begin{aligned} E &= E_i + E_r + E_w + E_w^s \qquad \text{for } x > 0, \\ &= E_t + E_w^t \qquad \text{for } x < 0. \end{aligned}$$

It can readily be verified that E and $\partial E/\partial x$ are continuous at $x = 0$.

The value of the current I is now found from the additional boundary condition that $E = -Iz_i \exp\left[i(2\pi/\lambda) y \sin\theta\right]$ where E is the field at the surface of the wire and z_i is the internal impedance of the wire. It can be assumed that the field is uniform around the wire since $a \ll d$ and $a \ll \lambda$ and hence z_i can be calculated by known methods and is given by[11]

$$z_i = \frac{\bar{\eta} I_0(\bar{\gamma} a)}{2\pi a I_1(\gamma a)} \tag{10a}$$

where $\bar{\eta} = \left[i\bar{\mu}\omega/(\bar{\sigma} + i\omega\bar{\epsilon})\right]^{1/2}$ and $\bar{\gamma} = \left[i\bar{\mu}\omega(\bar{\sigma} + i\omega\bar{\epsilon})\right]^{1/2}$ and $\bar{\mu}$, $\bar{\sigma}$, and $\bar{\epsilon}$ are the permeability, conductivity, and dielectric constant of the wire material. I_0 and I_1 are modified Bessel functions of or order of zero and unity. For metallic wires, the displacement currents are negligible since $\omega\bar{\epsilon} \ll \bar{\sigma}$ even for microwaves. In addition, the frequency is usually sufficiently high so that $|\bar{\gamma} a| \gg 1$ and hence

$$z_i \simeq \left(\frac{\bar{\mu}\omega}{2\bar{\sigma}}\right)^{1/2} \frac{1+i}{2\pi a} \cdot \tag{10b}$$

Invoking the boundary condition at the wire leads to

$$I = \frac{E_0 d\left\{\exp\left[i(2\pi/\lambda) h\cos\theta\right] + R\exp\left[-i(2\pi/\lambda) h\cos\theta\right]\right\}}{(\eta/2\cos\theta)(1 + R\exp\left[-i(4\pi/\lambda)\ h\cos\theta\right]) + Z_g} \tag{11}$$

where R_m is defined in (9) and R_{-m} is obtained by replacing m with $-m$. The current I on the grid wires is now specified in terms of known quantities. An immediate partial check is obtained by noting that I reduces to (10) of an earlier paper[10] when ϵ' approaches infinity corresponding to a perfectly conducting plane at $x = 0$.

The Distant Field

Although the complete solution of the problem has now been obtained, it is very desirable to focus attention on the distant scattered field. For example, if $(x = h) \gg \lambda$ it is evident that only the terms for $m = 0$ are significant for $d/\lambda < 1/(1 + \sin|\theta|)$ and $d/\lambda' < 1/(1 + \sin|\theta'|)$. The higher values of m correspond to evanescent waves which are highly damped in the positive and negative x directions. For larger values of d, additional undamped waves can be scattered from the grid. The discussion will be limited here to the smaller grid spacings satisfying the above inequality. The distant fields are then given by

$$\begin{aligned} E = E_0 \exp\left[i(2\pi/\lambda)(x\cos\theta + y\sin\theta)\right] \\ + \left\{E_0 R + \frac{I\eta}{2d\cos\theta}\left[\exp\left(i2\pi H\cos\theta\right)\right.\right. \\ \left. + R\exp\left(-i2\pi H\cos\theta\right)\right] \\ \left.\cdot\exp\left[i(2\pi/\lambda)\cdot(-x\cos\theta + y\sin\theta)\right]\right\} \end{aligned} \tag{14}$$

for large positive x, and

$$E = \left\{E_0 T + \frac{I\eta}{2d\cos\theta} T \exp(-i2\pi H\cos\theta)\right\} \cdot \exp\left[i(2\pi/\lambda')(x\cos\theta' + y\sin\theta')\right] \quad (15)$$

for large negative x, where

$$R = T - 1 = (K' - K)/(K' + K) \quad (16)$$

with $K = \eta/\cos\theta$ and $K' = \eta'/\cos\theta'$ with $H = h/\lambda$.

The equivalent circuit, which may be taken as the analog of the wire grid is shown in Fig. 2. The space to the right of the interface, $(x>0)$, is represented by a transmission line of characteristic impedance K and propagation constant Γ. The line constants for the space to the left $(x<0)$ are K' and Γ'. At $x=h$, the line is *shunted* by an impedance Z_g. The voltage V across the line and the current in the line J can now be identified with the electric field E and the magnetic field component H_y respectively. The characteristic impedances have been defined earlier and the propagation constants are given by

$$\Gamma = i(2\pi/\lambda)\cos\theta \quad \text{and} \quad \Gamma' = i(2\pi/\lambda')\cos\theta'.$$

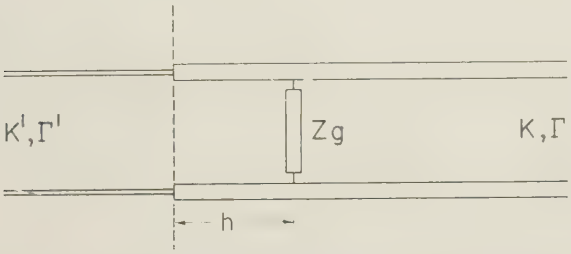

Fig. 2—The equivalent circuit consisting of two semi-infinite transmission lines with shunt element across one.

In the case of normal incidence $(\theta=\theta'=0)$, (12) reduces to

$$Z_g = i\frac{d}{\lambda}\eta\left[\log\frac{d}{2\pi a} + \Delta\right] + (1+i)\frac{d}{2\pi a}\left(\frac{\bar{\mu}\omega}{2\bar{\sigma}}\right) \quad (17)$$

$$\Delta = \sum_{m=1}^{\infty}\left\{\frac{1 + R_m\exp\left[-4\pi(H/D)\sqrt{m^2-D^2}\right]}{\sqrt{m^2-D^2}} - \frac{1}{m}\right\} \quad (18)$$

and

$$R_m = \frac{\sqrt{m^2-D^2} - \sqrt{m^2-(ND)^2}}{\sqrt{m^2-D^2} + \sqrt{m^2-(ND)^2}}. \quad (19)$$

Numerical Discussion

Some numerical values of Δ for normal incidence $(\theta=0)$ and $\lambda'/\lambda = 1.57$ are given in Table I. The ratio of the wavelengths between the medium surrounding the grid and the exterior medium (*i.e.*, 1.57) is typical for a dielectric lens. The case of $H=0$ corresponds to the grid in the interface and $H=\infty$ corresponds to the grid within the dielectric lens medium when the interface is effectively at an infinite distance. Since for reactive-wall matching, H is of the order $\frac{1}{8}$, it is seen that the correction factor Δ can be appreciably different from the corresponding value for $H=\infty$ if D is of the order of one half-wave length or greater. When the grid is in the interface, the value of Δ can be expected to be influenced equally by the electrical properties of both media. This is demonstrated by considering the case $H=0$, $\theta=\theta'=0$, whence[13]

TABLE I
Values of Δ

$D=$	0.2	0.3	0.4	0.5	0.6	0.7	0.8
$H=0$	0.0170	0.0456	0.0728	0.1210	0.1865	0.1262	0.2216
$=\frac{1}{16}$	0.0245	0.0567	0.1027	0.1620	0.2561	0.3813	0.4614
$=\frac{1}{8}$	0.0246	0.0573	0.1067	0.1774	0.2771	0.4227	0.5856
$=\frac{1}{4}$	0.0246	0.0574	0.1068	0.1808	0.2882	0.4532	0.7433
$=\infty$	0.0246	0.0575	0.1068	0.1809	0.2882	0.4535	0.7477

$$\Delta = \sum_{m=1}^{\infty}\frac{2}{\sqrt{m^2-D^2} + \sqrt{m^2-(ND)^2}} - \frac{1}{m} \quad (20)$$

which can be approximated by

$$\Delta \simeq 0.301(N^2+1)D^2 \quad (21)$$

subject to $(ND)^4$ and $(D)^4 \ll 1$. This can be rewritten

$$\Delta \simeq 0.601(k_e D/2\pi)^2 \quad (22)$$

where ik_e is the effective propagation constant for a thin wire in an interface between two media whose propagation constants are $ik(=2\pi i/\lambda')$ and $ik'(=2\pi i/\lambda')$. Therefore subject to the above approximations

$$ik_e = i\sqrt{[(k)^2 + (k')^2]/2}. \quad (23)$$

This simple formula for the effective propagation constant was suggested previously on intuitive grounds.[14]

Conclusion

This analysis provides an exact expression for the equivalent shunt impedance Z_g of a thin wire grid situated parallel to the interface between two homogeneous dielectrics. The results indicate that Z_g is dependent on the distance h from the grid to the interface. The error incurred, however, in neglecting this effect in applications to surface-matching[12] of dielectric lenses is unimportant if the grid spacing d is less than about 0.5λ for normal incidence. This condition can become more stringent when the E vector is not parallel to the wires.[15]

[13] This particular formula is identical to one quoted to me by G. D. Monteath of the British Broadcasting Corp. recently. He says it can be obtained directly using a quasi-static method. I am indebted to Mr. Monteath for a stimulating discussion of this matter.

[14] J. R. Wait and W. A. Pope," Input resistance of l. f. unipole aerials (with radial wire earth systems)," *Wireless Eng.*, vol. 32, pp. 131–138; May, 1955.

[15] J. R. Wait, "On the theory of reflection (at arbitrary incidence) from a wire grid parallel to an interface between homogeneous media," *Appl. Sci. Res.*, vol. BV, 1957 (in press).

Semicircular Ridges in Rectangular Waveguides*

J. VAN BLADEL† AND O. VON ROHR JR.‡

Summary—The two-dimensional Helmholtz equation is solved in a rectangle having two semicircular projections in the center of its broad faces. More particularly, the lowest two eigenvalues are determined for Neumann's boundary condition, and the lowest eigenvalue for Dirichlet's boundary condition. The results are of interest in various fields of physics, such as vibrations of a membrane, but are of particular importance in the study of waveguide propagation. The latter application is stressed in the article, in accordance with the practical importance of ridged waveguides.

Introduction

THE LOWEST mode of a rectangular waveguide, *i.e.*, the TE_{10} mode, has a cutoff frequency f_1 equal to $c/2a$, where c is the velocity of light in the dielectric filling the guide (see Fig. 1). The next to lowest mode is either the TE_{01} mode, with cutoff frequency $c/2b$, or the TE_{20}, with cutoff frequency c/a, the choice between these two modes being determined by the aspect ratio b/a of the cross section. At most, the ratio of the lowest two cutoff frequencies (termed mode separation factor) is seen to be equal to two. Insertion of rectangular ridges has the following effects:[1,2]

1) A decrease in the lowest cutoff frequency. This is shown in Fig. 3, where, as in the rest of the article, frequencies are measured in terms of $c/2a$. The penetration of the ridge is expressed by the insertion coefficient i, a quantity which is defined as $2d/b$ for the rectangular shape and $2R/b$ for the semicircular shape. In particular, i takes the value one when the ridges touch each other. It is seen that the presence of the ridges makes the waveguide more compact for any given value of the lowest cutoff frequency.
2) An increase in mode separation, as seen in Fig. 6. Consequently, "one-mode" propagation is possible over a broader band of frequencies. This important property has led to the use of ridged waveguide in airborne weather-radar, where the two wavelengths of importance for precipitation detection, *viz.*, 3.2 cm and 5.6 cm, must be alternatively accommodated by the same waveguide run, excite a single mode, and still lie sufficiently far from cutoff values.
3) An increase in power attenuation, as evidenced by the two isolated points in Fig. 7. This is objectionable for energy transmission purposes, although desirable in the design of certain microwave devices.[1]
4) An increase of the maximum electric field intensity in the cross section, namely at the protruding corners of the ridges. This lowers the maximum power which can be transmitted without breakdown. To counteract this effect, corners of the ridge are slightly rounded off in practice. The question then naturally arises as to what would be the effect of rounding off much more drastically, *i.e.*, what desirable and undesirable properties of the rectangular ridge would result when one goes over to the "cornerless" semicircular ridge. It is the purpose of the present paper to give an answer to that question.

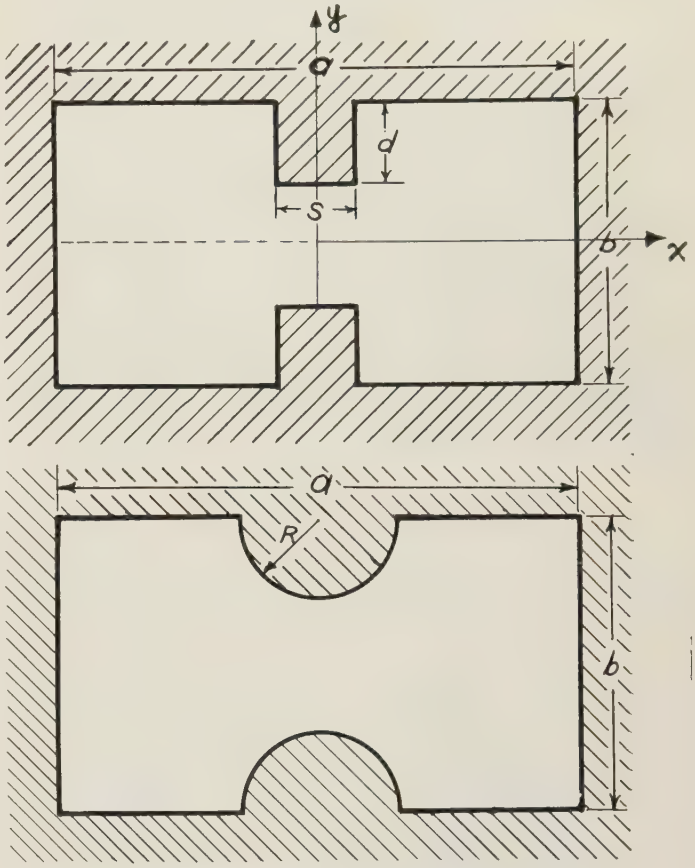

Fig. 1—Rectangular and semicircular ridges.

Numerical Calculations

The structure and properties of a waveguide mode are determined by solving the following two-dimensional eigenvalue problems:[3]

* Manuscript received by the PGMTT, June 25, 1956.
† Dept. of Elec. Eng. Univ. of Wisconsin, Madison, Wis. This work was written while the author was at Washington Univ., St. Louis, Mo.
‡ Dept. of Elec. Eng., Washington Univ., St. Louis, Mo.
[1] S. B. Cohn, "Properties of ridge wave guide," PROC. IRE, vol. 35, pp. 783–788; August, 1947.
[2] S. Hopfer, "The design of ridged waveguides," IRE TRANS., vol. MTT-3, pp. 20–29; October, 1955.
[3] S. Ramo and J. R. Whinnery, "Fields and Waves in Modern Radio," John Wiley & Sons, Inc., New York, N.Y., 2nd ed., ch. 8; 1953.

TE modes: $\nabla^2\phi + k^2\phi = 0$ with

$$\frac{\partial\phi}{\partial n} = 0 \text{ on cross section contour} \quad (1)$$

TM modes: $\nabla^2\phi + k^2\phi = 0$ with

$$\phi = 0 \text{ on cross section contour.} \quad (2)$$

To each eigenvalue k^2 and eigenfunction ϕ corresponds a different mode, the cutoff frequency of which is equal to $ck/2\pi$. The eigenvalue problem of the present article has been solved by classical difference equation methods.[4] Iteration methods have been found more suitable than relaxation methods for the purpose. In brief, the technique consists of starting with a small ridge radius, a coarse net, and a distribution ϕ^0 of net point values corresponding to the unperturbed eigenfunction (*i.e.*, relative to the rectangular boundary of same aspect ratio, but without ridge). A first estimate of k^2 is obtained by the Rayleigh quotient

$$(k^0)^2 = \frac{-\sum \phi^0\nabla^2\phi^0}{\sum (\phi^0)^2}. \quad (3)$$

Better values of ϕ are obtained by going around the net and replacing the initial values ϕ^0 by (see Fig. 2).

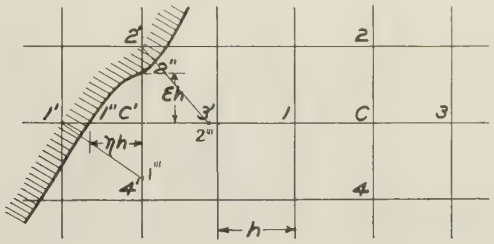

Fig. 2—Points of the nets used in the iteration method.

$$\phi_c' = \frac{\phi_1 + \phi_2 + \phi_3 + \phi_4}{4 - h^2(k^0)^2} \quad (4)$$

for an ordinary point.

$$\phi_c' = \frac{\frac{2}{\eta(1+\eta)}\phi_{1''} + \frac{2}{\epsilon(1+\epsilon)}\phi_{2''} + \frac{2}{1+\eta}\phi_{3''} + \frac{2}{1+\epsilon}\phi_{4''}}{\frac{2}{\epsilon} + \frac{2}{\eta} - (k^0)^2h^2} \quad (5)$$

for a boundary point.

From this new set of values, k^2 is again computed from (3), and the process is repeated until k^2 converges. One then goes over the finer nets, and computes the corresponding values of k^2. The final nets, in the present work, contained some 400 points on the average.[5] A typical sequence of values for k^2 is $11.1/a^2$, $8.3/a^2$, and $7.7/a^2$ for nets containing respectively 19, 97, and 425 points. The extrapolated value, in this particular example, was taken to be $7.6/a^2$. The results of the computations are shown in Figs. 3 to 6. Each curve contains five calculated points, and the over-all accuracy is believed to be better than 2 per cent, which is satisfactory for general engineering purposes. Computations were made on a desk calculator, in the absence of a suitable automatic computer. Interest is focused on the lowest two TE modes, which determine the mode separation factor. However, cutoff frequencies of the lowest TM mode have been added, both because it was found desirable to check whether they remain higher than those of the investigated TE modes, and also because they represent the fundamental frequency of the clamped membrane having the contour depicted in the lowest part of Fig. 1. It will be noticed from Fig. 4 that the TE_{20} mode is the second lowest mode for small aspect ratios. This characteristic property was also displayed by the ridge-

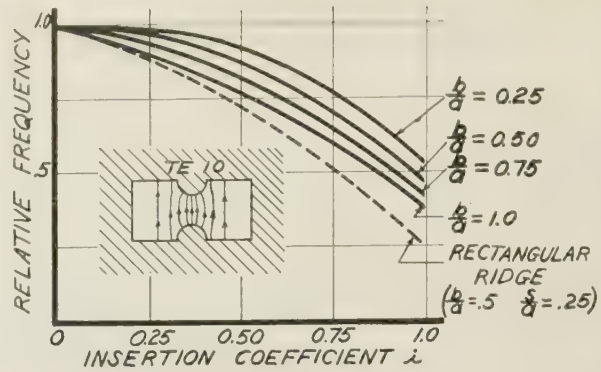

Fig. 3—Cutoff frequency of the lowest mode as a function of the ridge penetration. The dashed curve is relative to a rectangular ridge. The insert shows the lines of force of the electric field in the waveguide cross section.

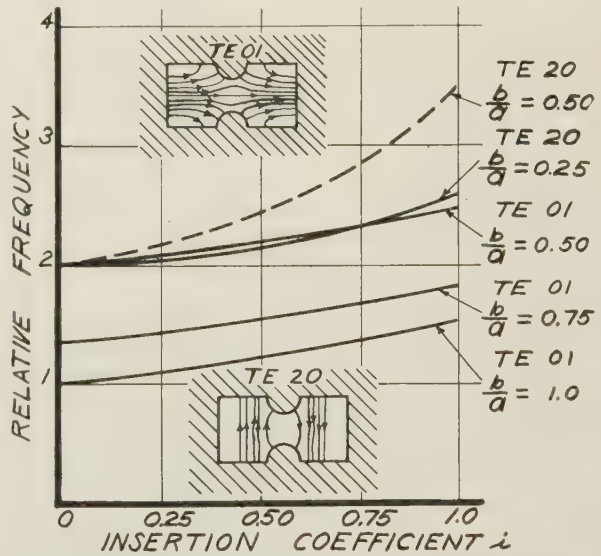

Fig. 4—Cutoff frequency of the second lowest mode as a function of ridge penetration. The inserts show the lines of force of the electric field in the waveguide cross section. The dashed curve, which represents the third lowest mode for $b/a = 0.50$, has been added to allow interpolation of the TE_{20} characteristics between $b/a = 0.50$ and $b/a = 0$.

[4] D. N. deG. Allen, "Relaxation Methods," McGraw-Hill Book Co., Inc., New York, N. Y., 1st ed., ch. 5, 6, and 12, 1954.

[5] For more details, see O. Von Rohr's thesis, submitted to the Sever Inst. of Tech. in partial fulfillment of the requirements for the degree of Master of Science in electrical engineering.

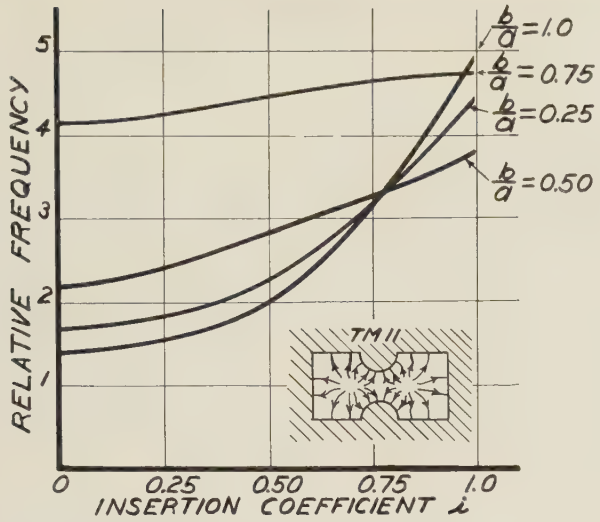

Fig. 5—Cutoff frequency of the lowest TM mode as a function of ridge penetration. The insert shows the lines of force of the electric field in the waveguide cross section.

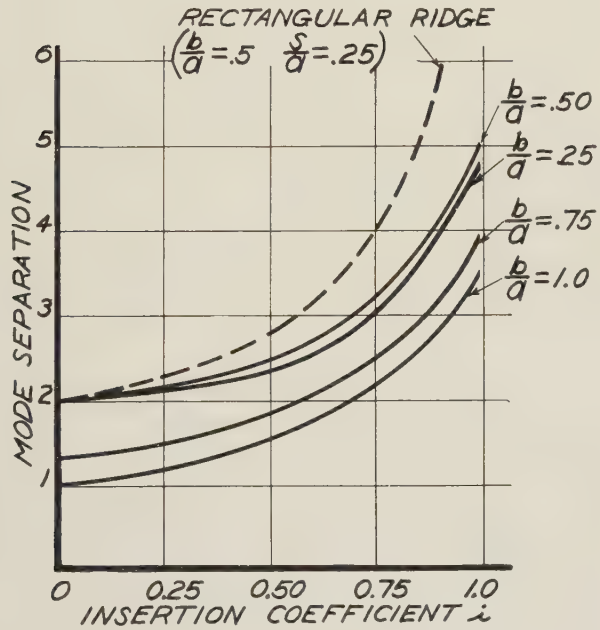

Fig. 6—Mode separation factor as a function of insertion coefficient. The dashed curve, added for comparison purposes, is relative to a rectangular ridge.

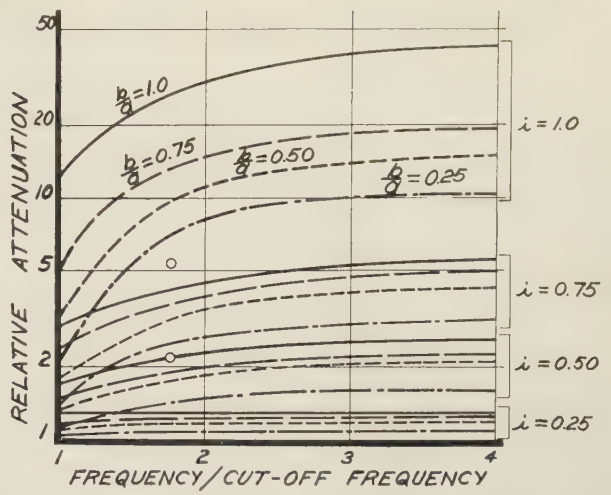

Fig. 7—Attenuation coefficient in terms of the attenuation coefficient relative to a ridgeless waveguide of identical aspect ratio and cut-off frequency. The curves are relative to the lowest mode. The two isolated points refer to the relative attenuation for a rectangular ridge ($S/a=0.25$, $b/a=0.5$) of insertion coefficients 0.5 and 0.75 respectively.

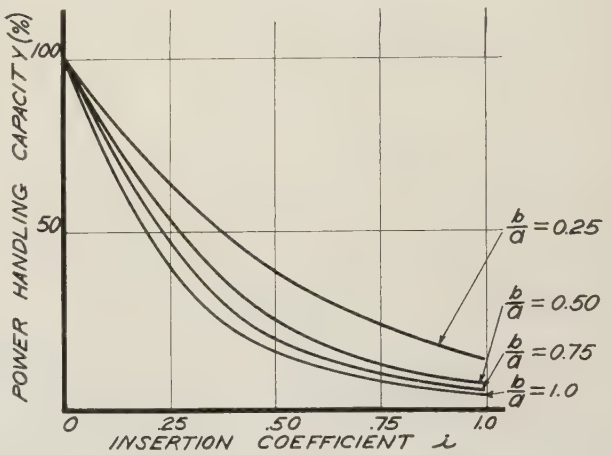

Fig. 8—Decrease of power handling capacity with ridge penetration.

less guide. The value of b/a, however, at which the transition from TE_{01} to TE_{20} takes place, is no longer 0.5, but is somewhat smaller. Notice also from Fig. 6 that the mode separation is optimum for an aspect ratio of 0.4 approximately.

The knowledge of the eigenfunction ϕ relative to the lowest mode makes it possible, by using classical formulas,[3] to compute the attenuation and the power handling capacity of the guide. The results are shown in Figs. 7 and 8. It has been found useful, for comparison purposes, to display the attenuation constant relatively to that of a ridgeless rectangular guide of identical material, aspect ratio, and cutoff frequency. The values of the attenuation constant of the latter guide can be found in the literature.[3] The relative power handling capacity curves indicate that, as the ridge penetration increases, the lowest power level which will cause breakdown (*i.e.*, create, somewhere in the cross section, an electric field equal to the breakdown value) becomes smaller and smaller.

Comparison Between Ridges

The best over-all properties, for a rectangular ridge and an aspect ratio of 0.5, are obtained[2] for $s/a=0.25$ (Fig. 1). An inspection of Fig. 6 indicates that such a rectangular ridge ensures a better mode separation than the semicircular ridge, for any given insertion coefficient. This is not surprising, for the rectangular ridge covers a larger proportion of the cross section than its semicircular counterpart. The comparison, however, should be made on a mode separation basis. For a given mode separation factor, the semicircular ridge is evidently greatly superior as far as power handling capacity is concerned. The latter is actually zero for a rectangular ridge (that is, if we take maximum local electric field as

a criterion). The relative attenuations are roughly identical for both ridges, as can easily be checked by considering the two representative points of Fig. 7. It consequently appears that the semicircular ridge has all the favorable features of its rectangular counterpart, and shows, in addition, considerable improvement in power handling capacity.

Experimental Verification

To obtain an idea of the accuracy of the curves, it was decided to check two points where the accuracy was expected to be low. These points were relative to the TE_{01} mode (the nets of which contained, in general, fewer points than for the TE_{10} mode) and to a waveguide with aspect ratio $b/a=0.466$ (namely the RG-49/U guide). The value of the cutoff wavelength, for insertion coefficients of 0.5 and 0.75, was found, by interpolation from the curves, to be 4.15 cm and 3.95 cm respectively. The measured values were 4.25 cm and 4.08 cm, off by 2 or 3 per cent. This discrepancy is within the limits of the expected 2 per cent over-all accuracy, if one takes into account the additional error introduced by the interpolation process.

Appendix

The following details about the computation method are of interest:

1) Each mode has certain symmetry or antisymmetry properties with respect to the $0x$ and $0y$ axes (Fig. 1). The TE_{10} mode, for example, is symmetrical for $0x$, and antisymmetrical for $0y$. These properties allow computations to be restricted to a quarter of the cross section.

2) The boundary condition $\phi=0$ is imposed by setting $\phi_{1''}=\phi_{2''}=0$ in (5). The condition $\partial\phi/\partial n=0$ is imposed by the use of Fox's method,[6] which consists of computing the value at c' (see Fig. 2) with the formula relative to an ordinary point, *i.e.*, (4). The values of the function at $2'$ and $1'$ are taken to be the same as in $2'''$ and $1'''$, points situated on the perpendicular to the boundary, and where ϕ can be obtained by interpolation between ϕ_c, and ϕ_3, ϕ_c, and ϕ_4, respectively.

3) Iteration with formulas (4) and (5) increases the proportion of lowest modes in the initial distribution ϕ^0. Indeed, the iteration process consists essentially of solving $\nabla^2\phi^1=-(k^0)^2\phi^0$. Assuming the initial distribution to be expanded in the still unknown eigenfunctions ϕ_1, ϕ_2, $\cdots$, ϕ_n, $\cdots$, as

$$\phi^0 = c_1\phi_1 + c_2\phi_2 + \cdots + c_n\phi_n + \cdots. \tag{6}$$

Then the "better" approximation ϕ^1 is seen to be

$$\phi^1 = c_1\frac{(k^0)^2}{(k_1)^2}\phi_1 + \cdots + c_n\frac{(k^0)^2}{(k_n)^2}\phi_n + \cdots \tag{7}$$

and, because $k_1^2<k_2^2<k_3^2$, $\cdots$, the coefficient of the lowest mode ϕ_1 has been proportionally increased as compared to the coefficients of ϕ_2, ϕ_3, $\cdots$, (and similarly for the coefficient of ϕ_n as compared with ϕ_{n+1}, ϕ_{n+2}, ϕ_{n+3}, etc.). Convergence will then be ultimately to the lowest mode ϕ_1, whatever the initial distribution ϕ^0, except if $c_1=0$, *i.e.*, the initial distribution was orthogonal to ϕ_1. This was fortunately easy enough to ensure in the present problem. Assume that one tries to converge to the TE_{10} mode, the eigenfunction of which is ϕ_2. The lowest eigenfunction ϕ_1 is a constant, *i.e.*, independent of position. If one takes the initial distribution to be symmetrical for $0x$, antisymmetrical for $0y$ (as ϕ_2 should be), then c_1 is automatically zero, and convergence will be to the desired eigenfunction ϕ_2. Similarly, symmetry properties allow convergence for the TE_{01} mode without any trouble. The TE_{20} mode, however, must be treated carefully. It is symmetrical with respect to $0x$ and $0y$, so that c_1 is not automatically zero anymore; coefficient c_1 is kept equal to zero only if, after each iteration, the function ϕ is adjusted, by addition of a constant, to have an average value equal to zero.

[6] L. Fox, "Solution by relaxation methods of plane potential problems with mixed boundary conditions," *Quart. Appl. Math.*, vol. 2, pp. 251–257; October, 1944.

Synthesis of a Class of Microwave Filters*

HAROLD SEIDEL†

Summary—This paper deals with the development of a new model for a class of microwave filters. With this model one can reproduce and systematize from a general viewpoint results now in the literature. Its most prominent feature, however, is that the use of the model permits the development of a synthesis procedure for the wide-band filter. From this single model a wide variety of structural realizations are readily obtained. Designs employing this model, and the appropriate synthesis, show significant improvement of desired characteristics over conventional designs. The general multiple quarter wave matching transformer problem is also discussed.

I. Introduction

THE PURPOSE of this paper is to unify various representations and designs of a class of reactive filters, of which the quarter wave coupled cavity filter[1] is representative. Herein structures are sought that have symmetric insertion loss characteristics about a given frequency and are characterized by an even polynomial loss function in terms of an appropriate frequency sensitive variable. Among others of possible interest included in this class are Tchebycheff and maximally flat responses. The form of the filter representation also leads simply to the design of multiple quarter wave matching transformers. This design is included in one section of this paper.

The building block chosen in a pair of equal transformers, as shown in Fig. 1, separated by a transmission

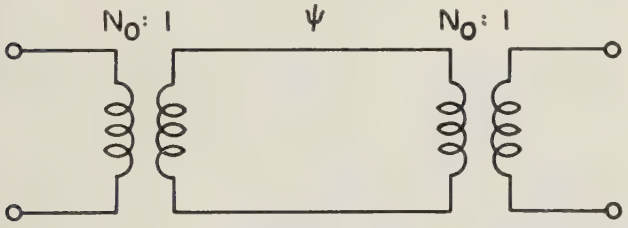

Fig. 1—Transformer representation of a resonant cavity.

line of electrical length ψ and having a relative characteristic impedance of value unity. When ψ takes on a quarter wavelength value, this network transmits without reflection and behaves in the manner of a resonant cavity. Since the cavity has been somewhat ambiguously represented in the literature, Fig. 1 will be taken as a defining representation to within the appendage of a quarter wavelength transmission line.

This representation has two features of interest: 1) the transmission line length at resonance is not a function of the transformer value, and, 2) direct cascades of resonant cavities of the form of Fig. 1 lead to polynomial insertion losses in the variable $\cos \psi$. These features permit a simple representation of a structural realization without the necessity of taking into account small phase corrections associated with the cavity loading or the interaction of adjacent cavities.[2] A symmetric array of cavity Q values leads to even polynomial insertion losses covering the class of present interest. These cavity loadings, or Q values, will be discussed more explicitly in the text.

The class of filters to be discussed is roughly similar to that of ladder networks in lumped element theory and, indeed, it will be shown that the ladder is the limiting microwave filter representation in the narrow band region of design. All the structures to be examined are formed from cascades of simple elements and are minimum phase networks. The multimode or bridge type structures[3–5] are excluded because they are not of this category. The filter is analyzed through the use of a transfer matrix[6] ($ABCD$ matrix), with a minor modification of the current flow convention.

The rigorous synthesis procedure described for arbitrary bandwidth filters extends the Darlington procedure for lumped element networks to the case of distributed line elements. A method of factoring is used in a fashion similar to that for lumped element synthesis, but with appropriate radical quantities involved in the factors characterizing the distribution effects.

The following section presents a review of certain aspects of four-pole theory and transformer equivalents. Section III is concerned with filter equivalents. Section IV extends the prior section to show its relation to quarter wave matching transformer design. Finally, section V covers the synthesis and realization of a general filter design.

II. Reactive Four-Pole Equivalents

A. Transfer Matrix Properties

The transfer matrix is defined by means of the conventions indicated in Fig. 2.

$$\begin{pmatrix} E_1 \\ I_1 \end{pmatrix} = \begin{pmatrix} A & i\beta \\ i\gamma & D \end{pmatrix} \begin{pmatrix} E_2 \\ I_2 \end{pmatrix}. \tag{1}$$

* Manuscript received by the PGMTT, June 28, 1956. This paper is a portion of a dissertation submitted in partial fulfillment of the degree of Doctor of electrical engineering at the Polytech. Inst. of Brooklyn, Brooklyn, N. Y.; May, 1954.

† Bell Telephone Labs., Inc., Murray Hill, N. J.

[1] R. M. Fano and A. W. Lawson, "Microwave filters using quarter-wave couplings," Proc. IRE, vol. 35, pp. 1318–1324; November, 1947.

[2] W. W. Mumford, "Maximally flat filters in waveguide," *Bell Sys. Tech. J.*, vol. 27, pp. 684–713; October, 1948.

[3] J. R. Whinnery, "Design of Microwave Filters," Symposium on Modern Network Synthesis, Brooklyn Polytech. Inst., Brooklyn, N. Y., pp. 293–301; April, 1952.

[4] S. B. Cohn, "Analysis of a wide-band waveguide filter," Proc. IRE, vol. 37, pp. 651–656; June, 1949.

[5] S. B. Cohn, "Design relations for the wide-band waveguide filter," Proc. IRE, vol. 38, pp. 799–803; July, 1950.

[6] E. A. Guillemin, "Communication Networks, Vol. II," John Wiley and Sons, Inc., London, Eng., pp. 144–152; 1935.

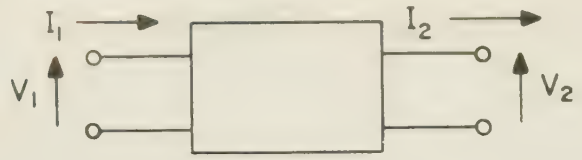

Fig. 2—Four-pole conventions.

A, D, β, and γ are all real for a reactive structure, and the matrix determinant is of unit value. The insertion loss L, which is defined as the ratio of the power transmitted into a matched load from a direct connection to the generator to that obtained with the four-pole inserted, is related to the elements of the transfer matrix by

$$L = 1 + \tfrac{1}{4}[(A - D)^2 + (\beta - \gamma)^2]. \qquad (2)$$

The input impedance to side 1, with a unit normalized terminating impedance, is given by

$$Z = \frac{A + i\beta}{i\gamma + D}. \qquad (3)$$

It is through (3) that synthesis will eventually be performed, since it gives a simply ordered array of the matrix elements.

Four-pole behavior with the insertion of frequency invariant quarter and half-wavelength transmission lines will be of interest in various aspects of this study. The half-wavelength line is an all-pass 180 degrees phase shift network and is employed as an identity operation with respect to insertion loss when employed in cascade. A simultaneous application of quarter wave lines as cascades before and after a four-pole interchanges diagonal terms in the transfer matrix. This transformation has the effect of inverting transformers, inverting the relative characteristic impedance of a transmission line, and interchanging lumped series reactances and shunt susceptances. These invariant line lengths are to be distinguished from physical transmission lines, which pass through quarter and half wavelength values as a function of frequency.

B. Equivalent Representations Involving Ideal Transformers

Weissfloch[7] has shown that any reactive four-pole may be represented, at a frequency, as a transformer with associated transmission line lengths. Iris type filters are obtained later from the transformer cavity model through reference to the Weissfloch network equivalents, shown in Fig. 3, for lumped series and shunt elements. Symmetric employment of transformers (Fig. 4) furnishes a ready equivalence to the junction of two transmission lines of different characteristic impedance.

[7] A. Weissflock, "Anwendung des transformersatzes über verlustlose vierpolen auf die hinter einander schaltung, von vierpolen," *Hochfreq. Tech. Electr. Akust.*, vol. 61, pp. 19–28; January, 1943.

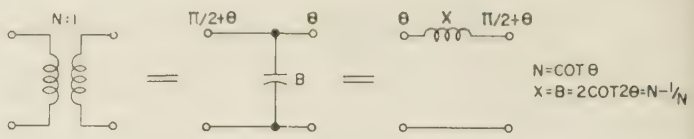

Fig. 3—Some transformer equivalents.

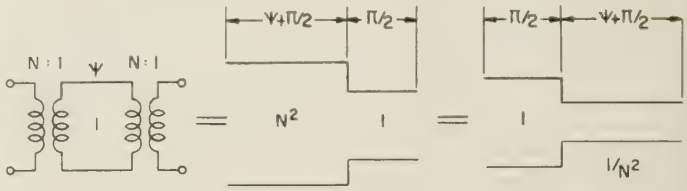

Fig. 4—Transmission line equivalents.

The transformer portion of the Weissfloch representation determines the insertion vswr of the four-pole. The transformer ratio, or its reciprocal, is equal to the square root of this vswr.

III. Filter Equivalents

A symmetrically loaded filter structure is illustrated in the transformer cavity representation of Fig. 5. Although symmetrically loaded, the network is electrically unsymmetric to within the addition of a quarter wavelength section. This construction is a direct coupled representation, since adjoining transformers coalesce. A quarter wave coupled construction results from the transformations shown in Fig. 6 which employ invariant half wavelength identity sections and quarter wavelength transformer inverting sections.

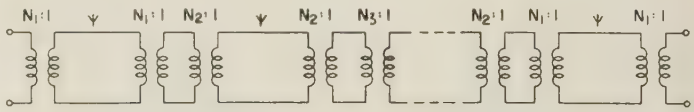

Fig. 5—Symmetric cavity array filter.

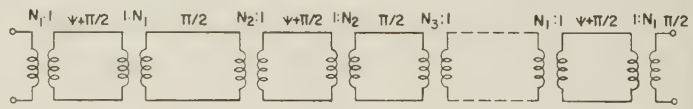

Fig. 6—Quarter wave coupled filter.

Fig. 6 is, at best, an idealized representation, since the coupling sections are of invariant quarter wave nature. The resonant cavity length $\psi+(\pi/2)$ is, however, permitted a realistic frequency variation, since ψ itself may undertake any appropriate variation as a function of frequency suitable to the radian length $\psi+(\pi/2)$.

The direct coupled structure of Fig. 5, as indicated, is incapable of realizing loss functions having a center-band mismatch. This situation may be overcome by considering the filter structure to be designed to a modified characteristic impedance. This situation, in turn, may be depicted simply by adding a pair of match-

ing transformers at the filter terminals. In practice, these added transformers may be realized by appropriately tapering the transmission line impedance to whatever value may be required at the filter terminals.

It may be demonstrated simply that a transformation of N to $1/N$ in these representations produces no effect on insertion loss. We shall, therefore, generally restrict the analysis to $N>1$.

A. Line Type Filters

Fig. 6 leads to the line filter structures shown in Fig. 7(a) and 7(b). These filters are each comprised of an array of sections, all of equal length, but varying in characteristic impedance. The second of these two figures is derived from the former by the inversion properties of the quarter wavelength sections. The structure shown in Fig. 7(b) has been used as a low pass structure, although there generally is no adherence to the requirement that the sections be of equal length. This lapse is permissible for small section lengths, since insertion losses there depend simply on the product of the characteristic impedance and line length, and either may modify the other. This is, however, an approximation valid only for small electrical line lengths and is improper in band-pass constructions.

Fig. 7(b) is an imperfect wideband structure, because of the existence of discontinuity effects. However, the compensation techniques of Section V adequately diminish these effects and this type of filter is employed eventually in wide-band operation. One may, however, directly obtain a coaxial line filter by the use of dielectric beads to effect impedance variations without discontinuity susceptances. The coaxial line, thus, permits a theoretically perfect realization of the filter design.

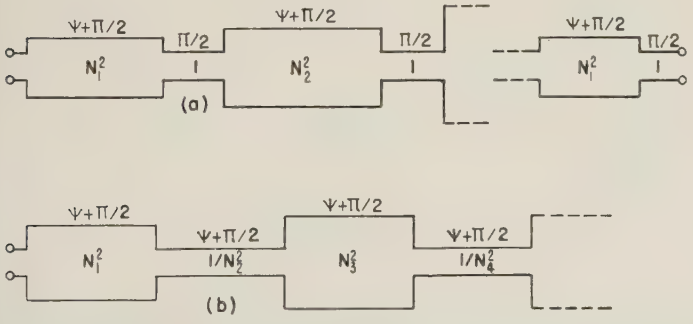

Fig. 7—Quarter wave and direct coupled line filters.

B. Iris Coupled Filters

The direct[8,9] and quarter wave coupled[1,2,10] iris type filters follow directly from Figs. 4–6. A filter comprised of series reactances is simply related to the susceptance (iris) type. The iris structures are shown in Fig. 8(a) and 8(b) where

$$\theta_n = \frac{1}{2}\operatorname{arc\,cot}\frac{B_n}{2}$$

$$\alpha_n = \frac{1}{2}\operatorname{arc\,cot}\frac{B_n}{2}$$

$$B_n = N_n - \frac{1}{N_n}$$

$$B_n' = N_{n-1}N_n - \frac{1}{N_{n-1}N_n}.$$

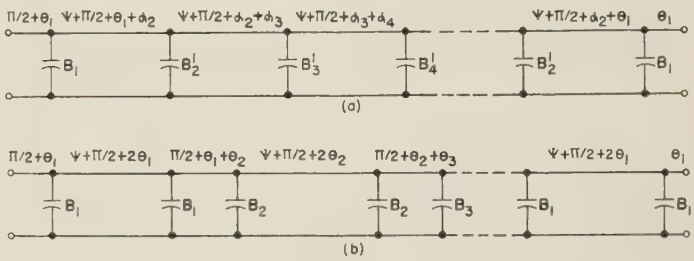

Fig. 8—Direct and quarter wave coupled iris filters.

The iris realizations are frequency sensitive, since the Weissfloch equivalent of the transformer is invariant and the physical elements approximating it are not. Nevertheless, we may expect the direct coupled filter to be the less frequency sensitive realization of the two types.

It will be of interest to remark on the properties of a two-section direct coupled iris filter. The central iris has an insertion vswr which is the square of that of either external iris. Thus, in the high susceptance limit, the central iris has a relative susceptance equal to the square of that of either external iris. In the low susceptance limit, the central iris takes on a susceptance value double that of either external iris. The cavity lengths vary from a half to a quarter wavelength over the same range of susceptance.

C. Narrow-Band Correspondence to Lumped Resonant Elements

The transfer matrix of the elementary transformer cavity of Fig. 1 is given by

$$T_1 = \begin{bmatrix} N^2\cos\psi & i\ \sin\psi \\ i\ \sin\psi & \dfrac{1}{N^2}\cos\psi \end{bmatrix}, \tag{4}$$

where the subscript on T indicates the matrix to be that of a single cavity. Narrow band approximation is achieved by placing $1/N^2$ equal to zero and setting $\sin\psi$ to unity. Thus, in the neighborhood of $\psi=\pi/2$

[8] J. Hessel, G. Goubau, and L. R. Battersby, "Microwave filter theory and design," Proc. IRE, vol. 37, pp. 990–1000; September, 1949.

[9] H. J. Riblet, "Synthesis of narrow-band direct-coupled filters," Proc. IRE, vol. 40, pp. 1219–1223; October, 1952.

[10] W. L. Pritchard, "Quarter wave coupled waveguide filters," *J. Appl. Phys.*, vol. 18; October, 1947.

$$T_1 \sim \begin{bmatrix} -\omega & N^2 \dfrac{d\psi}{d\omega}\dfrac{\delta\omega}{\omega} & i \\ i & & 0 \end{bmatrix}$$

$$= \begin{bmatrix} 0 & i \\ i & 0 \end{bmatrix} \begin{bmatrix} 1 & & 0 \\ i\left(\omega N^2 & \dfrac{d\psi}{d\omega}\dfrac{\delta\omega}{\omega}\right) & 1 \end{bmatrix}. \quad (5)$$

Eq. (5) suggests a decomposition into a quarter wavelength line and a shunt susceptance

$$\left(\omega N^2 \frac{d\psi}{d\omega}\right)\frac{\delta\omega}{\omega},$$

where the linear frequency variation of the susceptance indicates the neighborhood of resonance.

The susceptance of a shunt resonant network characterized by a doubly loaded value of Q is given as

$$B = 2Q\frac{\delta\omega}{\omega}.$$

Therefore,

$$N^2 = \frac{2Q}{\omega \dfrac{d\psi}{d\omega}\Big]_{\psi=\pi/2}}. \quad (6)$$

This relationship may be further simplified to

$$N^2 = \frac{Q}{m\pi}\left(\frac{\lambda_0}{\lambda_{g0}}\right)^2, \quad (7)$$

where m is the number of half wavelengths of the cavity, and where the zero subscript indicates evaluations made at centerband. λ_g is the guide wavelength and λ is that for free space.

Two narrow band equivalents of the cavity are shown in Fig. 9. Cascading the various cavity sections leads to a quarter wave coupled series array of lumped series resonant elements, a quarter wave coupled shunt array of lumped shunt resonant elements, or, finally, a direct coupled alternation of series and shunt elements in a ladder array.

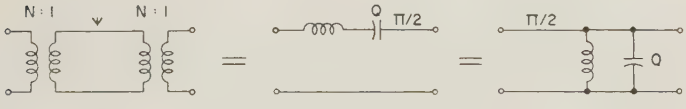

Fig. 9—Narrow band equivalents.

IV. Design of Quarter Wave Transformers

We may again utilize the symmetric application of transformers to a transmission line, but in a different fashion from that used earlier. A real impedance mismatch may be characterized by a matched load preceded by a transformer. We may achieve this representation by an appropriate construction in which the transformer used to mismatch the load is part of a filter array.

Consider the direct coupled filter of Fig. 10(a), opposite, where the additive transformers N_0 are included for completeness in representing the centerband mismatch case. Let us "purloin" a transformer of N:1 ratio from the last cavity section and rearrange the transformer array retrogressively, so that the transformers associated with any line section are symmetrically arranged. As shown in Fig. 10(b), an eventual accumulation occurs at the generator end of a transformer of value $\prod_i N_i : N$. This may be removed, by simply setting the ratio to unity so that

$$\prod_i N_i = N, \quad (8)$$

where the product extends over every transformer of the filter array. If the transformer N is employed to produce a load of relative resistance ρ, we have

$$N = \rho^{1/2}. \quad (9)$$

We then have the final configuration of Fig. 10(c).

For that frequency for which $\psi = \pi$, the filter of Fig. 10(a) appears as a single transformer of value $\prod_i N_i$, so that from (9), and given the polynomial insertion loss

$$L = 1 + R_n^2(\cos\psi), \quad (10)$$

we have,

$$L(1) = 1 + R_n^2(1) = 1 + \frac{(\rho-1)^2}{4\rho}. \quad (11)$$

It will be shown in the following section, that any even insertion loss function of the form of (10) is realizable as a symmetric cavity array, if R_n is an nth degree polynomial. Then, given any even or odd polynomial of nth degree $F_n(\cos\psi)$, we obtain the following general form of insertion loss of the quarter wave section matching transformer for the specified real termination impedance ρ:

$$L = 1 + \frac{(\rho-1)^2}{4\rho}\left[\frac{F_n(\cos\psi)}{F_n(1)}\right]^2. \quad (12)$$

V. A General Filter Synthesis and Its Realization

A. Synthesis

Synthesis of a filter, to a prescribed even insertion loss of polynomial nature of the form of (10), is accomplished by a modification of the Darlington[11] synthesis procedure, which takes the distributed nature of the line lengths into account.

[11] S. Darlington, "Synthesis of reactance 4-poles which produce prescribed insertion loss characteristics," *J. Math. Phys.*, vol. 18, pp. 257–353; September, 1939.

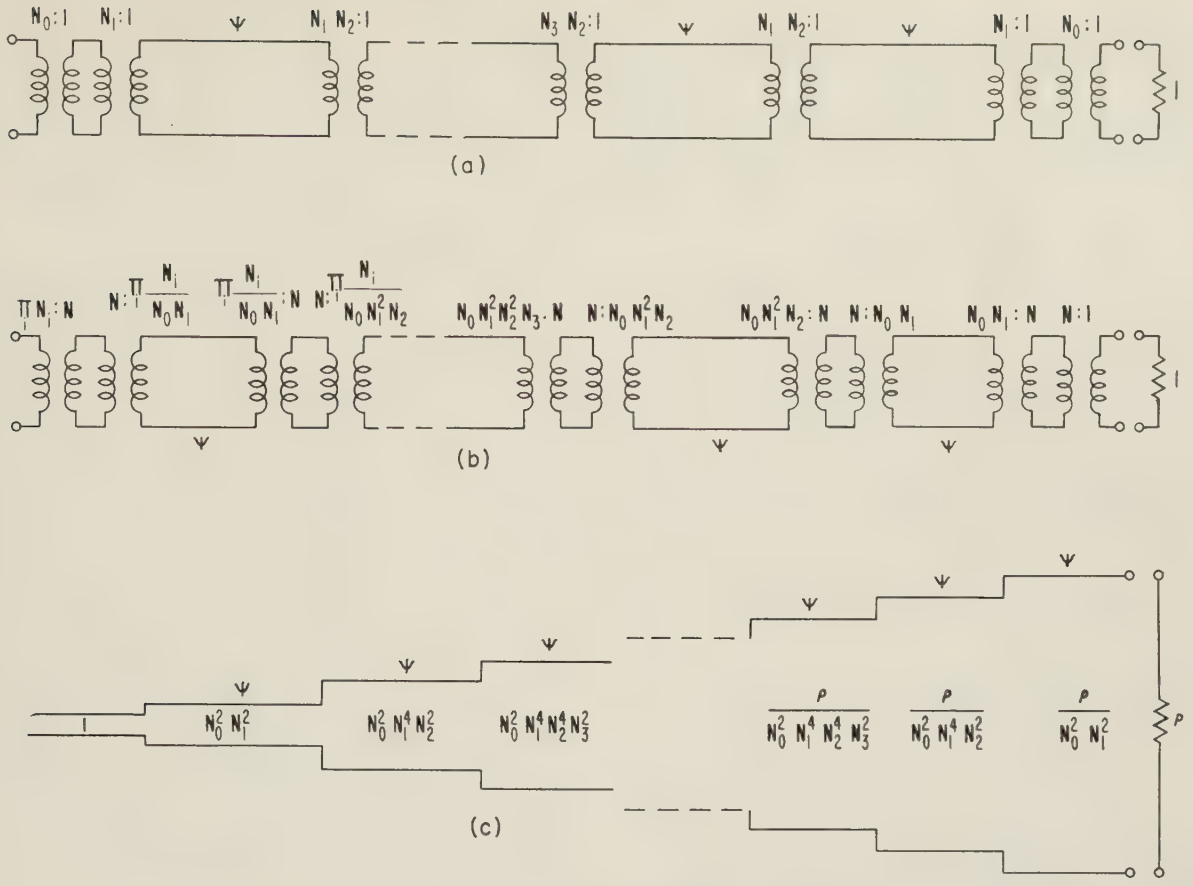

Fig. 10—Development of the quarter wave transformer.

Define:

$$u = \cos \psi,$$
$$p = -iu.$$

We now employ a "radical factoring" identity given as

$$(p-p_i)(p+p_i)(p-p_i^*)(p+p_i^*)$$
$$= |1+p_i^2|^2(p-\zeta_i\sqrt{1+p^2})(p+\zeta_i\sqrt{1+p^2})(p-\zeta^*\sqrt{1+p^2})$$
$$(p+\zeta_i^*\sqrt{1+p^2}) \qquad (13a)$$

where

$$\zeta_i^2 = \frac{p_i^2}{1+p_i^2}. \qquad (13b)$$

The special case in which p_j is real produces the modified identity

$$(p-p_i)(p+p_i)$$
$$= |1+p_i^2|(p-\zeta_i\sqrt{1+p^2})(p+\zeta_i\sqrt{1+p^2}). \qquad (14)$$

The quantities p_j are the roots of an expression that will be discussed shortly. These roots appear symmetrically about the origin in the complex plane, this array stemming from the even polynomial loss character of the filter. The left-hand side of (13) is just the decomposition that occurs in the Darlington theory. This decomposition is inadequate to describe transmission line filters which, as may be seen from the matrix expression of (4), require the existence of terms in $\sin \psi$ as well as $\cos \psi$. The radical expressions of the right of (13) are just the sine of ψ, giving the motivation to this factoring.

The method of synthesis may be described now. Let it be required, to obtain the following even insertion loss function, that

$$L = 1 + R_n^2(u), \qquad (10)$$

where $R_n(u)$ is an nth degree polynomial. It is appropriately odd or even from the requirement that $R_n^2(u) = R_n^2(-u)$. The insertion loss may also be described in terms of a reflection factor $k(u)$ and we have the relationship

$$|k(u)|^2 = k(u)k^*(u) = \frac{R_n^2(u)}{1+R_n^2(u)}. \qquad (15)$$

Employing (8), we may deduce the result

$$1 + R_n^2(u)$$
$$= [X(u) + i\sqrt{1-u^2}Y(u)][X(u) - i\sqrt{1-u^2}Y(u)], \qquad (16)$$

which is obtained by separating the quantities ζ_j into the left and right hand planes, respectively. $X(u)$ is an nth degree polynomial in u, and $Y(u)$ is of one degree less; both have even squares in u. A sufficient solution for $k(u)$ is given by

$$k(u) = \frac{R_n(u)}{X(u) + i\sqrt{1 - u^2}Y(u)}. \tag{16}$$

Discarding the arguments, we have the input impedance function

$$Z = \frac{1 + k}{1 - k} = \frac{(X + R_n) + i\sqrt{1 - u^2}Y}{i\sqrt{1 - u^2}Y + (X - R_n)}. \tag{17}$$

The total transfer matrix, subject to necessary conditions, is obtained through inspection of (3), namely

$$T_n = \begin{pmatrix} X + R_n & i\sqrt{1 - u^2}Y \\ i\sqrt{1 - u^2}Y & X - R_n \end{pmatrix}. \tag{18}$$

It may now be shown that T_n satisfies certain necessary conditions aside from satisfying (2). From (16)

$$| X + i\sqrt{1 - u^2}Y |^2 = X^2 + (1 - u^2)Y^2 = 1 + R_n^2. \tag{19}$$

T_n is thus seen to possess a unit determinant. Two other requirements imposed by the transformer form of representation are satisfied. They are: 1) the off diagonal terms are equal; and 2) the off diagonal terms possess the proper radical factors.

The major diagonal terms of T_n are even or odd polynomials and of nth degree. T_n may be decomposed by a "chipping away" procedure, where pairs of equal cavity sections are detached simultaneously from opposite sides of the filter, such that each element of the residual matrix is decreased by two degrees in u. Let T_1 be the leading transformer cavity in the array of T_n; then

$$T_{n-2} = T_1^{-1} T_n T_1^{-1}, \tag{20}$$

where

$$T_1^{-1} = \begin{pmatrix} \frac{1}{N_1^2} u & -i\sqrt{1 - u^2} \\ -i\sqrt{1 - u^2} & N_1^2 u \end{pmatrix}. \tag{21}$$

We thus obtain the recurrence

$$T_{n-2k} = T_k^{-1} T_{k-1}^{-1} \cdots T_2^{-1} T_1^{-1} T_n T_1^{-1} \cdots T_{k-1}^{-1} T_k^{-1}. \tag{22}$$

Let

$$T_{n-2k} = \begin{pmatrix} \alpha_k & i\sqrt{1 - u^2}\beta_k \\ i\sqrt{1 - u^2}\beta_k & \delta_k \end{pmatrix}, \tag{23}$$

where

$$\alpha_k = f_{n-2k}u^{n-2k} + f_{n-2k-2}u^{n-2k-2} + \cdots$$

$$\beta_k = g_{n-2k-1}u^{n-2k-1} + g_{n-2k-3}u^{n-2k-3} + \cdots$$

$$\delta_k = h_{n-2k}u^{n-2k} + u_{n-2k-2}u^{n-2k-2} + \cdots,$$

and where f, g, and h are constants.

It may be shown that a choice of

$$N_{k+1}^2 = \frac{f_{n-2k}}{g_{n-2k-1}} = \frac{g_{n-2k-1}}{h_{n-2k}} = \sqrt{\frac{f_{n-2k}}{h_{n-k2}}} \tag{24}$$

leads to a satisfactory determination of the transformer value, in that T_{n-2k-2} is reduced to proper degree. The structure may thus be appropriately reduced, eventually leading, at most, to the residue of a single transformer. This residue occurs only in the case of a filter having an even number of sections, since $R_n^2(0) \neq 0$.

As stated earlier, the centerband mismatch may be equally well accounted for with the transformer residue occurring not at the center of the structure, but being formed instead, equivalently, as two transformers applied equally to the filter terminals. Considering the quarter wave asymmetry inherent in the filter representation, these transformers act symmetrically to modify the filter characteristic impedance. Fig. 11 shows the manner of extraction of the transformer pair. It may be determined that

$$N_0 = [X(0) + R_n(0)]^{1/2}. \tag{25}$$

It may be shown, in general, that any admissible function $R_n(u)$, meeting the requirements stated in this paper, always leads to realizable filter structures.[12]

Fig. 11—Extraction of transformers causing centerband mismatch.

B. Structural Realization

The line type filter of Fig. 7(b) shows the greatest potential for wideband realization. The difficulty related to such realization, through the existence of discontinuity susceptances, may be mitigated by forming the individual sections into elementary, maximally flat two-section filters.

[12] Corresponding to every admissible polynomial R_n there is a unique transformer array N_i^2, based on the above method of development. The filter is unrealizable, if one or more values of N_i^2 goes negative. For this to occur, there must first be a region of R_n where some of the transformer values either tend toward zero or infinity. In either event, one of the elements in the matrix of (21) becomes singular, and this may be shown to contradict the finite nature of the loss function hypothesized for the filter.

Consider an individual section of a compensated structure, shown in Fig. 12, in which a value of susceptance has been inserted at the center of a line section double to that value occurring at either end. Given small values of the relative susceptance b, the line section is maximally flat in the neighborhood of a line length $\theta=\pi$. Maximal flatness indicates an approximate equivalence to a unit characteristic impedance transmission line with some phase shift alteration. This phase shift effect shows up as a modification of line length which, for capacitive susceptances, takes on the character of a new physical transmission line. Having such susceptances, one requires the following mechanical length for a half wave section of line:

$$l = \lambda_{g0}\left(\frac{1}{2} - \frac{b(0)}{\pi}\right), \tag{26}$$

where the zeros refer to centerband.

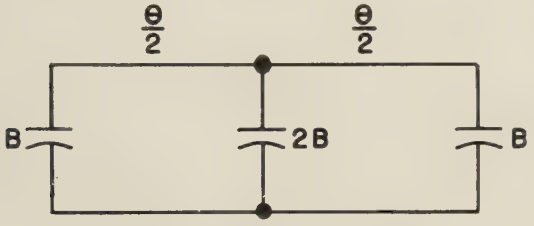

Fig. 12—Susceptance compensation.

The application of (26) is not unique. The susceptances occurring at a discontinuity may be absorbed between the two adjacent line sections in any arbitrary fashion, with susceptive irises possibly added at these discontinuities, to equalize susceptance values. The method adopted for design in this paper is such that each transmission line is made to appear identical to every other on a relative basis. The susceptances are then, in absolute value, divided proportionally to the line admittance at a discontinuity, with whatever positive susceptance required added, to provide equalization to other transmission lines. The justification of such a procedure is described below.

Let every compensated section be characterized by an impedance Z' and a length θ', both functions of frequency. The ratios of Z' remain identical with frequency from section to section, and all θ' are equal. The internal filter characteristic, therefore, perfectly realizes the design in terms of the quantity θ'. Since θ' differs from the ideal line length θ by second order quantities over the band of interest, the departure of internal characteristics is likewise of second order. Thus, compensation deviations of the equalized filter with equal length sections are not cumulative with respect to the number of sections. A small termination mismatch exists, due to the ratio of Z' to the actual line impedance. This is guaranteed small over a relatively large band by the choice of the maximally flat sections.

It is of interest to determine the limitations, if any, imposed by the discontinuities on the range of applicability of the line type filter. Given a junction between two rectangular waveguides of the same widths of large height ratios, the entire susceptance normalized to the smaller of the two guides[13] of the order of

$$b \sim \alpha H \ln \alpha,$$

where α is the ratio of the smaller to the larger height, and H is the height of the larger guide. H has an upper limit given by higher mode considerations, and b has a maximum value with respect to α. This value is never large, permitting the line type of design, in theory, for narrow as well as large bandwidths.

In the design of a 20 per cent bandwidth maximally flat four-section waveguide filter, a maximum susceptance occurs of value $b=0.15$. Since this is of the order of the largest susceptance to be expected, some numerical data are given in Table I. $\lambda_{g0}/\lambda_g=0.846$ gives the 3 db loss point.

TABLE I

Compensated Line Section

λ_g/λ_{g0}	θ	θ'	Z'
	degrees	degrees	
1	180	180	1
0.85	153	152.2	0.963
0.80	144	143.8	0.955

C. Typical Design

A test case was computed based on the following specifications:

Guide internal dimensions	2 inches × 1 inch
Center frequency	5.0 kmcs
3 db bandwidth	20 per cent
Type of characteristic	maximally flat.

The insertion loss function that results is given by

$$1 = 1 + 404\ (\cos \psi)^8.$$

The corresponding ideal line section filter is shown in Fig. 13.

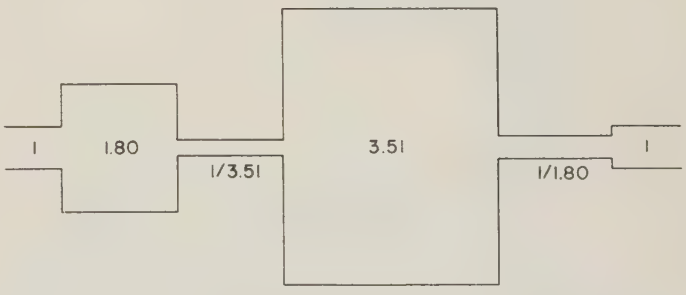

Fig. 13—Uncompensated 20 per cent bandwidth filter.

[13] Marcuvitz, "Waveguide Handbook, Vol. II," Mass. Inst. Tech. Rad. Lab. Series, McGraw-Hill Book Co., Inc., New York, N. Y.; 1951.

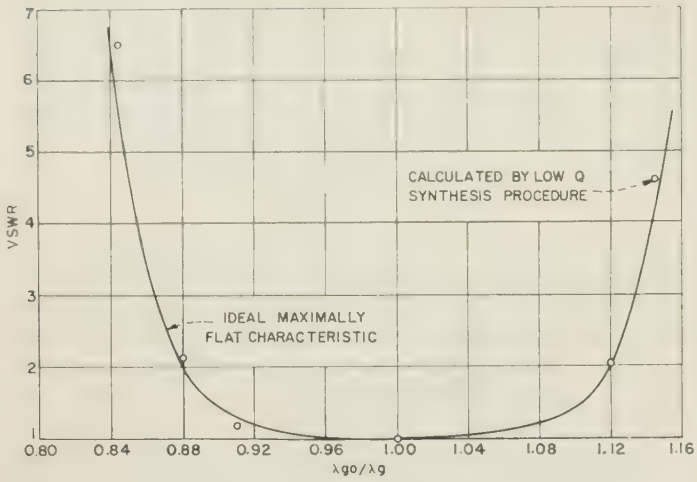

Fig. 14—Filter design employing compensated line type synthesis.

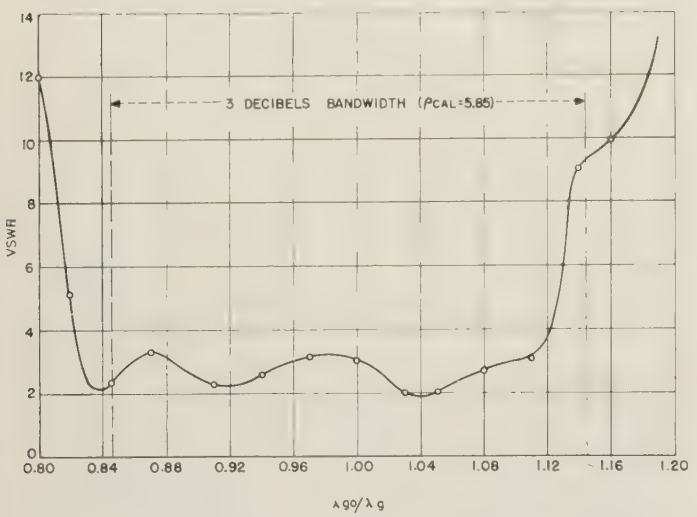

Fig. 15—Line type synthesis with discontinuity compensations omitted.

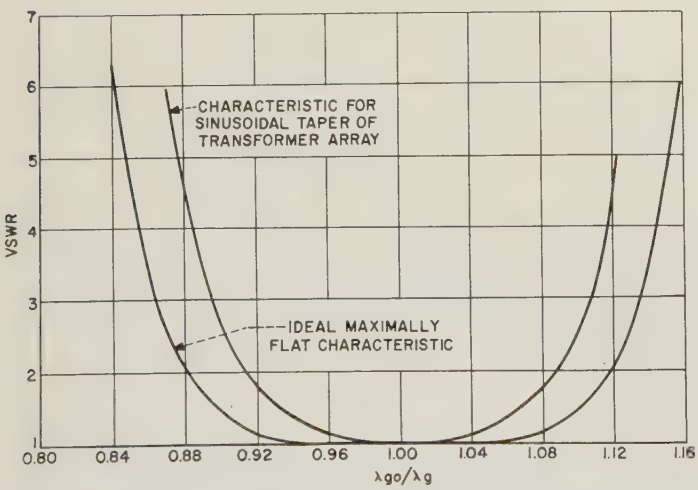

Fig. 16—Effect of ideal narrow-band synthesis application to a 20 per cent bandwidth filter.

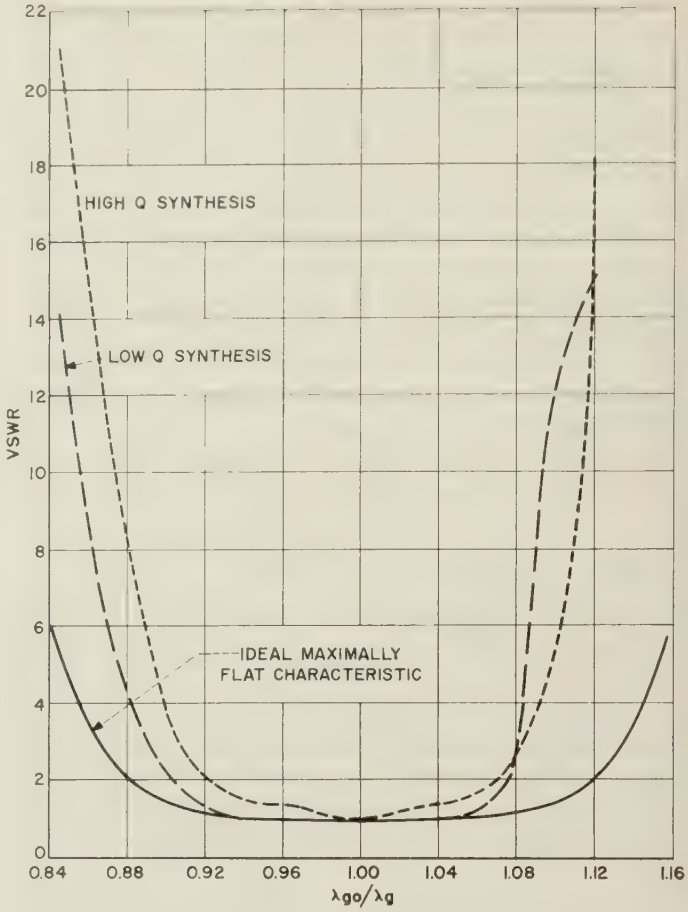

Fig. 17—Effect of use of narrow-band iris equivalents in wide-band filter synthesis.

Figs. 14–17 show the effects of the wide-band synthesis procedure.

Fig. 14 shows the nature of agreement of the voltage standing-wave-ratio characteristics of the synthesized compensated line type filter to the specified curve as a function of frequency. The deteriorating effects of the omission of susceptance compensations are shown by Fig. 15. Fig. 16 shows a comparison of the vswr characteristics of an ideal filter, designed by an unmodified Darlington procedure, to the specified vswr curve. Fig. 17 shows the effects of using an iris type direct coupled filter, designed by either the Darlington or radical factoring procedure.

Only Fig. 14 demonstrates good agreement to the specifications.

Acknowledgment

I should like to thank Dr. A. A. Oliner for his critical review and salient suggestions in the writing of this paper. I am indebted to my sister, Mrs. Ethel Maloy, for her collation of the dissertation manuscript. I also should like to express my appreciation to D. J. LeVine and J. A. Kostriza for their interest in this work.

Single Slab Arbitrary Polarization Surface Wave Structure*

ROBERT C. HANSEN†

Summary—A single grounded dielectric slab can support either TM or TE modes, but cannot propagate both with the same velocity. This paper concerns a modification of the single slab which enables either polarization to propagate with the same velocity. Such a structure could transmit a circularly polarized wave, and would be useful in transmission, feeder, and antenna applications.

The structure consists of a grounded dielectric slab with parallel metal plates imbedded in the dielectric, normal to and in contact with the ground plane. The plates do not reach the top of the slab. Propagation is *along* the plates, whereas corrugated surfaces propagate across the vanes. For small plate thickness, the TE field is undisturbed; hence, the entire slab thickness controls the velocity. The TM field, however, has an electric field component parallel to the plates, which is shorted out by the plates; thus, only the thickness of slab above the plates controls this mode, and the two modes can be independently controlled.

Since the plates are not a perfect short circuit, a boundary value analysis is given which finds the higher mode amplitudes, and the variation of effective short circuit with parameters. This analysis sets up a sum of modes in each region, and then solves the resulting sets of simultaneous transcendental equations by a contour integration-residue theory technique. The theory is illustrated by a specific example.

Introduction

SURFACE WAVE structures have received much attention in the literature during an interval of over fifty years. Most of the interest has been centered on two structures of practical importance: the corrugated metallic surface, and the dielectric surface, with or without an associated ground plane.[1,2] An excellent survey of the state of the art is given by Zucker, with 86 references.[3] Most of the surface wave antennas are of the endfire type.[4] All these structures, however, are essentially single polarization devices. The corrugated surfaces support only TM modes. A dielectric clad ground plane will support either TM or TE modes, but the propagation constants vary with the physical parameters in different fashions. It is not possible to design a single grounded dielectric slab to propagate both polarizations with the same velocity. Hence the array factors for the two polarizations differ when a given slab is used as an antenna.

In some transmission and antenna applications it is desirable to utilize surface wave structures with circular polarization. Two structures which can be designed to propagate both TM and TE surface waves with the same velocity are the two-layered dielectric slab with ground plane and the single-layer grounded slab with mode filter. The latter structure is the subject of this paper.

This structure, called the Single Slab Circular Polarization Structure, consists of a single dielectric layer on a ground plane with parallel metal plates or septa imbedded in the dielectric, normal to and in contact with the ground plane. Fig. 1 is an artist's sketch of the structure. Note that propagation is along the vanes while corrugated surfaces propagate a wave across the teeth. The TE mode has an electric field across the vanes, representing the TEM mode in a parallel plate transmission line; for small plate thickness the effect of

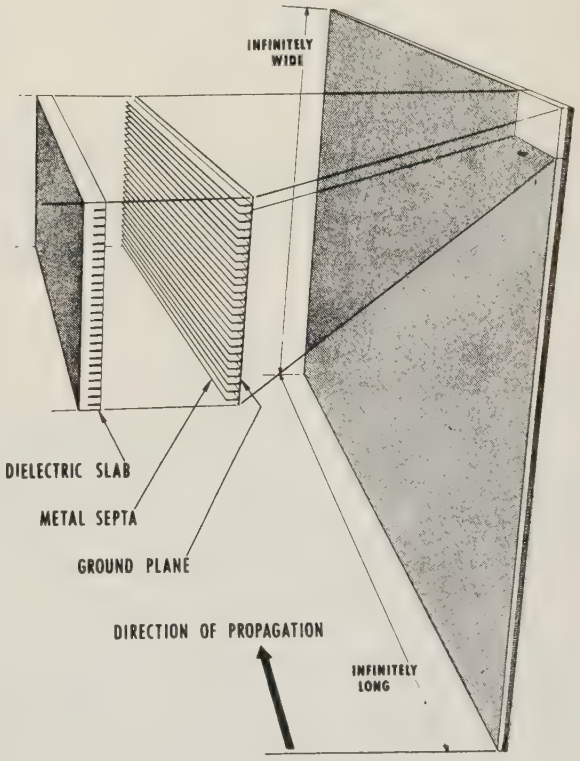

Fig. 1—Single slab arbitrary polarization structure.

* Manuscript received by the PGMTT, August 6, 1956. The work described in this paper was supported by the AF Cambridge Res. Ctr., Air Res. and Dev. Command, under Contract AF19 (604)-1317, and is an extract of Sci. Rep. No. 9, Hughes Aircraft Co., Culver City, Calif. The paper was presented at the URSI Meeting in Washington, D. C., May, 1956.

† Hughes Aircraft Co., Culver City, Calif.

[1] S. S. Attwood, "Surface wave propagation over a coated plane conductor," *J. Appl. Phys.*, vol. 22, pp. 504–509; April, 1951.

[2] R. S. Elliott, "On the theory of corrugated plane surfaces," IRE TRANS., vol. AP-2, pp. 71–81; April, 1954.

[3] F. J. Zucker, "The guiding and radiation of surface waves," *Proc. of Symp. on Modern Advances in Microwave Techniques*, Polytech. Inst. of Brooklyn, pp. 403–435; 1954.

[4] R. S. Elliott, "Pattern Shaping with Surface Wave Antennas," Tech. Memo. no. 360, Hughes Aircraft Co., March, 1955.

the plates is negligible and the entire slab controls the TE surface wave mode. For the TM mode, however, a parallel component of electric field is present. If the plates are sufficiently close together, this parallel electric field is shorted out, and the effective thickness of slab controlling the TM wave is nearly the thickness above the septa. It is the goal of this paper to determine the quantitative behavior of this effective thickness with the dimensions of the structure.

Single Grounded Slab Modes

The analysis of TM and TE surface waves on a single grounded dielectric (or permeable) slab is straightforward, and may be found in the literature.[5] Only the results are given here. If the surface wave propagation constant is β, and $k=\omega\sqrt{\mu\epsilon}$ for free space then the parameters of interest are the velocity ratio β/k and the slab thickness kc. The formulas are[5]

$$\text{TM} \qquad kc = \frac{\tan^{-1}\epsilon_1\sqrt{\dfrac{(\beta/k)^2-1}{\epsilon_1-(\beta/k)^2}}}{\sqrt{\epsilon_1-(\beta/k)^2}} \tag{1}$$

$$\text{TE} \qquad kc = \frac{\sin^{-1}\sqrt{\dfrac{\epsilon_1-(\beta/k)^2}{\epsilon_1-1}}}{\sqrt{\epsilon_1-(\beta/k)^2}}\,. \tag{2}$$

which give the thickness required for a slab of dielectric constant ϵ_1, to propagate each mode with velocity ω/β. The maximum value β/k can attain for either mode is $\sqrt{\epsilon_1}$. A typical curve of β/k vs slab thickness is Fig. 2 where it is seen that the TM mode is a dominant mode.

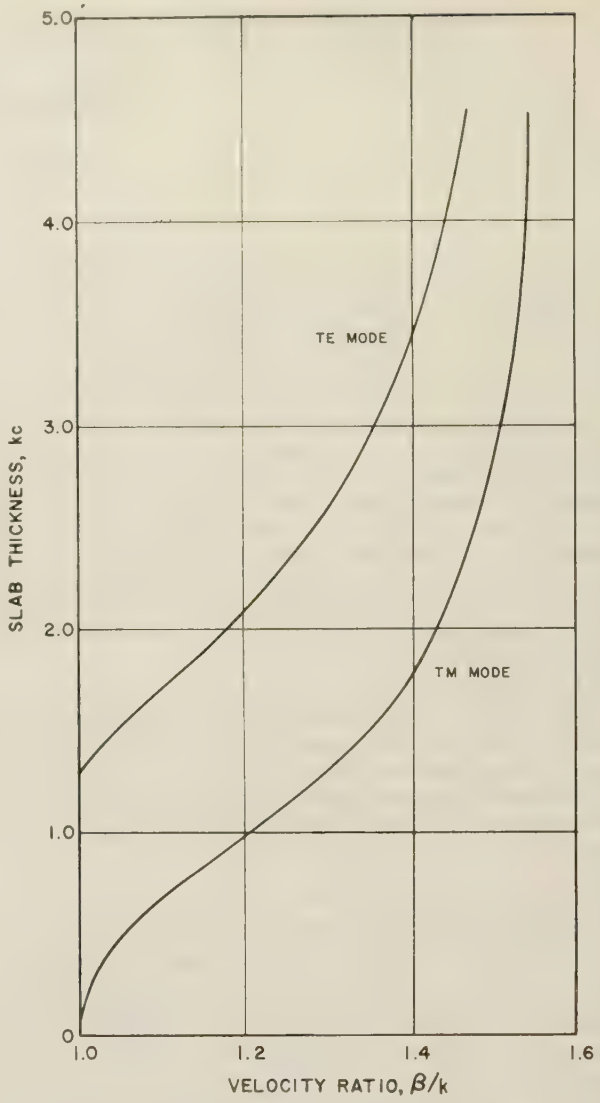

Fig. 2—Velocity ratio for a slab of $\epsilon=2.5$.

The Single Slab Arbitrary Polarization Structure

The single slab structure with septa was sketched in Fig. 1, and is shown in cross section in Fig. 3. The major effect of the septa is on the TM mode; thus this problem will be attacked. Surface waves are again the desired phenomenon; the lowest order TM mode will be assumed to propagate in the z direction as exp $(-j\beta z)$. Unlike the simple case in the section above, a single mode cannot exist either in the dielectric-air region or in the parallel plate waveguide region. Instead, each region has an infinite set of coupled modes, which satisfy boundary conditions and, of course, Maxwell's equations. Waves other than surface waves may exist on the structure, but attention here will be limited to the surface waves. The complete field in each region is written and the tangential fields at the boundaries are matched. This results in the usual infinite set of simultaneous equations in the unknown amplitudes and propagation constants. A residue theory technique is then used to solve the equations. This scheme augments the physical understanding by making explicit approximations but appears to be applicable only for plates of quite small thickness. The steps will be described briefly.

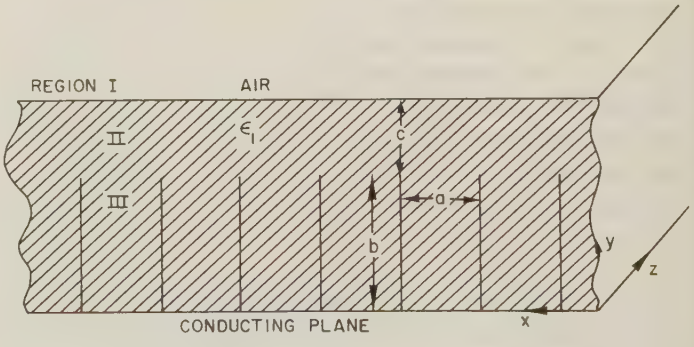

Fig. 3—Single slab structure in transverse section.

[5] Robert C. Hansen, "Single Slab Circular Polarization Surface Wave Structure," Sci. Rep. No. 9, Hughes Aircraft Co., February 14, 1956.

Field Equations in Three Regions

Except for the dominant TM mode, the field is composed of modes, transverse magnetic with respect to $\boldsymbol{y}$, derived from the scalar wave solution f:

$$\boldsymbol{E} = \frac{1}{j\omega\epsilon} \operatorname{curl} \operatorname{curl} \boldsymbol{a}_y f, \qquad \boldsymbol{H} = \operatorname{curl} \boldsymbol{a}_y f. \tag{3}$$

The reasons for using this type of field will be explained later. A y-directed unit vector is symbolized by $\boldsymbol{a}_y$. Since the parallel plate region is nonuniform in x, the higher modes will vary in x; from this variation may be deduced the y variation. Surface waves with $\exp(-j\beta z)$ are assumed. This assumption of a single propagation constant for the set of modes is valid because at each boundary the fields must match for all z. The factor $\exp(-j\beta z)$ will be suppressed throughout.

In Region II the field must be periodic in x with period a due to symmetry. The pythagorean relation forces the higher modes to be evanescent in y. Again it is stressed that propagation is parallel to the plates. Thus,

$$f = B_m \cos \frac{2m\pi x}{a} \sinh (D_m - \gamma_m y) \quad m \geq 1 \tag{4}$$

$$\epsilon_1 k^2 = \beta^2 + \left(\frac{2m\pi}{a}\right)^2 - \gamma_m{}^2. \tag{5}$$

The dominant mode is

$$\begin{aligned} E_y &= -(\beta\gamma/\omega\epsilon\epsilon_1) B \cos (D - \gamma y) \\ E_z &= -(\gamma^2/j\omega\epsilon\epsilon_1) B \sin (D - \gamma y) \\ H_x &= \gamma B \cos (D - \gamma y) \end{aligned} \tag{6}$$

where B is again the dominant mode coefficient. A device which allows this mode to be combined with the higher modes is that of replacing dominant mode coefficients by new symbols subscripted zero. Let

$$jB/\beta = B_0/\gamma_0, \quad j\gamma = \gamma_0, \quad D_0 = j(D + \pi/2). \tag{7}$$

Three of the components, which include the dominant mode, are

$$E_y = \sum_{m=0}^{\infty} \frac{B_m}{jw\epsilon\epsilon_1} \left[\left(\frac{2m\pi}{a}\right)^2 + \beta^2\right] \cos \frac{2m\pi x}{a} \cdot \sinh (D_m - \gamma_m y) \tag{8}$$

$$E_z = \sum_m (\beta\gamma_m B_m / w\epsilon\epsilon_1) \cos \frac{2m\pi x}{a} \cosh (D_m - \gamma_m y) \tag{9}$$

$$H_x = \sum_m j\beta B_m \cos \frac{2m\pi x}{a} \sinh (D_m - \gamma_m y). \tag{10}$$

In Region I, the field must have the same x variation as in Region II, and must decay exponentially in y because a surface wave contains its power in a region around the dielectric slab. Then the scalar function to use with (3) is

$$f = A_m \cos \frac{2m\pi x}{a} \exp (-\alpha_m y), \quad m \geq 1 \tag{11}$$

$$k^2 = \beta^2 + (2m\pi/a)^2 - \alpha_m{}^2. \tag{12}$$

The field is readily written from (3) and the above scalar, plus $E_y = (\alpha\beta/j\omega\epsilon) \exp(-\alpha y)$, $E_z = (-\alpha^2/j\omega\epsilon) \exp(-\alpha y)$, $H_x = -\alpha \exp(-\alpha y)$. At the dielectric-air boundary ($y = b + c$) this field must be continuous with the corresponding field in Region II, for all x and z. Orthogonality in x allows individual terms to be equated. In this problem it is possible to match all the tangential components only if the fields are transverse with respect to y, although it is natural to expect the higher modes to be derived from a z-directed Hertzian vector. The y direction represents a virtual direction of propagation. Later it will be seen that the waveguide region needs a TM field to match the dominant mode E_y in Region II; to match the guide field, a TM field is needed here. At $y = b + c$, matching gives two equations which are solved to yield

$$\gamma_m \coth [D_m - \gamma_m(b + c)] = \epsilon_1 \alpha_m \tag{13}$$

so for $m \geq 1$ the condition $D_m > \gamma_m(b + c)$ must be valid. For $m = 0$, the equation reduces to the analogous form of the equation for the single slab

$$\gamma \tan [\gamma(b + c) - D] = \epsilon_1 \alpha. \tag{14}$$

If D were known, then this equation would allow γ to be calculated.

For Region III, the parallel plate waveguide region, the field is obtained from

$$f = C_n \sin \frac{n\pi x}{a} \cosh \delta_n y \tag{15}$$

$$\epsilon_1 k^2 = \beta^2 + (n\pi/a)^2 - \delta_n{}^2 \tag{16}$$

which gives a field, TM with respect to the y direction, and represents waves originating at the discontinuity (cell mouth) and traveling in the y direction. Since $\sqrt{\epsilon_1} ka < \pi$, *all modes* are evanescent. Again the "propation" factor $\exp(-j\beta z)$ has been deleted for brevity.

The Approximate Physical Situation

To make the problem amenable to attack, the septa are assumed to be vanishingly thin. This assumption is reasonable physically as it is desirable to construct thin septa to avoid disturbing the TE surface wave. A second assumption neglects the reflected evanescent modes in the waveguide region. That is, the wave is attenuated so greatly in traveling from the guide mouth down to the guide end (ground plane) and back that the portion coming back can be discarded. From the equations to be given shortly it may be ascertained that the nth wave is attenuated by

$$\exp(-n\pi b/a)$$

in traversing the guide. For all practical designs, $b>a$ so even for $n=1$ the reflected wave is negligible.

The field will thus be approximated; the important components are

$$E_y = \sum_{n=1}^{\infty} \frac{C_n}{jw\epsilon\epsilon_1}\left[\left(\frac{n\pi}{a}\right)^2 + \beta^2\right] \sin\frac{n\pi x}{a} \exp(\delta_n y) \tag{17}$$

$$E_z = \sum_{n} -(\beta\delta_n C_n/w\epsilon\epsilon_1) \sin\frac{n\pi x}{a} \exp(\delta_n y) \tag{18}$$

$$H_x = \sum_{n} j\beta C_n \sin\frac{n\pi x}{a} \exp(\delta_n y) \tag{19}$$

Next this waveguide field is matched to the field in Region II, at the mouth of one parallel plate "cell," $y=b$. Only E_y, E_z, and H_x need be written.

$$\sum_{n=1}^{\infty} \frac{C_n}{jw\epsilon\epsilon_1}(\epsilon_1 k^2 + \delta_n^2) \sin\frac{n\pi x}{a} e^{\delta_n b}$$

$$= \sum_{m=0}^{\infty} \frac{B_m}{jw\epsilon\epsilon_1}(\epsilon_1 k^2 + \gamma_m^2) \cos\frac{2m\pi x}{a} \sinh\lfloor D_m - \gamma_m b\rfloor \tag{20}$$

$$\sum_{n} \frac{-\beta\delta_n C_n}{w\epsilon\epsilon_1} \sin\frac{n\pi x}{a} e^{\delta_n b}$$

$$= \sum_{m} \frac{\beta\gamma_m B_m}{w\epsilon\epsilon_1} \cos\frac{2m\pi x}{a} \cosh[D_m - \gamma_m b] \tag{21}$$

$$\sum_{n} j\beta C_n \sin\frac{n\pi x}{a} e^{\delta_n b}$$

$$= \sum_{m} j\beta B_m \cos\frac{2m\pi x}{a} \sinh[D_m - \gamma_m b]. \tag{22}$$

These equations are the usual infinite simultaneous equations obtained in boundary value problems. Next multiply (22) by $k^2/\beta\omega\epsilon$ and add it to (20) to give a new equation which, when simplified, is

$$\sum_{n} \delta_n^2 C_n \sin\frac{n\pi x}{a} e^{\delta_n b}$$

$$= \sum_{m} \gamma_m^2 B_m \cos\frac{2m\pi x}{a} \sinh[D_m - \gamma_m b]. \tag{23}$$

This equation and (21) will be used to obtain a solution. The right-hand side of each may be reduced to a single term due to the cosine orthogonality by multiplying each equation by $\cos 2q\pi x/a$ and integrating from **0** to ***a***. Since the resulting series in n is not uniformly convergent, one may question the validity of term by term integration. The result is, however, correct as may be shown by a Green's theorem argument.[6] The n series is not orthogonal to $\cos 2q\pi x/a$, and an integral formula (Dwight 465) must be used. So (23) and (21) become

$$(\pi\gamma_q^2 B_q/2\epsilon_q) \sinh(D_q - \gamma_q b) = \sum_{\substack{n=1\\ \text{odd}}}^{\infty} \frac{n\delta_n^2 C_n \exp(\delta_n b)}{n^2 - 4q^2} \tag{24}$$

$$(\pi\gamma_q B_q/2\epsilon_q) \cosh(D_q - \gamma_q b) = \sum_{\substack{n=1\\ \text{odd}}}^{\infty} \frac{-n\delta_n C_n \exp(\delta_n b)}{n^2 - 4q^2} \tag{25}$$

with ϵ_q the Neumann number,[7]

$$\epsilon_q = \begin{cases} 2 & q > 0 \\ 1 & q = 0. \end{cases}$$

Note that for n even, $C_n \equiv 0$. The pair of equations is not yet in the proper form; two simple manipulations are needed.

$$\text{Insert } n^2 - 4q^2 = \left(\frac{a}{\pi}\right)^2 (\delta_n^2 - \gamma_q^2)$$

and multiply the second equation by γ_q, and add and subtract to the first equation of the pair with the result

$$(\gamma_q^2 a^2 B_q/2\pi\epsilon_q) \exp(D_q - \gamma_q b) = \sum_{\substack{n=1\\ \text{odd}}}^{\infty} \frac{n\delta_n C_n \exp(\delta_n b)}{\delta_n + \gamma_q} \quad q = 0, 1, 2, \cdots \tag{26}$$

$$(\gamma_q^2 a^2 B_q/2\pi\epsilon_q) \exp(-D_q + \gamma_q b) = \sum_{n} \frac{-n\delta_n C_n \exp(\delta_n b)}{\delta_n - \gamma_q}. \tag{27}$$

For $q>0$ the $\exp(-D_q+\gamma_q b)$ represents an attenuated wave, a higher order evanescent wave which is reflected from the virtual ground plane at $y=b$. The amplitudes of these higher order reflected waves are small, and they will be neglected. Thus (27) is approximated by

$$(1/2\pi)\delta_{q0}\gamma_0^2 a^2 B_0 \exp(-D_0 + \gamma_0 b) = \sum_{\substack{n=1\\ \text{odd}}}^{\infty} \frac{-n\delta_n C_n \exp(\delta_n b)}{\delta_n - \gamma_q} \quad q = 0, 1, 2, \cdots. \tag{28}$$

The two infinite sets of simultaneous equations, (26) and (28), are a good physical approximation to the problem and need to be solved for the coefficients B_q and C_n and wave numbers δ_1 and γ_0. These equations will be solved exactly by function-theoretic methods.

The Contour Integral Solution

A contour integral is written whose residues form the terms of the series in (28). Then if the integral can be uniquely and explicitly determined, the solution is immediate. This method has been used with appreciable

[6] E. A. N. Whitehead, "Theory of Parallel Plate Media for Microwave Lenses," *Proc. I.E.E.*, vol. 98, pt. III, pp. 133–140; 1951.

[7] G. N. Watson, "Bessel Functions," Cambridge University Press, Cambridge, Eng., p. 22; 1952.

success by Hurd[8,9] Whitehead,[6] and others.[10–12] It is especially valuable for problems involving a semi-infinite region and for these cases can include one reflected wave on each side of the boundary. A general discussion of the function-theoretic method is given by Karp.[13]

Consider a complex function $f(w)$ which

1) has simple poles at δ_n, $n=1, 3, 5, \cdots$
2) has simple zeros at γ_q, $q=1, 2, 3, \cdots$
3) is elsewhere absolutely convergent in the strict sense
4) tends uniformly to zero as $|w| \to \infty$
5) obeys edge conditions.

Then by choosing a set of contours of increasingly large radius, selected to avoid the poles,[10]

$$\int_C \frac{f(w)dw}{w-\gamma_q} = \delta_{q0} f(\gamma_0) + \sum_{\substack{n=1 \\ \text{odd}}}^{\infty} \frac{R(\delta_n)}{\delta_n - \gamma_q} = 0 \quad (29)$$

where $R(\delta_n)$ is the residue of $f(w)$ at $w=\delta_n$.

If the function satisfies the above conditions, it is unique; hence (28) can be compared directly with (29), and it is found that

$$(1/2\pi)\gamma_0^2 a^2 B_0 \exp(-D_0 + \gamma_0 b) = f(\gamma_0) \quad (30)$$

$$n\delta_n C_n \exp(\delta_n b) = R(\delta_n). \quad (31)$$

Similarly

$$\int_C \frac{f(w)dw}{w+\gamma_q} = f(-\gamma_q) + \sum_{\substack{n=1 \\ \text{odd}}}^{\infty} \frac{R(\delta_n)}{\delta_n + \gamma_q} = 0 \quad (32)$$

which when compared with the set (26) gives the same formula for C_n and in addition

$$(-\gamma_q^2 a^2 B_q/2\pi\epsilon_q) \exp(D_q - \gamma_q b) = f(-\gamma_q). \quad (33)$$

Now by comparing (30) and (33) for $q=0$, a key equation is obtained:

$$-f(\gamma_0) = \exp(-2D_0 + 2\gamma_0 b) f(-\gamma_0). \quad (34)$$

This determinantal equation relates γ_0 and D_0.

To summarize, if the correct $f(w)$ were known, the mode amplitudes would be given directly by (31) and (33) and the determinantal equation would give γ_0 in terms of D_0. The next task is to construct the correct function. To this end two infinite products which display the needed zeros are defined.

$$\Pi_1(w) = \prod_{p=1}^{\infty} (w - \gamma_p)(-a/2p\pi) \exp(aw/2p\pi) \quad (35)$$

$$\Pi_2(w) = \prod_{\substack{p=1 \\ \text{odd}}}^{\infty} (w - \delta_p)(-a/p\pi) \exp(aw/p\pi). \quad (36)$$

It will appear below that the exponential factors make the products strictly convergent. Then if $g(w)$ is an entire function with $g(\gamma_0)=1$,

$$f(w) = g(w) \frac{B_0\gamma_0^2 a^2 \exp(-D_0 + \gamma_0 b)\Pi_1(w)\Pi_2(\gamma_0)}{2\pi\Pi_1(\gamma_0)\Pi_2(w)} \quad (37)$$

which contains the proper zeros and poles and also satisfies (30). The investigation of the asymptotic behavior of $f(w)$ is given in reference 5 and the $g(w)$ is determined from the edge conditions[14] in the same place. For $p>1$

$$\delta_p \simeq p\pi/a, \qquad \gamma_p \simeq 2p\pi/a$$

so that

$$\Pi_1(w) \simeq \prod_{p=1}^{\infty} [1 - aw/2p\pi] \exp(aw/2p\pi) \quad (38)$$

which is absolutely convergent for all w by Example 1 in Whittaker and Watson.[15] Similarly for Π_2. From Hansen,[5]

$$g(w) = \exp[(w - \gamma_0)a \ln 2/\pi]. \quad (39)$$

The determinantal (34) can now be solved for D in terms of γ_0. Inserting values for $f(\gamma_0)$ and $f(-\gamma_0)$ and solving for D gives the form

$$D = \gamma(b - a \ln 2/\pi) + (1/2j) \ln \frac{\Pi_1(-j\gamma)\Pi_2(j\gamma)}{\Pi_1(j\gamma)\Pi_2(-j\gamma)} \quad (40)$$

where the original γ is now used.

Note that no approximations were made here. Simplifying the last term yields the relationship between D and

$$D = \gamma(b - a \ln 2/\pi) + \sum_{p=1}^{\infty} (-1)^p \left[\sin^{-1}\frac{a\gamma}{p\pi} - \frac{a\gamma}{p\pi}\right]. \quad (41)$$

For most cases, $\gamma a/\pi \ll 1$. Then

$$D \simeq \gamma(b - a \ln 2/\pi) - (1/6)(\gamma a/\pi)^3. \quad (42)$$

This expression is the desired relationship among D, γ, and a. Note that b is not involved due to the neglect

[8] R. A. Hurd, "Propagation of an electromagnetic wave along an infinite corrugated surface," *Can. J. Phys.*, vol. 32, pp. 727–734; December, 1954.
[9] R. A. Hurd and H. Gruenberg, "H-plane bifurcation of rectangular waveguide," *Can. J. Phys.*, vol. 32, pp. 694–701; November, 1954.
[10] Z. Szekely, "Junction of Two Rectangular Waveguides," M. S. Thesis, Dept of Elec. Eng., Univ. of Toronto; May, 1953.
[11] L. Brillouin, "Wave guides for slow waves," *J. Appl. Phys.*, vol. 19, pp. 1023–1041; November, 1948.
[12] F. Berz, "Reflection and refraction of microwaves at a set of parallel metallic plates," *Proc. I.E.E.*, vol. 98, pt. III, pp. 47–55; 1951.
[13] S. N. Karp, "An Application of Sturm-Liouville Theory to a Class of Two-Part Boundary Value Problems," Rep. BR-13, New York Univ., New York, N. Y., August, 1955.
[14] The field must be singular in the proper manner at the septa edges.
[15] E. T. Whittaker and G. N. Watson, "Modern Analysis," Cambridge University Press, Cambridge, Eng., p. 34, 1952.

of evanescent reflected waves in the waveguide region. Result (42) is inserted into (14) to give the final transcendental equation determining γ. This equation is

$$\gamma c \tan [\gamma(c + a \ln 2/\pi) + (1/6)(\gamma a/\pi)^3] = \epsilon_1 \alpha c. \quad (43)$$

The equation can be solved by a perturbation scheme, first finding γ without the cubic correction term, then using this value in the complete equation and calculating a more correct γ. It is found that the cubic term has negligible effect for all γa where the theory is valid. Thus an excellent approximation to (43) is

$$\gamma c \tan \gamma(c + a \ln 2/\pi) = \epsilon_1 \alpha c \quad (44)$$

and the "effective height" c^* is given very simply by

$$c^* = c + a \ln 2/\pi. \quad (45)$$

An example, which will be of use later, has been chosen. In this example $\epsilon_1 = 4$ and $kc = 0.379$ which would yield a β/k of 1.05 if the slab were placed directly on the ground plane. Fig. 4 contains a plot of β/k vs plate

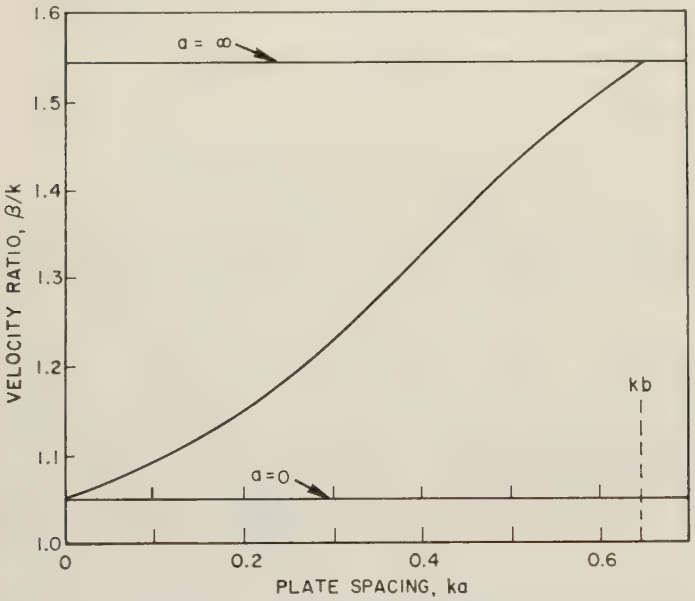

Fig. 4—Variation of propagation constant with septum spacing ka.

spacing for the example. When the plate spacing a becomes comparable with the plate height b, the evanescent modes which were not accounted for in the theory become important. This fact is observed in the graph, as the true β/k can never exceed the value produced by the entire slab thickness, regardless of plate spacing. That the theory did not allow for reflected modes higher than the first in Region II (above the plates) is an important fact because in practice b will usually be greater than a, but c will be less than a.

The effective height c^* obtained is, except for the cubic correction term, just that obtained from the electrostatic problem of a semi-infinite capacitor. Fringing of the field between the inner and outer plates is equivalent[16] to adding a section of plate, with uniform field, of length $(a \ln 2/\pi)$. The virtues of the function-theoretic approach are that it indicates exactly what approximations are used to obtain an answer and that the mode amplitudes can be calculated. Mode amplitudes have been calculated[5] for the example quoted; Table I compares the higher mode amplitudes to the

TABLE I
Amplitude Ratios at Interface

m	Ratio at Interface	Ratio at Cell Mouths
1	0.032	0.208
2	0.0015	0.0780
3	0.00010	0.0435
4	0.000009	0.0284

dominant mode amplitude at the dielectric-air interface, and at the cell mouths. The dominant mode in the dielectric of Region II originates at the interface and decays exponentially toward the waveguide cells. On the other hand, the higher order modes in the same region originate at the cell mouths, where they are needed to match the boundary conditions, and decay toward the interface. Hence Table I indicates that the *higher modes are insignificant at the interface but appreciable at the cell mouths.*

Conclusion

The Single Slab Arbitrary Polarization Structure is a practical structure which should find use in surface wave antennas and other devices. Finite spacing of the plates lowers the effective short circuit plane by an amount proportional to the plate spacing. This fact and the data presented allow a structure to be designed for a desired β/k ratio. The function-theoretic technique used also divulged the mode amplitudes in each region. In the parallel plate guide and just above the guides appreciable quantities of higher modes exist. At the trapping interface, higher order modes are negligible; thus this structure would not degrade the performance of an antenna.

A more precise theory will need to be cognizant of reflected evanescent waves in the dielectric region.

[16] W. R. Smythe, "Static and Dynamic Electricity," McGraw-Hill Book Co., Inc., New York, N. Y., p. 103, 1939. See prob. 26.

Attention is called to the following two papers, one by R. K. Moore, the other by W. L. Pritchard and J. A. Mullen. Since the papers are very closely related, the objection might arise that either one or the other should be published, but not both. However, the editorial board felt that both papers are deserving of considerable credit, and indeed the subject itself is of great interest, not only to microwave people, but to systems people as well.

Furthermore, although Mr. Moore's paper was received by the Editor of these TRANSACTIONS on August 7, 1956, whereas Messrs. Pritchard and Mullen's paper was not received until October 1, 1956, it is only fair to point out that the latter paper had been submitted to the Editor of PROCEEDINGS some time prior to September of last year.—*The Editor*

The Effects of Reflections from Randomly Spaced Discontinuities in Transmission Lines*

RICHARD K. MOORE†

Summary—**Reflections from randomly spaced transmission line discontinuities can cause serious attenuation and distortion of pulses in the lines, and the presence of reflections at the sending end may be undesirable. The effect of these discontinuities may be described in terms of the mathematics for combining outputs from oscillators with random frequencies. The location of the discontinuity corresponds to the frequency of an oscillator. The phase constant of the transmission line is analogous to time for the oscillators. Use of spectrum and filter analogies permits approximate determination of discontinuity locations from measurements. Use of known space and size distributions permits statistical prediction of attenuation and of size of reflected wave at the sending end.**

TRANSMISSION lines often contain small discontinuities which may affect their operation—either by causing undesired reflections at the input, or by increasing the attenuation over that which would be present without the discontinuities.[1–4] These discontinuities may be regularly spaced due to such things as beads supporting center conductors for coaxial transmission lines, couplings between individual sections of waveguide, or bends associated with the way in which a coaxial line was rolled up during storage. On the other hand, they may be randomly spaced due to such things as random breakage during manufacture, dents in outer conductors of solid coaxial lines or in waveguide, random migration of the center conductor in coaxial lines, either flexible or solid, and pinching of a coaxial line by various causes. In this paper, expressions are developed for the additional attenuation and reflection due to randomly spaced small discontinuities.

For randomly spaced discontinuities, a statistical relation has been established between the reflection or attenuation-vs-frequency curve and the spacing of discontinuities. It is shown that the mathematics for reflections from randomly spaced discontinuities is the same as that for the combination of large numbers of oscillators with random frequencies. The technique of analysis used to obtain the frequency spectrum for the oscillators has been used here to locate the discontinuities. Our analogy compares the frequency of the individual oscillator with the coordinate (on the transmission line) of the individual discontinuity. The time variable, in the case of oscillators, is analogous to the phase constant of the transmission line.

The methods shown may be used to calculate the effects of discontinuities on attenuation and reflection if the sizes and magnitude of the discontinuities are known. They may also be used to ascertain, as nearly as possible, the size and location of discontinuities by using a measurement of the attenuation or reflection as a function of frequency. Because this measurement may be made over only a limited range of frequencies in any practical case, the exact location and number of discontinuities cannot be specified. Rather, a spectrum may be specified which gives the best idea as to the size and location of discontinuities which can be obtained with any specified frequency range for the measurement.

Fig. 1 represents a cable with discontinuities spaced a distance Δx_i apart along its entire length. The reflec-

* Manuscript received by the PGMTT, August 7, 1956. This work was done while the author was a consultant to Sandia Corp., Albuquerque, N. M.

† Elec. Eng. Dept., University of New Mexico, Albuquerque, N. M.

[1] D. A. Alsberg, "More on the sweep-frequency response of RG/6U cable," PROC. IRE, vol. 41, p. 936; July, 1953.

[2] W. T. Blackband, "The sweep-frequency response of RG/6U," PROC. IRE, vol. 40, pp. 995–996; August, 1952.

[3] D. A. Alsberg, "A precise sweep-frequency method of vector impedance measurement," PROC. IRE, vol. 49, pp. 1393–1400; November, 1951.

[4] W. T. Blackband and D. R. Brown, "The two-point method of measuring characteristic impedance and attenuation of cables at 3,000 mc," *J. IEE*, vol. 93, Part IIIA, pp. 1383–1386; September, 1946.

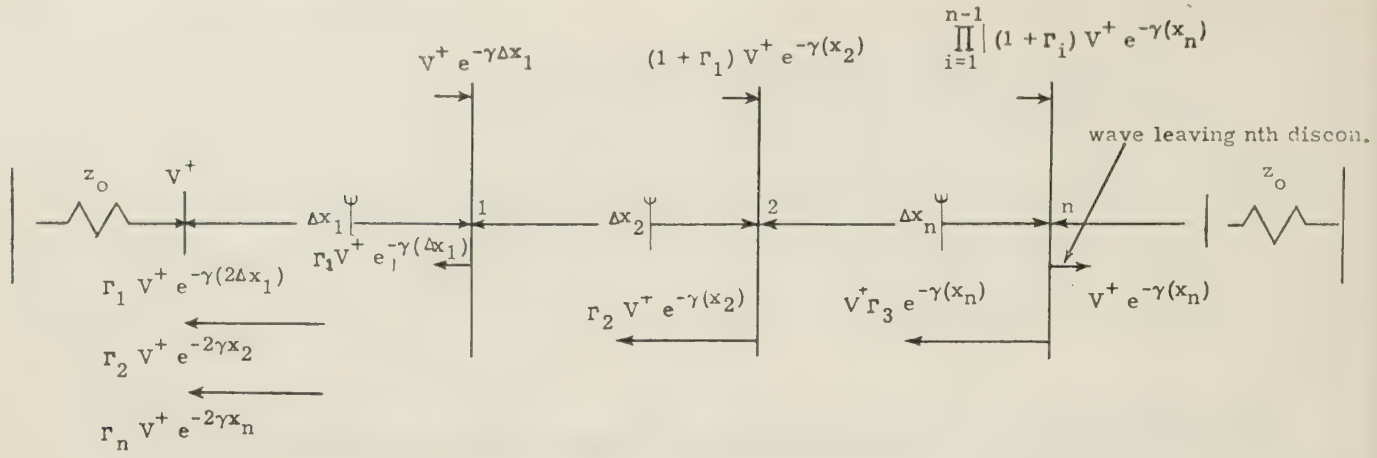

Fig. 1.

tion coefficient Γ_i for voltage is assumed to be small so that only first-order reflections need be considered; *i.e.*, $|\Gamma_i| \ll 1$.

In the figure and subsequent discussion,

V^+ = incident input;
V^- = reflected wave at input;
V_i = total input = $V^+ + V^-$;
V_t = total output;
$\gamma = \alpha + j\beta$, the propagation constant;
L = line length;
n = index of discontinuities;
N = total number of discontinuities;
Γ = voltage reflection coefficient.

The voltage reflected back to the origin of the line is given, in the notation of this paper, by

$$V^- = \sum_{n=1}^{N} (V^+ e^{-\alpha x_n} \Gamma_n e^{-j\beta x_n})(e^{-\alpha x_n} e^{-j\beta x_n}). \tag{1}$$

Here, the coordinate of the nth reflecting discontinuity is given by x_n. This equation is made up in the following manner. The first bracket represents the magnitude and phase of the reflected wave at the nth discontinuity. The magnitude of the incident wave at the origin is given by V^+. The first exponential gives the effect of attenuation on the line from the origin to the point of discontinuity. Γ_n represents the magnitude of the voltage reflection coefficient, and the second exponential term represents the phase shift down the line from the origin to the nth discontinuity. The expression in the second bracket shows the additional effect of transmitting this wave from the reflection point back to the origin, with both phase and amplitude terms. In this equation only first-order reflections are considered. If $|\Gamma|$ is large enough, second-order effects may be significant; so the analysis here only applies to small $|\Gamma|$.

Note also that the effect on the transmitted wave has been neglected. In Fig. 1, this effect is shown at the top but not at the bottom.

To simplify the form of this expression for calculating the probable amplitude of the reflected wave, the attenuation factors and the reflection coefficients have been combined in one symbol, A, and the two phase factors have also been combined. The result is given by

$$V^- = V^+ \sum_{n=1}^{N} A_n e^{-j2\beta x_n}. \tag{2}$$

If we assume random spacing for the discontinuities so that the principal value of the phase term $(2\beta x_n)$ may with equal likelihood take on any value between zero and 2π, then we may treat the resulting sum in the same way that one would treat the result of combining the outputs of a large number of oscillators having frequency $2x_n$ and time variation as $(-\beta)$.

When the conditions stated in the preceding paragraphs are met, whether it be for reflections from randomly spaced discontinuities or for waves from oscillators of various frequencies, the mean square value of the resultant vector obtained by summing up all the components is given by the sum of the squares of the various component vectors. This is indicated by

$$\overline{|V^-|^2} = (V^+)^2 \sum_{n=1}^{N} A_n^2. \tag{3}$$

For time variations, rather than variations with β, this is the same as saying the average power resulting from a large number of waves of different fre quencies is equal to the sum of the power contained in the various waves. This is a well-known phenomenon and applies even though the waves are harmonically related.

Eq. (3) is an average over β, the phase propagation constant. If will be recognized that, for the transverse electromagnetic mode, β varies only as the first power of frequency and, therefore, this may also be considered as an average over frequency; thus, it might be measured by making measurements at a large number of frequencies and averaging them. In a waveguide, of course, or in an inhomogeneous medium, β may vary

with some other parameter besides frequency or may vary with frequency in a more complex manner than a straight linear variation.

If one is to utilize measurements of the reflected wave or transmitted wave to determine an average discontinuity, or conversely, if one is to use an average value of discontinuity to determine the reflected voltage or transmitted voltage, it is necessary to separate the effect of the reflection coefficient from the attenuation in the line. If there is no relationship between the individual reflection coefficients and their position on the line, that is, if their variations about the average reflection coefficient are random and independent of location, one may assume

$$A_n = \overline{\Gamma} e^{-2\alpha x_n}, \tag{4}$$

where $\overline{\Gamma}$ represents the mean value of the reflection coefficient. The assumption of random distribution of the coordinates x_n means that

$$\text{Prob}\,(x < x_n < x + dx) = \frac{dx}{L}, \tag{5}$$

that is, the probability of finding x_n in any interval dx for a line of length L is the length of the interval divided by the total length of the line.

Utilizing this probability, one may compute the expected value for the mean square voltage as given by (3) by use of the relation

$$E\left(\sum_{n=1}^{N} A_n^2\right) = N\int_0^L (\overline{\Gamma})^2 e^{-4\alpha x}\,\frac{dx}{L} = N\overline{A^2}. \tag{6}$$

It should be noted that this represents propagation continuously down the transmission line; that is, the entire length of the line is illuminated at any one time.

Eq. (6) defines a mean square value of A which can be used in analysis of the performance of lines from measurements or in prediction of their performance based upon knowledge of discontinuities and their location. The result is given by

$$\overline{|V^-|^2} = (V^+)^2\,\frac{N\overline{\Gamma}^2}{4\alpha L}\,(1 - e^{-4\alpha L}). \tag{7}$$

From this we can see that the magnitude of the reflected root-mean-square voltage is given by

$$V_a^- = (\overline{|V^-|^2})^{1/2} = V^+\overline{\Gamma}\sqrt{\frac{N(1-e^{-4\alpha L})}{4\alpha L}}. \tag{8}$$

The input voltage to the line is the sum of the incident and reflected voltages, as measured at the input. For the case discussed above, the input voltage is, therefore, given by

$$V_i = V^+\left(1 + \frac{|V^-|}{V^+}\,e^{j\phi}\right), \tag{9}$$

where ϕ is the phase angle of V^-.

The relationship of the phase of the reflected wave to that of the transmitted wave is important in determining the magnitude of the input voltage. The phase angle may take on with equal likelihood any value between zero and 2π, hence

$$\text{Prob}\,(\phi < \phi_n < \phi + d\phi) = \frac{d\phi}{2\pi}. \tag{10}$$

It should be noted that the reflected voltage has a magnitude which is known only statistically for any given β. Its variation is the same as that for the magnitude of a white noise voltage since (2) indicates that the same representation may be used for reflected voltage, with β as the variable, as is used for noise voltage where time is the variable.

The distribution function for the reflected voltage is called the Rayleigh distribution if the total number of terms in the sum of (2) approaches infinity. The Rayleigh distribution is the result of an infinite-step random walk in a plane, and this is a well-known problem of statistics. It is readily seen upon examination of the distribution functions for Rayleigh and for finite random walks that, at least in the case where all steps are equal in length, a five-step random walk gives essentially the same distribution curve, except in the extreme limits, as an infinite number of steps would give. Since, in general, one is interested here in the situation in which there is a fairly large number of discontinuities, one may without large error replace the distribution for the resultant voltage with a finite number of discontinuities by the equivalent Rayleigh distribution. The result of doing this is shown by

$$\text{Prob}\,(V < |V^-| < V + dV) = \frac{2V}{N\overline{A^2}}\,e^{-V^2/N\overline{A^2}}dV. \tag{11}$$

The distribution of V^- [or $(|V^-|/V^+)e^{j\phi}$ of (5)] is a two-dimensional one given by

$$P(V^-)dVd\phi = \frac{1}{2\pi}\,P(|V^-|)dVd\phi. \tag{12}$$

Hence

$$P\left(\frac{V_i}{V^+}\right) = P\left[\left(1 + \frac{|V^-|\,e^{j\phi}}{V^+}\right)\right]. \tag{13}$$

It should be noted that this is identical statistically to the problem of the combination of a large steady signal and a Rayleigh distributed signal.[5] The resulting distribution function for the magnitude, converted from Rice's notation to ours, is given by

[5] S. O. Rice, "Mathematical analysis of random noise," *Bell Sys. Tech. J.*, vol. 23, pp. 282–332; July, 1944, and vol. 24, pp. 46–156; January, 1945.

$$P\left(\frac{V_i}{V^+}\right) = \frac{|V_i|}{V^+}\sqrt{\frac{2}{N\bar{A}^2}} \cdot \exp\left[-\frac{1+\left(\frac{|V_i|}{V^+}\right)^2}{N\bar{A}^2}\right] I_0\left(\frac{2|V_i|}{V^+N\bar{A}^2}\right), \quad (14)$$

where I_0 is the Bessel function of the first kind with imaginary argument. One may use this expression to calculate the probable loss in the transmission line. The ratio of output to input voltage of the line is given by

$$\text{Loss} = \left|\frac{V_t}{V_i}\right| = \left|\frac{V_t/V^+}{V_i/V^+}\right| = R. \quad (15)$$

The distribution for loss may be obtained from (14) by use of the identity from probability theory

$$P(x) = Q(y)\left|\frac{dy}{dx}\right| .$$

If we assume that V_t does not vary with β (to a first-order approximation), the resultant loss distribution is given by

$$Q(R) = R^2\frac{P\left(\frac{|V_i|}{V^+}\right)}{|V_t|/V^+} = \frac{R^2P\left(\frac{|V_t|}{V^+R}\right)}{|V_t|/V^+} . \quad (16)$$

Curves of $P(|V_i|/V^+)$ are given by Rice and others so that this probability may be readily plotted. Utilizing results which may be derived for V_t, we have

$$Q(R) = \frac{R^2P\left[\frac{(1+\bar{\Gamma})^Ne^{-\alpha L}}{R}\right]}{(1+\Gamma)^Ne^{-\alpha L}} = \text{Prob}\,[R < \text{Loss} < R + dR]. \quad (16a)$$

Eqs. (11) and (16a) give the probability of any amplitude of reflection or loss, respectively. Thus, if one is interested in the reflected signal, he may use (11) to find the probability of it taking on any value; and if one is interested in the attenuation to a transmitted wave, he may use (16a).

Normally, one would not be interested in a reflection if the wave filled the entire line as the case of a continuous wave. On the other hand, if a short pulse were transmitted down the line, only a portion of the line would be illuminated at any given time and a reflected signal would occur after the end of the transmitted pulse which might have some deleterious or desirable effect on equipment located at the transmitting point. When the short pulse is used, the integral of (6) must be carried out over the limits of the illuminated region as indicated in

$$E\left(\sum_{N=1}^{M} A_n^2\right) = M\int_{c(t-\tau)/2}^{ct/2} (\bar{\Gamma})^2e^{-4\alpha x}\,\frac{dx}{(c\tau/2)} \quad (16b)$$

where M is the number of discontinuities illuminated, t is the time from start of transmission of the pulse, τ is the pulse length, and all the other quantities are the same as in (6).

The illumination of the line is illustrated in Fig. 2. At a given time during transmission of the pulse the illumination is as indicated in Fig. 2(a), but the portion contributing to the reflection at that time is shown in Fig. 2(c). Since the reflected wave must travel down and back, only the illuminated region corresponding to a *round-trip* time t will contribute. This has the same effect as if the transmission velocity were halved in the line, insofar as reflected waves are concerned. Figs. 2(b) and 2(d) show the situation where the end of the pulse has occurred (16b).

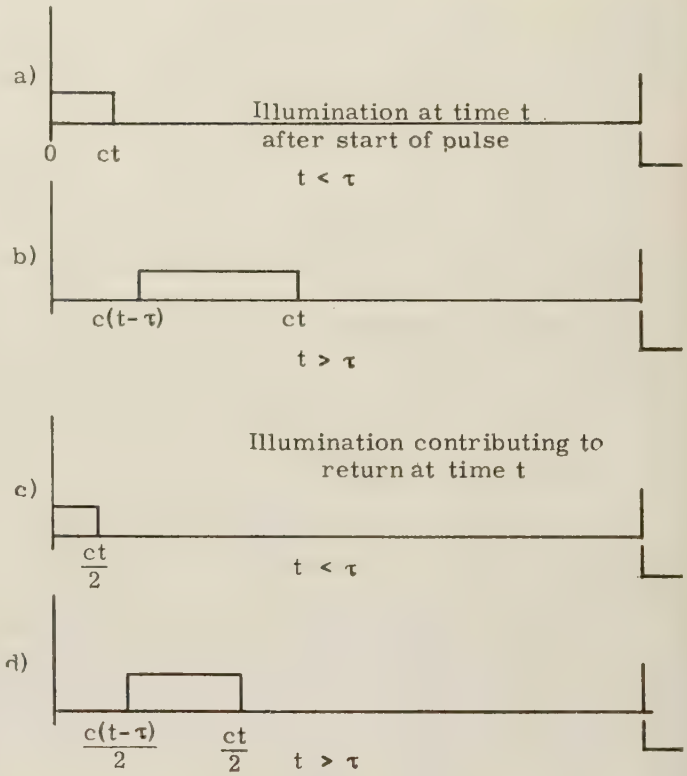

Fig. 2.

When this situation prevails, the effect of the reflected wave on the total loss is noted as a reduction in amplitude plus an effect on V_i, similar to that involved in derivation of (16), in which the reflections which occur during transmission of the pulse are the only ones which are significant. Thus, in such a case, the integration for determining V_i modification would have to be carried out no further than from zero to $\frac{1}{2}$ pulse length along the line. The transmitted pulse would be distorted at different points by an amount determined by carrying this integration to an appropriate upper limit.

Information about the spacing, magnitude, and location of the discontinuities in the line can be found by

studying the magnitude of the reflected wave as a function of β. In the succeeding development, it will be assumed that one is actually measuring the amplitude of the reflected wave. This can be done by using a pulse to excite a portion of the line, or it can be done by going backwards through the development which results in (16).

Consider the reflected wave as a function of β as indicated in

$$A(\beta) = \left| \sum_{n=1}^{N} A_n e^{-j2x_n\beta} \right|. \tag{17}$$

This is a quantity which may be measured, provided one knows the magnitude of the incident pulse. The autocorrelation vs β of such a measured function may be calculated; (β would be varied by varying frequency). The autocorrelation is given by

$$B(\beta) = \lim_{F\to\infty} \int_0^F |A(b)|\,|A(b+\beta)|\,db. \tag{18}$$

By itself the autocorrelation has no particular significance in this case since we are really interested in the space variation, not β variation. Typical examples of $A(\beta)$ and $B(\beta)$ are shown in Fig. 3.

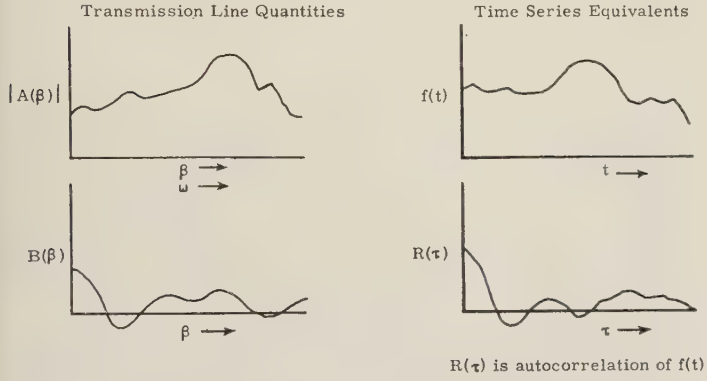

Fig. 3—Reflected wave functions and their time series analogs.

We may obtain the space variation from the autocorrelation by utilizing the relationship that the cosine transform of the autocorrelation function is the power spectrum. This is used in time series analysis quite frequently, in which case the autocorrelation vs time is computed and the transform is taken to obtain the spectrum of power as a function of frequency. In this case, we compute the autocorrelation as a function of β and transform in such a way as to obtain a power spectrum as a function of x. Actually, of course, since there are discrete discontinuities, the power spectrum of reflection vs x should contain discrete lines; and, in fact, a complete Fourier analysis would give the lines. This is indicated in Fig. 4. Since we cannot measure a complete range of β, it is not possible to obtain the exact locations and magnitudes of the discontinuities.

If, instead of a number of discrete discontinuities, there were a continuum of small discontinuities, then the spectrum would itself be continuous as a function of distance. In that case, the magnitude of the spectrum would be the reflected power within a length dx at a distance x from the origin. Because of our incomplete information (due to lack of an infinite range in frequency), such a continuous spectrum will be obtained anyway, and it will give some indication of the location of the discrete reflectors. Fig. 5 illustrates this effect, and the various quantities used in describing it.

Fig. 4—Discontinuities and time series analogs.

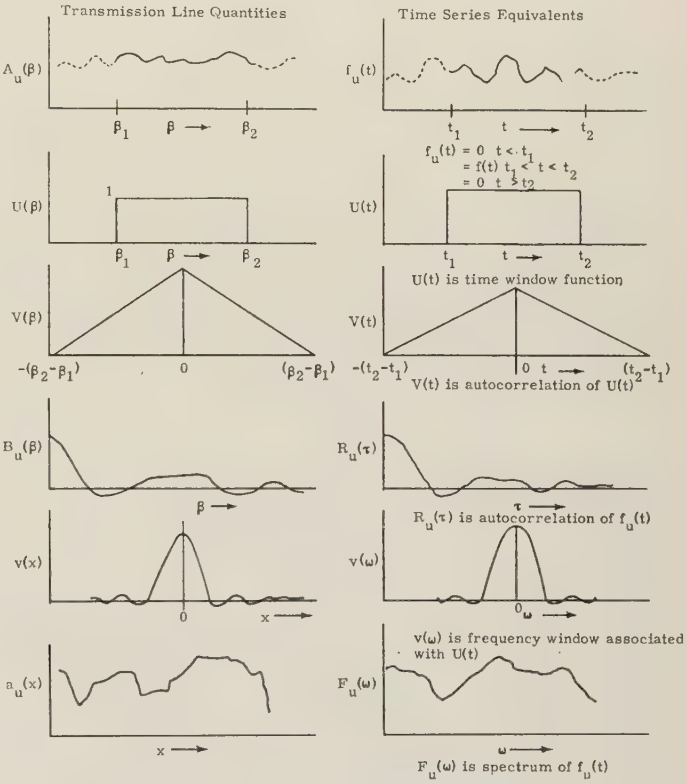

Fig. 5—Effect of finite frequency range of measurement on inferred distance spectrum of discontinuities, and its time-series analog.

The expression for determining the spectrum is given by

$$a(x) = 4\int_0^\infty A(\beta)\cos x\beta\, d\beta. \tag{19}$$

Instead of the reflection function A, we will actually use a function A_u which is measured over the range β_1 to β_2, since it would be impossible to make measurements over the entire range of β (or frequency).

$$\begin{aligned} A_u(\beta) &= 0, && \beta < \beta_1 \\ &= A(\beta), && \beta_1 < \beta < \beta_2 \\ &= 0, && \beta_2 < \beta. \end{aligned} \tag{20}$$

Associated with this will be an autocorrelation function

$$B_u(\beta) = \int_0^\infty | A_u(b) | \, | A_u(b+\beta) | \, db \tag{21}$$

and associated with the autocorrelation function will be a modified space power spectrum given by

$$a_u(x) = 4 \int_0^\infty B_u(\beta) \cos x\beta d\beta. \tag{22}$$

It is possible to write B_u in terms of A instead of A_u by introducing a function:

$$\begin{aligned} U(\beta) &= 0, && \beta < \beta_1 \\ &= 1, && \beta_1 < \beta < \beta_2 \\ &= 0, && \beta_2 < \beta. \end{aligned}$$

When this is done, we have B_u

$$B_u(\beta) = \int_0^\infty [\, | A(b) | \, | A(\beta + b) | \,][U(b)U(b+\beta)]db. \tag{21a}$$

A is a stochastic variable and U may be considered as an independent stochastic variable; that is, the probability of an occurrence of one should have no effect on the probability of occurrence of the other. If we assume this sort of independence of A's and U's, we may utilize a theorem of probability which states that

$$\overline{xy} = \bar{x}\,\bar{y}. \tag{23}$$

The result of application of this theorem to (21a) is

$$\begin{aligned} B_u(\beta) &= \int_0^\infty | A(b) | \, | A(b+\beta) | \, db \int_0^\infty U(b)U(b+\beta)db \\ &= B(\beta)V(\beta), \end{aligned} \tag{21b}$$

where V is a triangular window function associated with the autocorrelation and given by

$$\begin{aligned} V(\beta) &= 0, && \beta < -(\beta_2 - \beta_1) \\ &= (1+\beta)(\beta_2 - \beta_1), && -(\beta_2 - \beta_1) < \beta < 0 \\ &= (1-\beta)(\beta_2 - \beta_1), && 0 < \beta < (\beta_2 - \beta_1) \\ &= 0. && (\beta_2 - \beta_1) < \beta. \end{aligned} \tag{21c}$$

In this notation, (22) becomes

$$a_u(x) = 4 \int_0^\infty B(\beta)V(\beta) \cos x\beta d\beta, \tag{22a}$$

and a_u may also be given in terms of the convolution of a and v as

$$a_u(x) = a(x) * v(x) \tag{24}$$

where v is the transform of V and is given by

$$v(x) = \frac{\beta_2 - \beta_1}{2} \left[\frac{\sin x\left(\frac{\beta_2 - \beta_1}{4}\right)}{x\left(\frac{\beta_2 - \beta_1}{4}\right)} \right]^2. \tag{25}$$

The physical meaning of this is that the lines of the spectrum, a, are looked at through a space window or a space filter v, which has the form of $(\sin ax/x)^2$. This means that, instead of the discrete lines, one sees each line spread out to the shape of v. If the lines are far enough apart in the power spectrum (that is, if the discontinuities are far enough apart), then the spectrum measured will be a succession of these window functions and one can easily locate the individual lines and their magnitudes and, hence, the individual discontinuities and their magnitude. On the other hand, if the discontinuities are fairly close together, there will be a jumbling of these responses to the various discontinuities and it will not be possible to determine the exact location and magnitude of the individual discontinuities but only the average distribution of discontinuities and their average magnitude at any given spot. This corresponds closely to the time function situation in which one is looking for discrete lines in a frequency spectrum but is forced to take an inaccurate determination of these lines due to the fact that he must use a finite sample rather than observing for an infinite period of time.

Using this method of analysis on the reflected pulse should make it possible to determine without too much difficulty the location and size of discontinuities. The application of this method to the case where loss is measured will be somewhat harder because of the complications introduced by going through the process of (15), but still should be quite feasible.

It has been shown that distribution functions of the values for reflected and transmitted waves on a transmission line with randomly spaced discontinuities may be computed if something is known of the probability distribution, average size, and number of the discontinuities. Conversely, it is shown that a measurement of transmission or reflection as a function of frequency may be used to locate approximately the discontinuities causing the reflection.

The techniques illustrated here should be useful both in determining the performance of known transmission lines and in establishing the mechanism and location for reflections in transmission lines whose discontinuous properties are not known.

Acknowledgement

The editorial assistance of Miss L. D. Patterson of Sandia Corporation is gratefully acknowledged. Colleagues whose comments have been particularly helpful include Dr. B. L. Basore and Mr. D. M. Gragg.

The Statistical Prediction of Voltage Standing-Wave Ratio*

J. A. MULLEN† AND W. L. PRITCHARD‡

Summary—The problem of predicting the probability distribution of vswr for many randomly spaced discontinuities is solved using the "central limit theorem." Assuming that reflection factors add in the complex plane and using the "central limit theorem" the result is shown to be a Rayleigh distribution in terms of the reflection factor.

The probability of the vswr over a band of frequencies is calculated using the concept that this band of frequencies can be considered as a number of statistically independent samples.

Distribution Function for Voltage Standing-Wave Ratio

THE DESIGNER of microwave systems is faced with the problem of estimating the voltage standing-wave ratio resulting from the combined reflections of many components. Typically, a radar system may contain an antenna reflector, radome, horn feed, polarizing devices, two or three rotating joints, a waveguide switch, duplexer, and perhaps twenty or thirty bends, twists, and flanges. In the worst conceivable case the over-all voltage standing-wave ratio will be the product of the component voltage standing-wave ratios. With reasonably attainable values of voltage standing-wave ratio for the components this worst case is often too horrible to contemplate. Conversely, an acceptable value of maximum over-all voltage standing-wave ratio leads to impossibly small values for the components. An exact computation of the over-all voltage standing-wave ratio from the values of component voltage standing-wave ratios and line lengths is extraordinarily complicated. Even worse, the line lengths are often not known until late in the system development and long after the components are designed. In the past, equipment designers have relied on accumulated experience to estimate the practical result, *i.e.*, to take advantage of the small statistical probability that the individual mismatches will combine to give the worst case.

It is the purpose of this paper to treat the problem statistically, *i.e.*, to obtain the distribution function of over-all standing-wave ratio in terms of the number of discontinuities and their mean squared reflection factor.

Note that we are not considering the production problem of quality control which is that of predicting the variation of voltage standing-wave ratio of an assembly when the line lengths vary from their design values. This problem has been dealt with by Brown.[1]

In order to make the problem analytically tractable we assume that the reflection factors (complex) add, *i.e.*,

$$\hat{\gamma} = \sum_{i=1}^{n} \gamma_i \epsilon^{j2\theta_i}$$

$$\hat{\gamma} = \sum_{i=1}^{n} \gamma_i \cos 2\theta_i + j \sum_{i=1}^{n} \gamma_i \sin 2\theta_i$$

$$\hat{\gamma} = \gamma_x + j\gamma_y. \tag{1}$$

This is a reasonable approximation if the magnitude of the individual reflection factors are small. Practical system designs usually involve magnitudes of γ well within these limits. It should be noted that, mathematically at least, this assumption permits over-all magnitudes of γ greater than unity, which is physically impossible. However, the mathematics will also show that the probability of γ anywhere near unity (where the additive approximation is invalid) is exceedingly slight.

We further assume that the line lengths between discontinuities are independent of each other and that all values of θ between 0 and 2π are equally probable. These assumptions seem reasonable in view of the fact that electrical line lengths in a complicated microwave system are generally much longer than 2π and are chosen for random mechanical reasons.

We finally assume that n, the total number of discontinuities, is large ($n > 8$). If the system has periodic discontinuities, *e.g.*, flanges recurring at equal intervals, they should be considered as a single discontinuity, the magnitude of which is calculable separately and exactly.

These assumptions are sufficient to use the "central limit theorem" of probability theory.[2]

The central limit theorem can be stated for our purposes as follows: the joint distribution function of the real and imaginary parts of the sum of a large number of independent complex random variables asymptotically approaches normal regardless of the distribution functions of the individual random variables.[3]

Eq. (1) for the complex reflection factor is the sum of a large number of independent random variables

* Manuscript received by the PGMTT, October 1, 1956.
† Raytheon Mfg. Co., Waltham, Mass.
‡ Raytheon Mfg. Co., Wayland, Mass.

[1] L. W. Brown, "Problems and practice in the production of waveguide transmission systems," *Proc. IEE*, vol. 93A, pp. 639–646; 1946.

[2] J. V. Uspensky, "Introduction to Mathematical Probability," McGraw-Hill Book Co., New York, N. Y. ch. 15; 1947.

[3] There are only slight restrictions not applicable here.

and, as such, comes within the scope of the central limit theorem.

The joint distribution of the real and imaginary components of $\hat{\gamma}$ is now given in the two dimensional normal form.[4]

$$W(\gamma_x, \gamma_y) = \frac{1}{2\pi\sigma^2\sqrt{1-r^2}} \exp\left\{-\frac{\gamma_x^2 - 2r\gamma_x\gamma_y + \gamma_y^2}{2\sigma^2(1-r^2)}\right\}. \quad (2)$$

Eq. (2) is the joint normal distribution where the mean values of γ_x and γ_y vanish and where the mean squared values are equal and calculated as follows:

$$\gamma_x^2 = \sum_i \sum_j \gamma_i \cos 2\theta_i \gamma_j \cos 2\theta_j. \quad (3)$$

In averaging the right hand side over θ_i and θ_j their independence when $i \neq j$ causes their joint average to be the same as their separate averages, and the uniform distribution of θ_i and θ_j causes these averages to be zero. Thus we can write

$$\overline{\gamma_x^2} = \overline{\sum_i \gamma_i^2 \cos^2 2\theta_i} \quad (4)$$

$$= \sum_i \overline{\gamma_i^2 \cos^2 2\theta_i}. \quad (4a)$$

Since θ_i is uniformly distributed we can make use of the fact that the mean squared value of a cosine is equal to $\frac{1}{2}$ and write:

$$\overline{\gamma_x^2} = 1/2 \sum_{i=1}^{n} \gamma_i^2. \quad (5)$$

Similarly

$$\overline{\gamma_y^2} = 1/2 \sum_{i=1}^{n} \gamma_i^2$$

and by definition

$$\sigma^2 = \overline{\gamma_x^2} = \overline{\gamma_y^2}. \quad (5a)$$

We must now calculate r, the correlation coefficient, which is defined as follows:

$$\sigma^2 r = \overline{\gamma_x \gamma_y}. \quad (6)$$

Using an argument identical to that following (3) we proceed:

$$\sigma^2 r = \overline{\sum_i \sum_j \gamma_i \cos 2\theta_i \gamma_j \sin 2\theta_j \delta_{ij}}$$

$$= \sum_i \gamma_i^2 \overline{\cos 2\theta_i \sin 2\theta_i}$$

$$= 1/2 \sum_i \overline{\gamma_i^2 \sin 4\theta_j}.$$

Thus

$$\sigma r = 0. \quad (6a)$$

Now, we can write the joint distribution simplified as:

$$W(\gamma_x, \gamma_y) = \frac{1}{2\pi\sigma^2} \exp -\left(\frac{\gamma_x^2 + \gamma_y^2}{2\sigma^2}\right). \quad (7)$$

Since we are seeking the distribution of the magnitude of the reflection factor we must transform from rectangular to polar coordinates.

The element of area goes from $d\gamma_x d\gamma_y$ to $\gamma d\gamma d\theta$. With γ_x and γ_y expressed in polar coordinates, the joint density function becomes

$$W(\gamma_x, \gamma_y) d\gamma_x d\gamma_y = \frac{1}{2\pi\sigma^2} \epsilon^{-\gamma^2/2\sigma^2} \gamma d\gamma d\theta. \quad (8)$$

From the definition of $W(\gamma, \theta)$[5] we have that

$$W(\gamma, \theta) = \frac{\gamma}{2\pi\sigma^2} \epsilon^{-\gamma^2/2\sigma^2}. \quad (9)$$

By integrating over θ the distribution of γ is seen to be

$$W(\gamma) = \frac{\gamma}{\sigma^2} \epsilon^{-\gamma^2/2\sigma^2}. \quad (10)$$

This is the well-known Rayleigh distribution. In fact we have just rederived in a different context the two dimensional "random walk" problem for a large number of steps.[6-8]

The value which maximizes $W(\gamma)$ is defined as the most probable value of γ and is designated γ_m. Since γ_m is found equal to σ, we have

$$W(\gamma) = \frac{\gamma}{\gamma_m^2} \epsilon^{-\gamma^2/2\gamma_m^2}. \quad (11)$$

The distribution of over-all reflection factor has been plotted using (11) for representative values of γ_m in Fig. 1. Note that the smaller γ_m, the sharper and higher is the distribution function. The most probable value, γ_m, is calculated from the individual reflection factors as follows:

$$\gamma_m = \sigma = \frac{1}{\sqrt{2}}\left(\sum_{i=1}^{n} \gamma_i^2\right)^{1/2}. \quad (12)$$

If γ_0 is the rms value of the γ_i's, we can rewrite (12) to show explicitly the dependence on n as

$$\gamma_m = \sqrt{\frac{n}{2}}\, \gamma_0. \quad (13)$$

[4] H. Cramer, "The Elements of Probability Theory," John Wiley and Sons, New York, N. Y., ch. 9, sec. 4; 1955.

[5] $W(\gamma, \theta)$ stands for the probability density of the random variable within the parentheses and does *not* reprersent the same function for different random variables.

[6] L. Rayleigh, *Phil. Mag.*, vol. 10, p. 73; 1880.

[7] K. Pearson, Drapers Co. Res. Memo No. 4, Biometric Series No. III; 1906.

[8] J. L. Lawson and G. E. Uhlenbeck, "Threshold Signals," Rad. Lab. Ser. No. 24, McGraw-Hill Book Co., Inc., New York, N. Y.; 1950.

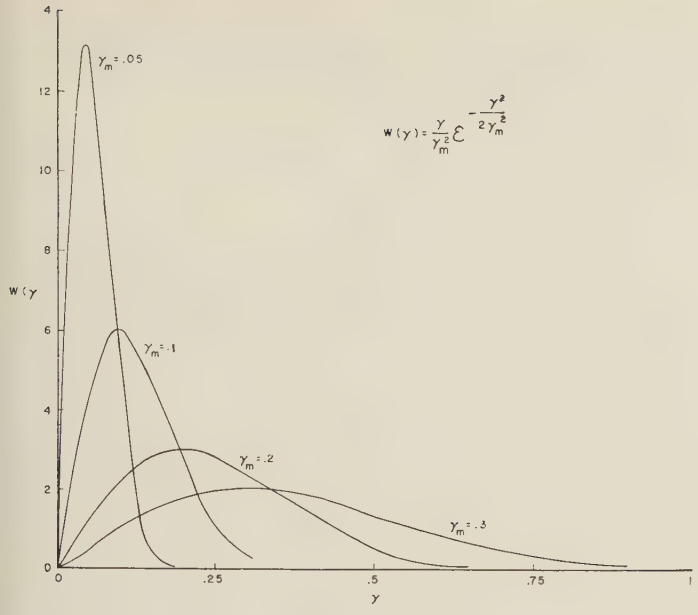

Fig. 1—Probability density of reflection factor with the most probable over-all reflection factor as parameter.

We note that the probability density in the region where the additive approximation becomes questionable ($\gamma \cong 0.5$) is extremely small.

The probability $P(\gamma)$ that the reflection factor is less than γ is given by

$$P(\gamma) = \int_0^{\gamma} W(\gamma)d\gamma = 1 - \epsilon^{-\gamma^2/2\gamma_m^2}. \tag{14}$$

The convenience of the results is increased by writing the probability in terms of ρ, the vswr, rather than γ. γ and ρ are related by

$$\gamma = \frac{\rho - 1}{\rho + 1}. \tag{15}$$

Defining ρ_m to correspond to γ_m using (15), we can write

$$P(\rho) = 1 - \exp\left\{-1/2\left(\frac{\rho - 1}{\rho + 1}\right)^2\left(\frac{\rho_m + 1}{\rho_m - 1}\right)^2\right\}. \tag{16}$$

$P(\rho)$ is plotted in Fig. 2 for the same values of ρ_m as in Fig. 1. These curves can be used to compute the probability that, among a large number of possible designs with the same set of discontinuities, the vswr of a particular design will be less than ρ. Note that the probability of being less than ρ_m is only 0.4, so that ρ_m is not a conclusive design parameter, but for moderately larger values of ρ the asymptotic approach to unity is rapid.

To plot these results in a still more useful form we define $\rho_{.9}$ as that value of vswr that we have only a ten per cent probability of exceeding. From (14) we find

$$\gamma_{.9} = \sqrt{2 \text{ Log } 10}\gamma_m = 1.52\sqrt{n}\gamma_0 \tag{17}$$

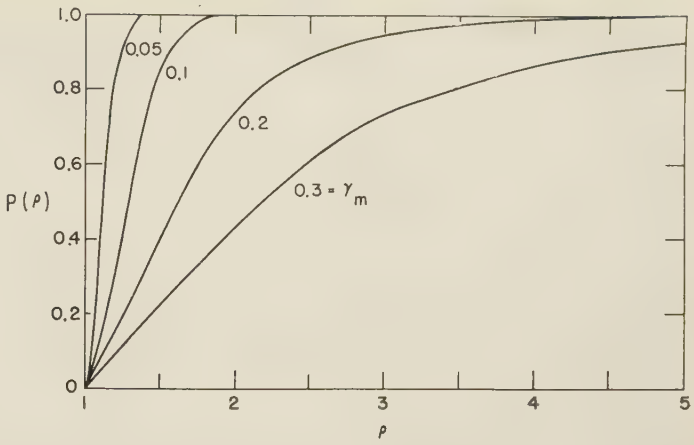

Fig. 2—Cumulative probability of voltage standing-wave ratio with the most probable over-all reflection factor as parameter.

whence

$$\rho_{.9} = \frac{1 + \gamma_{.9}}{1 - \gamma_{.9}}. \tag{17a}$$

Eq. (17), using the variable of (17a), is plotted in Fig. 3 for representative values of n. These curves permit a system designer to predict, given a number of discontinuities and their typical values, a very conservative result for the over-all vswr. Using the preceding methods a set of curves is easily constructed to predict a less conservative result, *e.g.*, $P(\rho) = \frac{2}{3}$.

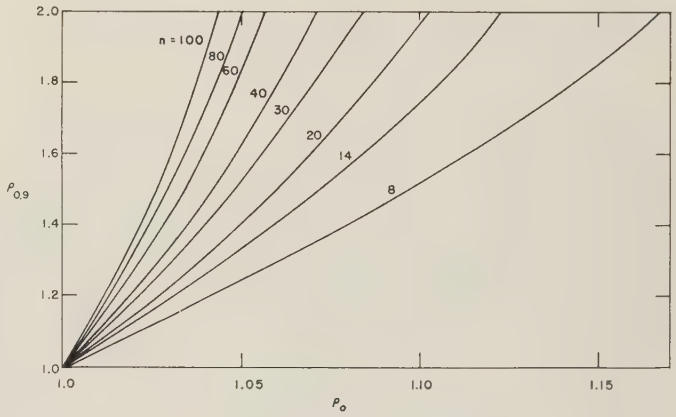

Fig. 3—The value of vswer exceeded in only 10 per cent of the possible designs plotted vs the vswr of a typical discontinuity, with the number of discontinuities as a parameter.

Prediction Over a Wide-Frequency Band

So far the theory has considered results at a single frequency only and cannot be used to predict results over a band of frequencies. We have approached this latter problem by considering it as a "sampling" problem. In other words, if the frequency range is wide, we actually have a multiplicity of problems, each the same as that solved in the first section. The difficulty, of course, is in deciding how many independent samples

the frequency band contains. We estimate this number and show that the answer is insensitive to this estimate.

There are two possibilities, that the reflection factor is greater than γ or less than γ. The joint probability that in N tries, represented by the N independent frequency points, there will be N favorable results, *i.e.*, vswr less than γ, is simply $P^N(\gamma)$.[9]

$P^N(\gamma)$ is plotted in Fig. 4 using a normalized abscissa scale. Note that for a constant probability the value of γ varies about as log N. This dependence is insensitive to N which is fortunate since the awkward aspect of this problem is in deciding on the number of independent frequencies.

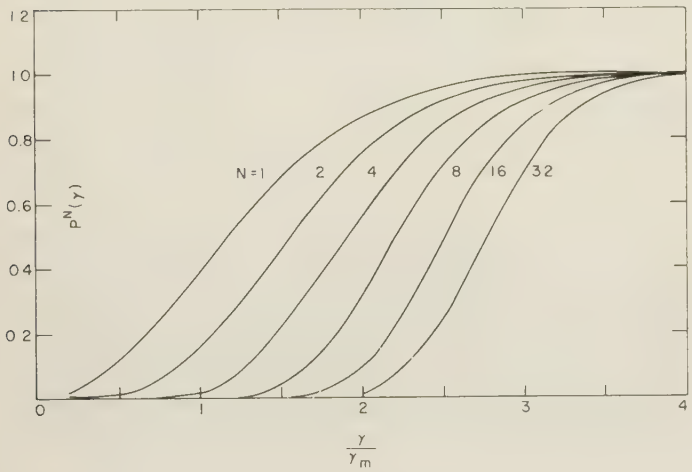

Fig. 4—The cumulative probability that the reflection factor is less than γ in a bandwidth B plotted against γ/γ_m with the number of independent samples (determined from B) as parameter.

Our method is based on the following considerations. When the frequency has changed sufficiently that the average electrical length between discontinuities has changed by π, the individual reflection factors have changed their phases enough so that their sum can be considered as a new random variable. On this basis, N is given by

$$N = \frac{B}{\Delta f} = 2\,\frac{B}{f}\,\frac{L}{\lambda}\cdot \tag{18}$$

This estimate of N is optimistic and realistic system planning should use a value of N probably twice that given by (18).

In many typical systems, one length (*e.g.*, a smooth run from transmitter to antenna) is much longer than any of the others. This problem should not be considered statistically on an over-all basis, but should be resolved into two or more separate statistical problems, whose results are combined by conventional methods. In other words, at some point in the frequency band, corresponding to a single independent sample, two groups of discontinuities separated by a very long length of line will combine in the most unfavorable phase; so that the most probable vswr is the product of the most probable vswr's of the separate groups.

If the magnitude of the vswr's of the individual discontinuities varies over the band, a conservative approach to system design would use the largest values in calculating γ_0.

[9] We have used γ rather than ρ as an independent variable in order to achieve a universal curve.

Conclusion

We have determined the probability distribution at a single frequency for many randomly spaced small discontinuities, and plotted results in several convenient forms. This theory has been extended in an intuitive fashion to cover a band of frequencies.

List of Symbols

- γ magnitude of over-all reflection factor.
- $\hat{\gamma}$ over-all complex reflection factor.
- γ_i magnitude of the reflection factor of the ith discontinuity.
- γ_x real component of over-all reflection factor.
- γ_y imaginary component of over-all reflection factor.
- γ_0 rms value of the γ_i's.
- γ_m the most probable value of γ.
- λ midband wavelength.
- θ_i electrical line length, in excess of a whole number of 2π's, to ith discontinuity.
- n total number of discontinuities.
- r correlation coefficient between γ_x and γ_y.
- σ standard deviation of either γ_x or γ_y.
- δ_i. Kronecker delta $\delta_{ij} = \begin{cases} 0 & i \neq j \\ 1 & i = j \end{cases}$.
- L average length between discontinuities.
- $W(\cdot)$ probability *density* (distribution function) of variable included in parentheses.
- N number of independent samples in the system bandwidth.
- ρ over-all voltage standing-wave ratio.
- $\rho_{.9}$ that value of over-all vswr exceeded in only 10 per cent of the possible designs.
- ρ_m the most probable value of ρ.
- $P(\cdot)$ the probability that the random variable is less than the value in parentheses.
- B total system bandwidth.
- f midband frequency.
- — a bar over any term indicates the taking of its arithmetic mean.
- Δf frequency spacing between independent samples.

Performance of Three-Millimeter Harmonic Generators and Crystal Detectors*

J. M. RICHARDSON† AND R. B. RILEY‡

Summary—**Because of growing applications of millimeter wave measurements, a fairly thorough investigation of what could be expected from sources and detectors in the 3 mm region was made. The sources consisted of fourth-harmonic generators from a 1.25 cm fundamental. A type of crystal holder for both harmonic generators and detectors in which a small crystal wafer is positioned in the broad wall of the millimeter waveguide, being contacted by a whisker passing across the waveguide (the open-guide type) was found to be superior in general to units using crystal cartridges or modifications thereof. Factors affecting the performance of these units have been investigated statistically. It was found that the short-circuit current sensitivity in microamperes per microwatt of a good crystal detector of the type described above is not greatly less than the value for crystals at lower microwave frequencies, so that the minimum detectable signal is about the same. As an additional result, evidence for an important effect in which the harmonic generation process degrades the signal-to-noise ratio of the source is presented and discussed.**

Introduction

THE GROWING number of applications for millimeter waves in the last few years has increased the need for convenient sources and detectors of wide dynamic range. In most applications, such as microwave spectroscopy, microwave optics, or dielectric measurements, coherence and excellent monochromaticity are primary requirements. These requirements virtually dictate that the millimeter waves be produced by harmonic generation in a nonlinear element such as a crystal diode excited by radiation from a microwave vacuum tube source. There are numerous reports of such devices.[1–4]

During construction of a precision millimeter wave interferometer, it became desirable to produce a source-detector combination at 3 mm possessing large signal-to-noise ratio, freedom from spurious modulations, and convenience of operation. The latter requirement indicated a simple crystal rectifier or bolometer type of detector rather than a superheterodyne type. [Johnson and Schlesinger[5] have described a superheterodyne receiver in which the mixer crystal is driven by a (swept) local oscillator near the same fundamental frequency from which the signal harmonic is generated. The signal then mixes with the local oscillator such that a high order beat near the IF can be recovered.] If the sensitivity of the simpler crystal or bolometer should prove adequate, then of course it would be the best for the application at hand. Thus, a fairly extensive investigation of performance of such generators and detectors was made with the purpose of finding the combination of variables best satisfying the above requirements.

Measurement

The measuring apparatus is shown in Fig. 1, which is largely selfexplanatory. The slotted section was included to determine the degree of match into the multiplier produced by the E/H tuner. The waveguide lead from multiplier to detector would not support any harmonics of 1.25 cm below the fourth.

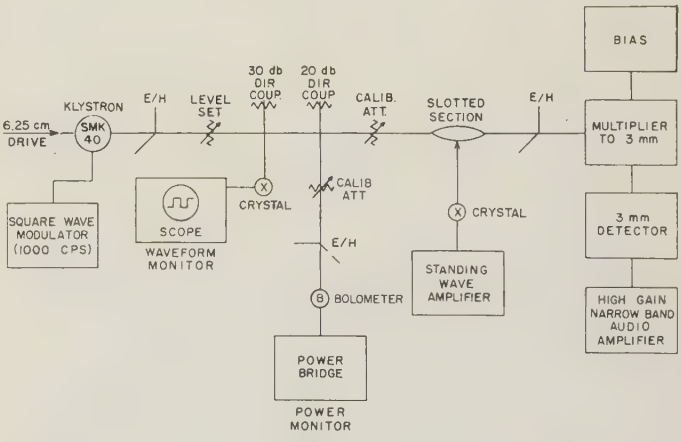

Fig. 1—Block diagram of measuring apparatus.

A drawing of the multiplier unit is shown in Fig. 2. The detector units were similar, but with the omission of the large waveguide. These units were modelled closely on the design of Johnson, Slager, and King,[3] and are designated as open-guide types. Two units of each were tested to see if significant performance differences occurred in units presumably machined in the same way from the same drawings.

* Manuscript received by the PGMTT, September 4, 1956. Part of this work was carried out under a program of research and development in basic instrumentation cooperatively supported by ONR, AFOSR, AEC, and NBS.

† Nat. Bur. of Standards, Boulder, Colo.

‡ Hewlett-Packard Co., Palo Alto, Calif. Formerly with the Nat. Bur. of Standards, Boulder, Colo.

[1] C. H. Townes and A. L. Schawlow, "Microwave Spectroscopy," McGraw-Hill Book Co., Inc., New York, N. Y., 1955.

[2] J. A. Klein, J. H. N. Loubser, A. H. Nethercot, and C. H. Townes, "Magnetron harmonics at millimeter wavelengths," *Rev. Sci. Instr.*, vol. 23, p. 78; February, 1952.

[3] C. M. Johnson, D. M. Slager, and D. D. King, "Millimeter waves from harmonic generators," *Rev. Sci. Instr.*, vol. 25, pp. 213–217; March, 1954.

[4] W. C. King and W. Gordy, "One-to-two millimeter wave spectroscopy. IV. Experimental methods and results for OCS, CH_3F, and H_2O," *Phys. Rev.*, vol. 93, pp. 407–412; February 1, 1954.

[5] C. M. Johnson and S. P. Schlesinger, "Superheterodyne receiver for the 100 to 150 kMc region," Johns Hopkins Univ. Radiation Lab., Internal Memo., June 21, 1954.

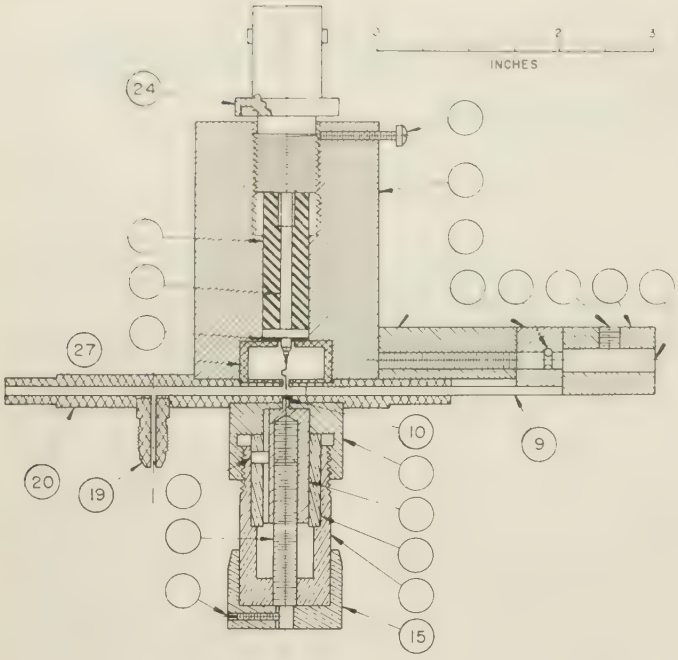

Fig. 2—Assembly of 3 mm multiplier unit. Crystal, 10; RG-66/U fundamental waveguide, 27; RG-138/U harmonic waveguide, 20; shorting stub, 9; bias connector, 24; contact adjusting knob, 15; fitting for coolant gas line, 19.

Silicon wafers extracted from several different commercial crystal cartridges were used. These included type 1N31, 1N32, 1N26, and 1N78, made by one manufacturer and type 1N26 made by another manufacturer. Although all these crystals are generally fabricated from the same source of silicon, differences in rf performance nevertheless do appear, and are the basis for classification by type number. It was asked whether differences accounting for the various classifications also produced differences in 3-mm performance. Two samples of each crystal type were tested. Difficulty was experienced in mounting 1N53 wafers on the crystal posts of our units, so that after one measurement on a 1N53 wafer indicated good but not outstanding performance, further attempts to use them were abandoned.

The question was asked whether silicon surface condition influenced performance. One surface condition, designated as "original," resulted from merely wiping the wafer clean and rinsing with alcohol. Another condition, designated as "cleaned," resulted from a thorough cleaning in concentrated sulfuric acid. A few observations were made on crystals freshly etched electrolytically in hydrofluoric acid.

Three states of whisker point condition were studied, "straight," "convex," and "used," as shown in Fig. 3. The first two were produced by slightly differing techniques of electrolytic pointing. The used point was one which had contacted a crystal once or more and had usually become blunted or bent.

Provision was made for conveniently biasing the multiplier units with various combinations of resistance and voltage.

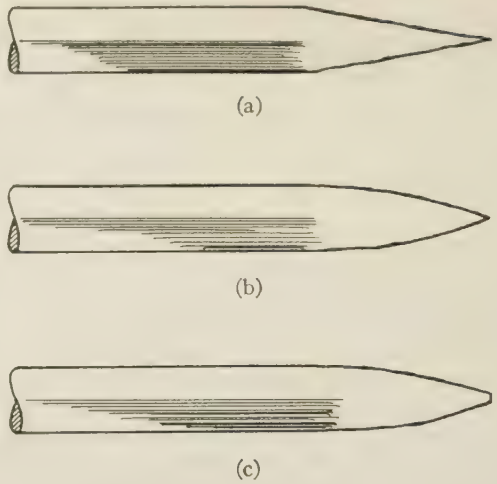

Fig. 3—Sketch of whisker point conditions: (a) straight; (b) convex; (c) used.

Multiplier performance was measured in terms of the indication of a commercial bolometer detector in RG-98/U waveguide size with taper to RG-138/U size. The observations are reported in Table I, opposite, as average 3 mm output power expressed in db above 1 μw. Because of ignorance at this wavelength about mount efficiency and the validity of dc-rf substitution, the absolute power quoted may be in error by 3 db as a best guess, but the relative values should not be seriously affected. Contact between whisker and crystal was made with only a few milliwatts incident. Contact force and incident power were then increased alternately, maintaining bias resistance and all tuning controls optimized. Each entry in Table I represents the best of two or three contacts. The best was chosen rather than an average because anyone desiring millimeter wave power will usually reject poor, average, or even good contacts until an outstanding one is achieved.

Detector observations are reported in Table II and represent the 1000 cps detected output of a detector expressed in db above 1 μv into a 600-ohm load with 5 μw average power, square-wave modulated, incident on the detector, tuning and bias controls being optimized.

What was observed was essentially the conversion efficiency of the crystals, first in converting 24 kmc power to 96 kmc power, and then in converting modulated 96 kmc power to audio power. Strictly speaking, it is not these quantities but rather the attainable signal-to-noise ratios which are of critical interest. The measurement of a signal-to-noise ratio is much more inconvenient and unreliable to make, however, so that in a practical case where the worker is seeking a good multiplier or detector, he will probably use the conversion efficiency as a criterion. The writers believe on the basis of experience that this criterion is valid; *i.e.*, the signal-to-noise ratio for given operating conditions is greater for a crystal of greater conversion efficiency, although perhaps not proportionately greater. The situation is further complicated by the dependence of both the con-

TABLE I

Observations on 3 mm Multiplier Units*

Multiplier Unit		C				D			
Crystal Condition		Original		Cleaned		Original		Cleaned	
Point Condition		Convex	Used	Convex	Used	Convex	Used	Convex	Used
1N31	*a*	9.5	6	—	—	8.5	4	—	—
	b	8	−4	—	—	5	−2	—	—
1N32	*a*	12.5	4	—	—	12	8	13.5	—
	b	11	6	—	—	12.5	—	14.5	—
1N26 Mfg. "A"	*a*	11	1	—	—	12	8	—	—
	b	13	3	—	—	14.5	−1.5	17	—
1N26 Mfg. "B"	*a*	—	—	—	—	11	—	—	—
	b	12	—	—	—	12.5	—	—	—
1N78	*a*	10.5	−2	—	—	9.5	4	—	—
	b	—	—	—	—	—	—	—	—

* Entries are expressed in db above 1 μw (average) of rf power with 100 mw (average) incident on the multiplier. Designations *a*, *b*, refer to assigned sample numbers.

TABLE II

Observations on 3 mm Detector Units*

Detector Unit		A				B			
Crystal Condition		Original		Cleaned		Original		Cleaned	
Point Condition		Convex	Used	Convex	Used	Convex	Used	Convex	Used
1N31	*a*	66	64	—	—	56	60	—	—
	b	62	48	—	—	54	56	—	—
1N32	*a*	60	49	—	—	46	—	—	—
	b	60	50	66	62	48	—	—	—
1N26 Mfg. "A"	*a*	46	50	—	—	54	—	—	—
	b	46	60	—	—	50	—	—	—
1N26 Mfg. "B"	*a*	48	—	—	—	—	—	—	—
	b	56	62	—	—	42	—	—	—
1N78	*a*	54	60	—	—	52	—	—	—
	b	—	—	—	—	—	—	—	—

* Entries are expressed in db above 1 μv into a 600-ohm load with 5 μw (average) incident on the detector. Designations *a*, *b*, refer to assigned sample numbers.

version efficiency and the generated noise on input power, and results on these effects are forthcoming from another investigation in this laboratory.

Results

Statistically Significant Results

The wide range of the data as experimental conditions were varied indicated that a statistical analysis should be used to distinguish true effects from experimental fluctuations. Some parts of the experiment may be considered complete factorial experiments in that all levels of all factors of such a part are represented. The factors involved are type of silicon, number assigned to the sample (a random assignment included only for replication), the manufacturer, the multiplier (or detector) unit, the silicon surface treatment, and the whisker point condition. Such results can be analyzed by the statistical technique called "analysis of variance"[6] which will supply a test as to whether either main effects or interactions of the various factors are statistically significant. The results are summarized in Tables III and IV above, in which a significance level of 10 per cent applies; that is, the existence of a positive effect would be concluded only 10 per cent of the time in the long run if in fact the true effect were null (*i.e.*, not significant). An indication of the "resolution" of the result or fineness of detection of an effect is given in each case. Interactions between factors were not found to be significant.

TABLE III

Statistical Results for Multipliers

Factor	Result	Approximate Amount
Type Silicon	1N31 < 1N32 < 1N26	0 < 3 < 4 db
Assignment of Sample No.	Null	Within 3 db
Manufacturer	Null	Within 3 db
Multiplier Unit	Null	Within 3 db
Surface Treatment	Original < Cleaned	2 db
Point Condition	Used < Convex	8 db

"<" means "better than" by the indicated amount.

TABLE IV

Statistical Results for Detectors

Factor	Result	Relative Amount
Type Silicon	1N26 < 1N32 < 1N31	0 < 4 < 10
Assignment of Sample No.	Null	Within 8 db
Manufacturer	Null	Within 25 db
Detector Unit	Null	Within 8 db
Surface Treatment	Null	Within 19 db
Point Condition	Null	Within 8 db

"<" means "better than" by the indicated amount.

The generalizations worth drawing are as follows:

1) Essentially the same performance can be expected from different holders (either multiplier or detector) made from the same machine drawings.
2) Essentially the same performance can be expected from different samples of a given type of silicon, for either multiplier or detector.
3) For a multiplier, silicon from 1N26 cartridges excels that from 1N32 cartridges, which in turn excels that from 1N31 cartridges. For a detector the inverse order of silicon type is true. Silicon from 1N78 cartridges was not greatly different from that from 1N31 cartridges, for either multiplier or detector.
4) For a multiplier, the first contact of a properly sharpened point is essential. For a detector, the point condition is largely immaterial.
5) A cleaned silicon surface is beneficial in a multiplier, and may be so in a detector.

[6] See any standard text on statistics, for example, Bernard Ostle, "Statistics in Research," Iowa State College Press, 1954.

6) The resolution of the experiment was not sufficient to disclose any difference in performance due to manufacturer.

Miscellaneous Observations and Inferences

Although the above results are the only statistically significant ones emerging from the investigation, it may be helpful to enumerate a host of miscellaneous observations made during the course of this work, and which we believe to be true. Statistical testing of the hypotheses listed below was not made simply because it did not seem worthwhile.

Results with "straight" points were in every case bettered with a "convex" point, possibly because the convex point was stronger and less subject to bending.

Observations on an electrolytically etched crystal showed improved detector performance but essentially no improvement in multiplier performance.

In addition to the open-guide multiplier studied above in detail, a survey was made of other types readily available in the laboratory. The best performance of the various types is indicated for comparison below, under conditions of 100 mw average incident power, square wave modulated.

1) Open-guide type. Best output (Table I), 50 μw. (Best efficiency observed at 5 mw in, 5 μw out.)
2) Windowed 1N26 cartridges. These were commercial 1N26 cartridges in which windows had been cut to expose the whisker. The cartridge was mounted in RG-66/U waveguide and the window looked into RG-138/U waveguide. Best output, 5 μw.
3) Windowed 1N53 cartridges similar to 2) above. Performance was worse than the windowed 1N26's.

Similarly, a survey of various other types of readily available 3 mm detectors was made. The best performance of the various types is indicated for comparison below. The experimental arrangement was 5 μw average incident power, square wave modulated, with 600-ohm load on the crystal detector. Figures given are microvolts across this load.

1) Open-guide type. Best output (from Table II), 2000 μv.
2) 1N53 crystal cartridges in RG-96/U (30 kmc) commercial waveguide mount, with taper from RG-96/U to RG-138/U. Best output of 20 different cartridges, 275 μv.
3) Windowed 1N26 cartridges, the window looking into RG-138/U waveguide. Best output 100 μv.
4) Wafer bolometer in RG-98/U waveguide mount, with taper from RG-98/U to RG-138/U. Bias current of about 3 ma. Output, 100 μv.
5) 1N26 crystal cartridges in RG-66/U (24 kmc) commercial waveguide mount, with taper from RG-66/U to RG-138/U. Best output of 40 different cartridges, 65 μv.
6) Windowed 1N53 cartridges, similar to 3) above. Performance was worse than windowed 1N26's.

A typical variation of 3-mm output power vs K-band input power in an open-guide multiplier with a 1N26 crystal chip and a good contact is shown in Fig. 4. 100 mw was chosen as a standard input power because it was about the maximum power that could be applied to the open-guide multipliers without causing rapid deterioration of the harmonic power with time. It was found that some contacts deteriorated quite rapidly at this power level while other contacts were stable. In general, the contact force had to be fairly heavy to minimize deterioration.

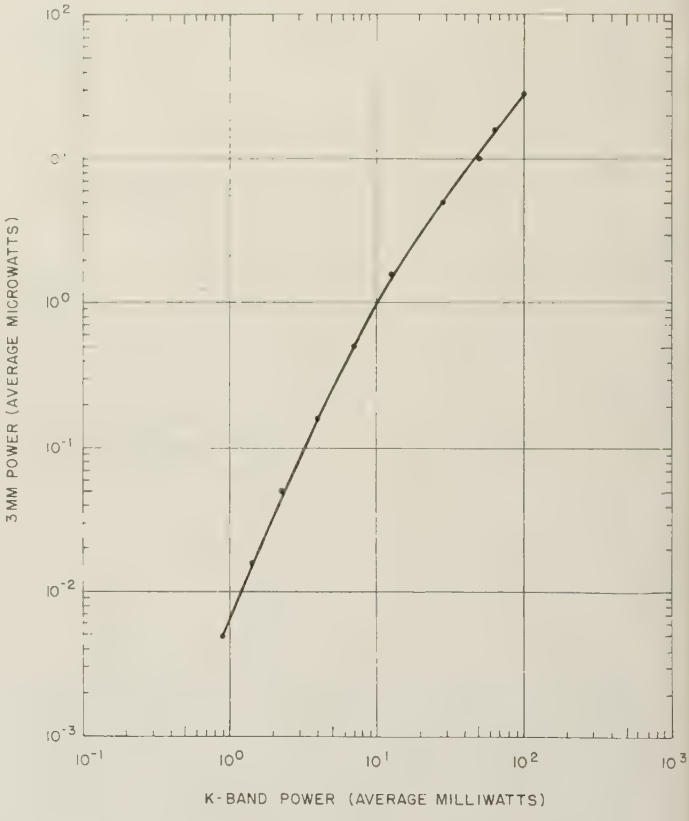

Fig. 4—3-mm output power vs K-band input power for an open-guide multiplier with a 1N26 crystal chip and a good contact.

Discussion

Sensitivity and Minimum Detectable Signal

The short circuit current sensitivity was found to be 0.75 μa/μw for the best 3-mm detector. This is to be compared with the frequently given value of 1 μa/μw for a good crystal at lower microwave frequencies, such as S-band. It is seen that the detection sensitivity has not suffered greatly by working in the millimeter region. On the other hand, as pointed out above, there are unsuitable crystal detectors whose sensitivity is as poor or

worse than that of the inherently insensitive bolometer. This figure allows an estimate of minimum detectable signal of -83 dbm (5×10^{-12} w-sec$^{1/2}$) to be made assuming 1 cps bandwidth, amplifier noise figure of 4, and video impedance of 5000 ohms. Thus with the production of 50 μw average square wave modulated power, a dynamic range of 70 db is available for experimentation using careful matching and a 1 cps band.

Noise Introduced by the Multiplication Process

A measurement of the noisiness of the fourth harmonic at 3 mm was made, and is included to bring out the important point that noise is introduced in the multiplication process. We cannot quantitatively explain the mechanism of the noise introduction at this writing, but the effect is definite, and forms the subject of another current investigation in this laboratory.[7] A likely qualitative explanation is that the excitation of the multiplier crystal by large amounts (100 mw) of fundamental power produces, as is well-known, excess noise obeying the $1/f$ power spectrum. This leads to the presence of fairly strong noise currents near, for example, 1000 cps flowing in the nonlinear crystal rectifier along with currents at 24 kmc, the fundamental microwave frequency. It is supposed that the low-frequency noise currents mix with the harmonics of the 24 kmc to modulate them, thus producing noise sidebands on the 3-mm output in particular. The noise sideband spectrum will be greatest closest to the carrier, in accordance with the $1/f$ spectrum of the excess noise which produced the sidebands. When the 3-mm carrier is demodulated and observed through a filter or narrow-band amplifier we will then expect to see the demodulated noise at the filter frequency (in addition to any other noise present).

By choosing a bolometer as a square law demodulating device, and calibrating its sensitivity to power variations with a known square wave, it was possible to observe both the average power of the 4th harmonic output and the absolute magnitude of its power fluctuations caused by noise. From these data it is easy to arrive at either an effective amplitude modulation index, m, or the ratio of noise power, P_n, to carrier power, P_c for the band in use, assuming this power results from amplitude modulation alone. The same procedure was applied to the fundamental microwave, and the following results obtained reduced to 1 cps bandwidth.

$$\text{Fundamental:}\quad P_n/P_c = 0.8\times10^{-12}$$
$$m = 1.3\times10^{-6}$$
$$\text{4th Harmonic:}\quad P_n/P_c = 20\times10^{-12}$$
$$m = 6\times10^{-6}.$$

Thus by some mechanism the multiplication process has degraded the signal purity by 14 db. This degradation appears too large to be explained simply by the production and superposition at the demodulation frequency of harmonics and beats among noise components existing in the slightly impure input.

From information such as just presented, estimates may be made concerning such things as the minimum detectable modulation produced by some external modulating agency (Stark modulation in a microwave spectrometer, for example), or the smallest detectable change in signal level in an interference or transmission experiment.

Conclusion

Increasing activity in the millimeter wave region has made it desirable to investigate the characteristics of sources and detectors with a view toward optimizing available designs and describing the best performance which may be attained. The open-guide type of crystal holder has been found superior in general to more primitive types for both harmonic generators and detectors. There is a significant difference among silicon wafers extracted from various types of commercial crystals, so that choice of silicon is important. Sharpness of the whisker point is absolutely essential for a good harmonic generator. Cleanliness of the silicon surface is also significant.

The range of results produced by these factors either individually or in combination is rather large, so that the "best" combination may be some 20 db or more better than the "worst" combination. Thus, individual trial and adjustment by an experimenter is still necessary, for no specifications can yet be set down which will guarantee a given performance.

The best fourth-harmonic generators may be expected to exhibit a conversion loss rising from 30 db at 5 mw input power to 33 db at 100 mw input power. Although many of the rectifying contacts may deteriorate at input power levels above 100 mw, some may still be usable, so as to give a greater absolute value of output power.

Detector crystal sensitivity of the *best* units compares favorably with that of typical crystals for lower microwave frequencies, so that the minimum detectable signal for a given bandwidth is about the same.[8] The factor limiting the dynamic range of measurement is the maximum 3 mm power that can be produced, which is still in the microwatt region.

As an additional result, evidence of an important effect in which the harmonic generation process degrades the signal-to-noise ratio of the source was found.

[7] J. M. Richardson and J. J. Faris, "Excess noise in microwave crystal diodes used as rectifiers and harmonic generators," to be published in IRE Transactions on Microwave Theory and Techniques; July, 1957.

[8] See, for example, the discussion in Carol G. Montgomery, "Technique of Microwave Measurements," Rad. Lab. Series, vol. 11, McGraw-Hill Book Co., Inc., New York, N. Y. p. 547f; 1947.

Circularly Polarized Microwave Cavity Filters*

CONRAD E. NELSON†

Summary—A new group of circularly polarized microwave cavity filters is described. With a single circularly polarized cavity, a reflectionless filter is achieved that couples nearly 100 per cent of the energy from the main waveguide at the cavity resonant frequency. Two degenerate cavity modes may be excited, to produce a circularly polarized field, by coupling to the transverse and longitudinal waveguide magnetic fields or to the transverse electric and magnetic waveguide fields.

A theoretical analysis is presented as well as experimental results. The loss between the band-pass terminals of the reflectionless cirlarly polarized filter is identical with the loss in a conventional reflection-type band-pass filter with the same bandwidth and cavity-wall losses. The null at resonance between the band-elimination terminals of the reflectionless circularly polarized filter is limited only by the asymmetries of the cavity and not by the cavity-wall losses. Design equations and curves are given for eight of the lower order, circularly cylindrical, degenerate cavity modes that are coupled to a rectangular waveguide at the point of circularly polarized waveguide magnetic fields.

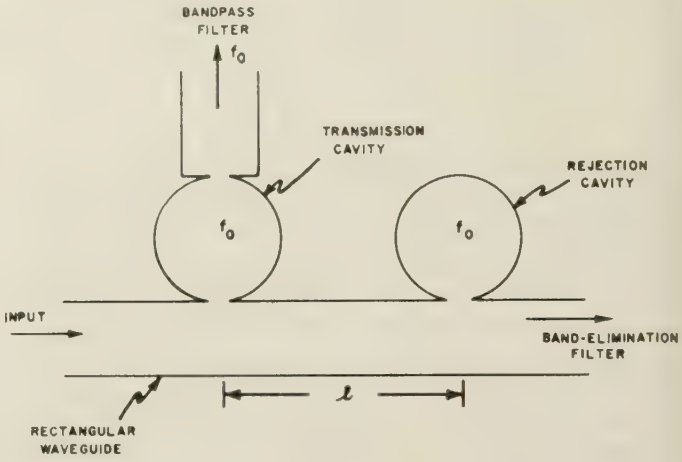

Fig. 1—Conventional waveguide diplexer.

I. Introduction

IN THE CONVENTIONAL design of three terminal microwave cavity filters, at least two cavities are required to produce a matched filter capable of coupling nearly 100 per cent of the power from the main waveguide at resonance. Fig. 1 illustrates this method of diplexing.

A low-loss "rejection" cavity must be spaced a critical distance from the main cavity. The single circularly polarized cavity described in this paper can replace these two cavities and perform the same function. The theoretical loss for the two systems is the same (assuming that each system has the same band-width and cavity loss). However, the isolation at resonance for the conventional two-cavity diplexer is limited by the rejection cavity losses, while the isolation of the circularly polarized cavity is limited only by asymmetries of the cavity.

There are many applications for the circularly polarized single-cavity filter. Since this filter is essentially reflectionless, several may be placed in series without producing large reflections. The circularly polarized cavity may be used as a passive duplexer for a circularly polarized radar as well as a nonreciprocal, tunable filter by placing a ferrite in the circularly polarized magnetic fields in the cavity. The use of a ferrite also permits the design of a narrow-band duplexer for use with linearly polarized radar systems.

II. Principle of Operation

One configuration of the circularly polarized microwave cavity filter is shown in Fig. 2(a). It has four waveguide ports and only one circularly cylindrical cavity.[1] The cavity is designed to operate with two orthogonal, degenerate, TE_{112} modes (several other cavity modes will work just as well). Two circular coupling holes are centered at each end of the cavity, but they are offset from the waveguide centerline. Fig. 2(b) shows the cavity rf magnetic fields;[2] these fields are coupled to the transverse (H_x) and longitudinal (H_z) waveguide magnetic fields. In this example, the circular coupling holes are placed in the waveguides at the point of circular polarization of the waveguide magnetic fields [Fig. 2(c)].

The operation of the filter is as follows. Energy enters the waveguide at port A [Fig. 2(a)] and excites the cavity in a circularly polarized TE_{112} mode, since H_x and H_z in the waveguide are 90 degrees out of time phase. The excited cavity radiates into waveguides A-B and C-D. However, due to the direction of circulation of the cavity modes, the cavity will radiate only toward waveguide ports B and C. Therefore, with an input signal at port A, there should be no reflection back to port A, and the output energy will divide between ports B and C.

The fact that the filter is reflectionless is important, but an even more important characteristic is that nearly 100 per cent of the energy entering port A can be coupled into arm C at the cavity resonant frequency (neglecting cavity-wall losses). Normally, a single-mode cavity must share the input energy with the load in arm B, since the two are either in series or in parallel. However,

* Manuscript received by the PGMTT, October 3, 1956.
† Res. Labs., Hughes Aircraft Co., Culver City, Calif.

[1] This type of filter is being investigated independently by S. B. Cohn and F. S. Coale at the Stanford Res. Inst. See "Directional channel-separation filters," 1956 IRE Convention Record, part 5, pp. 106–112.

[2] S. Ramo and J. Whinnery, "Fields and Waves in Modern Radio," John Wiley and Sons, Inc., New York, N. Y.; 1947.

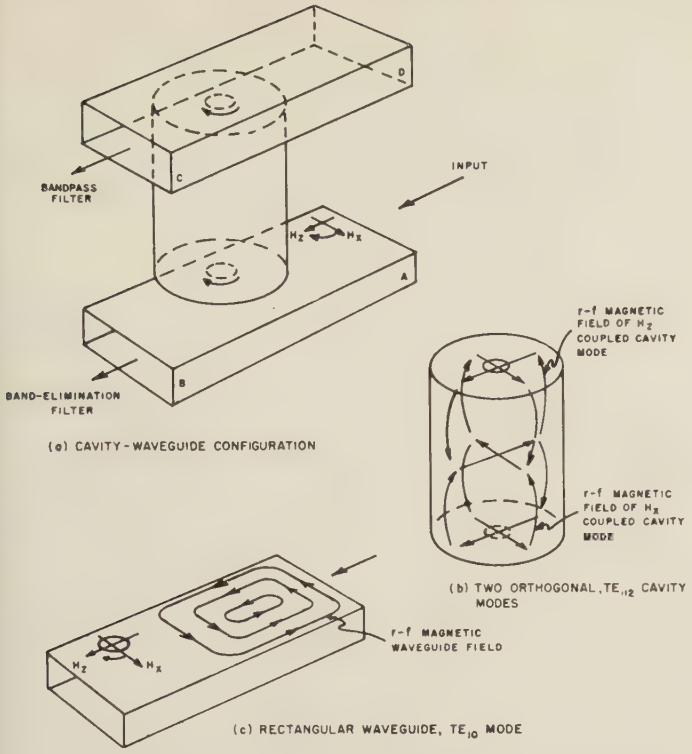

Fig. 2—A circularly polarized microwave cavity filter using magnetic field coupling.

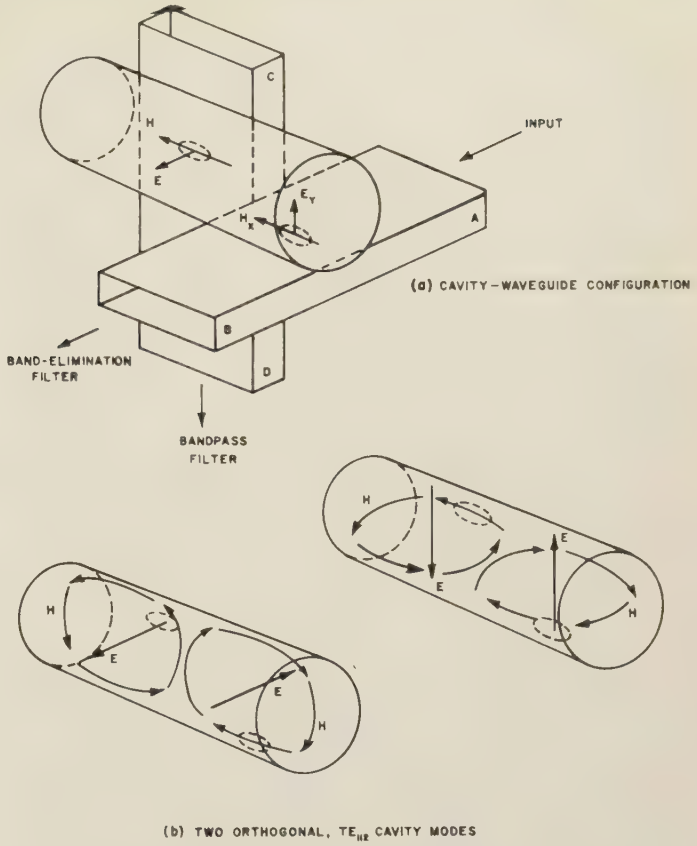

Fig. 3—A circularly polarized microwave cavity filter using electric and magnetic field coupling.

with the dual-mode cavity, each cavity mode couples out one half of the incident energy at resonance, and this produces a null in arm B. Far off resonance, the cavity will not couple to the waveguide, and all the energy entering port A will leave port B. The result is a single-cavity, reflectionless filter that is band-elimination between ports A-B and band-pass between ports A-C.

In the preceding example, a circularly polarized cavity mode is attained by coupling to the circularly polarized waveguide magnetic fields. Another arrangement that will produce a circularly polarized cavity mode is shown in Fig. 3. The cavity is designed to operate with two orthogonal, degenerate, TE_{112} modes. Two coupling holes are spaced between the end plates of the cavity and on the waveguide centerline. Fig. 3(b) shows the cavity rf magnetic and electric fields. These fields are coupled to the waveguide transverse magnetic (H_x) and transverse electric (E_y) fields. In the waveguide, the transverse components of electric and magnetic fields are in phase, but in a cavity, E and H for one mode are 90 degrees out of time phase. Therefore, the magnetic field of the E_y-coupled cavity mode lags (or leads, depending upon assigned directions of mode orientation) the magnetic field of the H_x-coupled cavity mode by 90 degrees. The coupling holes are centered in the waveguide, to couple to the peak of the transverse waveguide fields. The slot is adjusted in shape to produce equal coupling to the two cavity modes, because the electric and magnetic fields are different in the waveguide as well as in the cavity.

The operation of the E_y- and H_x-coupled cavity is similar to the H_x- and H_z-coupled cavity. Energy entering port A excites the cavity in a circularly polarized TE_{112} mode. The excited cavity then radiates into waveguides A-B and C-D. However, the radiations of the two cavity modes back to port A will cancel, since they are 180 degrees out of time phase. In waveguide C-D, the energy from both cavity modes cancels at port C, but adds at port D. As before, a reflectionless band-elimination and band-pass filter results.

Any combination of the above two coupling methods may be used, as well as different waveguide orientations. The coupling holes in the E and H coupling technique do not have to be at right angles but may be opposite each other, provided that the cavity mode configuration is favorable. Also many degenerate cavity modes have more than one position on the end plate at which a circularly polarized magnetic field results.

III. Analysis of Dual-Mode Cavity With Four Waveguide Ports

Fig. 2 is an example of a cavity system to which the following analysis applies. Several other cavity modes, coupling-hole shapes, positions, and waveguide orientations will work just as well. Some of these will be described later. The important requirement of the reflectionless filter is that two orthogonal waveguide fields are

coupled to two orthogonal cavity modes that are resonant at the same frequency and are 90 degrees out of time phase. The coupling to the two cavity modes must take place in the same transverse waveguide plane. As the analysis will show, the coupling-hole position or shape must be adjusted, to produce an equal coupling to each cavity mode. In general, the analysis also applies to the cavity system shown in Fig. 3; however, the equivalent circuit will be slightly different. Although this analysis applies primarily to the dual-mode cavity with four waveguide ports and two coupling holes, only slight modifications are required, to cover the case of a cavity system with two waveguide ports and only one coupling hole.

The conventional microwave cavity filter analysis will be reviewed briefly, since most of these circuit equations and equivalent circuits can be applied to the solution of the reflectionless dual-mode cavity filter.

A. Series Coupling

A cavity, coupled only to the transverse magnetic field (H_x) of the TE_{10} rectangular waveguide mode, acts in series with the waveguide. It is assumed that all cavity modes except the desired one are far off resonance and will not affect the equivalent circuit. The waveguide is represented as a transmission line of characteristic impedance Z_0 and the cavity (H-coupled) presents an impedance Z_c in series with the transmission line. Fig. 4(a) illustrates the cavity-waveguide arrangement. Either the impedance Z_c or the normalized impedance z is a parallel tuned circuit as shown in Fig. 4(b). However, a more useful equivalent circuit [Fig. 4(c)] is obtained by letting the cavity internal impedance be a series tuned circuit and then having a special transformer reverse this impedance, so that the transmission line (TL) sees a parallel tuned circuit.[3,4] The normalized impedance

$$\frac{1}{Q_c} + j\left(\frac{f}{f_0} - \frac{f_0}{f}\right)$$

is the "internal" cavity loss and reactance. The cavity Q, Q_c, represents the cavity losses, such as a lossy cavity dielectric and cavity wall losses. The cavity current I_c represents the actual current in the cavity walls and, hence, is proportional to the magnitude of the cavity fields. The relations between the cavity and TL normalized currents and voltages are

$$\left.\begin{aligned} I_c &= \pm j\sqrt{Q_w}V_2 \\ V_c &= \pm j\frac{I_1}{\sqrt{Q_w}} \\ \frac{V_c}{I_c} &= \frac{1}{Q_c} + j\left(\frac{f}{f_0} - \frac{f_0}{f}\right) \end{aligned}\right\} \quad (1)$$

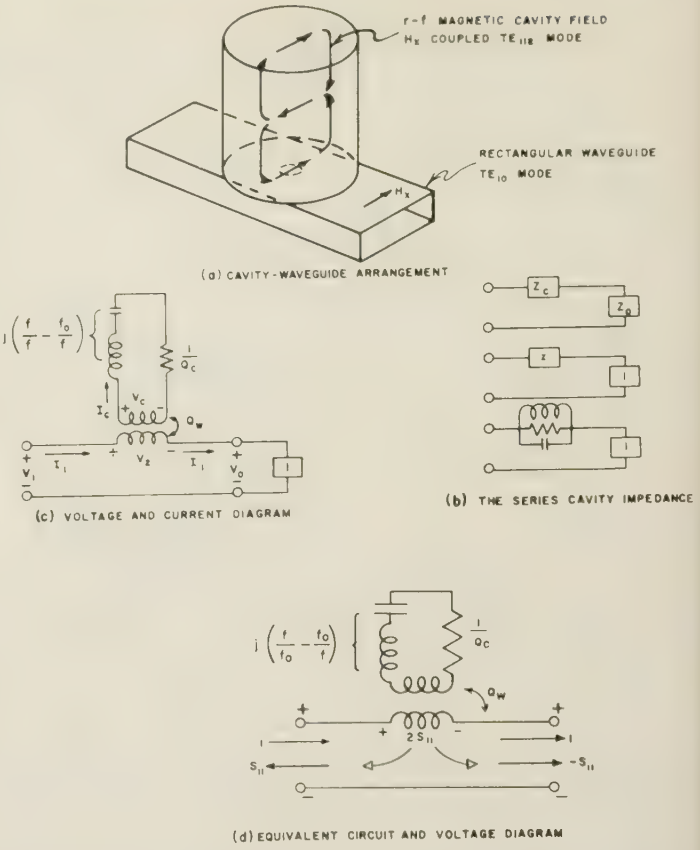

Fig. 4—Series-coupled cavity with two waveguide ports.

where

Q_w = window Q or window-coupling factor[5]
Q_c = cavity Q
f_0 = cavity resonant frequency
f = frequency.

The signs of the internal cavity current, I_c, and voltage, V_c, depend upon the assigned polarity of the cavity mode. The normalized cavity impedance in series with the TL is

$$z = \frac{V_2}{I_1} = \frac{1}{Q_w}\frac{I_c}{V_c} = \frac{1}{\frac{Q_w}{Q_c} + jQ_w\left(\frac{f}{f_0} - \frac{f_0}{f}\right)}. \quad (2)$$

The special transformer, represented by the window coupling factor Q_w, has no impedance itself, but only inverts the "internal" cavity impedance. The reciprocal of the window-coupling factor Q_w represents the amount of coupling between the cavity and the waveguide. Without a coupling hole, the coupling is zero, Q_w is infinite, and the cavity impedance z is zero. As the coupling hole is made larger Q_w decreases and z increases. H. A. Bethe has determined Q_w, and numerical values of Q_w are given in Section V. It should be noted that in (2) the value of Q_w differs by a factor of two from that

[3] H. A. Bethe, "Theory of Side Windows in Waveguides," M.I.T. Rad. Lab. Rep. No. 43-27.
[4] H. A. Bethe, "Excitation of Cavities Through Windows," M.I.T. Rad. Lab. Rep. No. 43-30.
[5] Q_w is the same as the external or radiation Q given by C. G. Montgomery, "Technique of Microwave Measurements," McGraw-Hill Book Co., Inc., New York, N. Y.; 1947.

for Q_w in Bethe's article. This is because of the definition of Q_w given in (2).

For an impedance (or cavity) in series with the TL the normalized input impedance z_i with a matched load is $z+1$. The voltage scattering matrix coefficients are

$$S_{11} = \frac{z_i - 1}{z_i + 1} = \frac{z}{2 + z}, \tag{3}$$

and

$$S_{12} = 1 - S_{11}.$$

If a unit voltage is incident upon the cavity system, it will travel along the waveguide, excite the cavity, and proceed to the output terminal. However, the excited cavity radiates back into the waveguide with the voltage equally divided between input and output terminals. The voltage radiated or reflected back to the input terminals is $+S_{11}$, and the net voltage at the input terminals is $1+S_{11}$. The voltage appearing at the output terminals is $1-S_{11}$. The voltage $-S_{11}$ is due to the cavity radiation or cavity impedance [see Fig. 4(d)], The concept of the cavity radiating back into the waveguide to produce two traveling voltages, S_{11} and $-S_{11}$, is important and is required when the series and parallel coupled cavities are combined. Fig. 5 illustrates a more complicated series-coupled cavity system; it also represents the series-coupling equivalent circuit for the dual-mode cavity system. With a unit incident voltage at port A, the cavity will be excited, and the incident voltage will appear at port B. The excited cavity will radiate into waveguides A-B and C-D. The resulting voltages, due to the cavity, will be S_{11}, $-S_{11}$, S_{13}, and $-S_{13}$. The normalized cavity impedance in series with waveguide A-B is

$$z = \frac{1}{\frac{Q_{w1}}{Q_{c1}} + jQ_{w1}\left(\frac{f}{f_1} - \frac{f_1}{f}\right) + \frac{1}{2}\frac{Q_{w1}}{Q_{w2}}}. \tag{4}$$

There is a factor of two in (4), since the cavity coupled to waveguide C-D sees ports C and D in series. The coefficient S_{11} is

$$S_{11} = \frac{1}{1 + \frac{Q_{w1}}{Q_{w2}} + \frac{2Q_{w1}}{Q_{c1}} + j2Q_{w1}\left(\frac{f}{f_1} - \frac{f_1}{f}\right)}. \tag{5}$$

The coefficient S_{13} is obtained as follows. The voltage across the cavity terminals in waveguide A-B is $2S_{11}$, and the voltage across the cavity terminals in waveguide C-D is $2S_{13}$. The "interval" cavity current I_c is

$$I_c = j2S_{11}\sqrt{Q_{w1}} = j2S_{13}\sqrt{Q_{w2}},$$

therefore,

$$S_{13} = \sqrt{\frac{Q_{w1}}{Q_{w2}}}\, S_{11}. \tag{6}$$

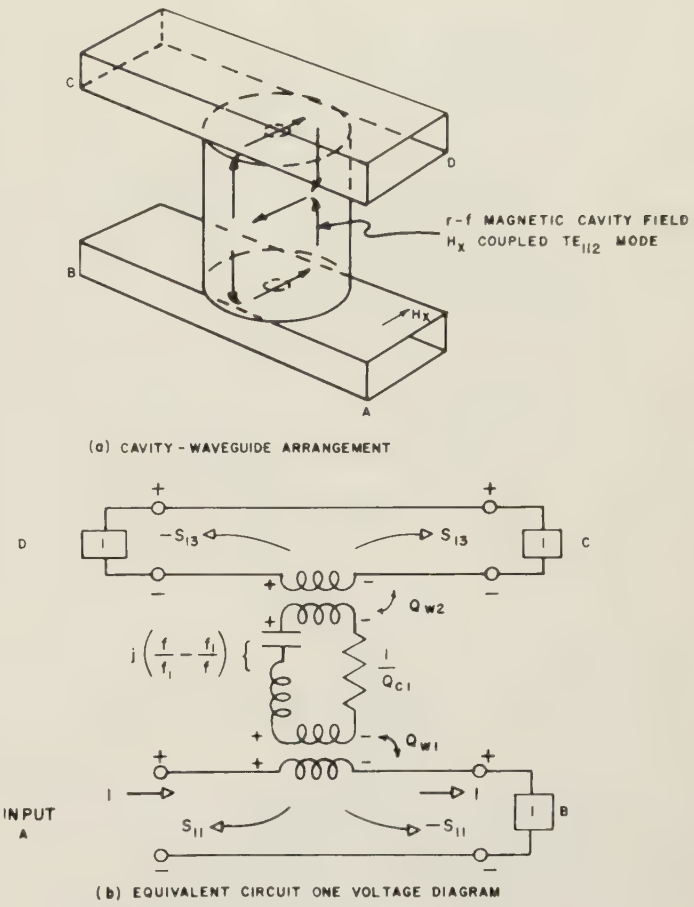

Fig. 5—Series-coupled cavity with four waveguide ports.

The signs of the voltage S_{13} and cavity current I_c may be plus or minus, depending upon the direction of the magnetic fields in the cavity. The sign of S_{13} is chosen as plus, and the same sign convention is used in the parallel-coupled cavity.

B. Parallel Coupling

Let us consider the cavity shown in Fig. 6(a), which couples only longitudinal magnetic fields (H_z) of two waveguides. In the equivalent circuit [Fig. 6(b)] the cavity is in parallel with the TL. This is because a short circuit in arm B, placed one half of a guide wavelength from the cavity coupling hole, would produce a standing wave with zero H_z (and E_y) at the coupling hole. The cavity would not be excited—hence, it would be shorted out as if it were in parallel with the TL. A quarter wavelength TL is needed in the equivalent circuit, to invert the impedance and to present a 90-degree time lag in the voltage reaching the cavity (the H_z waveguide component is 90 degrees behind the H_x and E_y components, which are assigned zero time phase). The internal cavity current for this type of coupling lags by 90 degrees the cavity current for the series-coupled cavity.

With a unit incident voltage at port A, shown in Fig. 6(b), the cavity causes voltages T_{11}, T_{11}, T_{13}, and T_{13} to appear at the four waveguide ports. Normalized, parallel cavity admittance seen by waveguide A-B is

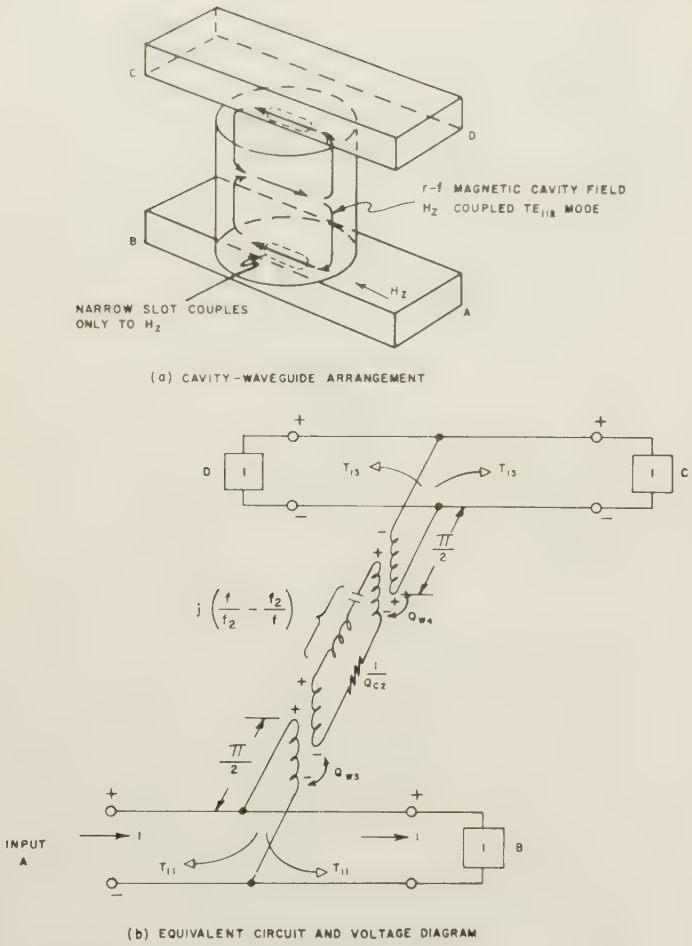

Fig. 6—Parallel-coupled cavity with four waveguide ports.

$$y = \frac{1}{\frac{Q_{w3}}{Q_{c2}} + jQ_{w3}\left(\frac{f}{f_2} - \frac{f_2}{f}\right) + \frac{1}{2}\frac{Q_{w3}}{Q_{w4}}}. \tag{7}$$

The coefficient T_{11} is

$$T_{11} = \frac{1 - (y+1)}{1 + (y+1)} = -\frac{y}{2+y} \tag{8}$$

$$T_{11} = \frac{-1}{1 + \frac{Q_{w3}}{Q_{w4}} + \frac{2Q_{w3}}{Q_{c2}} + j2Q_{w3}\left(\frac{f}{f_2} - \frac{f_2}{f}\right)}. \tag{9}$$

As before (with considerable manipulation),

$$T_{13} = -\sqrt{\frac{Q_{w3}}{Q_{w4}}}\, T_{11}. \tag{10}$$

A negative sign was added to (10), to make it consistent with the assumed polarity of S_{13}.

C. Circularly Polarized Coupling

The complex cavity shown in Fig. 2 can now be analyzed. It should be noted that the coupling hole is offset from the waveguide centerline and couples the orthogonal waveguide H_x and H_z components to the two orthogonal, degenerate, TE_{112} circularly cylindrical cavity modes. There is a component of electric field (E_y) in the coupling hole, due to the waveguide fields, but, since the TE_{112} cavity mode has a zero electric field at the center of the end plate, this component does not provide additional coupling to this mode, and the other cavity modes are far off resonance.

The transverse waveguide field H_x couples to the first cavity mode (with constants Q_{w1}, Q_{w2}, Q_{c1}, and f_1). The longitudinal waveguide field H_z couples to the second cavity mode (with constants Q_{w3}, Q_{w4}, Q_{c2}, and f_2). There is no interaction between the series- and parallel-coupled cavity modes, because the cavity modes are orthogonal and are excited by orthogonal fields in the waveguide. Furthermore, the waveguide ports B, C, and D are terminated in matched loads. With a unit incident voltage at port A, the series cavity produces voltages S_{11}, $-S_{11}$, S_{13}, and $-S_{13}$, and the parallel cavity produces voltages T_{11}, T_{11}, T_{13}, and T_{13}. The resulting voltages at each of the waveguide ports are listed below.

Port	Voltage
A	Incident voltage $=1$
A	Reflected voltage $V_a = S_{11} + T_{11}$
B	Output voltage $V_b = 1 - S_{11} + T_{11}$
C	Output voltage $V_c = S_{13} + T_{13}$
D	Output voltage $V_d = -S_{13} + T_{13}$

A comparison of (5) and (8) shows that, if the normalized, series cavity impedance is equal to the normalized, parallel cavity admittance, then

$$z = y$$

and

$$S_{11} = -T_{11}$$
$$S_{13} = +T_{13}$$

the resulting output voltages (for a unit incident voltage at port A) are

$$V_a = 0$$
$$V_b = 1 - 2S_{11} = \frac{2-z}{2+z}$$
$$V_c = 2S_{13} = \frac{2z}{2+z}\sqrt{\frac{Q_{w1}}{Q_{w2}}}$$
$$V_d = 0. \tag{11}$$

The requirements for a reflectionless filter are

$$Q_{w1} = Q_{w3} \text{ (in waveguide A-B)}$$
$$Q_{w2} = Q_{w4} \text{ (in waveguide C-D)}$$
$$Q_{c1} = Q_{c2}$$
$$f_1 = f_2. \tag{12}$$

Therefore, a reflectionless filter results when each cavity mode has the same resonant frequency, loss, and coupling to the waveguide fields. The electromagnetic fields in the two cavity modes are equal in amplitude, but are

90 degrees out of phase; hence, a true circularly polarized mode results. If a circular coupling hole is used, it must be placed at a position of circular polarization of waveguide magnetic fields, since the cavity modes are identical. If an asymmetrical slot is used, it must be placed in the waveguide in a manner that will compensate for its symmetry and produce equal coupling.

The power transfer characteristics for the circularly polarized filter can be expressed in simplified terms. Assume a unit incident power (of frequency f) at port A; then, the resulting output powers are

$$P_a = 0$$

$$P_b = \frac{m + x^2}{1 + x^2}$$

$$P_c = \frac{n}{1 + x^2}$$

$$P_d = 0, \tag{13}$$

where

$$P = |V|^2 = \frac{\text{Output Power}}{\text{Incident Power at A}}$$

$$x = \frac{2(f - f_0)}{BW} \tag{14}$$

$$m = \left[\frac{\frac{1}{Q_{w2}} - \frac{1}{Q_{w1}} + \frac{2}{Q_c}}{\frac{1}{Q_{w2}} + \frac{1}{Q_{w1}} + \frac{2}{Q_c}}\right]^2 \sim 0 \tag{15}$$

$$n = \frac{1}{\left[\frac{1}{2}\left(\sqrt{\frac{Q_{w1}}{Q_{w2}}} + \sqrt{\frac{Q_{w2}}{Q_{w1}}}\right) + \frac{\sqrt{Q_{w1}Q_{w2}}}{Q_c}\right]^2} \sim 1 \tag{16}$$

$$\frac{1}{Q_L} = \frac{BW}{f_0} = \frac{1}{2}\left(\frac{1}{Q_{w1}} + \frac{1}{Q_{w2}}\right) + \frac{1}{Q_c} \tag{17}$$

BW = 3-db bandwidth.

Eq. (13) predicts three important characteristics of this system:

1) Throughout the operating frequency band including resonance there will be practically no reflection back to port A.
2) At resonance there will be a power null of amplitude m at port B. This results in a "reflectionless band-elimination filter."
3) At resonance, energy will be coupled through the cavity and will produce power output of amplitude n at port C. This results in a "reflectionless band-pass filter."

D. Equivalent Circuit

An equivalent circuit for the filter illustrated in Fig. 2 is shown in Fig. 7. The special transformer for the series-coupled cavity is center-tapped, and each leg has an equivalent window-coupling factor of $4Q_w$, because

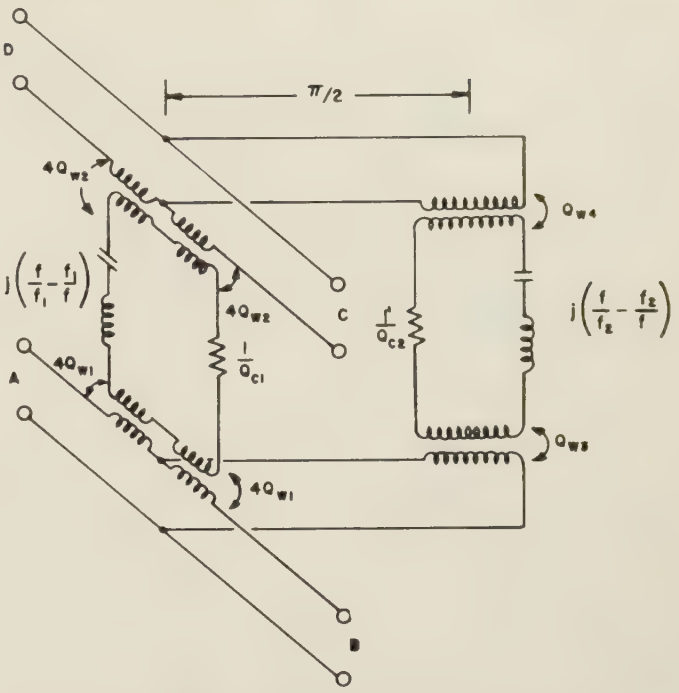

Fig. 7—Equivalent circuit for the dual-mode cavity with four ports.

the coupling is actually proportional to the reciprocal of the square root of Q_w. Different currents are in each leg of the series-coupling transformer, and this produces the effect required to achieve unity coupling between ports A and C (neglecting losses). By observing the electromagnetic fields and the type of coupling in any cavity and waveguide system, the proper equivalent circuit can be determined as well as the direction of power flow at resonance.

E. Optimum Band-pass Filter

The condition of maximum power transfer between ports A and C is achieved when coupling holes of the same size are placed in waveguides A-B and C-D. The resulting equations are

$$Q_w = Q_{w1} = Q_{w2} = Q_{w3} = Q_{w4}$$

$$\frac{1}{Q_L} = \frac{1}{Q_w} + \frac{1}{Q_c} = \frac{BW}{f_0}$$

$$n = \left[1 - \frac{Q_L}{Q_c}\right]^2$$

$$m = \left[\frac{Q_L}{Q_c}\right]^2. \tag{18}$$

With zero cavity-wall losses, unity coupling from the main waveguide at resonance can theoretically be achieved. The system is symmetrical, inasmuch as the operations from A to C, C to A, B to D, and D to B are identical. It should also be pointed out that the band-pass filter loss for the circularly polarized filter is identical with the loss in a conventional band-pass filter or with the two cavity filters shown in Fig. 1 (assuming the same bandwidth and cavity Q). Eq. (18) also indi-

cates that, with maximum power transfer between ports A and C (Fig. 2), the isolation at resonance between ports A and B is not optimum. Isolation at resonance can theoretically be made to approach infinity with an unnoticeable increase in loss between ports A and C.

F. Optimum Band-Elimination Filter

The isolation between ports A and B can theoretically be made infinite by making the coupling hole in waveguide C-D slightly smaller than that in waveguide A-B. The resulting equations are

$$\begin{aligned} Q_{w1} &= Q_{w3} = Q_L \\ Q_{w2} &= Q_{w4} = \frac{Q_{w1}}{1 - \frac{2Q_{w1}}{Q_c}} \geq Q_{w1} \\ n &= 1 - \frac{2Q_L}{Q_c} \\ m &= 0. \end{aligned} \tag{19}$$

In a conventional band-elimination filter, the cavity loss limits the isolation at resonance. In the circularly polarized filter, there is no theoretical limitation on isolation, only a practical limitation. When the isolation is larger than 30 or 40 db, the null is usually too sharp to be of any use. With coupling holes of different sizes, there is optimum isolation only between ports A and B or B and A.

G. Two-Port Band-Elimination Filter

The equations for the band-elimination filter, when waveguide C-D is removed, are

$$\begin{aligned} Q_{w2} &= Q_{w4} = \infty \\ \frac{1}{Q_L} &= \frac{1}{2Q_{w1}} + \frac{1}{Q_c} \\ \sqrt{m} &= \frac{\frac{Q_{w1}}{Q_c} - \frac{1}{2}}{\frac{Q_{w1}}{Q_c} + \frac{1}{2}}. \end{aligned} \tag{20}$$

The null in output power at resonance can be made zero by adding a lossy material to the cavity. If

$$Q_c = 2Q_{w1}, \tag{21}$$

then

$$\begin{aligned} Q_L &= Q_{w1} \\ m &= 0 \\ P_b &= \frac{x^2}{1 + x^2}. \end{aligned}$$

Now the cavity Q, Q_c, includes the lossy material in the cavity. If too much loss is added to the cavity, the null will not be zero. Only a specified cavity loss will produce a zero null, as indicated by (21).

If an isolation of 30 db is required over a narrow frequency band, the 3-db bandwidth will have to be large, because 30 db is maintained only over 3.16 per cent of the 3-db bandwidth ($m = 0$). If two identical cavity systems having a zero null and the same resonant frequency are placed in series along a waveguide (the spacing is not critical, since each cavity system is reflectionless), the normalized output power is

$$P_b = \left[\frac{x^2}{1 + x^2}\right]^2 = \left[\frac{u^2}{0.4142 + u^2}\right]^2 \tag{22}$$

where

$$\begin{aligned} x &= \frac{2(f - f_0)}{f_0} Q_{w1} \\ u &= \frac{2(f - f_0)}{f_0} Q_L \\ Q_L &= \sqrt{\sqrt{2} - 1} Q_{w1} \\ Q_c &= 2Q_{w1}. \end{aligned}$$

Therefore, an isolation of 30 db is maintained over 11.6 per cent of the 3-db bandwidth. If the resonant frequencies of the two cavity systems are separated until the response has a 30-db ripple, then the ratio of the 30-db bandwidth to the 3-db bandwidth increases to 16.4 per cent. Note that a single-cavity system has two cavity modes resonant at the same frequency.

If two cavity systems are placed in parallel (two coupling holes in the same transverse waveguide plane), then, with a ripple in the response, the theoretical ratio of the 30-db bandwidth to 3-db bandwidth is 24.8 per cent.

IV. Discussion of Cavity Modes and Coupling

In section III, it has been shown that, when a waveguide excites a circularly polarized cavity field by means of two orthogonal couplings in the same transverse waveguide plane, a reflectionless microwave filter results. Therefore, a single-cavity, reflectionless filter may be constructed using a spherical, a square, or a circular cylindrical cavity, with aperture, loop, or probe coupling. Loop coupling would be advantageous at the lower frequencies. However, the following discussion is restricted to aperture-coupled, circular cylindrical cavities.

A given cavity shape can support an infinite number of cavity modes. The use of higher order cavity modes will, in general, result in the following characteristics: 1) higher cavity Q, *i.e.*, lower wall losses; 2) larger size; 3) smaller available coupling (smaller bandwidth for a given coupling-hole size); and 4) other modes that have resonant frequencies close to that of the desired mode. Therefore, it seems expedient at this time to list the lower order cavity modes that may be circularly polarized. Eight of the lower order circular cylindrical cavity modes that, when circularly polarized, have a circularly polarized magnetic field at the center of the end plate

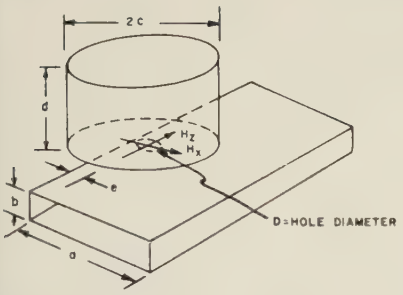

(a) TYPE A COUPLING

Lowest-order Usable modes

TE_{111} TM_{110}
TE_{121} TM_{120}
TE_{112} TM_{111}
TM_{121}
TM_{112}

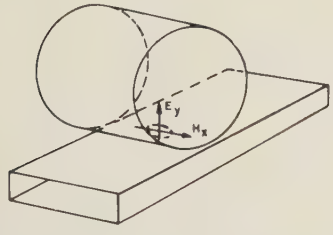

(b) TYPE B COUPLING

TE_{111}
TE_{211}
TE_{311}
TE_{112}

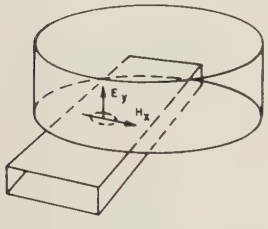

(c) TYPE C COUPLING

TM_{110}
TM_{210}
TM_{310}
TM_{120}
TM_{111}
TM_{211}

Fig. 8—Types of coupling for circularly polarized cavity modes using circularly cylindrical cavities.

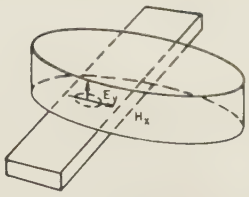

(a) CAVITY – WAVEGUIDE CONFIGURATION

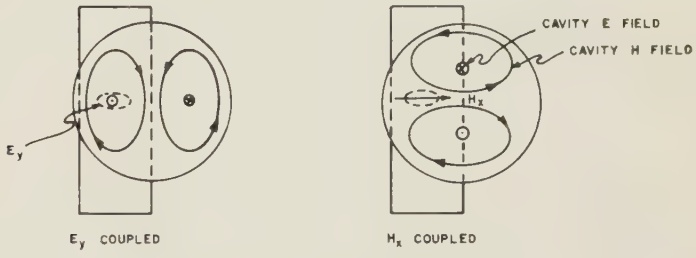

(b) TWO ORTHOGONAL, TM_{110} CAVITY MODES

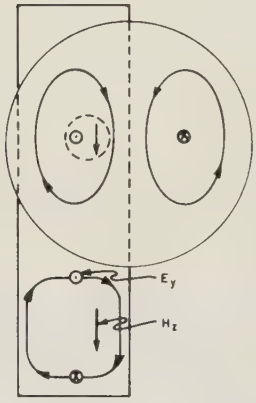

(c) E_y AND H_z COUPLING TO ONE MODE

Fig. 9—Circularly polarized cavity, TM_{110} mode.

are listed in Fig. 8(a). These modes are coupled to the H_x and H_z waveguide fields (Type A coupling). Four of the lower order, degenerate, TE modes that may be E_y- and H_x-coupled (Type B coupling) are given in Fig. 8(b), and six of the lower order, degenerate, TM modes that may be E_y- and H_x-coupled (Type C coupling) are listed in Fig. 8(c). For the cavity-waveguide configuration illustrated in Fig. 8(b), only the TE cavity modes have a longitudinal magnetic field. Similarly in Fig. 8(c), only the TM cavity modes have a longitudinal electric field. Fig. 9(a) and 9(b) illustrates Type C coupling to two orthogonal, TM_{110} cavity modes. The coupling hole is on the waveguide centerline and at the position of maximum electric field in the cavity for one TM_{110} mode. The shape of the coupling hole is adjusted, to vary the electric and magnetic polarization of the aperture, and to obtain a circularly polarized cavity field. The position of the coupling hole does not permit H_z coupling between the waveguide and the E_y-coupled cavity mode. However, it may be advantageous to allow a certain amount of H_z coupling. For example, if it were desired to use a circular coupling hole in Fig. 9(a) for all ratios of cavity diameter to cavity length, then the position of the circular hole would be varied in the waveguide and cavity, to produce a circularly polarized cavity mode. In this case, a combination of H_x, E_y, and H_z coupling is being used. As illustrated in Fig. 9(c), a slight movement of the coupling hole in the waveguide and cavity allows a small amount of H_z coupling. The H_z coupling affects only the E_y-coupled mode, and it either adds or subtracts to the amount of E_y coupling. If the hole in the waveguide and cavity is moved in the same direction, as in Fig. 9(c), then the H_z coupling adds to the E_y coupling, since H_z lags E_y by 90 degrees in the waveguide, and H lags E by 90 degrees in the cavity for the given field directions.

The coupling hole in a cavity alters the electromagnetic cavity fields so that the cavity resonant frequency is different from the resonant frequency calculated from the cavity diameter and length. Bethe's analysis[4] shows that a cavity mode with a magnetic field in the aperture lowers the resonant frequency, and that an electric field in the coupling aperture raises the resonant frequency. Therefore, with Type A coupling, each cavity-mode resonant frequency will be lowered by nearly the same amount. For large coupling holes, the magnetic field of one cavity mode in the coupling aperture sees the waveguide wall in closer proximity than does the magnetic field of the other cavity mode. In such a case, a small tuning screw is required for one of the cavity modes, in

order to adjust both modes to the same resonant frequency. With Types B and C coupling, the resonant frequency of the two cavity modes is changed in opposite directions, due to the coupling hole, and a larger tuning screw for one of the modes will be required.

However, when a symmetrical coupling system is used (as in Fig. 3), each cavity mode uses both E and H coupling, and the resonant frequency of each mode should be the same. Even though the resonant frequencies are theoretically the same, very small tuning screws are usually required to compensate for manufacturing tolerances.

V. Window-Coupling Factor, Q_w

The value of the window-coupling factor Q_w is a measure of the coupling between the waveguide and cavity. This coupling and the cavity losses determine the bandwidth of a particular filter, as was shown in section III. The basic equation for Q_w has been determined by Bethe using small-coupling-hole theory (the hole size is much smaller than the wavelength, and the hole is in a uniform cavity and waveguide field).[3,4,6] As the coupling hole increases in size, the error in the calculated value of Q_w increases. With this restriction in mind, theoretical curves of Q_w, for Type A coupling, are shown in Fig. 10. Theoretical curves of Q_w, for Types B and C coupling, are omitted, since their derivation is much more involved.

The values of Q_w for the cavity diameter-length ratios given in Fig. 10 were computed for a standard X-band waveguide (0.9 by 0.4 inch) with a cavity resonant frequency of 9000 mc. At this frequency, the point of circularly polarized magnetic field in the waveguide is 0.234 inch from one side wall. The maximum coupling-hole diameter is then 0.468 inch, which is the hole size used for the curves shown in Fig. 10. To find the window-coupling factor[7] for a hole with a diameter of D inches, multiply the value of Q_w in Fig. 10 by

$$\left[\frac{0.468}{D}\right]^6. \tag{23}$$

These theoretical curves indicate the minimum value of Q_w attainable for a given cavity diameter-to-length ratio. For example, if a 20-mc bandwidth was required ($Q_L = 450$) using a TE_{112} mode in a band-pass filter, the value of Q_w would be approximately 465 [from (18) and by assuming that $Q_c = 14{,}000$]. Then (from Fig. 10), it is determined that the cavity would have to have a diameter-to-length ratio approximately between 0.4 and 1.4. If the cavity diameter-to-length ratio is 0.8, then the required coupling-hole diameter is

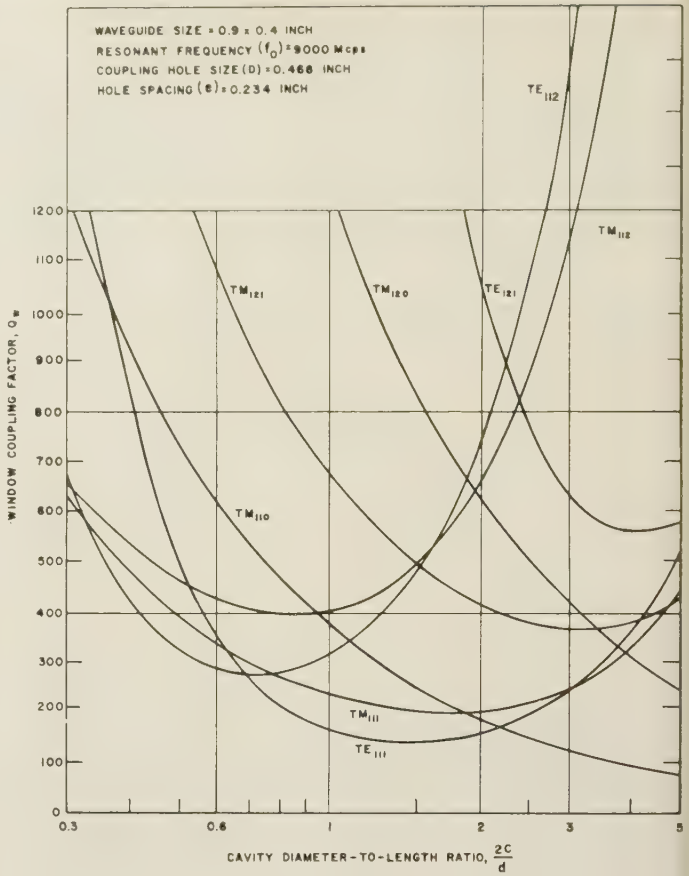

Fig. 10—Window coupling factors for circularly cylindrical cavities using type A coupling.

$$D = 0.468\left[\frac{280}{465}\right]^{1/6} = 0.430 \text{ inch.}$$

Actually, for a window size this large, the value of the curves for Q_w may be as much as 30 per cent in error. The window size should probably be made 0.440 inch instead of 0.430 inch. The optimum diameter would have to be determined experimentally. Therefore, Fig. 10 should be used only as a design aid. However, the curves are useful in determining approximate values of Q_w or D, as well as in determining which cavity modes do not have sufficient coupling, for a given bandwidth requirement. Theoretical curves for both cavity Q and the resonant frequency of most of the modes shown in Fig. 10 are given by Montgomery.[5]

Because of its length, a theoretical analysis of Q_w is not included in this paper. However, the value of Q_w is proportional to

$$\frac{a^3 b\lambda^2}{D^6\sqrt{1-\left(\frac{\lambda}{2a}\right)^2}}, \tag{24}$$

for a given cavity diameter-to-length ratio. Fig. 8(a) illustrates cavity-waveguide dimensions as given in (24).

[6] H. A. Bethe, "Formal Theory of Waveguides of Arbitrary Cross Section," M.I.T. Rad. Lab. Rep. No. 43-26.

[7] M. Surdin, "Directive couplers in waveguides," *J. IEE*, part IIIA, vol. 93, pp. 725–736; March–May, 1956.

VI. Applications

There are many applications for the reflectionless microwave filter. The simplest filter is the band-elimination filter with two waveguide ports. Normally, a TE_{111} circularly cylindrical cavity mode, Type A coupled, would be used, since it is very small and does not require a high cavity Q. The four-port, reflectionless diplexer (Figs. 2 and 3) can be constructed in several ways. Each cavity mode and type of coupling has certain advantages and disadvantages as far as loss, available bandwidth, unwanted modes, and availability for temperature compensation are concerned. Therefore, the type of cavity to be used will depend upon the application.

A circular polarization separator may be constructed, as shown in Fig. 11, by using a single cavity, a rectangular waveguide, and a circular waveguide. At the cavity resonant frequency, energy entering port A will be coupled to arm C. At port C, the energy will be in the form of a circularly polarized TE_{11} mode. If the input was at port B, then the energy coupled to arm C would be circularly polarized in the opposite direction. Therefore, this device would be suitable as a duplexer for a fixed-frequency circularly polarized radar. The transmitter, receiver, and antenna would be connected to ports A, B, and C, respectively. The cavity would be tuned to the transmitter frequency. Transmitted energy would be coupled from arm A to arm C and would radiate from the antenna as a circularly polarized field. Target reflections would be received by the antenna and coupled from arm C to B. There would be approximately 40-db isolation between the transmitter and receiver. This system sees twice the cavity loss; therefore, a large cavity bandwidth should be used to minimize this loss.

The addition of a ferrite in the circularly polarized cavities at the point of circularly polarized magnetic field produces a reflectionless filter that is nonreciprocal and tunable. An important application of the ferrite-loaded reflectionless filter is a passive duplexer for a fixed-frequency radar (see Nelson[8]).

VII. Sample Designs and Experimental Results

Several cavities with Type A coupling have been built and tested. The tests results verify the analysis and indicate the degree of accuracy of the theoretical curves of window-coupling factor Q_w.

The reflectionless filter shown in Fig. 2 was constructed using the TE_{111} circularly cylindrical cavity mode. The internal cavity length is 0.800 inch and the diameter is 1.350 inches. Two coupling holes 0.370 inch in diameter, with a 0.020-inch wall thickness, were placed 0.212 inch from the centerline in a standard,

[8] C. E. Nelson, "Ferrite tunable microwave cavities and the introduction of a new reflectionless, tunable microwave filter," presented at the Symposium on Microwave Properties and Applications of Ferrites, Harvard Univ., Cambridge, Mass.; April 2, 1956.

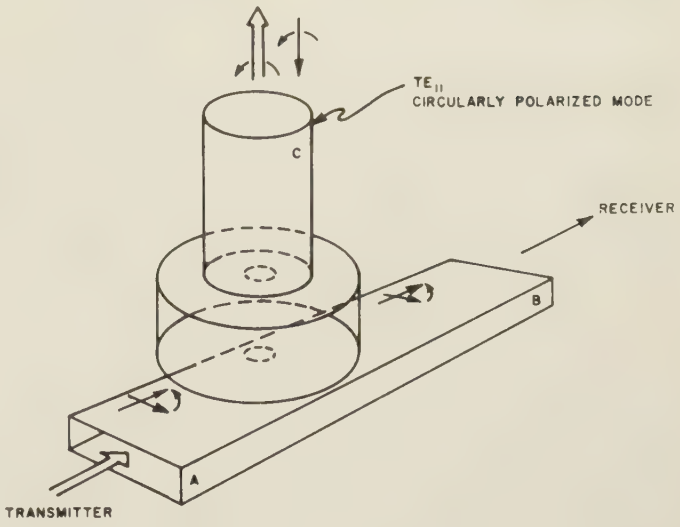

Fig. 11—Circular polarization separator.

X-band rectangular waveguide (0.400 by 0.900 inch). Five turns of an 0–80 NF metal screw, that was placed midway between the cavity end-plates, were required to reduce the resonant frequency of one cavity mode, so that both cavity modes were resonant at the same frequency (in order to produce a minimum reflection at the input waveguide). The TE_{111} cavity mode is resonant at 8755 mc, and there are no other mode resonances between 8300 and 10,000 mc. Between waveguide terminals A and C, the loss at resonance is 0.9 db and the bandwidth is 11.8 mc. The isolation between terminals A and B and between terminals A and D at resonance is 19.9 db and 27.9 db, respectively. For coupling holes of equal size, (18) may be transformed into

$$Q_w = \frac{Q_L}{\sqrt{n}}$$

$$Q_c = \frac{Q_L}{1 - \sqrt{n}}$$

$$m = (1 - \sqrt{n})^2,$$

where $n = 0.814$ for a 0.9-db loss. Using this experimental data, the calculated values of Q_L, Q_w, Q_c, and m are 742, 823, 6810, and 19.3 db, respectively. The calculated value of m (the isolation between A and B at resonance) corresponds very well with the measured value of 19.9 db. The value of Q_w is 32 per cent higher than that predicted in Fig. 10 and by (23) and (24). The cavity Q, Q_c, is 50 per cent lower than the theoretical value for solid silver cavity walls. A polished cavity with silver plated walls should have about 70 to 80 per cent of the theoretical cavity Q, because of the porosity and surface finish of the plated silver. The test cavity was slightly oxidized; this would account for the reduction in cavity Q from 70 to 50 per cent. The analysis indicates that, if the coupling hole in the main waveguide (A-B) is increased in size, then the isolation between terminals A

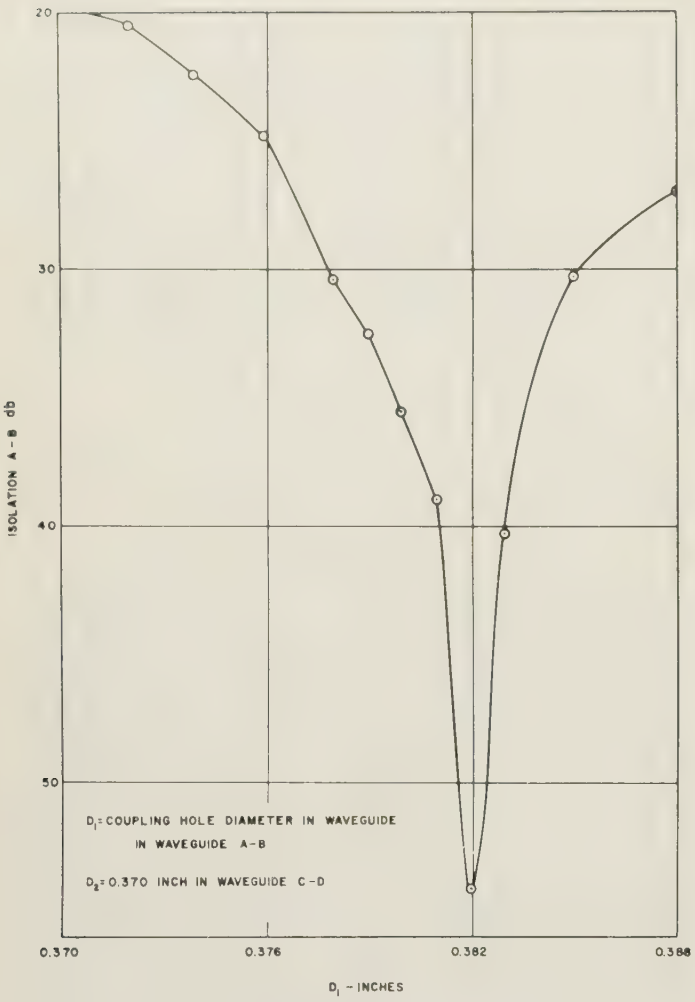

Fig. 12—Isolation between ports A and B for four-port TE_{111} mode cavity filter using type A coupling.

and B at resonance should also increase. The theoretical coupling-hole size for maximum isolation between A and B may be found from (19) and (23).

$$\frac{Q_{w2}}{Q_{w1}} = 1 + \frac{2Q_{w2}}{Q_e} = \left(\frac{D_1}{D_2}\right)^6$$

or

$$\left(\frac{D_1}{0.370}\right)^6 = 1 + \frac{2 \times 823}{6810},$$

then

$$D_1 = 0.3836 \text{ inch.}$$

If the coupling hole in waveguide A-B is 0.0136 inch larger than the hole in waveguide C-D (which is 0.370 inch in diameter), then an infinite isolation at resonance between terminals A-B should result. Fig. 12 shows the experimental measurements of isolation for increasing hole size in waveguide A-B. The maximum isolation (about 54 db) occurred with a hole 0.382 inch in diameter. Fig. 13 is a typical input vswr curve for this filter without a matching button in the waveguide. The off-resonance reactance of the coupling hole in the waveguide produces a vswr of about 1.10. Near resonance, the cavity impedance produces a small reflection that adds to, or subtracts from, the off-resonance reflection. This small reflection caused by the cavity impedance may be due to a slight inequality in the H_x and H_z window-coupling factors or to the finite window size.

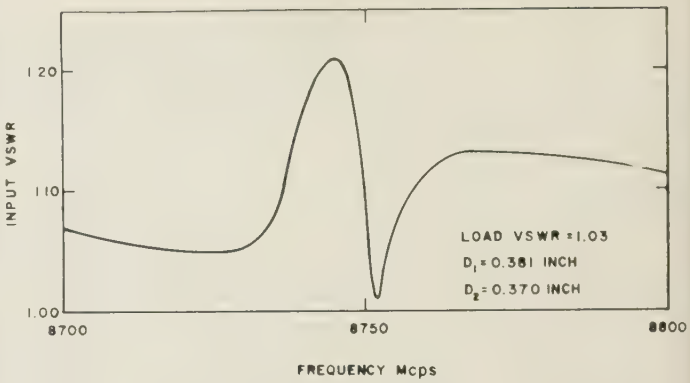

Fig. 13—Input vswr for four-port, TE_{111} mode cavity filter using type A coupling.

A similar filter was constructed using the TE_{121} circular cylindrical cavity mode. The internal cavity length is 1.200 inches and the diameter is 2.590 inches. Two coupling holes, each 0.458 inch in diameter, were used. The TE_{121} cavity mode is resonant at 9107 mc, and there are other resonances at 8920, 9130, 9499, and 9869 mc (some of these are quite small). The TE_{121} cavity mode has very low cavity-wall losses; therefore, the loss at resonance should also be low. Between terminals A-C (Fig. 2), the loss at resonance is 0.5 db and the bandwidth is 6.6 mc. The isolation between terminals A and B and between terminals A and D at resonance is 27.7 db and 25.3 db, respectively. The measured value of the window-coupling factor Q_w is 39 per cent higher than the theoretical value found by using small-aperture theory. The measured value of cavity Q is 25,200. This is 70 per cent of the theoretical value. Fig. 14 illustrates the isolation between terminals A and C and between terminals A and D, for frequencies near resonance. As is typical of microwave cavities, the band-pass filter response is asymmetrical.

A reflectionless band-elimination filter was constructed that had only one waveguide and a circular cylindrical TE_{111} cavity mode [see Fig. 8(a)]. The cavity diameter and length are 1.350 and 0.800 inches, respectively. A single coupling hole, 0.360 inch in diameter, was used. Midway between the cavity end-plates, four 0–80 NF screws were equally spaced about the cavity circumference. Two of the screws were metal; the others were lossy dielectric screws. All were adjusted for approximately minimum reflection and maximum absorption at resonance. The isolation at resonance between input and output is 36 db with a 3-db bandwidth of 11 mc and a 10-db bandwidth of 3.7 mc. The loss in output power at $f_0 \pm 11$ mc is theoretically (for $m = 0$)

$$\frac{(2)^2}{1 + (2)^2} = -0.97 \text{ db};$$

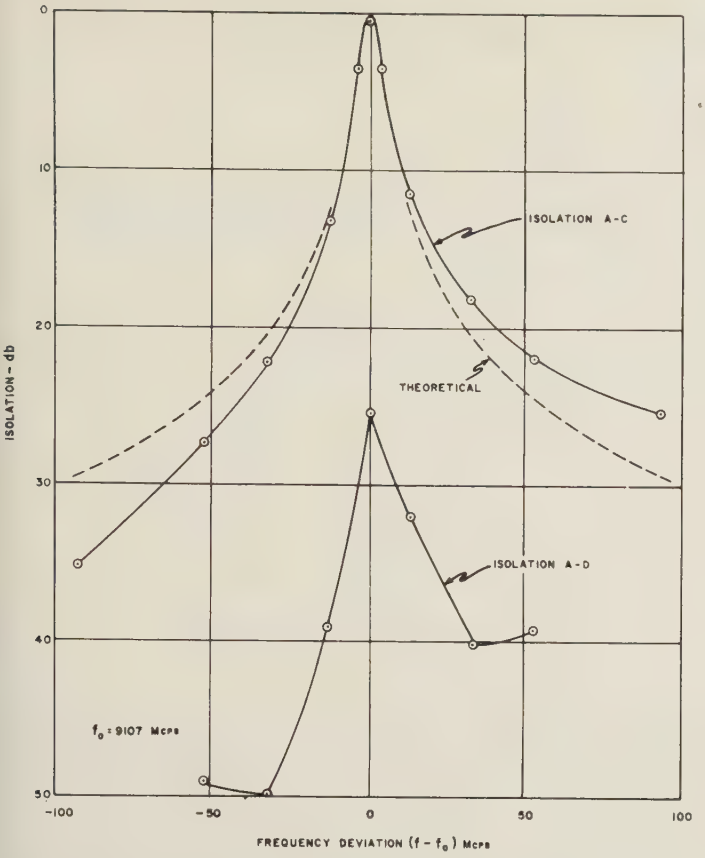

Fig. 14—Isolation between ports A and C and between A and D for four-port TE_{121} mode cavity filter using type A coupling.

the measured values above and below resonance are 1.0 and 1.1 db, respectively. The input vswr of the band-elimination filter without matching is shown in Fig. 15. The test results correspond very well with the theory.

A circular polarization separator (Fig. 11) was constructed using a TE_{111} circular cylindrical cavity mode. The cavity-wall losses were rather high, but the device functioned in the manner predicted. Without a mode-tuning screw, power into terminal A produced an elliptically polarized waveguide field at terminal C. When

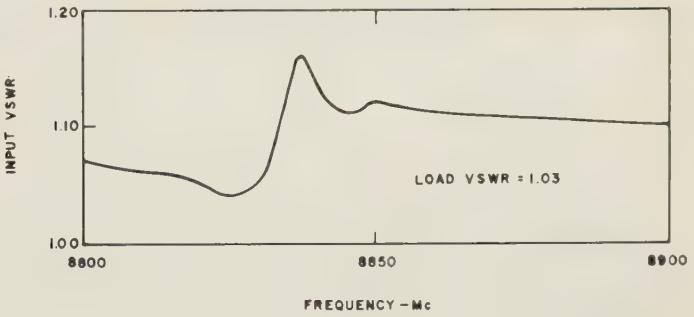

Fig. 15—Input vswr for two-port, TE_{111} mode cavity filter using type A coupling.

the tuning screw was adjusted for minimum reflection at terminal A, the vswr in the circumferential direction in arm C dropped to about 1.05. This is equivalent to a 32-db ratio in the amplitudes of the two directions of circularly polarized fields. Some experimental data on the ferrite loading of circularly polarized cavities are given by Nelson.[8]

VIII. Conclusion

Theoretical analysis proves that a single, circularly polarized cavity may be used to construct a reflectionless band-pass and band-elimination filter that is capable of coupling nearly 100 per cent of the energy from the main waveguide at resonance. The theoretical loss of the band-pass portion of this filter is identical with that in any conventional band-pass cavity filter. Among many other applications, the circularly polarized cavities may also be used in the design of diplexers and tunable nonreciprocal filters.

Experimental results verify the analysis for a degenerate cavity mode coupled to the rectangular waveguide, magnetic field components at the point of circular polarization. The input vswr of the experimental cavities is below 1.2 without matching. The amount of energy coupled from the main waveguide at resonance could be adjusted to produce an isolation greater than 50 db.

Reference Cavity Design Considerations*

WILLIAM A. GERARD†

Summary—The design problems in a reference cavity include coupling, cavity Q, temperature compensation, stability, and hysteresis. Temperature compensation is shown to be a problem in second order compensation theory and is solved by material changes. Stability is achieved by novel mechanical design and by elimination of hysteresis producing members.

Reference Cavity Design Considerations

THE 1Q SERIES reference cavity has held a unique place in the field of microwave devices. It has remained virtually unchanged in over 10 years of use. The introduction of the standing-wave discriminator has created a need for cavities matched to waveguide impedance with bandwidth and transmission characteristics of the 1Q retained. Furthermore a demand has arisen for a frequency standard that would maintain frequency at very low temperatures. The problem then resolved itself to what can be done that will result in a major improvement in compensation and stability on the 1Q.

The Matching Problem

The desirability of a matched cavity for the standing-wave discriminator has been demonstrated by Denton, Wilson, and Margolin.[1] Their results show that maximum sensitivity results when the cavity is matched to the waveguide. The scheme of operation is shown in Fig. 1. As generator frequency changes, the vswr pattern shifts and increases in amplitude. Two crystals are located symmetrically about the position of vswr minimum, and, when the pattern shifts, there is an unbalance which is used to actuate a feedback system. This in turn is used to correct the generator frequency.

To match the 1Q series reference cavity, a study was undertaken in which the windows were varied in size and the measured coupled characteristics of the cavity were compared with the theoretical characteristics of an ideal cavity. Plots of the coupled characteristics of a 1Q are shown in Fig. 2 and the characteristics of an ideal cavity[2] are shown in Fig. 3 (both opposite). The latter is plotted in terms of the coupling parameters B_1 and B_2, the former in terms of actual window diameters. The window diameters are directly related to the B parameters. Comparison of the curves shows general similarity, the major difference being that the unloaded Q in an actual cavity changes as windows are opened. The measured curves for the 1Q cavity were obtained by selecting several cavities with similar characteristics (especially unloaded Q) and successively machining the windows. The cavity was degreased after each machining operation to eliminate oil films which would otherwise cause poor results. The theoretical curves show that if an input match better than 1.4 is to be achieved with the same transmission fraction (T) as the 1Q (equivalent to 5 db insertion loss), a Q of 1650 would result.

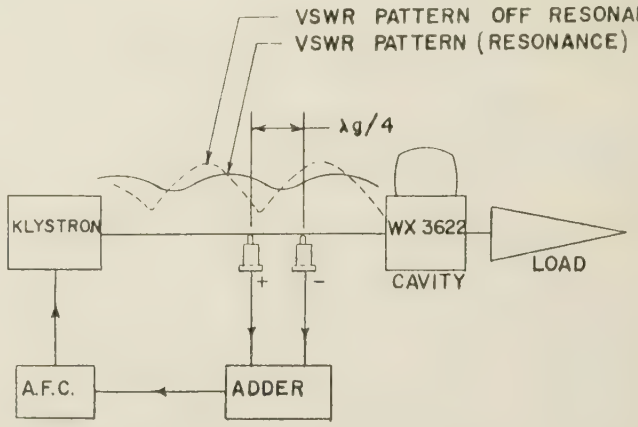

Fig. 1—Standing-wave discriminator.

The present design of the 1Q was dictated by considerations developed by Pound,[3] where maximum sensitivity for a transmission system is shown to be obtained when the cavity has equal input and output coupling. For a cavity with fixed unloaded Q, this results in a maximum TQ_L product. Obviously the matched 1Q will no longer exhibit the same TQ_L product since the matched cavity for fixed transmission fraction has a lower Q_L. The lower Q_L would also lower the sensitivity of the standing-wave discriminator. The best solution would be to raise the unloaded Q from the 5000 of the 1Q design to about 6500 where both applications could be served with equal ease.

Unloaded Q

To understand the unloaded Q changes contemplated, it is helpful to examine the nature of the mode used in the 1Q. Barrow and Mieher[4] have sketched the effect of the addition of a rod or nose on the perfect cylindrical TM_{010} mode.

* Manuscript received by the PGMTT, October 5, 1956.
† Westinghouse Electric Corp., Horseheads, N. Y.
[1] R. F. Denton, T. A. Wilson, and A. R. Margolin, "Automatic Frequency Control of High-Power Klystron," NEC, Chicago, Ill., 1952.
[2] C. G. Montgomery, "Technique of Microwave Measurements," vol. 11, M.I.T. Rad. Lab. Ser., McGraw-Hill Book Co., New York, N. Y., pp. 286–291.
[3] R. V. Pound, "Microwave Mixers," vol. 16, M.I.T. Rad. Lab. Ser., pp. 215–218.
[4] W. L. Barrow and W. W. Mieher, "Natural oscillations of electrical cavity resonators," Proc. IRE, vol. 28, pp. 184–191; April, 1940.

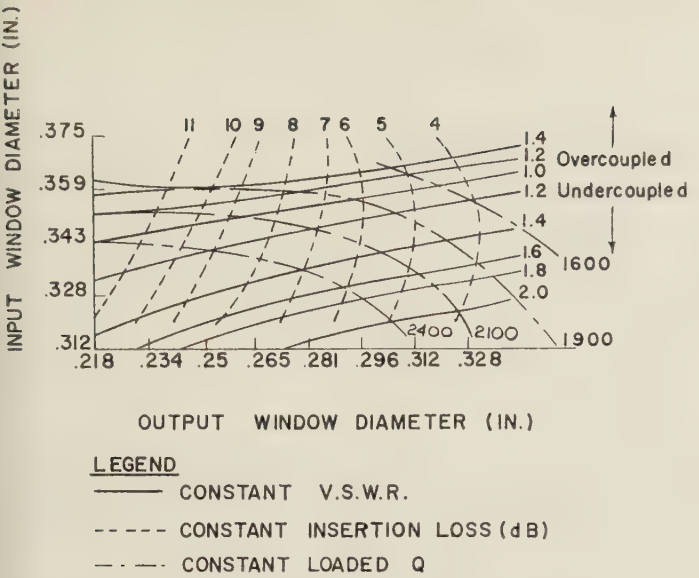

Fig. 2—Coupled properties of 1Q cavity. $f=9280$ mc.

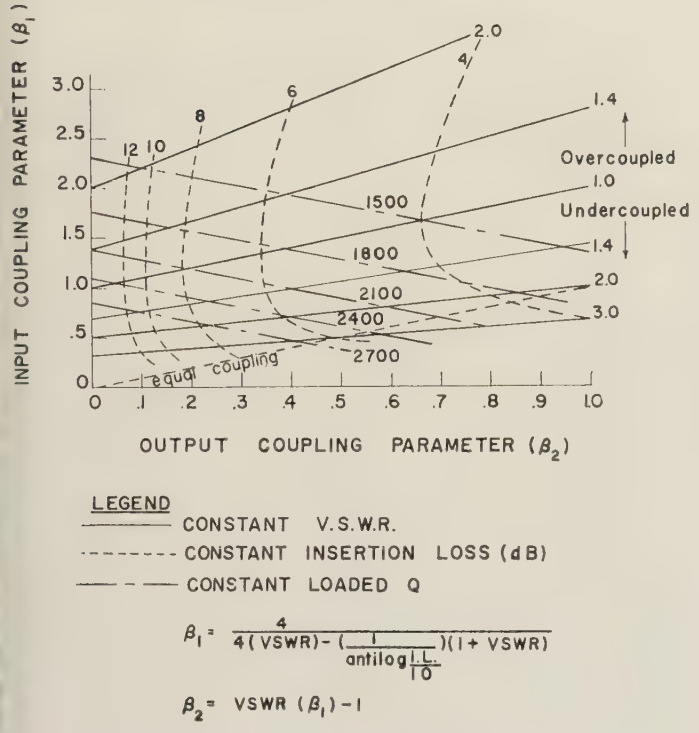

Fig. 3—Coupled properties of an ideal cavity. $Qu=5000$.

The 1Q series cavity uses a configuration that is much closer to the TM_{010} mode than to the TM_{001} capacity loaded coaxial mode that has been more widely treated due to its application to klystron design. The desirable feature of the nosed-in cavity is that the presence of the nose provides a high tuning rate for compensation purposes. The nose, however, will lower the Q as compared to the associated TM_{010} cavity. This is borne out in Fig. 4, which gives the relative Qu values for nosed-in cavities as a function of their geometry. Frequency is held constant. To calculate the frequency to a sufficient

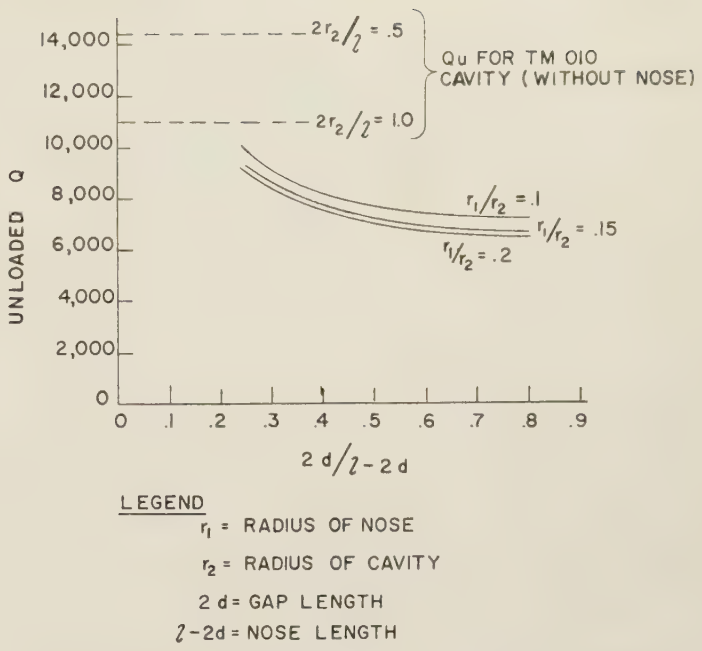

Fig. 4—Unloaded Q for nosed-in cavity. Material—copper.

accuracy (1 per cent) for the geometries of greatest interest, it was necessary to extrapolate the curves given by Holstein and Mayer.[5] The Q values were calculated from a method given by Warnecke and Guenard[6] for nosed-in cavities in the capacity loaded coaxial mode. The legitimacy of

$$Qu = 4\pi^{3/2}\cdot 10^{-7} f^{1/2}\sigma^{1/2}\mu^{-1/2}K\,\frac{(r_2^2 - r_1^2)l\cdot + r_1^2 2d}{[r_2(r_2-1) + r_1(l-2d)]}$$

$u = 4\times 10^{-7}$

σ = conductivity

f = frequency

$$K = \text{geometric parameter} = \left[\frac{1/V\iiint H^2 dV}{1/S\iint H^2 dS}\right]$$

(approximately unity, also see Fig. 134 of footnote 6)

$r_1, r_2, l, 2d$ = cavity dimensions, [Fig. 5(a) next page]

the use of their formula is justified by comparison with the value of Qu computed for nearly equivalent TM_{010} cavities and by subsequent experiment. Fig. 4 shows that the final choice of geometry thus represents a compromise between tuning rate, size, and Qu.

These curves give a Qu of 6800 for the 1Q while measurements yield a Qu of 5000. Studies of the various surface conditions and assembly techniques were under-

[5] T. Holstein and E. Mayer, "Resonant Frequencies of the Nosed-in Cavity," Westinghouse Electric Corp., Res. Rep. SR-281.

[6] R. Warnecke and P. Guénard, "Tubes Electronique à Modulation de Vitesse," Gauthier-Villars, Paris, France, p. 234.

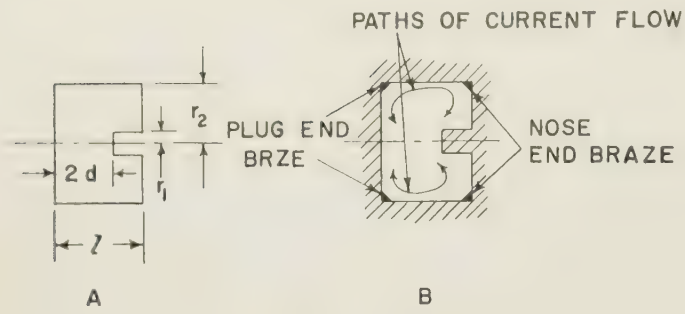

Fig. 5—Nosed-in cavity nomenclature and assembly.

taken to see whether higher Q could be obtained in practice. Tests showed that the smoother side wall surface obtained by ball-burnishing was no better than a machined side wall. The corrugated diaphragm was equally as good as a smooth machined surface. The chief loss of Q that could be improved by changing fabrication technique was in the braze joints. Poor joints resulted in extremely low Q values because cavity currents flow perpendicular to these joints. Even the best of joints using silver-copper eutectic solder resulted in a substantial loss of Q. A special set of cavities was constructed that were machined in different fashions. Referring to Fig. 5(b) and Table I we can see that the

TABLE I

Qu	
6380 7120	brazes at both ends
7320 7800	nose end brazes only
7340 8250	plug end brazes only

elimination of at least one braze joint made a substantial contribution to the unloaded Q of a WX-3622 cavity having a theoretical unloaded Q of 9000. Cavities made with joints parallel to the path of current flow showed almost no reduction of Q, but construction of this type is difficult. The size of the coupling holes affected Qu but the size ultimately is dictated by the coupled characteristics of the cavity. The input and output windows also decreased the unloaded Q by adding dielectric loss. This was substantially eliminated by the use of 7070 glass.

Temperature Compensation

The theory of 2nd order compensation has been treated by Wheeler.[7] We may review these results before applying them to this compensation problem. If cavity wavelength scales linearly with change in dimension, we may write cavity frequency as a function of temperature.

$$\Delta f = -f_0(\alpha_1 \Delta t + \beta_1 \Delta t^2)$$

[7] M. S. Wheeler, "Tunable temperature compensated reference cavity," *Wireless Eng.*, vol. 32, pp. 201–205; August, 1955.

where

Δf = frequency change in mc
f_0 = resonant frequency
Δt = change in temperature in °C
α_1, α_2 = 1st order coefficients of thermal expansion
β_1, β_2 = 2nd order coefficients of thermal expansion.

As shown in Fig. 7, we may then introduce a tuner of length L (of a second metal having expansion coefficients α_2, β_2) which has a tuning rate of R mc per mil. Then

$$\Delta f = -f_0(\alpha_1 \Delta t + \beta_1 \Delta t^2) + RL\{(\alpha_2 - \alpha_1)\Delta t + (\beta_2 - \beta_1)\Delta t^2\}.$$

If we multiply through by $1/\Delta t$ and setting $\Delta f/\Delta t$ equal to 0, we obtain the equation of 1st order compensation.

$$0 = \frac{\Delta f}{\Delta t} = -f_0\alpha_1 + RL(\alpha_2 - \alpha_1) + \text{second order terms } [-f_0\beta_1 + RL(\beta_2 - \beta_1)]\Delta t. = -f_0\alpha_1 + RL(\alpha_2 - \alpha_1).$$

When RL is made equal to $f_0\alpha_1(\alpha_2 - \alpha_1)$ the first order error is zero. Using this value of RL in the original expression will give us the residual shift that can not be eliminated by a bimetal.

$$\Delta f = f_0 \Delta t^2 \frac{(\alpha_1\beta_2 - \alpha_2\beta_1)}{(\alpha_2 - \alpha_1)}.$$

The resulting equation shows that for a given temperature change, the change in frequency is a function of the material properties only. An examination of Fig. 6 shows that copper can be best compensated with iron, but the resulting bimetal would be too long due to the small difference in α values. These curves should serve as a guide as actual materials do not behave precisely as the published expansion figures. Many of these curves, however, were confirmed by measurements on uncompensated cavities. The concave upward characteristic of tungsten will be shown to be desirable for it will compensate for nonlinearities in the tuning rate (R) characteristic. The tungsten compensator will fit the nosed-in cavity compensation requirements nicely since a low expansion system moving the nose would compensate a copper cavity. This is most fortunate since tungsten is easily fabricated in rod form. If we were required to work with a TE_{111} cavity, for example, we would be required to attach the copper to one side wall and make the cavity *body* out of tungsten.

Several configurations could be considered as possible alternate designs for a nosed-in cavity. Referring to Fig. 7, configuration #1 is essentially the 1Q structure with a tungsten strut substituted for the invar. This design shows pronounced hysteresis (changes in room temperature frequency with temperature cycling) and requires a high conductivity plating on the tungsten.

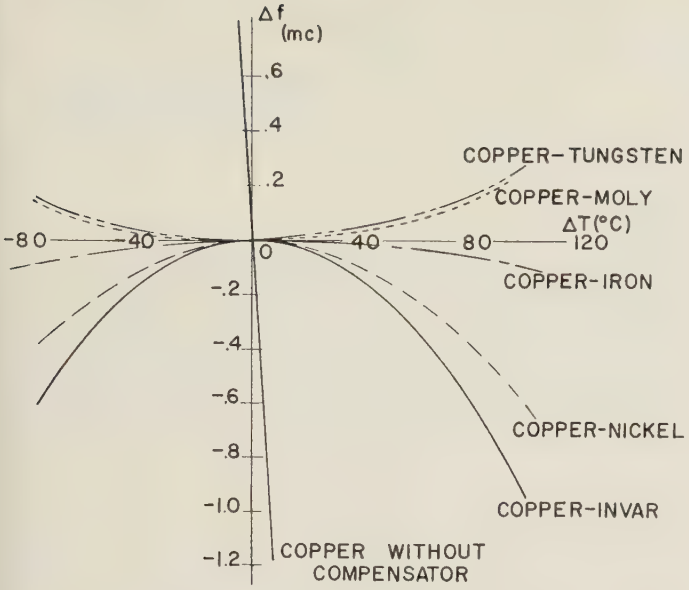

Fig. 6—Residual temperature compensation.

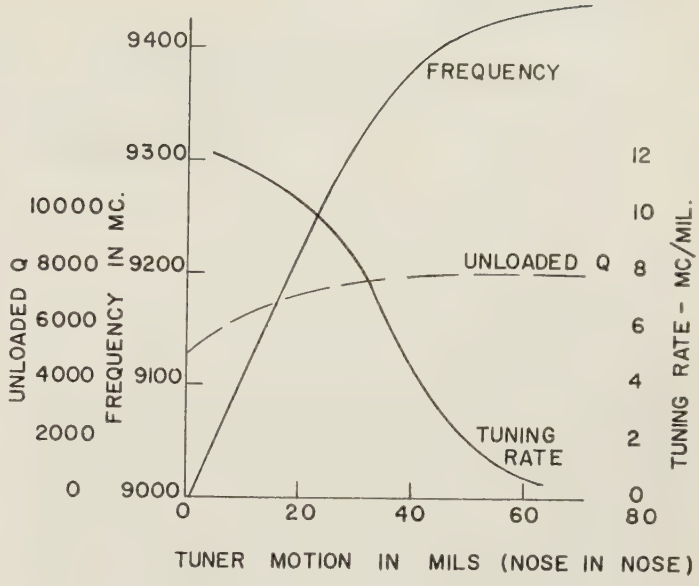

Fig 8—Tuning rate and Qu for nose-in-nose cavity

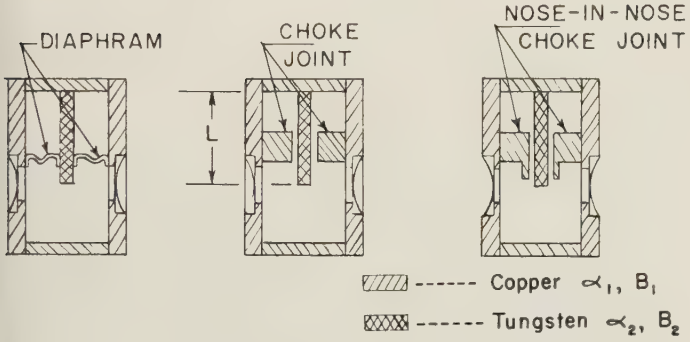

Fig. 7—Nosed-in cavity configurations

The portion of the tuner within the cavity might have been made of copper but this would have increased the over-all size. The hysteresis is the result of cold working the diaphragm during temperature cycling. This has been measured as high as 0.4 mc for a 9280 mc cavity. Configuration #2 offers a method of eliminating diaphragm hysteresis by use of a choke joint to allow the bimetallic action. Unfortunately, the nose plating is still a problem, and the design has low unloaded Q due to the break in the cavity wall. The base of the nose is a high current point. The choke would be better located as it is in configuration #3 where a nose-in-nose structure is chosen. Here the choke joint is located close to the current zero which appears at the center of the end of the nose. This design offers greater latitude in choke joint design and the nose plating problem is eased due to the smaller current flowing over it.

Fig. 8 shows the tuning properties and unloaded Q for a cavity with a nose-in-nose configuration. As the inner nose is advanced into the cavity, tuning rate increases as frequency and unloaded Q decrease. The tuning rate R is chosen depending on the compensator length that can be used, over-all size being the determining factor. A typical value might be 9.4 mc/mil. Note the nature of the tuning rate curve in terms of compensator action. As the cavity system is heated, the inner nose is withdrawn by the bimetal to compensate. However, the tuning rate decreases as the inner nose is withdrawn. When the cavity is cooled, the opposite effect takes place. This has the effect of adding first order error to the curve for copper-tungsten shown in Fig. 6. The net effect is to pull the concave upward into one that is concave downward. This is shown in Fig. 10 to be less than 0.1 mc from −55°C to +71°C. The nonlinearity of the tuning rate may be used to advantage to adjust the value of compensation on individual cavities.

The Westinghouse WX3622 cavity was developed along the lines of thought described above. It is a tungsten compensated copper cavity which is evacuated and sealed. The mechanical isolation from the waveguide of the 1Q series[8] was preserved by holding the cavity in an aluminum block with thin mounting rings. The input vswr was held to 1.4 max, with transmission fraction $\frac{1}{4}$, and loaded Q 2100 to 2400. To insure the accuracy of the compensation and frequency setting, considerable work was done to improve present frequency measuring systems. Great pains were taken to match the test systems. The most important improvement was the change in presentation technique. By use of an electronic switch, the cavity response was placed on the scope along with the swept klystron mode. This allows accurate tuning of the klystron. Improper "peaking" of the klystron turned out to be a chief source of error in previous work. Pulses are generated by beating

[8] D. Alpert *et al.*, U.S. Patent No. 2,584,717.

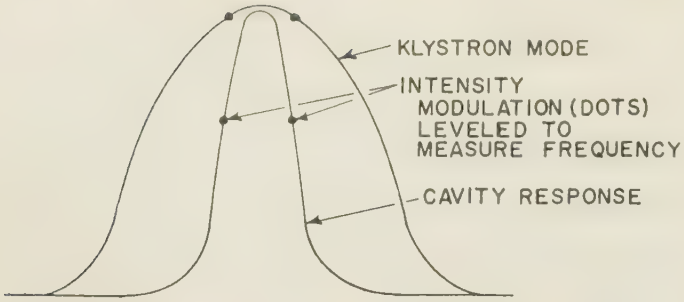

Fig. 9—Oscilloscope trace for frequency measurement.

a standard frequency harmonic against the swept klystron. The pulses become intensity modulation (dots) on the scope and frequency is measured by leveling these dots. It can be seen in Fig. 9 that if the klystron is tuned so that cavity frequency is on the sloping portion of the caracteristic, an error will result in frequency reading. Present technique calls for leveling the dots on both the cavity response and on the klystron mode. Under these conditions equal power at the measurement level is assured and klystron tuning error is eliminated.

These improvements in technique allow a more thorough evaluation of cavity performance. Fig. 10 shows the performance of a WX3622 cavity, a 1Q cavity and the performance of a cavity exhibiting pronounced hysteresis, such as might be expected in a diaphragm cavity. The amount of hysteresis in a diaphragm cavity varies and is related to the amount of movement in temperature cycling that occurs. Compensation better than 0.1 mc can be achieved over the temperature range from −55°C to +71°C. This includes hysteresis effects. The second curve also represents the performance of a tungsten strut diaphragm cavity. The difference in performance is due to diaphragm setting. A great deal of time was spent in studying and eliminating long term drift in these cavities. Originally, glassed Kovar washers soft soldered to the body were used as windows for the coupling holes. Temperature cycling cavities with these windows produced a negative frequency shift or set each cycle, always occurring after a cold (−55°C) cycle. Apparently the soft solder joint was sufficiently hard at the cold temperature to firmly bond the Kovar washer to the copper body and prevent its normal contraction. The result was a net outward distortion of the copper body. At higher temperatures the solder was soft enough to yield and no strain was transmitted to the copper body. This phenomenon was traced up to 25 cycles. By eliminating the Kovar and substituting a copper washer and a resin to glass joint, the soft solder no longer affected the cavity stability. Cavities have been cycled up to 50 cycles from 100° to −55°C with less than 0.1 mc change in room temperature frequency. Most of this occurs in the first few cycles and some sort of aging is required before the cavity is judged to be stable.

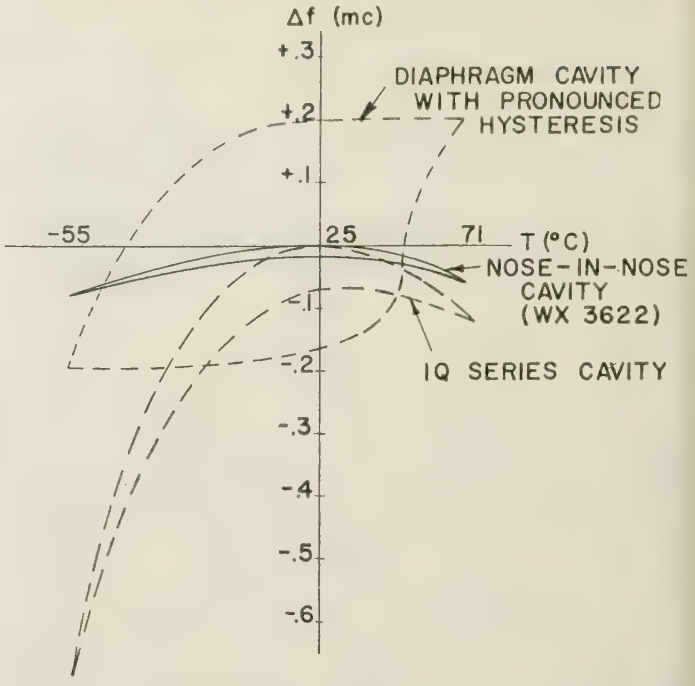

Fig. 10—Cavity compensation.

Acknowledgment

I wish to acknowledge the assistance of R. G. Larson who shared the development. E. C. Okress and W. R. Hayter, Jr., provided help with the theory used to describe the cavity and offered many valuable suggestions. I wish to thank D. E. Marshall for his guidance especially during the uncertain phases of the development.

The Relationship of Physical Applications of Fourier Transforms in Various Fields of Wave Theory and Circuitry*

E. FOLKE BOLINDER†

Summary—**A procedure is presented for connecting some known physical applications of Fourier transform pairs in different branches of the theory of waves and circuitry. After an investigation of the cases of diffraction, reflection, and coupling of waves, deflection of particles (which includes the cathode-ray-tube case and so-called gap effect) and the closely related scanning problem are examined. Finally, extension to random functions is discussed briefly.**

Introduction

DURING the last decades, more and more engineers and physicists have started to use the Laplace and Fourier transformations in solving their problems. The idea is that a problem that is difficult to solve in one domain might be easily solved after transformation to another domain, whereupon a transformation is made back into the original domain. Actually, every engineer is performing the same type of operations in multiplying two numbers by adding their logarithms on his sliderule.

In this paper, only the Fourier transformation arising from integration along the real axis in the two domains will be considered. The connection between this transformation, the Fourier transformation in the complex plane, the two-sided and the one-sided Laplace transformations has been lucidly described by van der Pol and Bremmer.[1] The method of extending real integrals into the complex plane is well known from the residue calculus. When even the complex integral is difficult to calculate, approximate integration has to be used. Until about eight years ago only two methods were known, both giving asymptotic series as results. The methods are called the saddlepoint method and the stationary phase method. Since that time, Cerrillo at M.I.T. has created a new theory of approximate integration founded on five new methods, all giving uniformly convergent series[2] as results.

* Manuscript received by the PGMTT, October 5, 1956. Reprinted from *Acta Polytechnica, Physics*, including *Nucleonics* Series, vol. 3, p. 189, 1956. The work was made possible by research grants from the Swedish Gov. Tech. Res. Council, Stockholm, Sweden, and Telefonaktiebolaget LM Ericsson, Stockholm, Sweden.

† Formerly with the Royal Inst. of Tech., Div. of Radio Eng., Stockholm, Sweden; now at the Res. Lab. of Electronics, Mass. Inst. of Tech., Cambridge, Mass.

[1] B. van der Pol and H. Bremmer, "Operational Calculus Based on the Two-Sided Laplace Integral," Cambridge University Press, London, Eng.; 1950.

[2] M. V. Cerrillo, "On the Evaluation of Integrals of the Type

$$f(\tau_1, \tau_2, \cdots, \tau_n) = \frac{1}{2\pi i}\int F(s)e^{W(s,\tau_1,\tau_2,\cdots,\tau_n)}ds$$

and the Mechanism of Formation of Transient Phenomena," Tech. Rep. No. 55, Res. Lab. of Electronics, Mass. Inst. Tech., Cambridge, Mass. Of six parts, no. 2a, "An Elementary Introduction to the Theory of the Saddlepoint Method of Integration," has been published; May 3, 1950.

In this paper, an elementary theory is formulated for connecting some known physical interpretations of Fourier transform pairs in different branches of the theory of waves and circuitry. This way of putting things may be considered a little unusual. Ordinarily, a specific problem is stated and the mathematical tools for solving it are looked for. Here, the tool, Fourier transformation, is given, and the connection between some known problems that can be solved by means of Fourier transforms is studied.

So many papers have been published on the use of Fourier transforms in engineering and physics that the author is compelled to refer only to certain specific papers in the different fields.

The Fourier Transformation

As is well known,[1] a Fourier series expansion may be written in the exponential form

$$\begin{cases} f(v) = \sum_{n=-\infty}^{\infty} a_n e^{j(2\pi nv/d)}, \text{ where} & (1) \\ a_n = \frac{1}{d}\int_{-d/2}^{d/2} f(v)e^{-j(2\pi nv/d)}dv. & (2) \end{cases}$$

By means of a limiting process, this series expansion can be transformed to an integral

$$f(v) = \int_{-\infty}^{\infty}\left[\int_{-\infty}^{\infty} f(y)e^{-j2\pi uy}dy\right]e^{j2\pi uv}du. \quad (3)$$

Separating:

$$\begin{cases} F(u) = \int_{-\infty}^{\infty} f(v)e^{-j2\pi uv}dv & (4) \\ f(v) = \int_{-\infty}^{\infty} F(u)e^{j2\pi uv}du. & (5) \end{cases}$$

The function $F(u)$ is called the Fourier transform of $f(v)$; $f(v)$ is called the inverse Fourier transform of $F(u)$. Together they form a Fourier pair. This Fourier pair, (4) and (5) has been tabulated; the most extensive table is the one by Campbell and Foster.[3]

[3] G. A. Campbell and R. M. Foster, "The practical application of the Fourier integral," *Bell Syst. Tech. J.*, vol. 7, pp. 639–707; October, 1928.

Campbell and Foster, "Fourier Integrals for Practical Applications," *Bell Syst. Tech. J.*, Monograph B584; September, 1931, and D. Van Nostrand Co., Inc., New York, N. Y., 1948.

When $f(v)$ and $F(u)$ are discontinuous, (4) and (5) have to be written as Fourier-Stieltjes integrals:

$$F(u) = \int_{-\infty}^{\infty} e^{-j2\pi uv} dg(v) \tag{6}$$

$$f(v) = \int_{-\infty}^{\infty} e^{j2\pi uv} dG(u) \tag{7}$$

where

$$g(v) = \int_{-\infty}^{v} f(\alpha) d\alpha \tag{8}$$

$$G(u) = \int_{-\infty}^{u} F(\beta) d\beta. \tag{9}$$

The functions $g(v)$ and $G(u)$ are called distribution functions; $f(\alpha)$ and $F(\beta)$ are called density distribution functions.

Very often the function $F(u)$ is "normalized":

$$F(u)_{\text{norm}} = \frac{F(u)}{F(u)_{u=0}} = \frac{\int_{-\infty}^{\infty} f(v) e^{-j2\pi uv} dv}{\int_{-\infty}^{\infty} f(v) dv}. \tag{10}$$

When the first derivatives of $f(v)$ or $F(u)$ are discontinuous, the so-called first corner theorem, stated by Cerrillo in a rigorous mathematical form,[4] has to be used. When, for simplicity, in the following we mainly treat continuous functions satisfying (4) and (5), it is understood that a small change of this Fourier pair makes it rigorously applicable as well to discontinuous functions and impulse functions.

Diffraction of Waves

Let us assume that we have a finite aperture in the interval $-(d/2) \leq x \leq (d/2)$, and that the aperture is excited by a wave, see Fig. 1, so that all elements of the aperture are in phase and have a density distribution function $f(x)$. We now select a point P in the so-called Fraunhofer region; *i.e.*, at such a distance from the origin that rays from the aperture towards P may be considered to be parallel. Adding the contributions of all element waves from the aperture at P we get

$$F_1(\theta, k) = \int_{-d/2}^{d/2} f(x) e^{j2\pi kx \sin\theta} dx \tag{11}$$

where $F_1(\theta, k)$ equals $F(\theta, k)$ multiplied by a phase factor determined by P's exact position, θ is the angle between the rays and a line perpendicular to the x axis, and the wave number $k = 1/\lambda$.

Putting

$$-k \sin\theta = u \tag{12}$$

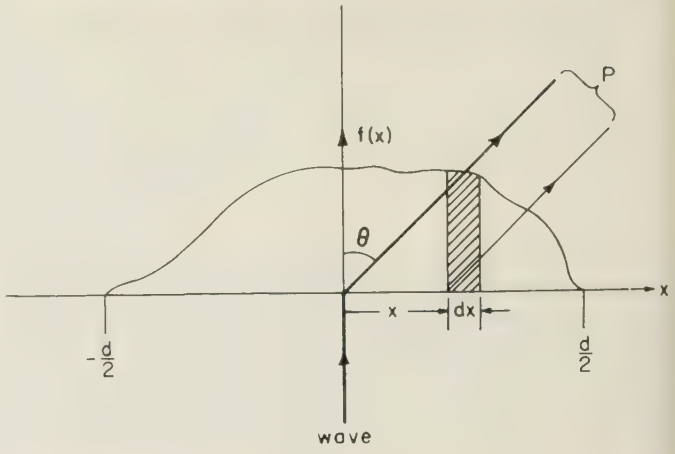

Fig. 1—Diffraction of a wave.

we get

$$F_1(u) = \int_{-d/2}^{d/2} f(x) e^{-j2\pi ux} dx. \tag{13}$$

This is a Fourier integral, because $f(x) = 0$, $|x| > (d/2)$. The inverse Fourier transform is

$$f(x) = \int_{-\infty}^{\infty} F_1(u) e^{j2\pi ux} du. \tag{14}$$

We now have two cases to consider:

1) k is a constant, θ is a variable.

This case, known by Michelson in 1905, has been extensively treated in literature. A critical examination of the conditions under which it is right to consider $F_1(u)$ to be an antenna polar diagram was lately made by Booker and Clemmow.[5] They introduced a powerful concept called angular spectrum.

The integrals (13) and (14) can easily be extended to two or three dimensions, and have proved to be of great value in works dealing with diffraction of X rays and electrons by crystals. They have also been used, for example, in optics, in antenna theory, and in acoustics. The first to suggest the use of Fourier series in crystal analysis problems is thought to be W. H. Bragg in 1915. Since then, many papers have been published in that field; an article by Patterson[6] and a monograph by Wrinch[7] may be mentioned as examples.

During the second world war, Ramsay created an antenna theory[8] by interpreting the theorems in the Campbell-Foster table, mentioned above, in terms of antenna theory. At the same time Booker and his group

[4] M. V. Cerrillo and E. F. Bolinder, "On Basic Existence Theorems in Network Synthesis, Part IV: Transmission of Pulses," Tech. Rep. No. 246, Res. Lab. of Electronics, M.I.T., Cambridge, Mass.; August, 1952.

[5] H. G. Booker and P. C. Clemmow, "The concept of an angular spectrum of plane waves, and its relation to that of polar diagram and aperture distribution," *Proc. IEE*, part III, pp. 11–17; January, 1950.

[6] A. L. Patterson, "The diffraction of X-rays by small crystalline particles," *Phys. Rev.*, vol. 56, pp. 972–977; November, 1939.

[7] D. Wrinch, "Fourier transforms and structure factors," Axsred Monograph no. 2, The American Society of X-ray and Electron Diffraction, Murray Printing Co., Cambridge, Mass.; February, 1946.

[8] J. F. Ramsay, "Fourier transforms in the aerial theory," six parts in the *Marconi Rev.*, 1946–1948, based on two reports written in 1942–1943.

used Fourier transforms for determining cosec θ antenna patterns. On the basis of analogies in optics, Spencer[9] independently constructed an equivalent antenna theory. A book on the applications of Fourier integrals in optics has been published by Duffieux.[10]

In acoustics the Fourier pair, (13) and (14), has been used in designing microphones and loudspeakers.[11]

Both in electromagnetic theory and in acoustics, it is common to extend this Fourier pair to two dimensions and, after that, to make a transformation to polar coordinates. In that way, a Fourier-Bessel transform pair originates. For this pair the author has not been able to find any extensive table corresponding to the Campbell-Foster tables.

2) θ is a constant $= -90$ degrees, k is a variable.

In this case we get

$$\begin{cases} F(k) = \int_{-d/2}^{d/2} f(x)e^{-j2\pi kx}dx & (15) \\ f(x) = \int_{-\infty}^{\infty} F(k)e^{j2\pi kx}dk & (16) \end{cases}$$

and the point P is located as shown in Fig. 2.

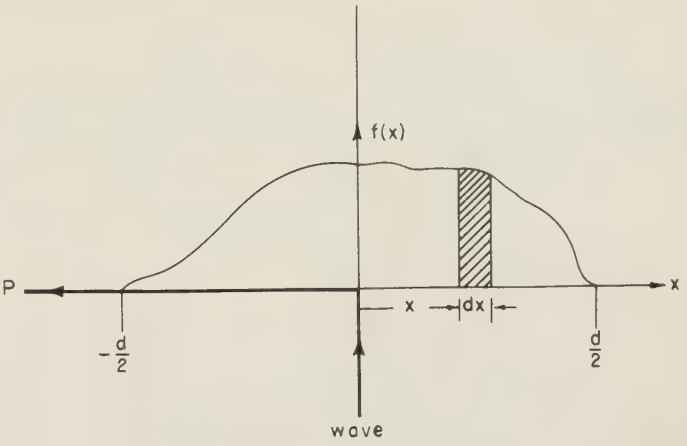

Fig. 2—Diffraction of a wave, $\theta = -90°$.

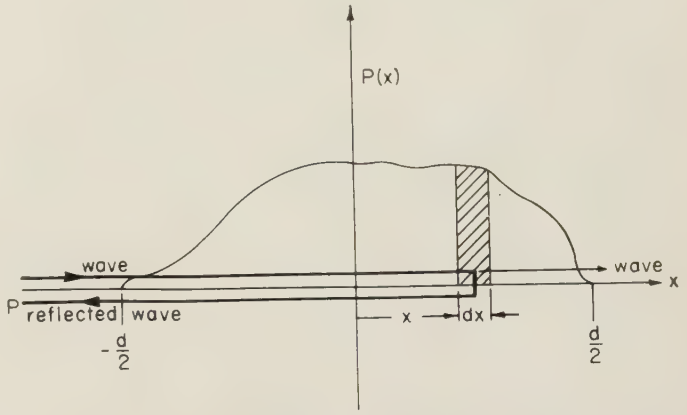

Fig. 3—Reflections in an inhomogeneous medium.

Reflection of Waves

In the diffraction case, Fig. 2, the wave exciting the aperture may be thought of as having its wavefront parallel to the x axis. If, instead, we assume that the wave is coming in toward the interval $-(d/2) \leq x \leq (d/2)$ in the positive x direction (Fig. 3) and is partly reflected in the interval, we get the following integral for the reflection coefficient at P:

$$\rho_1(k) = \int_{-d/2}^{d/2} P(x)e^{-j2\pi k2x}dx \qquad (17)$$

where $P(x)$ is the variable reflection coefficient in the interval. Since there are no reflections for $|x| > (d/2)$, the limits may be replaced by $-\infty$ and ∞ in the same way as in the diffraction case. The Fourier transform originating has the following mate:

$$P(x) = \int_{-\infty}^{\infty} \rho_1(k)e^{j2\pi k2x}dk. \qquad (18)$$

Since the wave travels back and forth, distance x in the diffraction case is now replaced by distance $2x$.

Practically, the simplest way of realizing this situation is by means of a dispersion-free coaxial tapered line. See Fig. 4. It can easily be shown that the connection

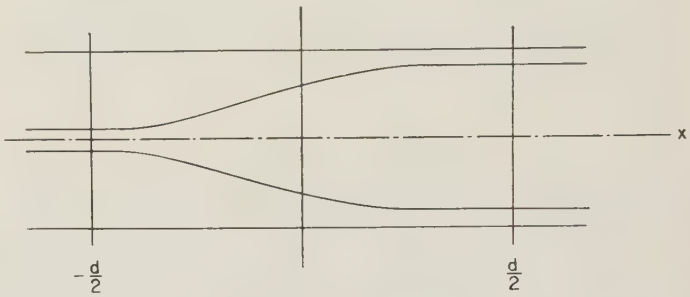

Fig. 4—Coaxial tapered line.

between the variable reflection coefficient $P(x)$, and the variable characteristic impedance, $Z_0(x)$, is the following:[12]

$$P(x) = \frac{1}{2} \frac{d \ln Z_0(x)}{dx}. \qquad (19)$$

Some restrictions have to be imposed on the reflection coefficients so that the Fourier integrals will be valid with great accuracy. These restrictions are that, in order to retain a plane field in the line, both $P(x)$ and $\rho_1(k)$ have to be small compared to unity.

[9] R. C. Spencer, "Fourier Integral Methods of Pattern Analysis," Rad. Lab. Rep. 762-1, M.I.T., Cambridge Mass.; PB 15305; January, 1946.

[10] P. M. Duffieux, "L'intégrale de Fourier et ses applications à l'optique," Société Anonyme des Imprimeries Oberthur, Rennes, France; 1946.

[11] H. F. Olsen, "Elements of Acoustical Engineering," D. Van Nostrand Co., Inc. New York. N.Y.; 1940.

[12] E. F. Bolinder, "Fourier transforms in the theory of inhomogeneous transmission lines," *Trans. Royal Inst. Tech.* (Stockholm, Sweden), no. 48; 1951. Also see Proc. IRE, vol. 38, p. 1354; November, 1950.

Coupling of Waves

By exchanging the concept of reflection for that of coupling in the preceding section, we obtain an approximate theory of, for instance, the directional coupler.[13] The Fourier transform pair is directly

$$I_{rev}(k) = \int_{-d/2}^{d/2} I(x)e^{-j2\pi k2x}dx \tag{20}$$

$$I(x) = \int_{-\infty}^{\infty} I_{rev}(k)e^{j2\pi k2x}dk \tag{21}$$

where $I(x)$ is the coupled wave at a distance x, and I_{rev} is the total reversed wave in the coupled transmission line.

In the tapered line case the incident wave and the reflected element waves were enclosed in the same transmission line. In the coupling case the incident wave and the reflected waves travel in different transmission lines. See Fig. 5. Independent of the above theory, Miller, at the Bell Telephone Laboratories, recognized the Fourier transform formulation of the directivity of directional couplers. The work was presented in a joint paper with Mumford at the IRE Convention in 1951.[14]

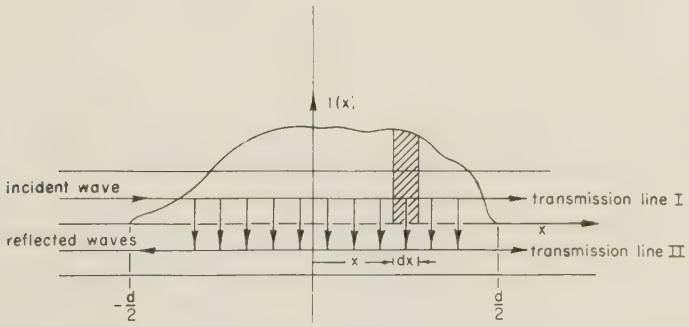

Fig. 5—Coupling of waves.

The directional couplers, both continuous and discrete, are well suited for frequencies in the microwave and vhf regions. For lower frequencies, it is possible to use a discrete folded directional coupler. See Fig. 6. Replacing the pieces of transmission lines between the coupling holes by delay networks and the couplings by amplifying devices, a distributed amplifier is obtained.

At low frequencies it is possible to use the upper half of the configuration in Fig. 6 and match it at the receiving end. See Fig. 7. The former coupling points are connected to phase-shifting attenuating or amplifying devices. Because of the low frequency, the tapping points T_1, T_2, $\cdots$, T_n may be connected together to a common output P. The type of filter originating was thoroughly investigated by Kallmann,[15] who called it a

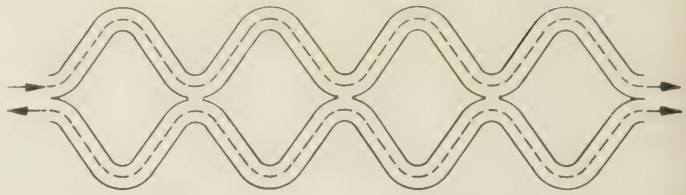

Fig. 6—A folded directional coupler.

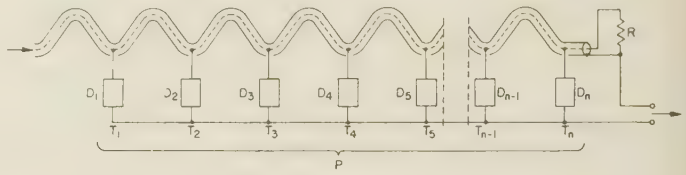

Fig. 7—Transversal filter.

"transversal" type of filter, to distinguish it from the ordinary "longitudinal" type of filter. The transversal filter has many features analogous to the grating spectroscope. Similar systems were described in patents filed in 1931 by Wiener and Lee.[16] By replacing the pieces of transmission lines in Fig. 7 by delay networks, Stutt[17] constructed a delay-line network with which transient phenomena, Fourier transforms, convolution integrals, and so on, can be studied on a cathode-ray tube.

At still lower frequencies the concept of distance completely loses its significance. By putting $x=ct$, $k=f/c$, where c is the velocity of light, we obtain the well-known Fourier pair in time-frequency domains:

$$F(f) = \int_{-\infty}^{\infty} f(t)e^{-j2\pi ft}dt \tag{22}$$

$$f(t) = \int_{-\infty}^{\infty} F(f)e^{j2\pi ft}df. \tag{23}$$

Refraction and Polarization of Waves

For the sake of completeness, it would have been nice if the concept of reflection given above could also be exchanged for the concepts of refraction or polarization. However, as shown by Fig. 8, in these cases no interference is obtained between element waves in the same sense as in the other cases, so that no Fourier transform pairs similar to the ones above are obtained.

Deflection of Particles: The Scanning Problem

In the different cases above, we have assumed that the point P is fixed, and that the waves move and are added at P. We may, however, just as well assume that we have a fixed field varying sinusoidally with time in the interval $-(d/2) \leq x \leq (d/2)$, and that P con-

[13] E. F. Bolinder, "Approximate theory of the directional coupler," Proc. IRE, vol. 39, p. 291; March, 1951.
[14] S. E. Miller and W. W. Mumford, "Multi-element directional couplers," presented before the IRE National Convention, New York, N. Y.; March, 1951.
[15] H. E. Kallmann, "Transversal filters," Proc. IRE, vol. 28, pp. 302–310; July, 1940.
[16] N. Wiener and Y. W. Lee, "Electrical network system," U.S. Patent No. 2024900; December 17, 1935 (filed September 2, 1931).
[17] C. A. Stutt, "Experimental Study of Optimum Filters," Tech. Rep. No. 182, Res. Lab. of Electronics, M.I.T., Cambridge, Mass.; May, 1951.

stitutes a particle moving through the interval. The field may be transversal or longitudinal and the particle may be of different kinds. During its travel through the field, the particle is exposed to influences from the field, and the influences are summed up after the particle has passed through the interval.

Because the particle P always travels with a velocity less than that of light, we have to introduce a fictitious wavelength $\lambda_e = 1/k_e$, if we want to use the same formulas as those given above. If v is the velocity of the particle P, and c is the velocity of light,

$$k_e = \frac{c}{v} k. \tag{24}$$

The Fourier transform pair is

$$\begin{cases} F_1(k_e) = \int_{-d/2}^{d/2} f(x) e^{-j2\pi k_e x} dx & (25) \\ f(x) = \int_{-\infty}^{\infty} F_1(k_e) e^{j2\pi k_e x} dk_e. & (26) \end{cases}$$

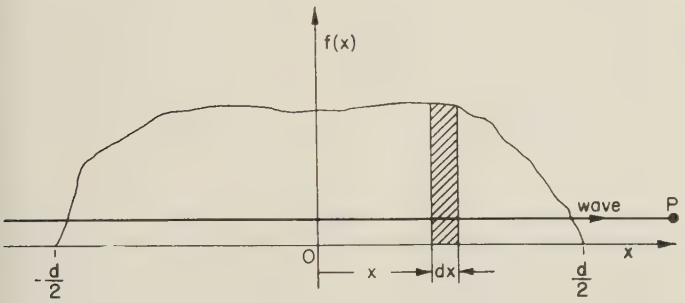

Fig. 8—A wave through a refracting or polarizing medium.

The Cathode-Ray-Tube Case

If the particle P constitutes an electron, and the density distribution function $f(x)$ is an electric field transverse to the x axis (formed, for instance, by metallic plates according to Fig. 9), then the cathode-ray-tube case is obtained. It has been shown[18] that in this case $F_1(k_e)$ is the dynamic sensitivity factor of the cathode-ray tube. Theoretically, the case may be thought of as originating from the reflection case by exchanging the concept of reflection for that of angular deflection. The corresponding approximations are that, both the variable angular deflection of the electron beam, $f(x) = \phi(x)$, and the total deflection angle at the end of the deflection, $F_1(k_e) = \phi_d(k_e)$, must be small.

The Gap (Slit) Effect

If an electron P, instead of passing through a transverse electric field, passes through a parallel field (see, for example, Fig. 10), the instantaneous velocity of P will be changed. If we assume that the velocity change

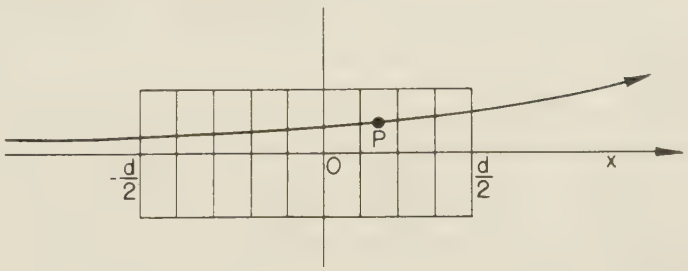

Fig. 9—An electron in a transversal field.

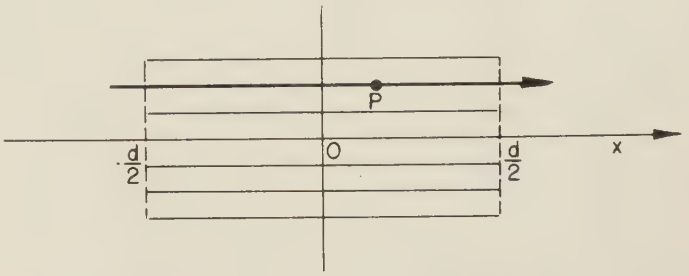

Fig. 10—An electron in a longitudinal field.

is small, so that the total transit time through the field can be assumed to be constant, then $F_1(k_e)$ constitutes the so-called beam coupling factor obtained, for instance, in klystron theory. An analogous transit time factor is obtained in transistor theory. The coining of the expression "gap effect" for these factors perhaps is still better understood in cases in which P constitutes a particle of a band running in front of a gap having a fixed field distribution. Examples are magnetic tape recording[19] and reproduction of movie film.[20,21] In all of the examples given above, the gap factor, which for a parallel slit of width d follows the well-known expression

$$F_1(k_e) = \frac{\sin \pi k_e d}{\pi k_e d} \tag{27}$$

may be changed, inside certain limits, by changing the field distribution in the slit.

The Scanning Problem

If, instead of a moving point P and a fixed aperture, we have a fixed point P and a moving aperture, the conditions of the scanning problem are fulfilled. Two fundamental papers dealing with the scanning problem in two dimensions have been written by Mertz and Gray[22] and Wheeler and Loughren.[23] Both papers are

[18] E. F. Bolinder, "A theory of determining the dynamic sensitivity of cathode-ray-tubes at very high frequencies by means of Fourier transforms," IRE Trans., vol. ED-2, pp. 44–50; January, 1955.

[19] F. Krones, "Die Magnetische Schallaufzeichnung in Theorie und Praxis," special edition of Radiotechnik, *Z. für Hochfrequenz.* Verlag B Erb, Wien, 1952.

[20] W. Meyer-Eppler, "Tonfilmspalt und filmfrequenzgang," *Kino-Technik*, part I, pp. 1–7; January, 1943; part II, pp. 16–18; February, 1943.

[21] W. Meyer-Eppler, "Verzerrungen, die durch die endliche durchlassbreite physikalischer apparate hervorgerufen werden, nebst Anwendung auf die Periodenforschung," *Ann. Phys.*, vol. 41, pp. 261–300; April, 1942.

[22] P. Mertz and F. Gray, "A theory of scanning and its relation to the characteristics of the transmitted signal in telephotography and television," *Bell Syst. Tech. J.*, vol. 13, pp. 464–515; July, 1934.

[23] H. A. Wheeler and A. V. Loughren, "The fine structure of television images," Proc. IRE, vol. 26, pp. 540–575; May, 1938.

concentrated on the scanning problem in television, but the latter paper stresses the analogous conditions in optics.

The step from the slit problem in optics to optical diffraction of an aperture is very small. Thus we may say that we have returned to our starting point.

Fourier Pairs in Time and Frequency Domains

In our modern world of pulse-modulated links, television sets, and radars, the Fourier pair in time and frequency domains, (22) and (23), known since the days of Fourier and Lord Rayleigh, has had extensive use. The author confines himself to pointing out two papers by Cherry[24] and Levy.[25]

This Fourier pair lately obtained special application in the theory of superregeneration.[26–29]. In this theory

$$f(t) = s(t) = \exp \int_0^t \alpha d\tau \tag{28}$$

where $s(t)$ represents the variation in impulse sensitivity with time and is, therefore, called "sensitivity pulse," $\alpha = G/2C$, G is the conductance, and C is the capacitance of a single tuned circuit.

Wheeler,[30] in 1942, recognized that the frequency function representing the selectivity of a simple superregenerative circuit is the Fourier transform of the sensitivity pulse.

Random Functions

The different Fourier transform pairs discussed above can be extended to be valid for random functions. The well-known Wiener-Khintchine theorem states that the power density spectrum and the correlation function are Fourier transforms of each other. Correlation functions have found applications, for example, in X-ray crystallography (Patterson diagrams), optics, antenna theory, acoustics, communication theory, and statistics. Much work has been done and is still going on, to figure out the exact interrelations among these different fields. A complete treatment of the random functions cases with references is, however, outside the scope of this paper.

Conclusion

The different physical applications of Fourier transform pairs discussed above show a selection of the great variety of problems which can be treated by one and the same mathematical tool, Fourier transformation theory. Thus, results in one field are immediately applicable in another field. Computations are simplified by existing tables and calculating machines. In the cases in which severe assumptions limit the practical use of the theory, the Fourier transform pairs have to be modified. Even in these idealized cases, however, the Fourier theory is of great value because it is simple and comprehensible. The presentation above constitutes an attempt to show, in a graphic way, how some known Fourier transform pair applications may be thought of as fitting together.

Acknowledgment

The work presented above was started in the summer of 1954, when the author was at the Royal Institute of Technology, Stockholm, Sweden; it was continued while he was a guest at Instituto Nacional de la Investigacion Cientifica, Mexico D. F., Mexico, during the winter of 1954–55; and it was completed at the Research Laboratory of Electronics, Massachusetts Institute of Technology, Cambridge, Mass., in the summer of 1955. The author expresses his gratitude to the Swedish Government Technical Research Council, Stockholm, Sweden, and Telefonaktiebolaget LM Ericsson, Stockholm, Sweden, for grants which made the Mexico-United States trip possible. He also takes great pleasure in thanking Dr. Manuel V. Cerrillo for his constructive criticism in reading the first part of the paper.

[24] E. C. Cherry, "Pulse response: a new approach to ac electric network theory and measurement," *J. IEE*, vol. 92, part III, pp. 183–196; September, 1945.
[25] M. M. Levy, "Fourier series and Fourier transform analysis," *J. Brit. IRE*, part I, vol. 6, pp. 64–73; March-May, 1946; part II, vol. 6, pp. 228–246; December, 1946.
[26] H. A. Wheeler, "A simple theory and design formulas for superregenerative receivers," Wheeler Monographs No. 3; June, 1948.
[27] H. A. Wheeler, "Superselectivity in a superregenerative receiver," Wheeler Monograph No. 7; November, 1948.
[28] W. E. Bradley, "Superregenerative detection theory," *Electronics*, vol. 21, pp. 96–98; September, 1948.
[29] A. Hazeltine, D. Richman, and B. D. Loughlin, "Superregenerative design," *Electronics*, vol. 21, pp. 99–102; September, 1948.
[30] H. A. Wheeler, private correspondence.

A Variant in the Measurement of Two-Port Junctions*

GEORGES DESCHAMPS†

Summary—Projective constructions are described for deducing the iconocenter of a two-port junction from input reflection coefficient measurements taken with a short circuit placed in various positions in the output waveguide. The wavelength in the ouput line is deduced from a four-point measurement. If this wavelength is known in advance, a three-point measurement gives all the information needed to construct the iconocenter.

Introduction

A DETERMINATION of the scattering matrix of a two-port junction and methods for making impedance measurements through such a junction have been described.[1–3] They all make use of the iconocenter, *i.e.*, of the input reflection coefficient corresponding to a matched output waveguide.

When no matched load is conveniently available, the iconocenter can be deduced from the input reflection coefficient measured for two pairs of reactive loads, each pair corresponding to short circuits spaced a quarter-wave apart.

As pointed out by Wentworth and Barthel[4] restricting the displacements of the short circuit to quarter-wave steps or to some fraction of the wavelength can be very inconvenient when taking measurement on a single junction over a large band of frequencies: it means an adjustment of the short positions for each new frequency. The authors propose a solution based on arbitrary fixed location of the short circuits and give a construction of the iconocenter based on the intersection of two circles.

The present note describes solutions to the same problem which are based on projective constructions. They are simpler in that they do not require drawing of a larger number of circles. They also have the advantage of *not requiring the knowledge of the wavelength* in the output waveguide.

These constructions were in fact originally devised to determine the wavelength in Microstrip by indirect measurement. They would apply to any medium where it is not convenient to move the short circuit back and forth. In the measurement on Microstrip for instance, the line under test was successively cut to produce the reactive termination of variable phase, and there was no possibility to adjust this phase before knowing the wavelength.

The constructions will be described for reactive junctions but apply just as well to lossy junctions. They give the "crossover" point from which the iconocenter follows by the construction ℬ.[2]

Experiment and Constructions

The experimental procedure (Fig. 1) consists of placing the short circuit in 4 positions—1, 2, 3, 4—equispaced but not in any relation to the wavelength. The "images" or input reflection coefficients are plotted on the reflection chart as M_1', M_2', M_3', M_4', and fall on the circle Γ'. (Γ' coincides with the unit circle Γ when the junction is loss free.)

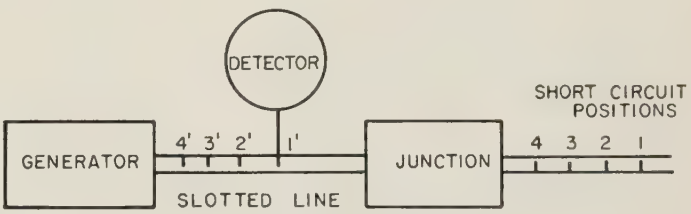

Fig. 1—Experimental setup.

Considering at first the 3 consecutive loads' positions 1, 2, and 3 in the output line, they are represented by M_1, M_2, M_3 on the unit circle Γ and the arc M_1M_2 equals the arc M_2M_3 [Fig. 2(a), next page]. The diameter of the circle Γ through the point M_2 therefore goes through the intersection T of the tangents to the circle Γ at the points M_1 and M_3. Using the projective representation of reflection coefficients[2] the image of this diameter [Fig. 2(b)] is therefore the line joining M_2' to the intersection T' of the tangents at points M_1' and M_3' to the circle Γ'. This is one locus for the image O' of O. Another straight line locus is deduced in the same manner from the points M_2', M_3', and M_4'. As shown in Fig. 3, O' is the intersection of the two lines, $T'M_2'$ and $U'M_3'$. The point O' image of O on the projective chart is called the cross-over point.[1–3] The iconocenter on the conformal (Smith) chart is related to it as described in these references.

There are many other versions of this projective construction. One that is particularly useful when the tangents to the circle Γ' do not intersect within the lim-

* Manuscript received by the PGMTT, October 11, 1956.
† Federal Telecommunication Labs, Nutley, N. J.

[1] G. A. Deschamps, "Determination of reflection coefficients and insertion loss of a waveguide junction," *J. Appl. Phys.*, vol. 24, pp. 1046–1050; August, 1953.
[2] G. A. Deschamps, "A Hyperbolic Protractor for Microwave Impedance Measurements and Other Purposes," Federal Telecommunication Labs, 1953.
[3] J. E. Storer, L. S. Sheingold, and S. Stein, "A simple graphical analysis of a two-port waveguide junction," PROC. IRE, vol. 41, pp. 1004–1013; August, 1953.
[4] F. L. Wentworth and D. R. Barthel, "A simplified calibration of two-port transmission line devices," IRE TRANS., vol. MTT-4, pp. 173–175; July, 1956.

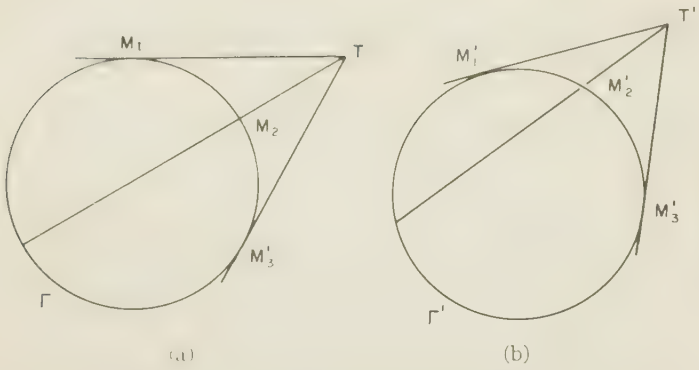

Fig. 2—Projective construction of the image of a diameter.

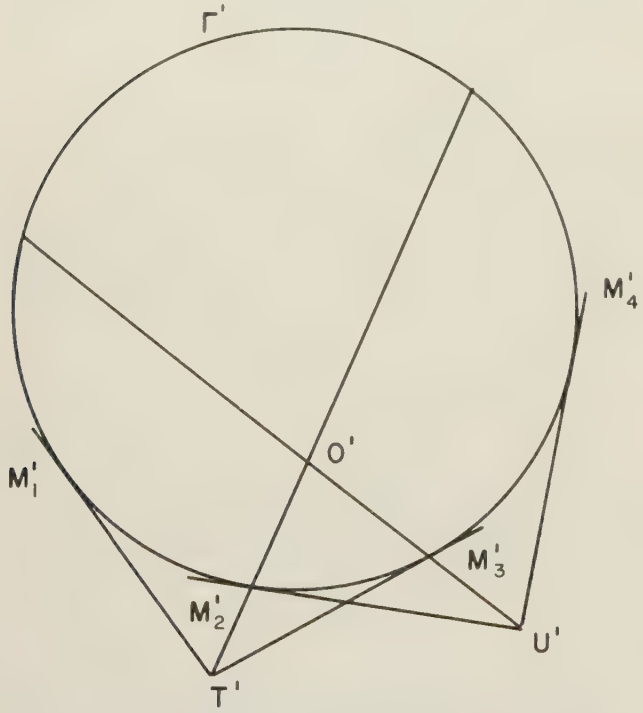

Fig. 3—Construction of the crossover point from the reflection coefficients for four equispaced loads (wavelength unknown).

its of the page is shown in Fig. 4(b). The transform or image of the diameter is the line $M_2'C'$ where C' is the intersection of $M_1'B'$ and $M_3'A'$. This is justified by considering Fig. 4(a) before the transformation.

Once O' has been found, projection of M_1', M_2', M_3', M_4' through O' onto the circle Γ' will give the points M_1'', M_2'', M_3'', and M_4'' which are equispaced along this circle. The angle between two successive points (M_1'', M_2'') for instance, is the electrical angle corresponding to the displacement from 1 to 2; hence this gives a means of *finding the wavelength* in the output waveguide.

This determination of the wavelength resulted from measurement on four arbitrary equispaced loads. Conversely, if the wavelength is known in advance, the point O' may be determined from a three-point measure-

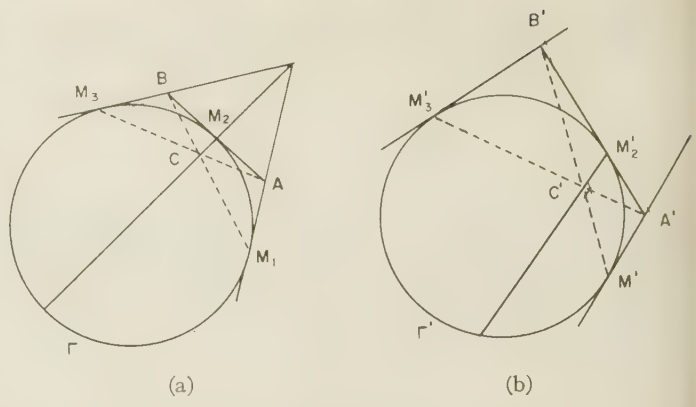

Fig. 4—Construction of the diameter image when the tangents at points M_1' and M_3' meet "out of bounds."

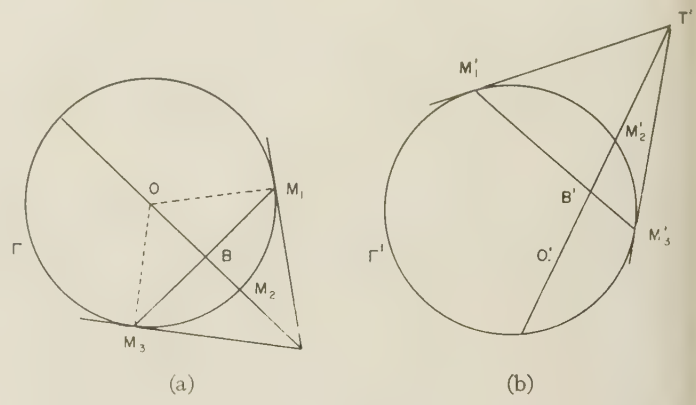

Fig. 5—Construction of the crossover point from a three-points measurement (wavelength known).

ment. This is what is done in the construction of Wentworth and Barthel. A projective construction that leads to the same result quicker and without drawing circles is shown in Fig. 5. The diameter $M_2'T'$ is found as above and O' is located on that diameter by using the invariance of the hyperbolic distance.[2]

$$\langle O'B' \rangle = \langle OB \rangle.$$

Fig. 5(a) is drawn making use of the known electrical angle α between 1 and 2 or 2 and 3. The "distance" $\langle OB \rangle$ is measured on that figure with the hyperbolic protractor or it is computed by

$$\langle OB \rangle = 10 \log_{10} \frac{1 + \cos \alpha}{1 - \cos \alpha} = 20 \log_{10} \cot \frac{\alpha}{2} \cdot$$

[In nepers the hyperbolic distance $\langle OB \rangle$ is the antigudermaniam of $(\pi/2) - \alpha$.] It is then used to lay out the distance $\langle O'B' \rangle$ on Fig. 5(b) by means of the hyperbolic protractor for instance.

There are many other projective constructions for three- or four-point measurements for completely arbitrary load positions that can be devised by anyone familiar with projective geometry. They are somewhat more laborious than those based on equispaced loads. The latter are therefore recommended since they are

still compatible with measurements at variable frequency taken with fixed loads.

Another practical recommendation is to use more than four loads in order to increase the precision by some averaging. This also makes it possible to choose for the construction the points that show the best configuration; for instance, to avoid the use of points that are too close together.

Finally it should be noted that at a single frequency and when the wavelength is known, the quarter-wave spacing leads to a simpler construction. For variable frequency the measurements take less time when fixed short-circuit positions are used, but the interpretation is slightly complicated.

An obvious requirement when using this method is to have a good control on the frequency. In regions where the measured reflection coefficients vary rapidly with frequency, it may be advisable to go back to a measurement where the frequency is set and the short circuit moved.

Correspondence

WESCON Papers' Deadline Set for May 1

Authors wishing to present papers at the 1957 WESCON Convention to be held in San Francisco, Calif., on August 20–23 should send 100–200 word abstracts, together with complete texts or additional detailed summaries, to the Technical Program Chairman, D. A. Watkins, Stanford Electronics Laboratories, Stanford University, Stanford, Calif., for consideration by the Technical Program Committee. Authors will be notified whether or not their papers have been accepted by June 1.

For the first time this year, an IRE WESCON Convention Record will be published. It will include every paper presented at the 1957 WESCON and will be published immediately following the convention, for national distribution.

The IRE "Affiliate" Plan—A New Venture in Engineering Society Structure and Service

On January 4, 1957, the IRE Board of Directors arrived at a decision which may in time prove to be one of the most far-reaching in its 45-year history. On that date the Board adopted a plan which will enable non-IRE members whose main professional interests lie outside the sphere of IRE activities to become affiliated with certain of the IRE Professional Groups *without* first having to join the IRE itself.

This plan is aimed at those specialists in other fields of science and technology whose work touches upon our own electronics and communications field only in specialized areas. In effect, the IRE is extending the specialized services of its Professional Groups to every field of science and engineering.

An outstanding example of where these services are needed may be found in the case of the medical and biological sciences. At the present time some 1400 IRE members enjoy the privileges of membership in the Professional Group on Medical Electronics. And yet there are hundreds, perhaps thousands, of medical doctors, biologists, and others to whom the activities of this Group would be of interest and value. Both they and the Group would benefit from their participation. To require these persons, who have no interest in radio engineering, to join the IRE in order to join the Group is unreasonable, and probably futile as well. In fact, it was largely to provide an answer to this particular problem that the "Affiliate" Plan was first conceived, although it pertains to other fields as well, such as Computers, etc.

The "Affiliate" Plan is admittedly an experiment. So far as is known, no other society has ever tried a similar scheme. The Board of Directors feels strongly that the benefits afforded by the plan justify the risk that some persons who should join the IRE will instead become Affiliates. To minimize this risk, the plan has been carefully worked out along the following lines:

1) Participation in the Plan is at the option of each Professional Group. It is not expected that all Groups will adopt it; only those which feel it serves a need in their particular field.

2) Each Group interested in initiating the "Affiliate" Plan must submit to the Chairman of the Professional Groups Committee a list of accredited organizations which has been selected and approved by its Administrative Committee, for official approval by the IRE Executive Committee.

3) To be an Affiliate of a Professional Group, a person must belong to an accredited organization approved by that Group and the IRE Executive Committee. Moreover, he shall not have been an IRE member during the five years prior to his application. He may affiliate with more than one Group, provided the accredited organization to which he belongs is recognized by the Groups concerned.

4) The fee for Affiliates shall be the assessment fee of the Group, plus $4.50. The latter covers IRE subsidies to the Group, Professional Group overhead expenses borne by IRE Headquarters, and 50 cents which is to be rebated to IRE Sections for mailing and meeting costs.

5) An Affiliate will be entitled to receive the TRANSACTIONS of his Group and that part of the IRE NATIONAL CONVENTION RECORD pertaining to his Group. He will be eligible for a Group award, and may attend local or national meetings of the Group by payment of charges assessed Group members.

6) An Affiliate cannot serve in an elective office in the Group or Group Chapter, nor vote for candidates for these offices.

7) An Affiliate may hold an appointive office in the Group or Group Chapter.

8) An Affiliate may not receive any IRE benefits that are derived through IRE membership.

The "Affiliate" Plan is a bold and far-sighted venture; one that recognizes and provides for the rapidly spreading influence of electronics in every walk of scientific and technological life, and one that enables the IRE to further its aims as a professional engineering society—the advancement of radio engineering and related fields of engineering and science.

W. R. G. BAKER, *Chairman*
IRE Professional Groups Committee

Matching the Sides of a Parallel-Plate Region*

One of the simplest forms of electromagnetic wave is a TEM wave propagating between parallel conducting planes which extend laterally to infinity. It is perhaps not

* Received by the PGMTT, December 27, 1956.

widely known that a TEM mode may be sustained in a parallel plane region of finite width by closing the sides and including dielectric slabs as in Fig. 1. The field in

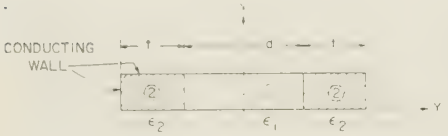

Fig. 1.

the dielectric-free region is strictly identical with a TEM mode at a single frequency (f_0) only; the curves of Fig. 2 have been prepared to show the bandwidth which may be achieved by permitting a given departure from a pure TEM mode.

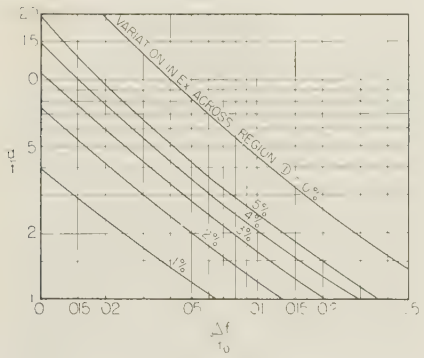

Fig. 2.

In region 1 of Fig. 1, the dependence of E_x on y may be expressed as

$$E_x \propto \cos \beta y. \tag{1}$$

The solution to Maxwell's equations for the case of Fig. 1 and assuming no variation with x is well known.

It is found that as the frequency is increased, β, which is real, decreases to zero and then becomes imaginary. The field which is identical to a TEM mode in region 1 is the degenerate case where $\beta=0$. In this case it may be shown that

$$\frac{t}{\lambda_1}\sqrt{\frac{\epsilon_2}{\epsilon_1}-1} = 0.25 \tag{2}$$

where the following nomenclature is used:

λ_1—Wavelength of a plane wave in an unbounded region of relative permittivity ϵ_1, *i.e.*, free space wavelength if region 1 is air-filled
ϵ_1—Relative permittivity in region 1
ϵ_2—Relative permittivity in region 2
t, d—Dimensions, in same units as λ_1
E_x—Electric field in x direction.

For a given wavelength and given value of ϵ_1 in region 1, (2) shows that there is a single infinity of pairs of t and ϵ_2 which are satisfactory, while d may have any value. If in a practical case, region 1 is the useful region, it would be desirable to minimize the width "t" of region 2. Eq. (1) shows that in this case the permittivity of the dielectric in region 2 should be as high as possible.

The above remarks apply only at a single frequency. To consider operation throughout a range of frequencies, the bandwidth may be defined in terms of allowable nonuniformity of E_x throughout region 1. This has been done in Fig. 2, which shows the amount of dielectric which must be used to obtain a given bandwidth. Curves are drawn for various allowable percentages of variation in E_x across region 1. At the low frequency end of the band the departure of E_x from uniformity across region 1 takes the form of a maximum at $y=0$, while at the high frequency end of the band E_x has a minimum at $y=0$.

For a given bandwidth (Δf) and permissible variation of E_x across region 1, Fig. 2 will give the parameter (d/t). By a slight rearrangement of (2):

$$\frac{d}{\lambda_1}\sqrt{\frac{\epsilon_2}{\epsilon_1}-1} = 0.25\frac{d}{t}. \tag{3}$$

Using this relation, and assuming λ_1 to be known,

$$d\sqrt{\frac{\epsilon_2}{\epsilon_1}-1}$$

is established. It is interesting to note that regardless of how large d is, the bandwidth requirement may be met in practice merely by reducing ϵ_2/ϵ_1 toward unity. In some cases this may imply the use of drilled or expanded dielectrics. There is no lower limit to d either, since if ϵ_2 becomes inconveniently large, it is merely necessary to choose a *better* condition, *i.e.*, smaller per cent variation in E_x, from Fig. 2.

The following explanation may help to provide a physical picture. The TE_{01} mode of a rectangular waveguide of width a has a wavelength longer than the free space wavelength of a plane wave. If the waveguide is now filled with dielectric, the wavelength will be reduced. Hence there must be some dielectric constant for each value of a which restores the wavelength to its free space value. This is identically the relation given by (2) if we consider: 1) "free space" has been generalized to any dielectric medium of permittivity ϵ_1; 2) $a=2t$; and 3) $d=0$.

If now we reintroduce region 1 by splitting the waveguide and tapering it outward as in Fig. 3, it is at least plausible

Fig. 3.

that the field in region 1 will resemble a TEM mode.

In practice, the configuration of Fig. 3 provides a possible method of setting up such a mode.

For completeness, it may be mentioned that the values of t and ϵ_2 could be different in each part of region 2.

Arthur C. Hudson,
National Research Council
Ottawa, Ontario, Canada

A Method of Analysis of Symmetrical Four-Port Networks*

The following errors appeared in the above article.[1] On page 248 the C term in the matrix for Fig. 11 should be $j(-a^2c^2+2ac+a^2-1)$. Also, on page 249 the term for T_{+-} for the rat race ring should be $T_{+-}=-j/\sqrt{2}$.

John Reed
Raytheon Mfg. Co.
Wayland, Mass.

* Received by the PGMTT, November 25, 1956.
[1] J. Reed and G. J. Wheeler, IRE Trans., vol. MTT-4, pp. 246–252; October, 1956.

Miniature Waveguide Flanges Unpressurized Contact Type*

I would like to call attention to the fact that RETMA Standard RS-166 with the above title and dated October, 1956, has been released. Copies of the Standard can be obtained through the Engineering Department of the RETMA, 11 West 42nd Street, New York 36, N. Y.

Tore N. Anderson
AIRTRON, Inc.
Linden, N. J.

* Received by the PGMTT, November 29, 1956.

Criteria for the Design of Loop-Type Directional Couplers for the L Band*

We have noted several errors in the above article[1] and the corrections are as follows:

Eq. 5(b) should read:

$$V_B \cong + \sqrt{\frac{Z_{20}}{Z_{01}}}\left(\frac{k_L - k_C}{4}\right) \cdot [1 - \cos\beta_0(k_C + k_L)l\epsilon^{-j2\beta_0 l}].$$

Eq. (7) should read:

$$D = 20\log_{10}\left|\frac{k_L - k_C}{k_L + k_C}\right|\frac{\sin\beta_0 l}{\beta_0 l}.$$

Richard F. Schwartz
Univ. of Pennsylvania
Philadelphia, Pa.

* Received by the PGMTT, November 1, 1956.
[1] P. P. Lombardi, R. F. Schwartz, and P. J. Kelly, IRE Trans., vol. MTT-4, pp. 234–239; October, 1956.

Planar Transmission Lines—Part III*

The following are a few comments on the above.[1] This paper purports to derive criteria for the optimum line from the standpoint of stability and attenuation. The conclusions arrived at, however, are erroneous.

The stability criterion derived, $0.03 < w/h < 0.75$, where w is the strip width and h is half the ground plane spacing, would limit the characteristic impedance to values greater than 120 ohms which would be most unfortunate if true. The basis for this choice is the rapid variation of $f(k^2)$ in the neighborhood of $k=0$ or 1. In the neighborhood of $k=0$, however,

$$f(k^2) \approx 4\left(\ln 2 + \frac{\pi w}{4h}\right)$$

so that it does not vary rapidly with the line dimensions and the upper limit on w/h is not necesasary.

An examination of stability might better be made by directly investigating the dependence of characteristic impedance on the dimensions. In the case of low impedance lines, $w \gg h$ and

$$Z_0 = \frac{15\pi^2}{\sqrt{k}} \frac{1}{\ln 2 + \dfrac{\pi w}{4h}} \approx \frac{60\pi}{\sqrt{k}} \frac{h}{w}.$$

Thus

$$\frac{dZ_0}{Z_0} = \frac{dh}{h} - \frac{dw}{w}$$

which indicates that low impedance lines are not unstable. For high impedance lines, $w \ll h$ and

$$Z_0 = \frac{60}{\sqrt{k}} \ln \frac{16h}{\pi w}.$$

In this case,

$$\frac{dZ_0}{Z_0} = \frac{60}{Z_0}\left(\frac{dh}{h} - \frac{dw}{w}\right)$$

which indicates that very high impedance lines are even more stable. This latter condition is generally true for any transmission line operating in the TEM mode as is obvious from the logarithmic dependence of the characteristic impedance on the line dimensions.

The statement that the attenuation decreases as w is decreased is contrary to fact, both experimental[2] and theoretical.[3] This error arose by neglecting the dependence of k^2 on the ratio w/h in (11) and (12). The dependence of the attenuation on w for a single strip line may be found from (33) of Park's original paper.[4]

This is[4]

$$\alpha \approx \frac{\eta\sqrt{k}}{120\pi h} \frac{4h}{\pi w}\left(\ln\frac{4h}{\pi t} + \frac{\pi w}{2h}\right); \quad \frac{\pi w}{4h} \gg \ln 2$$

$$\approx \frac{\eta\sqrt{k}}{120\pi h}\left(\frac{4h}{\pi w}\ln\frac{4h}{\pi t} + 2\right).$$

Then

$$\frac{\partial\alpha}{\partial w} = -\frac{\eta\sqrt{k}}{30\pi^2 w^2}\ln\frac{4h}{\pi t}.$$

showing that α decreases as w increases. This is also true for the case of a balanced strip line.

Karle S. Packard, Jr.
Airborne Instruments Lab. Inc.
Mineola, N. Y.

Author's Comment, Part IV[5]

In this note the characteristic impedance will be estimated for a transmission line composed of two wires of radius a and separation $2d$, embedded in a dielectric between two broad conducting strips which are a distance $2h$ apart and which extend for some distance beyond the wires on each side. For the notation and ideas, as well as a discussion of what is meant by "some distance," we refer to a previous paper.[4] The calculation is done by the method of images, and the approximation will be made that the radius of the wire is very small compared to the other dimensions of the system. If this is true, the charge distribution on each wire and its images will be nearly symmetrical about the center, and the work necessary to bring a unit charge from infinity to the surface of one of the wires is $(\lambda/2\pi\epsilon)\ln(2d/a)$ when only the fields of the two wires are taken into account. Considering next the fields due to the nth image of the pair of wires, located at a distance $2nh$ above them, we see easily that the corresponding work is $(-)^n\frac{1}{2}(\lambda/2\pi\epsilon)\ln[1+(d/nh)^2]$. Summing over all these pairs of images and including the original wires we get

$$V = \frac{\lambda}{2\pi\epsilon}\ln\left\{\frac{[1+(d/2h)^2][1+(d/4h)^2][1+(d/6h)^2]\cdots}{[1+(d/h)^2][1+(d/3h)^2][1+(d/5h)^2]\cdots}\cdot\frac{2d}{a}\right\}.$$

The infinite products converge and can be evaluated by means of the well-known products for sines and cosines to give

$$V = \frac{\lambda}{2\pi\epsilon}\ln\left\{\frac{2h}{\pi d}\frac{\sinh(\pi d/2h)}{\cosh(\pi d/2h)}\cdot\frac{2d}{a}\right\}.$$

The potential of a point on the other wire is the negative of this, and so the total potential difference is twice V. The characteristic impedance in the TEM mode is given by $Z=\sqrt{(\mu\epsilon)}/C$ where C, the line's capacity per unit length, is λ/V. Thus $Z=2\sqrt{(\mu\epsilon)}\,V/\lambda$, and

$$Z = \frac{120}{\sqrt{\kappa}}\ln\left\{\frac{4h}{\pi a}\tanh\frac{\pi d}{2h}\right\}.$$

This is the same as the equation before (22a),[4] if w there is replaced by $4a$. Thus it results that a flat central strip in a line of this kind is equivalent to (but more lossy than) a wire whose diameter is half the width of the strip.

Finally, a previous note in this journal[1] which purported to derive several restrictions on the dimensions of practical transmission lines must be amended. In fact the conditions imposed there were far too stringent, due to neglect of the fact that though the operating characteristics depend somewhat steeply on the parameter k^2 when k^2 is near the ends of its range, this does not mean that it depends very critically on the dimensions of the line, as can in fact easily be seen from the relevant formulas.[4] The restrictions are thus unnecessary. I would like to thank K. S. Packard for calling my attention to this mistake. Further, the numerical coefficients in (11) and (12)[1] should be corrected to read $7.4\times10^{-4}/b$ and $3.7\times10^{-4}/b$ respectively.

David Park
Williams College
Williamstown, Mass.

* Received by the PGMTT, June 29, 1956.
[1] D. Park, "Planar transmission lines—III," IRE Trans., vol. MTT-4, p. 130; April, 1956.
[2] E. G. Fubini, W. E. Fromm and H. Keen, "New techniques for high-Q strip microwave components," 1954, IRE Convention Record, Part 8, p. 91.
[3] S. Cohn, "Problems in strip transmission lines," IRE Trans., vol. MTT-3, p. 119; March, 1955.
[4] D. Park, "Planar transmission lines," IRE Trans., vol. MTT-3, p. 10; April, 1955.

[5] Received by the PGMTT, October 10, 1956.

A Low VSWR Matching Technique*

I would like to call your attention to a certain error in the above correspondence.[1] The admittance function plotted by the author on the Smith chart winds counterclockwise. This is contrary to the laws of nature for passive linear networks. These laws prescribed that the plot of the admittance function wind clockwise from the low to the high frequency.

Rotation of the admittance function to the generator would result in a loop instead of a point when the high-frequency end catches up with the low-frequency end. Furthermore, continued rotation causes f_h to pass f_l which is contrary to the author's figures.

Lenrod Goldstone
The W. L. Maxson Corp.
New York, N. Y.

* Received by the PGMTT, September 24, 1956.
[1] P. A. Rizzi, IRE Trans., vol. MTT-4, pp. 185–186; July, 1956.

Author's Comment[2]

In view of Mr. Goldstone's comment, the curvature of curves B and B' in Figs. 1 and 2 should be changed from concave with respect to the center of the chart to convex. Rotation of the resultant curve to the $g=1$ circle will, as Mr. Goldstone points out, yield an admittance plot which contains a small loop.

Nevertheless, the general matching procedure as outlined is still valid.

Peter A. Rizzi
Raytheon Mfg. Co.
Bedford, Mass.

[2] Received by the PGMTT, November, 1956.

A Broad-Band Microwave Circulator*

Edward A. Ohm[1] has recently shown some applications of microwave circulators, first suggested by A. G. Fox, S. E. Miller, and W. W. Mumford of the Bell Telephone Laboratories. One in particular, a circulator microwave modulator, I believe, needs some further discussion. This device is shown in Fig. 1. As shown, the energy from the oscillator travels to the port containing the modulator, where it is modulated, reflected from the short circuit, passed back through the modulator and to the output arm of the circulator. Let us consider what occurs if the modulator is a typical ferrite type modulator, like those commercially available. This modulator is shown in Fig. 2.

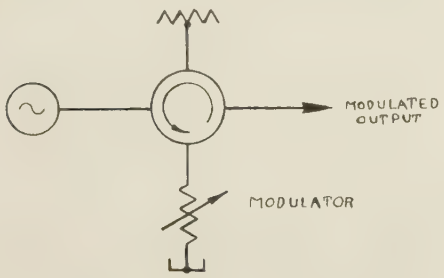

Fig. 1—A circulator microwave modulator.

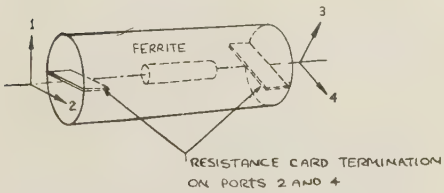

Fig. 2—Ferrite modulator.

When no field is applied to the modulator, the wave E_{incident} from the input port 1 splits between ports 3 and 4. With an applied ac field, the polarization is rotated first to port 3, the output, and then to port 4, which is terminated. The output wave at port 3 is

$$E_3 = \sin\left(\frac{\pi}{4} + m \sin \omega_m t\right) \tag{1}$$

where m is the index of modulation and ω_m is the angular modulation frequency.

If, in general, port 3 has a load reflection coefficient Γ, then due to the nonreciprocal rotation of the ferrite, the wave reflected back out of port 1 is

$$E_1 = \Gamma E_3 \cos\left(\frac{\pi}{4} + m \sin \omega_m t\right) \tag{2}$$

which reduces to

$$E_1 = \frac{\Gamma}{2} \sin\left(\frac{\pi}{2} + 2m \sin \omega t\right). \tag{3}$$

A sketch of the waveforms for (1) and (3) is shown in Fig. 3.

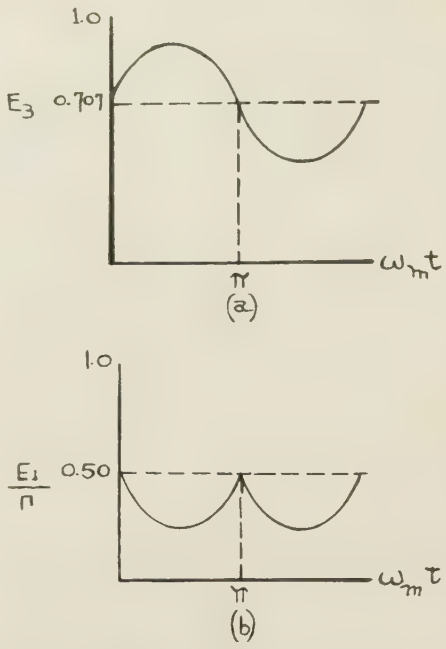

Fig. 3—Modulation envelope. (a) After passing through modulator once. (b) After being reflected from short and passing through modulator twice.

The harmonic content of (1) has been presented by Rizzi and Rich.[2] In a similar manner, the harmonic content of (3) can be analyzed; however, it is apparent that E_1 has a strong second harmonic component. Thus, the output of the circulator microwave modulator will not have good fidelity with respect to the driving voltage on the field coil. If the modulator were reciprocal instead of nonreciprocal, E_1 instead of equaling a cos sin term, would equal a $\sin^2$ term, which also has a strong second harmonic component.

From this discussion I believe it is also apparent that the use of a ferrite modulator in a microwave impedance test bench may have deleterious results, since the reflected power from the load to be measured will pull the test oscillator at approximately twice the modulation frequency. This will cause minimum filling in the standing-wave pattern and also results in a generator impedance $\neq z_0$ as a function of time.

A load isolator or attenuator should always be used with a ferrite modulator to reduce the amplitude of the wave reflected from the load.

Alvin Clavin
Rantec Corp.
Calasasas, Calif.

Author's Comment[3]

A modulator must be suited to its application and it appears that Mr. Clavin has selected a type which does not perform the task he requires. In this regard it can be shown that the fundamental modulation frequency envelope will not appear at the output of his modulator. Clavin's (3)

$$E_1 = \frac{\Gamma}{2} \sin\left(\frac{\pi}{2} + 2m \sin \omega_m t\right)$$

can be rewritten

$$E_1 = \frac{\Gamma}{2} \cos\left(2m \sin \omega_m t\right).$$

From (1) of Rizzi and Rich[2] it can be seen that this is identical to

$$E_1 = \frac{\Gamma}{2}\left[J_0(2m) + 2J_2(2m) \cos 2\omega_m t + 2J_4(2m) \cos 4\omega_m t \cdots\right]$$

and this makes it clear that E_1 does not vary at the rate of the fundamental modulation frequency.

This particular example may leave an impression that the modulation schematic shown in Fig. 6 of my paper[1] is not valid. However, since other, more successful, modulators can be designed which are in harmony with Fig. 6 it appears that some further discussion would be appropriate at this time.

One example of a more workable Faraday rotation assembly is depicted in Fig. 4. From this figure it can be shown that

$$E_{\text{reflected}} = E_{\text{in}} \cos\left(\pi/4 + 2\theta\right)$$

which is identical to

$$E_{\text{reflected}} = 0.707 E_{\text{in}}(\cos 2\theta - \sin 2\theta).$$

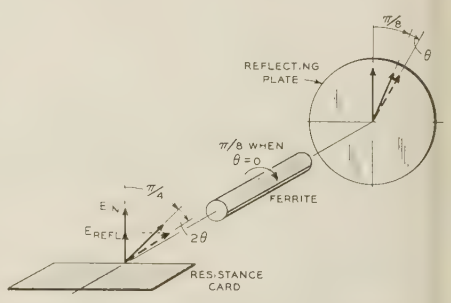

Fig. 4—A simple reflecting microwave modulator.

Now if θ varies sinusoidally at the modulation rate of ω_m with a maximum angle of rotation, $\theta_{\max}$, it can be written

$$\theta = \theta_{\max} \sin \omega_m t.$$

After inserting this value of θ, (1) of Rizzi and Rich[2] can again be used to show that $E_{\text{reflected}}$ varies at the fundamental modulation rate as well as at all of the even and odd harmonics of this rate.

$$E_{\text{reflected}} = 0.707 E_{\text{in}}[J_0(2\theta_{\max}) - 2J_1(2\theta_{\max}) \sin \omega_m t + 2J_2(2\theta_{\max}) \cos 2\omega_m t - 2J_3(2\theta_{\max}) \sin 3\omega_m t + 2J_4(2\theta_{\max}) \cos 4\omega_m t - \cdots].$$

An analysis of this equation reveals that the largest harmonic coefficients, the second and third, are down 19 db and 42 db respectively from the fundamental when the maximum value of $2\theta_{\max}$ is less than or equal to 25°. This is the value required to reduce the fundamental coefficient, $\sqrt{2}J_1(2\theta_{\max})E_{\text{in}}$, to 0.3 E_{in}, a value which corresponds to a 60 per cent modulation of a linear system.

If additional second harmonic discrimination is desired (without decreasing the fundamental component) the Faraday rota-

* Received by the PGMTT, November 13, 1956.
[1] E. A. Ohm, IRE Trans., vol. MTT-4, pp. 210–217; October, 1956.
[2] P. A. Rizzi and D. J. Rich, "A note on sidebands produced by ferrite modulators," Proc. IRE, vol. 44, p. 556; April, 1956.
[3] Received by the PGMTT, February, 1957.

tion assembly shown in Fig. 5 can be used. Although this assembly generates slightly larger odd harmonics it is generally superior to that of Fig. 1 because it does not generate even harmonics. It can be shown that

$$E_{\text{reflected}} = E_{\text{in}} \sin^2 \phi$$

where

$$\phi = (\pi/4 + \theta_{\max} \sin \omega_m t)$$

and that this is identical to

$$E_{\text{reflected}} = \frac{E_{\text{in}}}{2} [1 + \sin (2\theta_{\max} \sin \omega_m t)].$$

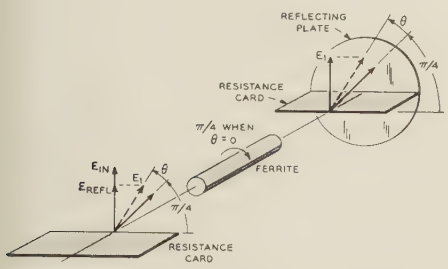

Fig. 5—A reflecting microwave modulator which does not generate even harmonics.

Again using (1) of Rizzi and Rich[2] it can be shown that the reflected voltage varies only at the fundamental and odd harmonic modulation rates.

$$E_{\text{reflected}} = E_{\text{in}}[1/2 + J_1(2\theta_{\max}) \sin \omega_m t + J_3(2\theta_{\max}) \sin 3\omega_m t + \cdots].$$

Thus, it appears that Mr. Clavin is in error when he claims that a strong second harmonic will result from a reflected voltage which varies as the $\sin^2 \phi$.

An analysis of this last equation yields data identical to that of Fig. 2 of Rizzi and Rich.[2] This figure shows how the largest harmonic coefficients, the third and fifth, vary with respect to the fundamental coefficient for different maximum values of $2\theta_{\max}$. In particular this figure shows that the third and fifth harmonics are down more than 36 db and 55 db respectively from the fundamental when the maximum value of $2\theta_{\max}$ is less than or equal to 36°, the value required to again reduce the fundamental coefficient, $J_1(2\theta_{\max})E_{\text{in}}$ to the same value of 0.3 E_{in} which corresponds to a 60 per cent modulation of a linear system.

Edward A. Ohm
Bell Telephone Labs.
Holmdel, N. J.

On Symmetrical Matching*

Mr. Mathis' note[1] is correct in that a match is achieved with the three shunt susceptances, but he is wrong in his assertion that no other positioning is possible for match. His method of matching is outlined in Fig. 1.

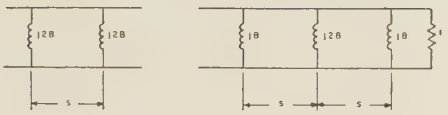

Fig. 1.

The distance s is computed so that two shunt susceptances, each of magnitude $2B$ will cancel each other,[2] thus $\tan 2\pi s/\lambda g = 1/B$. Then susceptances of magnitude B are spaced this distance away on either side and match is obtained. However, match is also obtained when $\tan 2\pi s/\lambda g = 2/B$ and thus the response is not symmetrical about the original frequency. The match can be checked by computing the admittance at the center of the network with a matched termination and, if it is purely real, the network is matched.[3]

The response can be made to be symmetrical (critically coupled) provided that the standing-wave ratios introduced by the three susceptances go in the ratios of r, r^2, r or the susceptances go as B, $B\sqrt{B^2+4}$, B. The spacing p between the three susceptances can be found on a Smith chart. See Fig. 2.

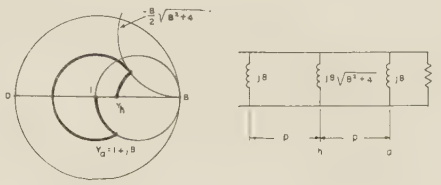

Fig. 2.

A matched termination at the right of the line makes the normalized admittance at point a $1+jB$. In Fig. 2, inductive susceptances which will have negative values are assumed. This admittance is transformed along the line toward the generator until the circle is tangent to the Smith chart circle for

$$-\frac{B}{2}\sqrt{B^2+4}.$$

The admittance at the center of the network then will be purely real and chart of the network will be the mirror image about the real axis. Therefore, the input admittance is matched. For small variations in length of line p corresponding to small changes in frequency the input admittance is still matched since the circles are tangent. This circuit is thus a critically-coupled double tuned arrangement. The value of the line length p is given by the formula.

$$\tan \frac{2\pi p}{\lambda g} = \frac{B^2 + 2 + \sqrt{B^2+4}}{B^3 + 3B}.$$

John Reed
Raytheon Mfg. Co.
Wayland, Mass.

Author's Comment[4]

Mr. Reed is correct in his remarks. My note was based on the theorem that *if one-sided matching for a lossless symmetrical discontinuity is achieved with a lossless symmetrical matching network, the matching network can be split and the part farther from the discontinuity moved to the opposite side of the discontinuity to obtain two-sided matching.* This theorem is correct, but all of the conclusions in my note were not correct.

In general, either the value of the shunt susceptances or their positions for symmetrical matching may be arbitrarily selected. When the value of the shunt susceptances is selected, there may be two pairs of positions which can be used. When the positions are selected, there may be two values of the shunt susceptances which can be used.

Procedures for finding the positions or the value of the shunt susceptances, when the other is given, are presented next. In the discussion which follows, it is assumed that the voltages, currents, and impedances are measured in units so that the characteristic impedance of the transmission line is one.

When the value B of the shunt susceptances is selected, the discontinuity is terminated in a matched load, and the input admittance Y_1 is determined and plotted on a Smith chart, as shown in Fig. 3. The admittance Y_2 given by the formula

$$Y_2 = \frac{16 + 12B^2 + 3B^4 - j(16B + 8B^3)}{16 + 12B^2 + B^4} \quad (1)$$

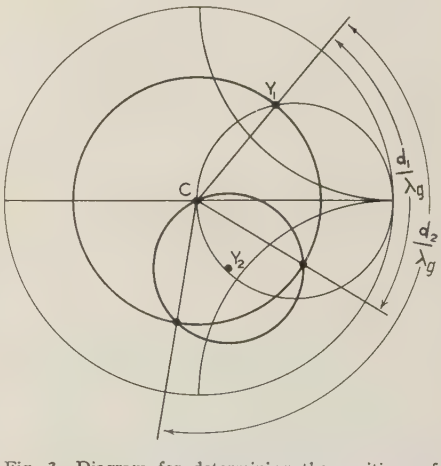

Fig. 3—Diagram for determining the positions of shunt susceptances.

is plotted on the Smith chart. A circle is drawn with its center at Y_2 which passes through the center C of the chart. (This circle must also pass through the point $Y = 1 - j2B$.) A circle is drawn with its center at C which passes through the point Y_1. The points of intersection of these circles determine the possible pairs of positions of the shunt susceptances. (For the second example given by Reed, the circles are tangent.) If the circles do not intersect, it is not possible to use this value of B. The distances d_1 and d_2 of these pairs of positions

* Received by the PGMTT, November 13, 1956.

[1] H. F. Mathis, IRE Trans., vol. MTT-4, p. 132; April, 1956.

[2] J. Reed, "Low-Q microwave filters," Proc. IRE, vol. 38, p. 794; July, 1950.

[3] *Ibid.* See (6).

[4] Received by the PGMTT, November 23, 1956.

from the discontinuity are determined on the Smith chart as indicated in Fig. 3.

When the positions of the shunt susceptances are selected, the input admittance $g+jb$ at one of the positions is determined with the opposite side of the discontinuity terminated in a matched load. The possible values B of the shunt susceptances are given by the formula

$$B = \frac{b \pm \sqrt{gb^2 + (g-1)^3}}{g-1}. \qquad (2)$$

If B is not real, it is not possible to use these positions.

Proof of Theorem

According to well-known circuit theory, any lossless four-terminal network can be represented by the matrix

$$\begin{pmatrix} A_{1,1} & jA_{1,2} \\ jA_{2,1} & A_{2,2} \end{pmatrix},$$

where the input voltage E_1 and the input current I_1 are related to the output voltage E_2 and the output current I_2 by the equations

$$E_1 = A_{1,1}E_2 + jA_{1,2}I_2,$$
$$I_1 = jA_{2,1}E_2 + A_{2,2}I_2.$$

The symbols $A_{1,1}$, $A_{1,2}$, $A_{2,1}$, and $A_{2,2}$ denote real quantities. If the network is symmetrical, $A_{1,1}=A_{2,2}$. If the network is reversed, the corresponding matrix is

$$\begin{pmatrix} A_{2,2} & jA_{1,2} \\ jA_{2,1} & A_{1,1} \end{pmatrix}.$$

If the input impedance is one when the load impedance is one, then $A_{1,1}=A_{2,2}$ and $A_{1,2}=A_{2,1}$. A section of lossless transmission line, with a characteristic impedance of one, is represented by the matrix

$$\begin{pmatrix} \cos\beta d & j\sin\beta d \\ j\sin\beta d & \cos\beta d \end{pmatrix}.$$

Let the symmetrical lossless discontinuity be represented by the matrix

$$\begin{pmatrix} M & jN \\ jP & M \end{pmatrix}.$$

The symmetrical one-sided lossless matching network is split into two networks which are represented by the matrices

$$\begin{pmatrix} m & jn \\ jp & q \end{pmatrix}$$

and

$$\begin{pmatrix} r & js \\ jt & u \end{pmatrix},$$

The matrix for the three networks connected in cascade is

$$\begin{pmatrix} A_{1,1} & jA_{1,2} \\ jA_{2,1} & A_{2,2} \end{pmatrix}$$
$$= \begin{pmatrix} m & jn \\ jp & q \end{pmatrix}\begin{pmatrix} r & js \\ jt & u \end{pmatrix}\begin{pmatrix} M & jN \\ jP & M \end{pmatrix}.$$

Since the matching network is symmetrical,

$$mr - nt = qu - ps.$$

Also, since the input impedance is one when the load impedance is one,

$$A_{1,1} = A_{2,2}$$
$$= (mr - nt)M - (ms + nu)P$$
$$= (qw - ps)M - (pr + qt)N$$

and

$$A_{1,2} = A_{2,1}$$
$$= (ms + nu)M + (mr - nt)N$$
$$= (pr + qt)M + (qu - ps)P.$$

If the part of the matching network farther from the discontinuity is moved to the opposite side of the discontinuity, the matrix for the resulting network is

$$\begin{pmatrix} B_{1,1} & jB_{1,2} \\ jB_{2,1} & B_{2,2} \end{pmatrix}$$
$$= \begin{pmatrix} r & js \\ jt & u \end{pmatrix}\begin{pmatrix} M & jN \\ jP & M \end{pmatrix}\begin{pmatrix} m & jn \\ jp & q \end{pmatrix}.$$

The values of $B_{1,1}$, $B_{1,2}$, $B_{2,1}$, and $B_{2,2}$ are given by the equations

$$B_{1,1} = (mr - ps)M - rtN - puP,$$
$$B_{1,2} = (nr + qs)M + qrN - nsP,$$
$$B_{2,1} = (mt + pu)M - ptN + muP,$$
$$B_{2,2} = (qu - nt)M - qtN - nuP.$$

By simple algebraic manipulations, it can be shown that the above equations require that $B_{1,1}=B_{2,2}$ and $B_{1,2}=B_{2,1}$. Consequently, if the load impedance is one, the input impedance is one. This completes the proof of the theorem.

Next, symmetrical matching is considered. In this case, the matrix for the combined network is

$$\begin{pmatrix} C_{1,1} & jC_{1,2} \\ jC_{2,1} & C_{2,2} \end{pmatrix}$$
$$= \begin{pmatrix} m & jn \\ jp & q \end{pmatrix}\begin{pmatrix} M & jN \\ jP & M \end{pmatrix}\begin{pmatrix} q & jn \\ jp & m \end{pmatrix}.$$

Since $C_{1,2}=C_{2,1}$,

$$2mnM + m^2N - n^2C = 2pqM - p^2N + q^2P.$$

If the right-hand network is moved to the left with a section of lossless transmission line between the two matching networks, the corresponding matrix is

$$\begin{pmatrix} D_{1,1} & jD_{1,2} \\ jD_{2,1} & D_{2,2} \end{pmatrix} = \begin{pmatrix} q & jn \\ jp & m \end{pmatrix}$$
$$\cdot\begin{pmatrix} \cos\beta d & j\sin\beta d \\ j\sin\beta d & \cos\beta d \end{pmatrix}\begin{pmatrix} m & jn \\ jp & q \end{pmatrix}\begin{pmatrix} M & N \\ jP & M \end{pmatrix}.$$

If βd is chosen so that $D_{1,1}=D_{2,2}$, then it can be shown by simple algebraic manipulations that $D_{1,2}=D_{2,1}$. Consequently, if symmetrical two-sided matching can be achieved, there exists a corresponding one-sided symmetrical matching network. So the procedures given above yield all possible symmetrical matching networks of the type considered.

Derivation of Procedures

According to the above theorem, if $Y_A=1$ for the circuit shown in Fig. 4, then $Y_B=1$ for the circuit shown in Fig. 5. It may be observed that the dimension d_3 does not appear in Fig. 5.

For the circuit shown in Fig. 4, let Y_1 denote the admittance at the input of the loss ess discontinuity, Y_a denote the admittance immediately to the right of the right shunt susceptance, Y_b denote the admittance immediately to the left of the right shunt susceptance, and Y_c denote the admittance immediately to the right of the left shunt susceptance. Let $Y_a=g+jb$. Now $Y_b=g+j(b+B)$. In order for the left shunt susceptance to complete the match, $Y_c=1-jB$. Three sets of these admittances are shown plotted on Smith charts in Figs. 6 and 7. (For these illustrations, the discontinuity consists of a shunt susceptance whose value is 1.6.)

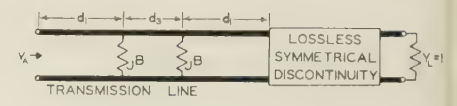

Fig. 4—One-sided matching.

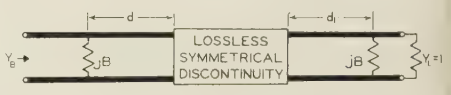

Fig. 5—Two-sided matching.

The point Y_b must lie on the circle C_1 through Y_c whose center is at C. Let C_2 denote the circle which is obtained by subtracting jB from the admittances on the circle C_1. Since $Y=1+jB$ lies on C_1, $Y=1$ must lie on C_2, *i.e.*, the circle C_2 must pass through C. The point Y_a must lie on C_2. The point Y_a must also lie on the circle C_3 through Y_1 whose center is at C. The distances d_1 and d_3 are indicated by the angles $\angle Y_1CY_a$ and $\angle Y_bCY_c$, respectively.

For a given value of B, the circle C_2 is fixed. In general, the circle C_3 intersects the circle C_2 at two points. This is illustrated in Figs. 3 and 6. The value of B is the same for Figs. 6(a) and (b), but d_1 and d_3 are different. (For Fig. 6, $Y_1=1+j1.6$ and $B=1$.)

The circle C_2 can be drawn by finding at least three points on it by subtracting jB from the admittances for points on the circle C_1, and then drawing a circle through these points. However, it is more convenient to compute the center of the circle. In the Γ-plane, the center of the circle is at $\Gamma=0$ and the radius of this circle is

$$\frac{B}{\sqrt{4+B^2}}.$$

The bilinear transformation[5]

$$Y = \frac{1+\Gamma}{1-\Gamma}$$

Y plane. The center of C_4 is at

$$Y = \frac{2+B^2}{2}$$

and the radius of C_4 is

$$\frac{B\sqrt{4+B^2}}{2}.$$

The circle C_5 in the Y plane is found by subtracting jB from the admittances on C_4. The center of C_5 is at

[5] H. F. Mathis, "Bilinear transformations," IRE Trans., vol. CT-3, p. 156; June, 1956.

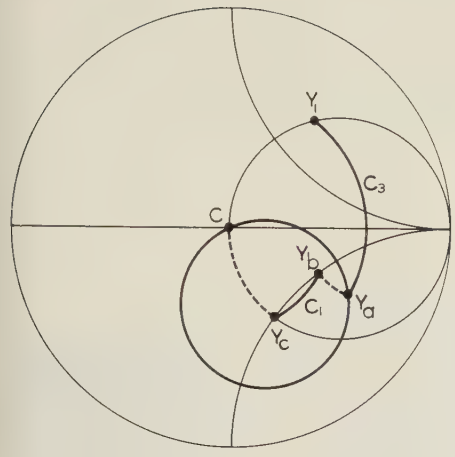

(a)

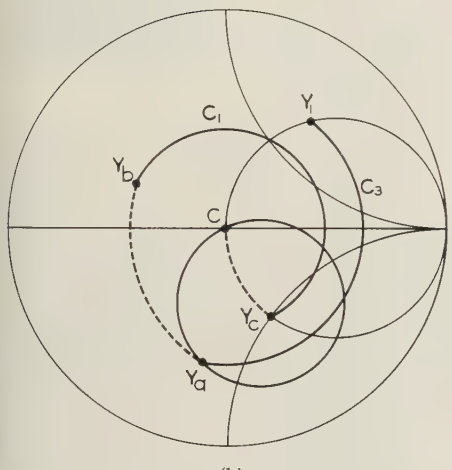

(b)

Fig. 6—Diagrams illustrating matching with fixed B.

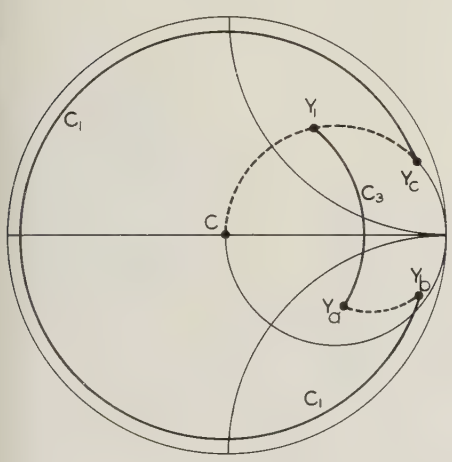

Fig. 7—Diagram illustrating matching with fixed d_1.

$$Y = \frac{2 + B^2}{2} - jB$$

and the radius of C_5 is the same as the radius of C_4. The transformation

$$\Gamma = \frac{Y - 1}{Y + 1}$$

maps the circle C_5 into the circle C_2 in the Γ plane. The center of the circle C_2 is at

$$= \frac{B^2 - i2B}{4 + 2B^2}.$$

The corresponding admittance of the center of C_2 is

$$Y_2 = \frac{1 + \Gamma}{1 - \Gamma}$$

$$= \frac{16 + 12B^2 + 3B^4 - j(16B + 8B^3)}{16 + 12B^2 + B^4}. \quad (1)$$

Let Γ_b and Γ_c denote the current reflection coefficients corresponding to Y_b and Y_c, respectively. The values of Γ_b and Γ_c are given by the equations

$$\Gamma_b = \frac{g + j(b + B) - 1}{g + j(b + B) + 1},$$

$$\Gamma_c = \frac{1 - jB - 1}{1 - jB + 1}.$$

Since Y_b and Y_c lie on the circle C_1,

$$|\Gamma_b|^2 = |\Gamma_c|^2 = \frac{(g - 1)^2 + (b + B)^2}{(g + 1)^2 + (b + B)^2}$$

$$= \frac{B^2}{2^2 + B^2}.$$

This equation can be solved for B to obtain (2). If $g = 1$, it is obvious that $2B = -b$. Thus for a given d_1 and the corresponding $Y_a = g + jb$, there are generally two possible values of B. This is illustrated in Figs. 6(a) and 7 where the value of Y_a is the same but the values of B are different. [For Fig. 6(a), $Y_a = 1.9 - j2$ and $B = 1$. For Fig. 7, $B = -5.4$.]

Harold F. Mathis
Goodyear Aircraft Corp.
Akron, Ohio

Letter from Mr. Reed[6]

Mr. Mathis' theorem is correct but the procedure resulting from this theorem does not give a good result from an engineering standpoint. The result of what he calls two-sided matching will give a match not only at the design center frequency, but also at some other frequency. Thus, the performance curve will *not* be symmetrical about the design center. The procedure suggested in my last note would give a symmetrical curve with maximally-flat response in which the two frequencies of match are the same.

Suppose it is desired to cancel out an inductive iris which has a normalized susceptance of -2. The reflection from this can be cancelled out by the use of another iris whose susceptance is also -2 spaced down the line toward the generator by three-eighths of a wavelength.

Thus, according to his theorem, we can split the matching into two susceptances of -1 on either side of the susceptance of -2 spaced 0.375 λg (tan $2\pi s/\lambda g = -1$) of a wavelength from it. But match would also occur if the spacing were 0.3245 λg(tan $2\pi s/\lambda g = -2$).

For critical coupling$B\sqrt{B^2+4}$ is set equal to -2 and the resulting equation solved for B giving B to -0.91018. This value of B is inserted into the formula for p, thus resulting in this case of a value of p equal to $0.3465\lambda g$. See Fig. 8.

[6] Received by the PGMTT, December 19, 1956.

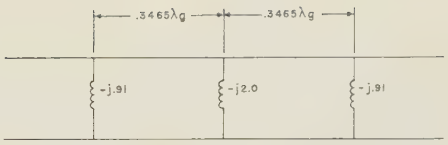

Fig. 8.

Approximate performance curves for one-sided matching, two-sided matching using the Mathis theory, and critically coupled performance as described above are shown below. Some improvements in the critically coupled performance can be obtained by letting the midband be mismatched but be matched on either side of the design frequency. See Fig. 9 below.

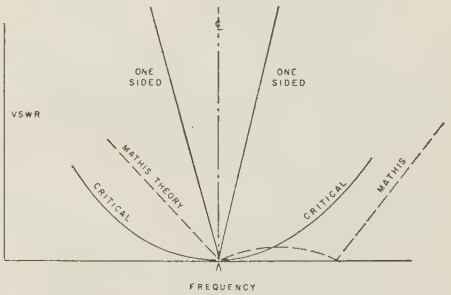

Fig. 9.

John Reed

Author's Comment[7]

I agree with the remarks in Mr. Reed's recent note. In my original brief notes, I did not consider the effects of varying the frequency. His two notes are most interesting and valuable. I do not think that I can add anything of value.

H. F. Mathis

[7] Received by the PGMTT, January 27, 1957.

The Available Power of a Matched Generator from the Measured Load Power in the Presence of Small Dissipation and Mismatch of the Connecting Network*

It is sometimes necessary to determine the available power of a matched generator in terms of the power dissipated in a load when the load is connected to the generator by means of a slightly mismatched 4-pole having small loss. (A piece of waveguide or short length of coaxial line could exemplify such a 4-pole; the discontinuities at flanges or at connectors and supporting beads could give rise to the slight mismatch.)

* Received by the PGMTT, October 1, 1956. The research reported in this document has been made possible through support and sponsorship extended by the Rome Air Dev. Ctr., Contract AF-30(602)-988. It is published for technical information only and does not represent recommendations or conclusions of the sponsoring agency.

Referring to Fig. 1,

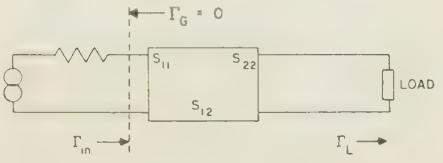

Fig. 1.

let

Γ_L = the reflection coefficient of the load
Γ_{in} = the reflection coefficient of the 4-pole and load
S_{11}, S_{22}, S_{12} = the scattering coefficients of the 4-pole
P_0 = the available power of the generator
P_L = the power dissipated in the load

$$P_L = KP_0. \tag{1}$$

The constant K may be expressed in terms of all or some of the scattering coefficients and only one of the reflection coefficients—either Γ_L or Γ_{in}. Thus,

$$K = \frac{|S_{12}|^2[1-|\Gamma_L|^2]}{|1-S_{22}\Gamma_L|^2} \tag{2}$$

$$K = \frac{|S_{12}^2+S_{22}(\Gamma_{in}-S_{11})|^2-|\Gamma_{in}-S_{11}|^2}{|S_{12}|^2}. \tag{3}$$

The question arises, which expression should be used to determine K if only the magnitudes (but not the phases) of the various scattering and reflection coefficients are known. If $|\Gamma_L|$ is known (and since the phase of Γ_L is arbitrary) the possible range of K may be determined from the maximum and minimum values of K given by (2), namely,

$$K_{max} = \frac{|S_{12}|^2[1-|\Gamma_L|^2]}{[1-|S_{22}\Gamma_L|]^2} \tag{4}$$

$$K_{min} = \frac{|S_{12}|^2[1-|\Gamma_L|^2]}{[1+|S_{22}\Gamma_L|]^2}. \tag{5}$$

(It is interesting to note that the db difference between K_{max} and K_{min},

$$20 \log \frac{1+|S_{22}\Gamma_L|}{1-|S_{22}\Gamma_L|},$$

is independent of S_{12}^2 and increases almost linearly with $|S_{22}\Gamma_L|$ for small values of this product.)

When $|\Gamma_{in}|$ is known (and is the only reflection coefficient accessible to direct measurement because the load is an integral part of a structure which cannot be readily taken apart) (3) must be used to estimate the possible range of K. If the worst possible phase combinations of the coefficients are used in the estimation, an unnecessarily large uncertainty in K will result if the phases of S_{11}, S_{22}, and S_{12} are assumed completely independent. In actuality the phases are restricted by the following relation if the 4-pole is to be physically realizable.[1]

[1] R. LaRosa and H. J. Carlin, "A general theory of wideband matching with dissipative 4-poles," *J. Math. and Phys.*, vol. 33, pp. 331–345; January, 1955.

TABLE I

Results Calculated from (2) for $|\Gamma_L| = 0.15$

	$\|S_{12}\|^2=0.98$				$\|S_{12}\|^2=0.95$				$\|S_{12}\|^2=0.90$			
$\|S_{11}\|$	K_{max}	K_{min}	K_0	Error	K_{max}	K_{min}	K_0	Error	K_{max}	K_{min}	K_0	Error
0.03	0.968	0.950	0.958	0.010	0.938	0.920	0.929	0.009	0.889	0.872	0.880	0.009
0.15	0.973	0.944	0.958	0.015	0.943	0.915	0.929	0.014	0.893	0.868	0.880	0.013
0.10	0.988	0.930	0.958	0.030	0.957	0.901	0.929	0.029	0.907	0.854	0.880	0.027

TABLE II

Results Calculated from (3) for $|\Gamma_{in}| = 0.15$

	$\|S_{12}\|^2=0.98$				$\|S_{12}\|^2=0.95$				$\|S_{12}\|^2=0.90$			
$\|S_{11}\|$	K_{max}	K_{min}	K_0	Error	K_{max}	K_{min}	K_0	Error	K_{max}	K_{min}	K_0	Error
0.03	0.964	0.952	0.957	0.007	0.937	0.916	0.926	0.011	0.892	0.852	0.875	0.023
0.05	0.965	0.954	0.957	0.008	0.942	0.912	0.926	0.016	0.899	0.836	0.875	0.039
0.10	0.970	0.964	0.957	0.013	0.947	0.922	0.926	0.021	0.905	0.847	0.875	0.030

$$(1-|S_{12}|^2)^2-|S_{22}|^2-|S_{11}|^2+|S_{11}S_{22}|^2 = 2\,\mathrm{Re}\,S_{12}^{*2}S_{11}S_{22}. \tag{6}$$

The maximum and minimum values of K should be computed from (3) taking into account the above restriction.

If $|S_{11}|$ is assumed equal to $|S_{22}|$, (3) may be transformed to

$$K = \frac{k_0 + k_1(\Phi,\psi)}{|S_{12}|^2} \tag{7}$$

where

$\psi = \arg\,(S_{12}^{*2}S_{11}S_{22})$
$\Phi = \arg\,(\Gamma_{in}^{*}\,S_{11})$
$k_0 = |S_{12}|^4+|S_{11}|^4-|S_{11}|^2-|\Gamma_{in}|^2$
$k_1(\Phi,\psi) = A\cos\Phi + B\cos(\psi-\Phi) - C\cos\psi$
$A = 2(1-|S_{11}|^2)|S_{11}\Gamma_{in}|$
$B = 2|S_{12}|^2|S_{11}\Gamma_{in}|$
$C = 2|S_{12}^2S_{11}S_{22}|$.

Eq. (6) then becomes

$$(1-|S_{12}|^2)^2-2|S_{11}|^2+|S_{11}|^4 \geq C\cos\psi. \tag{8}$$

Although Φ is an unrestricted angle, ψ is constrained by the above inequality to the region $\pi-\alpha \leqq \psi \leqq \pi+\alpha$, where α is a positive number $\leqq \pi$ whose value depends on $|S_{12}|^2$ and $|S_{11}|^2$. The extreme values of $k_1(\Phi,\psi)$ determine the extremes of k. The former can be obtained in the usual way by setting $\partial k_1/\partial\Phi$ and $\partial k_1/\partial\psi$ equal to zero and solving for the corresponding values of Φ and ψ. If a solution lies within the permissible region for Φ and ψ the corresponding maxima and minima of k_1 are evaluated. In addition solutions for the maxima and minima of k_1 on the boundary of the permissible region ($\psi=\pi-\alpha$, $\pi+\alpha$) are obtained by setting $\partial k_1/\partial\Phi$ equal to zero on the boundary. The extreme values thus obtained are compared with the values (if any) which lie within the region and the most extreme values are used in calculating k_{max} and k_{min}.

The values of K_{max} and K_{min} have been tabulated for two types of cases for typical values of the scattering coefficients. In the first type (Table I) $|\Gamma_L|$ is assumed known and (2) is used in estimating the uncertainty in K. In the second type (Table II) $|\Gamma_{in}|$ is assumed known, $|S_{11}|$ is assumed equal to $|S_{22}|$ and (3) is used subject to the restriction of (6). The uncertainty in K may be expressed by the difference between K_{max} or K_{min} and an intermediate value K_0, obtained by setting $|S_{11}| = |S_{22}| = 0$. By (2) and (3) respectively

$$K_0 = \frac{|S_{12}|^4-|\Gamma_{in}|^2}{|S_{12}|^2} \tag{9}$$

$$K_0 = |S_{12}|^2[1-|\Gamma_L|^2]. \tag{10}$$

The importance of the physical realizability criterion can best be appreciated by considering an example. Let $|S_{11}| = |S_{22}| = 0.1$, $|S_{12}|^2 = 0.95$ and $|\Gamma_{in}| = 0.15$. For the worst phase combinations (3) gives a maximum difference between K and K_0 of about 9 per cent if the phases are unrestricted. This is reduced to 2 per cent if the restriction of (6) is applied.

In most cases K_0 is not much different from a value midway between K_{max} and K_{min} and may therefore be used to represent K with minimum error. The only 4-pole parameter required to determine K_0 is the attenuation, $|S_{12}|^2$, of the 4-pole. For a structure such as a short piece of waveguide $|S_{12}|^2$ is usually a smooth and slowly varying function of frequency which can be determined once and for all.

In measuring P_L the coefficient $|\Gamma_{in}|$ can generally be determined at the same time, whereas $|\Gamma_L|$ must be derived from previous measurements, generally by interpolation between data points. Eq. (9) will therefore be more useful than (10). Moreover, for small attenuations ($|S_{12}|^2 \geqq 0.95$), (9) will yield a smaller uncertainty in K than (10). For larger attenuations (9) rapidly loses its usefulness and (10) yields smaller uncertainties. However, if interpolated values of $|\Gamma_L|$ are used and $|\Gamma_L|$ is an erratic function of frequency these uncertainties may be appreciably increased.

Acknowledgment

The aid and suggestions of Dr. H. J. Carlin of the Microwave Research Institute are gratefully acknowledged.

L. O. Sweet
Polytechnic Res. and Dev. Co.
Brooklyn, N. Y.
M. Sucher
Microwave Res. Inst.
Brooklyn, N. Y.

Contributors

For a photograph and biography of E. Folke Bolinder, please see page 187 of the July, 1956 issue of these TRANSACTIONS.

❖

Georges A. Deschamps (SM'51) was born in Vendome, France, on October 18, 1911. He graduated from the Ecole Normale Supérieure of Paris in 1934, and received the following degrees from the Sorbonne: license in mathematics and in physics, diplome d'étude supérieure, and agrégation in mathematics. After two years of research in pure mathematics, one in Paris and one at Princeton University he joined the Lycee Francais de New York as a professor of mathematics and physics. At that time he did some work on special relativity and the theory of elementary particles.

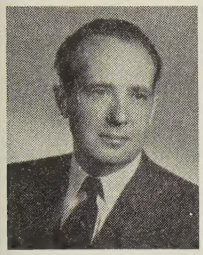

G. A. DESCHAMPS

Mr. Deschamps served in the French army during the war and, in 1947, joined Federal Telecommunication Laboratories where he is presently a senior project engineer in the Electronic Systems Laboratory.

He is a member of the American Physical Society.

❖

William A. Gerard (S'50–A'53) was born in Newark, N. J. on November 14, 1927. He was graduated from the Newark College of Engineering in 1951, receiving the B.S. degree in electrical engineering. After graduation he joined the Westinghouse Electric Corporation on the graduate student course. Since 1952 he has been an engineer of the electronic tube division at the Horseheads, N. Y. plant where he is engaged in the development of microwave tubes.

W. A. GERARD

❖

Robert C. Hansen (S'47–A'49–M'55) was born in St. Louis, Mo., in 1926. His college studies at the Missouri School of Mines and Metallurgy were interrupted by service in the United States Navy in 1945–46 as an RT instructor, after which he resumed studies at the same school, graduating in January, 1949 with the B.S. degree in electrical engineering. The M.S. degree was granted in 1950 by the University of Illinois.

For the next several years Dr. Hansen was, successively, research assistant and research associate in the Antenna Laboratory, University of Illinois. He was awarded the Ph.D. degree in electrical engineering by the University of Illinois in May, 1955. Since that time he has been a group leader in the Microwave Laboratory of Hughes Aircraft Company, working on surface waves and other antenna research. He is now head of the Electrical Research Section, Radome Department.

R. C. HANSEN

Dr. Hansen is a member of the American Institute of Physics, Tau Beta Pi, Phi Kappa Phi, Eta Kappa Nu, and Sigma Xi, and is a registered Professional Engineer in the state of Missouri.

❖

James D. Horgan was born in Grand Rapids, Mich., on May 21, 1922. He was a staff member at the M.I.T. Radiation Laboratory during World War II. In 1946 he returned to Marquette University and received the B.S. degree in electrical engineering in 1947, and the M.S. degree in 1951. Since 1947 he has been a member of the faculty there, and received the Ph.D. degree from the University of Wisconsin in February, 1957. He is now at Marquette as director of the department of electrical engineering.

J. D. HORGAN

Mr. Horgan is a member of Sigma Xi, Tau Beta Pi, and Eta Kappa Nu.

❖

For a photograph and biography of Donald D. King, please see page 76 of the January, 1957 issue of these TRANSACTIONS.

❖

Richard K. Moore (S'43–A'46–M'50–SM'54) was born November 13, 1923 in St. Louis, Mo. He received the B.S.E.E. degree from Washington University, St. Louis in 1943. Later he did graduate work at Washington and at Cornell University, receiving the Ph.D. degree from the latter in 1951.

Dr. Moore was employed as an engineer designing test equipment for RCA Victor Division in 1943–1944. He then entered the Navy, where he attended Bowdoin and M.I.T. radar schools and served as electronics and communications officer. During 1947–49, he was instructor of electrical engineering at Washington University and worked part-time on a research project on diversity reception. From 1949 to 1951 he was a research associate at Cornell University, working on tropospheric and ionospheric propagation, particularly that involving scatter by auroral ionization. In 1951 he joined Sandia Corporation where he directed a project involving radar return from the ground and from precipitation until leaving to become Chairman of the Electrical Engineering Department at the University of New Mexico, a position he now holds. Dr. Moore is still a consultant at Sandia Corporation.

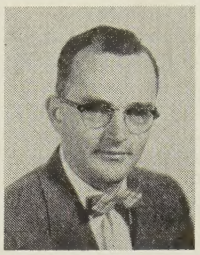

R. K. MOORE

He is a member of Phi Eta Sigma, Pi Mu Epsilon, Sigma Tau and Tau Beta Pi, and Sigma Xi. He belongs to AIEE and ASEE.

❖

James A. Mullen (S'50–A'55) was born May 28, 1928 in Malden, Mass. He received the B.S. degree in physics in 1950 from Providence College, Rhode Island after two year's service in the U. S. Army. He attended Harvard University and received the A.M. degree in 1951 and the Ph.D. degree in 1955 in the field of random processes.

J. A. MULLEN

Since the spring of 1955 he has been employed by the Research Division of Raytheon Manufacturing Company where he has been concerned with noise in electron tubes and communication systems

He is a member of Sigma Xi and the Society for Industrial and Applied Mathematics.

❖

Conrad E. Nelson (A'52) was born on December 4, 1927, on Long Island, N. Y. He received the B.S. degree in electrical engineering from the University of California at Los Angeles in 1949. In 1952, Mr. Nelson was graduated from the three year Advanced Engineering program at the Gen-

eral Electric Company, Schenectady, N. Y. and continued for three years at GE, Syracuse, N. Y., doing advance development of microwave components. Since 1955 Mr. Nelson has been in the Electronics Department of the Microwave Laboratory, Hughes Research Laboratories, Culver City, Calif.

C. E. NELSON

He has been a registered professional engineer in New York since 1955.

❖

Wilbur L. Pritchard (A'45–M'48–SM'52) was born in New York, N. Y., on May 31, 1923. He received the B.E.E. degree in 1943 from the City College of New York, and then engaged in part-time graduate study at Massachusetts Institute of Technology, from 1948 to 1951. He was an engineer with Philco Radio and Television Corp. from 1943 to 1946, and worked on developing airborne radar systems, home radios, and phonographs. In 1946 he joined Raytheon Manufacturing Company as a senior engineer.

W. L. PRITCHARD

Mr. Pritchard has had experience in microwave relay systems, rf and antenna design on radars, beacons, relay systems, and microwave cooking equipment. At present, he is manager of the Microwave and Transmitter Branch.

He is Chairman of the Boston Chapter and the Vice-Chairman of the PGMTT.

❖

John M. Richardson (S'56) was born September 5, 1921, in Rock Island, Ill. He received the B.A. in physics from the University of Colorado in 1942, and served as Electronics Officer in the USNR from 1943 to 1946. He received the M.A. and Ph.D. degrees from Harvard University, the latter in 1951. He was subsequently employed by the Denver Research Institute. In 1952, he went to work for the National Bureau of Standards. His work in the microwave physics section is concerned with the application of microwaves to problems of physical standards and constants, and he is currently working on a precision millimeter wave interferometer.

J. M. RICHARDSON

Dr. Richardson is a member of the American Physical Society, Sigma Xi, and the Research Society of America.

❖

Russell B. Riley was born in Kansas City, Mo., on July 31, 1933. He received the B.S. degree in electrical engineering from the University of Colorado in 1955. From 1952 to 1955 he worked part time for the National Bureau of Standards Laboratories in Boulder, first as a physical science aid and finally as an electronic scientist.

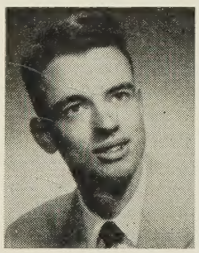

R. B. RILEY

In 1955 he joined the laboratory staff of the Hewlett-Packard company and is also engaged in part time school work at Stanford University.

He is a member of Tau Beta Pi, Eta Kappa Nu, Sigma Tau and RESA.

❖

Harold Seidel (A'47) received the B.E.E. degree from the College of the City of New York in 1943, and the M.E.E. and D.E.E. degrees from the Polytechnic Institute of Brooklyn in 1947 and 1954. After employment with the Microwave Research Institute of Polytechnic Institute of Brooklyn, Arma Corporation, and the Federal Telecommunications Laboratory he joined Bell Telephone Laboratories in 1953. His work there has generally been concerned with microwave problems. He is presently engaged in the analysis of ferrite devices.

H. SEIDEL

Dr. Seidel is a member of Sigma Xi, and the American Association for the Advancement of Science.

❖

Jean G. Van Bladel (M'54–SM'56) was born in Antwerp, Belgium, on July 24, 1922. He was graduated from Brussels University in 1947 with the title of ingénieur électricien et mécanicien. From 1948 through 1950, he was a graduate fellow of the Belgian American Educational Foundation at the University of Wisconsin, receiving the Ph.D. degree in electrical engineering from this university in 1950.

J. G. VAN BLADEL

After his graduation, Dr. Van Bladel became the head of the radar department at the M.B.L.E. factories in Brussels, Belgium, where he stayed until 1954. From 1954 until 1956 he was associate professor of electrical engineering at Washington University, St. Louis, Mo. Since 1956, he has been associate professor of electrical engineering at the University of Wisconsin, Madison, Wis., working half-time with the Midwestern Universities Research Association.

Dr. Van Bladel is a member of Sigma Xi, and the American Institute of Electrical Engineers.

❖

Oscar E. von Rohr, Jr. was born in St. Louis, Mo., June 30, 1917. He received the B.S. in electrical engineering from Washington University in June, 1953 and the M.S. in electrical engineering from the same university in June, 1956. Previous to attending Washington University, he was employed for four years as a radio engineer for Civil Service in which capacity he had charge of installations and maintenance of various types of radio and radar equipment. After obtaining the B.S. degree he worked one year for White Rogers Electric Company in the field of research and development of electronic equipment.

O. E. VON ROHR, JR.

From 1954 until the present time he has been employed as an instructor in the electrical engineering department at Washington University.

❖

For a photograph and biography of James R. Wait, please see page 189 of the July, 1956 issue of these TRANSACTIONS.

INSTITUTIONAL LISTINGS (Continued)

NATIONAL INSTRUMENT CO., INC., 23 E. 26 St., New York, N. Y.
Wide-Band Microwave Equipment, Simulated Flight Instruments, Lobe Switches, Custom Built Precision Apparatus

WEINSCHEL ENGINEERING CO. INC., Kensington, Md.
Attenuation Standards, Coaxial Attenuators and Insertion Loss Test Sets

WHEELER LABORATORIES, INC., 122 Cutter Mill Road, Great Neck, N. Y.
Consulting Services, Research & Development, Microwave Antennas & Waveguide Components

The charge for an Institutional Listing is $50.00 per issue or $140.00 for four consecutive issues. Applications for Institutional Listings and checks (made out to the Institute of Radio Engineers) should be sent to Mr. L. G. Cumming, Technical Secretary, Institute of Radio Engineers, 1 East 79th Street, New York 21, N. Y.

INSTITUTIONAL LISTINGS

The IRE Professional Group on Microwave Theory and Techniques is grateful for the assistance given by the firms listed below, and invites application for Institutional Listing from other firms interested in the Microwave field.

COLLINS RADIO CO., Cedar Rapids, Iowa
Complete Industrial Microwave, Communication, Navigation and Flight Control Systems

HUGHES AIRCRAFT COMPANY, Culver City, California
Radar Systems, Guided Missiles, Antennas, Radomes, Tubes, Solid State Physics, Computers

MARYLAND ELECTRONIC MANUFACTURING CORPORATION, College Park, Md.
Development and Production of Microwave Antennas and Waveguide Components

(Please see inside back cover for additional listings.)